

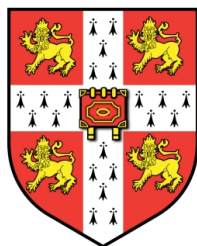
# Emission Properties of Radiative Chiral Nematic Liquid Crystals

This dissertation is submitted for the degree of  
Doctor of Philosophy

by

**Themistoklis K. Mavrogordatos**

Centre of Molecular Materials for Photonics and Electronics  
Photonics Doctoral Training Centre, Division B, Department of Engineering  
Jesus College, University of Cambridge  
Supervisor: Prof. Timothy D. Wilkinson



Cambridge

February 2014 (Rev. August 2014)

# Contents

<b>Declaration</b>	<b>v</b>
<b>Acknowledgments</b>	<b>vi</b>
<b>Abstract</b>	<b>vii</b>
<b>Introduction</b>	<b>x</b>
<b>1 The mechanics of liquid crystals</b>	<b>1</b>
1.1 Nematics . . . . .	1
1.2 Chiral nematics . . . . .	18
<b>2 Optical properties of LC cells</b>	<b>22</b>
2.1 The Belyakov formulation . . . . .	22
2.1.1 Kinematical approximation and exact solution . . . . .	22
2.1.2 Formation of the Boundary Value Problem . . . . .	28
2.2 The de Vries formulation . . . . .	35
2.3 Oblique incidence . . . . .	45
2.4 The Berreman method . . . . .	52
2.5 Optical feedback in nematic LC slabs . . . . .	56

<b>3</b>	<b>The density of photon states</b>	<b>67</b>
3.1	The rôle and the calculation of the DOS . . . . .	67
3.1.1	The quarter-wave stack . . . . .	84
3.2	The DOS in radiative chiral nematics . . . . .	89
3.2.1	Inclusion of absorption . . . . .	90
3.2.2	Inclusion of amplification . . . . .	97
<b>4</b>	<b>The Jaynes-Cummings model</b>	<b>111</b>
4.1	Hamiltonian, states and equations of motion . . . . .	112
4.2	Photonic Density of States revisited . . . . .	118
4.3	Main results for radiative chiral nematic LCs . . . . .	121
4.4	A 2D photonic crystal and the DOS . . . . .	124
4.5	Discussion of results . . . . .	130
4.6	More on the Fano-Anderson model . . . . .	136
<b>5</b>	<b>Adaptive pumping of radiative LC cells</b>	<b>145</b>
5.1	The method of adaptive pumping . . . . .	148
5.1.1	Sample preparation . . . . .	150
5.1.2	Pumping process . . . . .	151
5.2	Main results . . . . .	153
<b>6</b>	<b>Suggestions for further research</b>	<b>166</b>
6.1	Decay dynamics in the Jaynes-Cummings model . . . . .	166
6.2	The basic principles of the Resolvent Method . . . . .	169
6.3	Atomic radiation in free space . . . . .	173
6.4	Atomic radiation in cavities and waveguides . . . . .	177
6.5	Atomic radiation in a 1D periodic medium . . . . .	188

<b>Synoptic conclusions</b>	<b>192</b>
<b>Related publications</b>	<b>195</b>

# Declaration

This dissertation is the result of my own work and includes nothing which is the outcome of work done in collaboration except where specifically indicated in the text. No part of this thesis has been submitted for any other qualification. This dissertation contains 21 figures and less than 47.300 words, therefore it does not exceed the word limit for the respective Degree Committee.

Themistoklis K. Mavrogordatos

February 2014 (Revised August 2014)

# Acknowledgments

I would like to thank my supervisor, Prof. Timothy D. Wilkinson for his guidance, honesty and respect to freedom of opinion and expression. Very valuable help I also received from Dr. Stephen M. Morris throughout my PhD project, in both the theoretical and experimental parts of this work. In the latter, my colleague Simon Wood contributed significantly with an unusual perseverance and ardour. During my PhD studies, I had many stimulating and challenging discussions with most of the members of the CMMPE group, particularly with Dr. Flynn Castles. Some of the conclusive arguments constitute part of this thesis. In that regard, the academic collaboration with Prof. Vladimir A. Belyakov consisted a source of inspiration and rigour. His book on optics of periodic media, alongside relevant papers are referenced extensively throughout the thesis. As far as more practical matters are concerned, I would like to acknowledge financial support from the Onassis Foundation as well as from the EPSRC, towards my maintenance costs and tuition fees, respectively. Finally, on a more personal note, I am grateful to my friend Marcin Malinowski, who was the first physics student I supervised in Cambridge. He taught me to pay more attention to detail, and helped me remaining focussed and determined.

# Abstract

In this work, we calculate the density of photon states (DOS) of the normal modes in dye-doped chiral nematic liquid crystal (LC) cells in the presence of various loss mechanisms. Losses and gain are incorporated into the transmission characteristics through the introduction of a small imaginary part in the dielectric constant perpendicular and along the director, for which we assume no frequency dispersion. Theoretical results are presented on the DOS in the region of the photonic band gap for a range of values of the loss coefficient and different values of the optical anisotropy. The obtained values of the DOS at the photonic band gap edges predict a reversal of the dominant modes in the structure. Our results are found to be in good agreement with the experimentally obtained excitation thresholds in chiral nematic LC lasers. The behaviour of the DOS is also discussed for amplifying LC cells providing an additional insight to the lasing mechanism of these structures. We subsequently investigate the spontaneous emission properties, under the assumption that the electronic transition frequency is close to the photonic edge mode of the structure (resonance). We take into account the transition broadening and the decay of electromagnetic field modes supported by the so-called ‘mirror-less’ cavity. We employ the Jaynes-Cummings Hamiltonian

to describe the electron interaction with the electromagnetic field, focusing on the mode with the diffracting polarization in the chiral nematic layer. As known in these structures, the density of photon states, calculated via the Wigner method, has distinct peaks on either side of the photonic band gap, which manifests itself as a considerable modification of the emission spectrum. We demonstrate that, near resonance, there are notable differences between the behaviour of the density of states and the spontaneous emission profile of these structures. In addition, we examine in some detail the case of the logarithmic peak exhibited in the density of states in 2D photonic structures and obtain analytic relations for the Lamb shift and the broadening of the atomic transition in the emission spectrum. The dynamical behaviour of the atom-field system is described by a system of two first order differential equations, solved using the Green's function method and the Fourier transform. The emission spectra are then calculated and compared with experimental data.

Finally, we detail a new technique for the pumping of dye lasers which requires no moving parts or flushing mechanisms and is applicable to both solid state and liquid based devices. A reconfigurable hologram is used to control the position of incidence of a pump beam onto a dye laser and significant increases in device lifetimes are achieved. The technique is also applied to wavelength tune a dye laser. This offers access to higher repetition rates and larger average output powers. With higher repetition rate pump lasers it is feasible that the approach could allow such organic lasers to reach operating frequencies on the order of MHz. The unique nature of the adaptive pumping method also allows precise control of the spatial wave-front and configura-

tion of the pumping wave which allows greater versatility and functionality to be realised. It is possible to envisage that novel pump beam profiles that optimise propagation through the medium could also be demonstrated.

# Introduction

Photonic band edge lasing has been extensively demonstrated in dye-doped chiral nematic liquid crystal (LC) cells following the first pioneering experimental realisation in 1980 <sup>†</sup>. Feedback is provided by the modulation of the refractive index as the director precesses continually and orthogonally along the optical axis forming a helical structure with pitch. Optical gain, on the other hand, is provided through the addition of a gain medium such as a laser dye. In recent years, these lasers have attracted interest because of their remarkable emission characteristics in the form of broadband wavelength tuneability, narrow linewidth emission, and high slope efficiencies.

In the first two chapters we review the basic mechanical and optical properties of liquid crystals, aiming to build the required background to understand the enhancement of radiation from these molecular structures. The observed lasing behaviour near the edges of the photonic band gap can be explained by the drastic changes in the density of photon states (DOS). Divergence in the DOS at the band-edges in chiral nematic LCs was shown theoretically and experimentally who considered the fluorescence characteristics from a

---

<sup>†</sup>I.P. Il'chishin, E.A. Tikhonov, V.G. Tishchenko and M.T. Shpak, *Generation of a tunable radiation by impurity cholesteric liquid crystals*, JETP Lett., Vol. 32, 24-27 (1980).

dye-doped chiral nematic LC in the region of the photonic band gap. Subsequently, for laser emission it has been shown that, in analyzing the case of a Fabry-Pérot (FP) resonator, the threshold gain can be related directly to the DOS. Furthermore, according to the space-independent rate equations the slope efficiency can be shown to be inversely proportional to the threshold energy and therefore directly proportional to the DOS.

Losses will be important in the design of optimised practical systems: they will affect the DOS and hence the threshold gain and the slope efficiency. In this work we calculate the effect of losses and gain directly on the DOS. We modify the analysis of previous works to include imaginary parts in the parallel and perpendicular dielectric coefficients. We will show that small losses have appreciable and unexpected effects on the DOS, such as a reversal of the dominant edge mode, and hence also on the threshold gain. The modified DOS is investigated for various cell thicknesses and optical anisotropies. We then correlate our theoretical results with experimentally determined excitation thresholds, finding good agreement. The behaviour of the DOS corresponding to stimulated emission close to the lasing threshold condition is discussed.

In order to introduce losses in to the transmission coefficient it is first necessary to construct a formulation for the DOS in terms of the transmission coefficient. For a light wave propagating along the helix of a chiral nematic LC film there are two eigenmodes corresponding to elliptically polarized plane waves with an opposite sense of rotation. Their polarization is wavelength dependent. The probability of photon emission by an excited fluorescent molecule, as obtained by Dirac's rule is the product of the DOS and the

square of the matrix elements corresponding to the coupling of the electric field with the electric dipole moment of the gain medium. Furthermore, we consider a two-level system coupled to a quantum harmonic oscillator, frequently described with the Jaynes-Cummings (JC) Hamiltonian in which only ‘resonant’ terms feature. Such a consideration is permissible in the case of near resonance and weak coupling. Both conditions are satisfied for spontaneous emission in these periodic structures for small detuning. We put the analysis of spontaneous emission from 2D photonic crystals on a firmer basis providing analytical results, and explore in more detail the fluorescence properties in chiral nematic LCs, outlining common features that are attributed to resonance. Moreover, the discrepancy between the experimentally obtained emission spectra and the theoretically calculated DOS is addressed. Such a consideration aims to further the understanding of spontaneous and induced emission from these distributed feedback resonators.

Despite the advantages of organic solid-state dye lasers, liquid-dye lasers considerably outperform the solid-state organics when it comes to pulse duration. They can operate with pulses as short as 10 fs, and the pulse length can be made so long as to allow continuous-wave (CW) outputs. Solid-state dye lasers, which consist of an organic dye that is dispersed into a solid matrix, are not so versatile and are restricted to pulse durations are typically no longer than 10 ns. CW operation is generally prohibited because of bleaching issues caused by thermal degradation effects and also the accumulation of triplet excitons. In the case of triplet excitons, which possess an absorption band that overlaps the stimulated emission spectrum, suppression of the gain in the active region can occur, resulting in laser action being switched off.

In order to ensure that the population of triplet states is dissipated between the pulses, repetition rates of the pump laser are usually restricted to less than 10 kHz. However, even if the repetition rate is low enough that triplet excitons do not build-up it is still not necessarily the case that thermal effects are absent.

In order to combat these thermal and excited-state absorption effects, a solution is to remove the excited dye molecules out of the pump volume in sufficient timescales so as to maintain laser action. For liquid dye lasers, this involves a constant convective circulation of the organic species using a jet-stream with velocities on the order of 10s of  $\text{ms}^{-1}$  to replenish the dye molecules and thus avoid the bleaching effects that ultimately shut down laser action. Alternatively, for solid-state organic dye lasers, methodologies that mimic the approach of ‘flushing out’ the excited dye molecules have been demonstrated such as mechanically rotating a disc-shaped active gain medium at high speeds to constantly refresh the dye molecules. A common feature of the techniques that have been demonstrated to date require physically translating the active region in some way relative to the pump. This, therefore, requires the use of moving parts or fluid flow. In our work, we demonstrate that a potentially elegant solution in which the pump beam is moved relative to the solid-state organic dye laser using adaptive optics, which bypasses the need for any moving parts as the position of the pump beam is adjusted through the diffraction of light.

Finally, a chapter on further investigation is included, with emphasis on the Resolvent Method that can be employed to analyze spontaneous emission from radiative chiral nematic liquid crystals (where parallels are drawn with

atomic radiation in cavities and waveguides, with reference to the DOS). In particular, the knowledge of the DOS for periodic structures of finite length can help the understanding of spontaneous emission dynamics, where the departure from an exponential-decay behaviour is prominent.



# Chapter 1

## The mechanics of liquid crystals

In this introductory chapter we will focus more on the mechanics of deformations of the liquid crystals of interest (nematics and chiral nematics), rather than their on optical properties. Such a discussion is deemed necessary, in order to understand the properties of the molecular structures that will form the resonating cavities in both the theoretical and experimental aspects of this work.

### 1.1 Nematics

Nematic liquid crystals are substances which are both microscopically and macroscopically homogeneous in the undeformed state. The anisotropy of the medium is attributed to the anisotropic spatial orientation of the molecules. This anisotropy is fully defined-in the great majority of known nematics-by specifying a unit vector  $\mathbf{n}$  along one particular direction for each point in the medium. This vector is called the (molecular) director. The properties of

ordinary nematics, for every volume element, are invariant under a change in sign of all spatial co-ordinates (inversion). Hence, the state of a nematic crystal is determined by the specification of the director  $\mathbf{n}$  alongside the usual quantities (mass density  $\rho$ , pressure  $p$  and velocity  $\mathbf{v}$ ) for a liquid. In equilibrium, a nematic liquid crystal at rest under no external forces (including the forces exerted by the walls) is uniform and  $\mathbf{n}$  is constant throughout its volume. In a deformed nematic, the direction of  $\mathbf{n}$  varies slowly in space, such that the characteristic dimensions of the deformation are much greater than the molecular dimensions (as a result, the derivatives  $\partial n_i/\partial x_k$  can be regarded as small quantities).

The total free energy density of a deformed liquid crystal, being a scalar quantity itself, can contain only scalar combinations of the components of  $\mathbf{n}$  and its derivatives. The scalar combinations linear in the first derivatives are the true scalar  $\text{div}\mathbf{n}$  and the pseudoscalar  $\mathbf{n} \cdot \mathbf{curl}\mathbf{n}$ . Considering the bulk properties of the material, only the latter should be retained, as the former is transformed into a surface integral by virtue of Gauss's theorem. The true scalars that are quadratic to the first derivatives of the director can be found by considering the four-rank tensor  $\frac{\partial n_k}{\partial x_i} \frac{\partial n_l}{\partial x_m}$  and forming the invariant quantities resulting from contraction of some of its indices as well as from multiplication with  $\mathbf{n}$ . Bearing in mind that  $\mathbf{n}^2 \equiv 1$  we can form the invariant quantities  $(\mathbf{n} \times \mathbf{curl}\mathbf{n})^2$ ,  $\frac{\partial n_k}{\partial x_i} \frac{\partial n_k}{\partial x_i}$ ,  $\frac{\partial n_k}{\partial x_k} \frac{\partial n_i}{\partial x_i}$  and  $\frac{\partial n_k}{\partial x_i} \frac{\partial n_i}{\partial x_k}$ . The difference of the last two quantities can be written in the form [1]

$$\frac{\partial n_k}{\partial x_k} \frac{\partial n_i}{\partial x_i} - \frac{\partial n_k}{\partial x_i} \frac{\partial n_i}{\partial x_k} = \frac{\partial}{\partial x_i} \left( n_i \frac{\partial n_k}{\partial x_k} - n_k \frac{\partial n_i}{\partial x_k} \right), \quad (1.1)$$

which is a divergence that again contributes to the total free energy by an

integral over the surface of the body, and therefore will not be considered.

The invariant

$$\frac{\partial n_k}{\partial x_i} \frac{\partial n_k}{\partial x_i} = (\mathbf{n} \cdot \mathbf{curl} \mathbf{n})^2 + (\operatorname{div} \mathbf{n})^2 \quad (1.2)$$

and  $(\mathbf{n} \cdot \mathbf{curl} \mathbf{n})^2$  will be considered as the independent ones. Last, there is the quadratic in the first derivatives pseudoscalar  $(\mathbf{n} \cdot \mathbf{curl} \mathbf{n}) \cdot \operatorname{div} \mathbf{n}$ . Since  $\nabla \mathbf{n}^2 = 0 \Rightarrow (\mathbf{n} \cdot \nabla) \mathbf{n} = -\mathbf{n} \times \mathbf{curl} \mathbf{n}$ , the vector  $(\mathbf{n} \cdot \nabla) \mathbf{n}$  is perpendicular to  $\mathbf{curl} \mathbf{n}$ , hence  $[(\mathbf{n} \cdot \nabla) \mathbf{n}] \cdot \mathbf{curl} \mathbf{n} = 0$ .

Taking into account the above, the deformation energy of a nematic substance is given by an expression quadratic in the derivatives of  $\mathbf{n}$ , its general form being

$$\begin{aligned} F_d = F - F_0 = & c(\mathbf{n} \cdot \mathbf{curl} \mathbf{n}) \cdot \operatorname{div} \mathbf{n} + d(\mathbf{n} \cdot \mathbf{curl} \mathbf{n}) \\ & + \frac{1}{2} K_1 (\operatorname{div} \mathbf{n})^2 + \frac{1}{2} K_2 (\mathbf{n} \cdot \mathbf{curl} \mathbf{n})^2 + \frac{1}{2} K_3 (\mathbf{n} \times \mathbf{curl} \mathbf{n})^2. \end{aligned} \quad (1.3)$$

In order to meet the condition of equivalence between the directions  $\mathbf{n}$  and  $-\mathbf{n}$  we must set  $d = 0$  in the expression for the free energy. Moreover, the presence of a pseudoscalar for a medium containing planes as a symmetry element implies that the coefficients of these terms must be pseudo-scalars since the free energy is a true scalar. Therefore, on reflection from such a plane we will have  $c = -c$ . Hence, we are left with the relation

$$F_d = F - F_0 = \frac{1}{2} K_1 (\operatorname{div} \mathbf{n})^2 + \frac{1}{2} K_2 (\mathbf{n} \cdot \mathbf{curl} \mathbf{n})^2 + \frac{1}{2} K_3 (\mathbf{n} \times \mathbf{curl} \mathbf{n})^2, \quad (1.4)$$

where the last term can be also written as  $\frac{1}{2} K_3 [(\mathbf{n} \cdot \nabla) \mathbf{n}]^2$  by virtue of the relation  $\mathbf{n} \times \mathbf{curl} \mathbf{n} = \Delta \mathbf{n}^2 - (\mathbf{n} \cdot \nabla) \mathbf{n}$ , since  $\mathbf{n}^2 \equiv 1$ .

In chiral nematics there is no center of inversion among their symmetry elements, unlike nematics. The free energy density for a liquid crystal with an absence of a center of symmetry, where the directions  $\mathbf{n}$  and  $-\mathbf{n}$  are equivalent, is [2]

$$F = F_0 + \frac{1}{2}K_1(\text{div}\mathbf{n})^2 + \frac{1}{2}K_2(\mathbf{n} \cdot \mathbf{curl}\mathbf{n} + q_0)^2 + \frac{1}{2}K_3(\mathbf{n} \times \mathbf{curl}\mathbf{n})^2. \quad (1.5)$$

The inclusion of the pseudo-scalar  $\mathbf{n} \cdot \mathbf{curl}\mathbf{n}$  causes a fundamental change in the equilibrium state of the medium, such that it is no longer uniform in space, as in nematics. The equilibrium state for a chiral nematic liquid crystal corresponds to a distribution of directions for  $\mathbf{n}$  such that the free energy (1.5) attains its minimum value of zero. Hence we obtain the equations  $\text{div}\mathbf{n} = 0$ ,  $\mathbf{n} \cdot \mathbf{curl}\mathbf{n} = -q_0$  and  $\mathbf{n} \times \mathbf{curl}\mathbf{n} = \mathbf{0}$ , with solution  $n_x = \cos(q_0z)$ ,  $n_y = \sin(q_0z)$  and  $n_z = 0$ .

The orientational symmetry of a chiral nematic liquid crystal is periodic in one direction in space (z-axis) so that the correlation function can be written as  $\rho_{1,2} = \rho_{1,2}(z, \mathbf{r}_{12})$ . The vector  $\mathbf{n}$  acquires its original value after a step of length  $2\pi/q_0$  along the z-axis. However, since the direction  $\mathbf{n}$  and  $-\mathbf{n}$  are equivalent the actual spatial period of the crystal is  $\pi/q_0$ . The above considerations are valid only if the period of the helicoidal structure is large in comparison with molecular dimensions. The condition is in fact satisfied since in most chiral nematic liquid crystals  $\pi/q_0 \sim 10^{-7}$  m.

In order to determine the static deformations for nematics we start from the general thermodynamic condition of equilibrium: minimization of the functional  $\int FdV$  subject to the auxiliary condition  $\mathbf{n}^2 = 1$ . Using the method

of undetermined Lagrange coefficients, we equate to zero the variation

$$\begin{aligned} \delta \int \left\{ F - \frac{1}{2} \lambda(\mathbf{r}) \mathbf{n}^2 \right\} dV &= \int \left\{ \frac{\partial F}{\partial n_i} \delta n_i + \frac{\partial F}{\partial (\partial_k n_i)} \partial_k \delta n_i - \lambda(\mathbf{r}) n_i \delta n_i \right\} dV = \\ &= \int \left\{ \frac{\partial F}{\partial n_i} - \partial_k \frac{\partial F}{\partial (\partial_k n_i)} - \lambda(\mathbf{r}) n_i \right\} \delta n_i dV + \oint \frac{\partial F}{\partial (\partial_k n_i)} dn_i df_k, \end{aligned} \quad (1.6)$$

where in the last step we have applied integration by parts resulting in a surface integral (boundary term). Setting  $\delta \mathbf{n} = \mathbf{0}$  at the boundaries, we have

$$\int (\mathbf{H} + \lambda \mathbf{n}) \cdot \delta \mathbf{n} dV = 0, \quad (1.7)$$

with  $H_i = \partial_k \Pi_{ik} - (\partial F)/(\partial n_i)$  and  $\Pi_{ik} = \partial F/\partial (\partial_k n_i)$ . The vector  $\mathbf{H}$  is called the *molecular field*, and tends to “straighten out” the direction of  $\mathbf{n}$  [1]. Since the variation  $\delta \mathbf{n}$  is arbitrary the equilibrium equation is  $\mathbf{H} = -\lambda \mathbf{n}$  and by virtue of  $\mathbf{n}^2 = 1$  we obtain  $\lambda = -\mathbf{H} \cdot \mathbf{n}$ . Therefore, the equilibrium condition is written as  $\mathbf{h} \equiv \mathbf{H} - (\mathbf{n} \cdot \mathbf{H}) \mathbf{n} = 0$ . Once more, by virtue of the unit modulus of the director, the vector  $\mathbf{h}$  is perpendicular to  $\mathbf{n}$ . If a nematic is in equilibrium such that  $\mathbf{h} = \mathbf{0}$ , and moves as a whole with a constant spatial velocity, then the equation for the director expresses the fact that each liquid crystal particle moves in space with its own fixed  $\mathbf{n}$ . This is expressed by the equation

$$\frac{d\mathbf{n}}{dt} = \frac{\partial \mathbf{n}}{\partial t} + (\mathbf{v} \cdot \nabla) \mathbf{n} = 0. \quad (1.8)$$

Outside of equilibrium, the right handside of the above equation will contain terms than depend on the transverse part of the molecular field,  $\mathbf{h}$  and the spatial derivatives of the body, forming a tensor-in the first non-vanishing

hydrodynamic approximation-that can be divided into symmetric and anti-symmetric parts,  $v_{ik}$  and  $\Omega_{ik}$  respectively. The general form for the equation of motion of the director is [3]

$$\frac{dn_i}{dt} = \Omega_{ik}n_k + \lambda(\delta_{il} - n_in_l)n_kv_{kl} + h_i/\gamma \quad (1.9)$$

Contraction of the right handside of the above with  $n_i$  yields  $\Omega_{ki}n_kn_i + \lambda(n_l n_k v_{kl} - n_i n_i n_l n_k v_{kl}) + n_i h_i/\gamma = 0$ , since  $n_i h_i = 0$ ,  $n_i n_i = 1$ , and a contraction of a symmetric and an antisymmetric tensor yields zero. Hence, the above form is justified, since  $\mathbf{n}^2 = 1 \Rightarrow \mathbf{n} \cdot (\partial \mathbf{n} / \partial t) = 0$ . In the above, we define  $v_{ik} = \frac{1}{2}(\partial_i v_k + \partial_k v_i)$  and  $\Omega_{ik} = \frac{1}{2}(\partial_i v_k - \partial_k v_i)$ . In (1.9) the last term represents the relaxation of the director towards equilibrium under the action of the molecular field, the middle term the orienting effect of the velocity gradient of the director, and the first term the rotation of the director under uniform rotation of the nematic as a whole. All coefficients featuring are kinetic (the coefficient  $\gamma$  has dimensions of viscosity).

The equation for the time derivative of the velocity reads

$$\rho \left[ \frac{\partial v_i}{\partial t} + (\mathbf{v} \cdot \nabla) v_i \right] = \partial_k \sigma_{ik}. \quad (1.10)$$

In order to establish the form of the stress tensor, we invoke the energy conservation law in hydrodynamics, written as

$$\frac{\partial}{\partial t} \left( \frac{1}{2} \rho \mathbf{v}^2 + E \right) + \text{div} \mathbf{Q} = 0, \quad (1.11)$$

where  $E$  is the internal energy density and  $\mathbf{Q}$  is the energy flux density. The former can be written as  $E = E_0(\rho, S) + E_d$ , where  $E_0(\rho, S)$  pertains to the

undeformed homogeneous medium and  $E_d$  is attributed to the distortion of the field  $\mathbf{n}(\mathbf{r})$ . By using the thermodynamic relations

$$\left(\frac{\partial E}{\partial S}\right)_{\rho, \mathbf{n}} = T, \quad \left(\frac{\partial E}{\partial \rho}\right)_{S, \mathbf{n}} = \mu$$

with  $\mu$  being the chemical potential, we can expand the time derivative using the chain rule, as follows

$$\begin{aligned} & \frac{\partial}{\partial t} \left( \frac{1}{2} \rho \mathbf{v}^2 + E \right) \\ &= \frac{1}{2} v^2 \frac{\partial \rho}{\partial t} + \rho \mathbf{v} \frac{\partial \mathbf{v}}{\partial t} + \left( \frac{\partial E}{\partial \rho} \right)_{S, \mathbf{n}} \frac{\partial \rho}{\partial t} + \left( \frac{\partial E}{\partial S} \right)_{\rho, \mathbf{n}} \frac{\partial S}{\partial t} + \left( \frac{\partial E_d}{\partial t} \right)_{\rho, S} \\ &= \frac{1}{2} v^2 \frac{\partial \rho}{\partial t} + \rho \mathbf{v} \frac{\partial \mathbf{v}}{\partial t} + \mu \frac{\partial \rho}{\partial t} + T \frac{\partial S}{\partial t} + \left( \frac{\partial E_d}{\partial t} \right)_{\rho, S}. \end{aligned} \quad (1.12)$$

The last term can be recast in the following form

$$\begin{aligned} & \left( \frac{\partial E_d}{\partial t} \right)_{\rho, S} \\ &= \left( \frac{\partial E_d}{\partial n_i} \right)_{\rho, S} \frac{\partial n_i}{\partial t} + \left( \frac{\partial E_d}{\partial (\partial_k n_i)} \right)_{\rho, S} \partial_k \frac{\partial n_i}{\partial t} = \left( \frac{\partial E_d}{\partial n_i} \right)_{\rho, S} \frac{\partial n_i}{\partial t} + \Pi_{ki} \partial_k \frac{\partial n_i}{\partial t} \\ &= \left( \frac{\partial E_d}{\partial n_i} - \partial_k \Pi_{ki} \right) \frac{\partial n_i}{\partial t} + \partial_k \left( \Pi_{ki} \frac{\partial n_i}{\partial t} \right) = -\mathbf{h} \cdot \frac{\partial \mathbf{n}}{\partial t} + \partial_k \left( \Pi_{ki} \frac{\partial n_i}{\partial t} \right), \end{aligned} \quad (1.13)$$

where we have written  $\mathbf{h}$  instead of  $\mathbf{H}$  since  $\mathbf{n} \cdot (\partial \mathbf{n} / \partial t) = 0$ . Since

$$\frac{\partial \mathbf{n}}{\partial t} = \frac{d\mathbf{n}}{dt} - (\mathbf{v} \cdot \text{div}) \mathbf{n}$$

we write

$$\left( \frac{\partial E_d}{\partial t} \right)_{\rho, S} = h_i (v_k \partial_k n_i + \Omega_{ik} - \lambda v_{ik} n_k) - N_k h_k + \partial_k \left( \Pi_{ki} \frac{\partial n_i}{\partial t} \right), \quad (1.14)$$

where the last term is a total divergence. We now note that

$$\begin{aligned} v_{ik}n_k h_i &= \frac{1}{2}(\partial_i v_k + \partial_k v_i)n_k h_i = \frac{1}{2}(\partial_k v_i)(n_k h_i + n_i h_k) \\ &= \frac{1}{2}\{\partial_k[v_i(n_k h_i + n_i h_k)]\} - \frac{1}{2}v_i \partial_k(n_k h_i + n_i h_k) \end{aligned} \quad (1.15)$$

and that

$$\begin{aligned} \Omega_{ik}n_k h_i &= \frac{1}{2}(\partial_i v_k - \partial_k v_i)n_k h_i = -\frac{1}{2}(\partial_k v_i)(n_k h_i - n_i h_k) \\ &= -\frac{1}{2}\{\partial_k[v_i(n_k h_i - n_i h_k)]\} + \frac{1}{2}v_i \partial_k(n_k h_i - n_i h_k), \end{aligned} \quad (1.16)$$

so that we can write

$$\begin{aligned} \left(\frac{\partial E_d}{\partial t}\right)_{\rho,S} &= -G_i v_i - \frac{h^2}{\gamma} \\ &+ \partial_k \left( \Pi_{ki} \frac{\partial n_i}{\partial t} - \frac{1}{2}v_i(n_k h_i - n_i h_k) + \frac{\lambda}{2}v_i(n_k h_i + n_i h_k) \right), \end{aligned} \quad (1.17)$$

with

$$G_i = -h_k \partial_i n_k + \frac{1}{2}\partial_k(n_i h_k - n_k h_i) - \frac{\lambda}{2}\partial_k(n_i h_k + n_k h_i). \quad (1.18)$$

In a similar fashion to the partial time derivative considered above we have

$$\begin{aligned} (\partial_i E_d)_{\rho,S} &= \left(\frac{\partial E_d}{\partial n_k}\right)_{\rho,S} \partial_i n_k + \left(\frac{\partial E_d}{\partial(\partial_l n_k)}\right)_{\rho,S} \partial_i(\partial_l n_k) \\ &= \left(\frac{\partial E_d}{\partial n_k}\right)_{\rho,S} \partial_i n_k + \left(\frac{\partial E_d}{\partial(\partial_l n_k)}\right)_{\rho,S} \partial_l(\partial_i n_k) \\ &= \left(\frac{\partial E_d}{\partial n_k} - \partial_l \Pi_{lk}\right) \partial_i n_k + \partial_l(\Pi_{lk} \partial_i n_k) = -\mathbf{h} \cdot \partial_i \mathbf{n} + \partial_l(\Pi_{lk} \partial_i n_k) \\ &= -\mathbf{h} \cdot \partial_i \mathbf{n} + \partial_k(\Pi_{kl} \partial_i n_l), \end{aligned} \quad (1.19)$$

where we have interchanged the order of differentiation and we have replaced once more  $\mathbf{H}$  by  $\mathbf{h}$  since  $\mathbf{n}\partial_i\mathbf{n} = 0$ . The first term of  $G_i$ , then, can be recast in the form

$$-h_k\partial_i n_k = (\partial_i E_d)_{\rho,S} - \partial_k(\Pi_{kl}\partial_i n_l), \quad (1.20)$$

so that we can write

$$G_i = \partial_k\sigma_{ik}^{(r)} + (\partial_i E_d)_{\rho,S}, \quad (1.21)$$

where

$$\sigma_{ik}^{(r)} = -\Pi_{kl}\partial_i n_l + \frac{1}{2}(n_i h_k - n_k h_i) - \frac{\lambda}{2}(n_i h_k + n_k h_i). \quad (1.22)$$

As noted in [1], the definition of the tensor  $\sigma_{ik}^{(r)}$  is not unique, since the tensor  $\sigma'_{ik} = \sigma_{ik}^{(r)} + \partial_l\chi_{ilk}$  with  $\chi_{ilk} = -\chi_{ikl}$  would produce the same vector  $G_i$ , as the order of differentiation  $\partial_k\partial_l$  with respect to the indices  $k, l$  can be interchanged and the tensor  $\hat{\chi}$  is antisymmetric in  $k$  and  $l$  (the contraction of a symmetric and an antisymmetric tensor over a pair of indices is zero). The choice of the tensor  $\chi_{ikl}$  is arbitrary and will be of use when symmetrizing  $\sigma_{ik}^{(r)}$ . Assuming that the latter has been symmetrized we can write

$$(\partial_k\sigma_{(ik)}^{(r)})v_i = \partial_k(\sigma_{(ik)}^{(r)}v_i) - \sigma_{(ik)}^{(r)}(1/2)(\partial_i v_k + \partial_k v_i) = \partial_k(\sigma_{(ik)}^{(r)}v_i) - \sigma_{(ik)}^{(r)}v_{ik}$$

so that

$$\begin{aligned} \left(\frac{\partial E_d}{\partial t}\right)_{\rho,S} &= -N_i v_i + \sigma_{(ik)}^{(r)} v_{ik} - (\partial_i E)_{\rho,S} v_i \\ &+ \partial_k \left( \Pi_{ki} \frac{\partial n_i}{\partial t} - \frac{1}{2} v_i (n_k h_i - n_i h_k) + \frac{1}{2} v_i (n_k h_i - n_i h_k) + \sigma_{(ik)}^{(r)} v_i \right). \end{aligned} \quad (1.23)$$

We write the third term as

$$\begin{aligned} -(\partial_i E)_{\rho,S} v_i &= -v_i \partial_i E + \mu v_i \partial_i \rho + v_i T \partial_i S = (-v_i \partial_k E + \mu v_i \partial_k \rho + v_i T \partial_k S) \delta_{ik} \\ &= -\partial_k (E v_i \delta_{ik}) + E v_{ik} \delta_{ik} + \mu \partial_i (\rho v_i) - \mu \rho v_{ik} \delta_{ik} + T \partial_i (S v_i) - T S v_{ik} \delta_{ik}. \end{aligned} \quad (1.24)$$

We now return to (1.12) and substitute expressions (1.10), (1.23) as well as the mass and entropy continuity equations  $\partial \rho / \partial t = -\text{div}(\rho \mathbf{v})$  and  $\partial S / \partial t = -\text{div}(S \mathbf{v})$ , respectively. In the presence of dissipative processes, the latter is written

$$\partial S / \partial t = -\text{div}(S \mathbf{v} + \mathbf{q} / T) - 2R / T, \quad (1.25)$$

where  $\mathbf{q}$  is the heat flux density and  $R$  is the mechanical energy dissipation rate due to frictional forces. We then notice that

$$\begin{aligned} T \partial_i (S v_i) &= 2R - T \frac{\partial S}{\partial t} - T \partial_i \left( \frac{q_i}{T} \right) = 2R - T \frac{\partial S}{\partial t} + \frac{q_i}{T} \partial_i T + \partial_i q_i \\ \mu \frac{\partial \rho}{\partial t} &= -\mu \partial_i (\rho v_i) \\ \rho v_i \frac{\partial v_i}{\partial t} &= v_i \partial_k \sigma_{ik} - \rho v_i v_k \partial_k v_i \\ \frac{1}{2} v^2 \frac{\partial \rho}{\partial t} &= -\frac{1}{2} v^2 \partial_i (\rho v_i) = -\frac{1}{2} \partial_i (v^2 \rho v_i) + \rho v_i v_k \partial_i v_k \\ &= -\frac{1}{2} \partial_i (v^2 \rho v_i) + \rho v_i v_k \partial_k v_i. \end{aligned} \quad (1.26)$$

Collecting terms, we obtain

$$\frac{\partial}{\partial t} \left( \frac{1}{2} \rho \mathbf{v}^2 + E \right) = (\sigma_{(ik)}^{(r)} - p\delta_{ik} - \sigma_{ik})v_{ik} - N_i h_i + \frac{q_i}{T} \partial_i T + \partial_i(-Q_i), \quad (1.27)$$

where  $p = \rho\mu + TS - E = \Phi + TS - E$  is the pressure ( $\Phi$  is the Gibbs free energy) and  $\mathbf{Q}$  is the energy flux density. The components of this vector will be fully determined after having symmetrized  $\sigma_{ik}^{(r)}$ , as assumed throughout in our derivations. In order to calculate explicitly the antisymmetrical part of this tensor we use the fact that

$$B_{ik} = \frac{\partial E_d}{\partial n_i} + \Pi_{li} \partial_l n_k - \Pi_{kl} \partial_i n_l \quad (1.28)$$

is symmetric in the suffixes  $i$  and  $k$ . We will prove this indirectly as follows. Let us consider an infinitesimal rotation of the co-ordinates through an angle  $\delta\phi$ . The change in the director then is  $\delta n_i = \epsilon_{ijk} \delta\phi_j n_k = a_{ik} n_k$ , where  $\epsilon_{ijk}$  is the completely antisymmetric tensor, and  $a_{ik}$  is an antisymmetric tensor (in the suffixes  $i$  and  $k$ ), as a result of contraction of  $\epsilon_{ijk}$ . The change in the tensor  $\partial_k n_i$  is  $\delta(\partial_k n_i) = \delta(\partial_k) n_i + \partial_k(\delta n_i) = a_{kl} \partial_l n_i + a_{il} \partial_k n_l$ . The quantity  $E_d$  is a scalar, hence invariant under the infinitesimal arbitrary rotation.

$$\begin{aligned} \delta E_d &= \frac{\partial E_d}{\partial n_i} \delta n_i + \Pi_{ki} \delta(\partial_k n_i) = \frac{\partial E_d}{\partial n_i} a_{ik} n_k + \Pi_{ki} (a_{kl} \partial_l n_i + a_{il} \partial_k n_l) \\ &= \frac{\partial E_d}{\partial n_i} a_{ik} n_k + \Pi_{li} a_{ik} \partial_l n_k + \Pi_{kl} a_{ki} \partial_i n_l = a_{ik} B_{ik} = 0. \end{aligned} \quad (1.29)$$

In view of the arbitrariness of  $a_{ik}$  we infer that the non-zero tensor  $B_{ik}$  must indeed be symmetric. The tensor  $\sigma_{ik}^{(rn)} = \sigma_{ik}^{(r)} - (\lambda/2)(n_i h_k + n_k h_i)$  can be written as

$$\begin{aligned}
\sigma_{ik}^{(rn)} &= -\Pi_{kl}\partial_i n_l + \frac{1}{2}(n_i h_k - n_k h_i) \\
&= -\Pi_{kl}\partial_i n_l + \frac{\partial F}{\partial n_i} n_k + n_i \partial_l (\Pi_{lk}) - n_k \partial_l (\Pi_{li}) \\
&= \frac{\partial E_d}{\partial n_i} n_k + \partial_l (n_i \Pi_{lk} - n_k \Pi_{li}) + \Pi_{li} \partial_l n_k - \Pi_{kl} \partial_i n_l = B_{ik} - \Pi_{kl} \partial_i n_l
\end{aligned} \tag{1.30}$$

In the above we have used the theorem of small increments. As known from thermodynamics, knowledge of one of the thermodynamic potentials: internal energy  $E$ , Helmholtz free energy  $F$ , Gibbs free energy  $\Phi$  and the heat function  $W$ , is sufficient to determine the other variables, provided that the above are expressed as functions of  $S$  and  $V$ ,  $V$  and  $T$ ,  $P$  and  $T$ ,  $S$  and  $P$  respectively. If there are small parameters  $\zeta_i$  that determine a state of the system apart from its volume, the expression for the differential of the internal energy must involve terms proportional to the differentials  $d\zeta_i$  as below [4]

$$dE = TdS - PdV + \sum_i Z_i \zeta_i,$$

where  $M_i$  are the conjugate variables, functions of the state of the body. Since the transformation of the other thermodynamic potentials does not affect the parameters  $\zeta_i$ , similar terms will be added to the other potentials, therefore

$$dF = -SdT - PdV + \sum_i Z_i \zeta_i.$$

We conclude that  $E_d$  is the same as  $F_d$ , except that the elastic moduli  $K_{1-3}$  are expressed in terms of the density and entropy, instead of the temperature.

Based on (1.30), the antisymmetric part of  $\sigma_{ik}^{(r)}$  can be written as a divergence

$$\sigma_{ik}^{(r)} - \sigma_{ki}^{(r)} = 2\partial_l \phi_{ikl},$$

where  $\phi_{ikl} = (1/2)(n_i \Pi_{lk} - n_k \Pi_{li})$  is a tensor antisymmetric under exchange of the first pair of suffixes. From this result follows that the moment of forces over the whole volume of the body

$$M_{ik} = \oint (\sigma_{il}^{(r)} x_k - \sigma_{kl}^{(r)} x_i) df_l + \int (\sigma_{ki}^{(r)} - \sigma_{ik}^{(r)}) dV$$

is represented as an integral over the surface alone, since by virtue of Gauss's theorem the last term in the above can be written as

$$\int (\sigma_{ki}^{(r)} - \sigma_{ik}^{(r)}) dV = 2 \int \partial_l \phi_{ikl} dV = 2 \oint \phi_{ikl} df_l$$

The definition relation of the force components  $F_i = \partial_k \sigma_{ik}$  implies that the definition of  $\sigma_{ik}$  is not unique, since any other tensor of the form  $\bar{\sigma}_{ik} = \sigma_{ik} + \partial_l \chi_{ikl}$  with  $\chi_{ikl} = -\chi_{ilk}$  would produce the same component  $F_i$  (since we can interchange the order of differentiation). Selecting  $\chi_{ikl} = \phi_{kli} + \phi_{ilk} - \phi_{ikl}$  we can produce the symmetric tensor  $\chi_{ikl}^s = (1/2)(\phi_{kli} + \phi_{ilk} + \phi_{ikl} + \phi_{ilk} + \phi_{kli} - \phi_{kil}) = \phi_{kli} + \phi_{ilk}$ . Hence, the required symmetrical tensor  $\sigma_{(ik)}^{(r)}$  is produced by the unsymmetrical  $\sigma_{ik}^{(r)}$  as below

$$\begin{aligned} \sigma_{(ik)}^{(r)} &= \frac{1}{2}(\sigma_{ik}^{(r)} + \sigma_{ki}^{(r)}) + \partial_l (\phi_{kli} + \phi_{ilk}) = -\frac{\lambda}{2}(n_i h_k + n_k h_i) \\ &\quad - \frac{1}{2}(\Pi_{kl} \partial_i n_l - \Pi_{il} \partial_k n_l) - \frac{1}{2} \partial_l [(\Pi_{ik} + \Pi_{ki}) n_l - \Pi_{kl} n_i - \Pi_{il} n_k]. \end{aligned} \quad (1.31)$$

Comparing (1.27) with the energy conservation law

$$\frac{\partial}{\partial t} \left( \frac{1}{2} \rho v^2 + E \right) + \operatorname{div} \mathbf{Q} = 0$$

we identify the following terms [1]

$$\begin{aligned} 2R &= \sigma'_{ik} v_{ik} + N_i h_i - \frac{1}{T} q_i \partial_i T \\ Q_i &= \left( W + \frac{1}{2} v^2 \right) v_i - \Pi_{ik} [-v_l \partial_l n_k + \Omega_{li} n_l + \lambda n_l (v_{kl} - n_k n_m v_{lm})] \\ &\quad + \frac{1}{2} (n_i h_k - n_k h_i) + \frac{\lambda}{2} (n_i h_k + n_k h_i) - \sigma'_{ik} v_k - \kappa_{ik} \partial_k T, \end{aligned} \quad (1.32)$$

where  $\sigma'_{ik} = \sigma_{(ik)}^{(r)} - p\delta_{ik} - \sigma_{ik}$  is the viscous part of the stress tensor,  $q_i = -\kappa_{ik} \partial_k T$  with  $\kappa_{ik}$  being the thermal conductivity tensor and  $W = p + E$  is the heat function. The first equation in (1.32) determines the entropy increase due to dissipative processes (equal to the rate of dissipation of mechanical energy). The last term relates to the increase of total entropy of the nematic by irreversible processes of heat conduction. Also, the coefficient  $\lambda$  does not feature in this relation since the corresponding term quantifies a transport phenomenon not of a dissipative nature. The force density for a nematic medium in motion is

$$F_i = -\partial_i p + \partial_k \sigma_{(ik)}^{(r)} + \partial_k \sigma'_{ik} \equiv \partial_i p + F_i^{(r)} + F'_i. \quad (1.33)$$

If a medium is at rest in equilibrium, even if deformed,  $\mathbf{F} = \mathbf{F}' = 0$  and  $\mathbf{h} = 0$ . In that case  $G_i = 0$  therefore  $F_i^{(r)} = -(\partial_i E_d)_{\rho, S}$  and  $F_i = \partial_i p - (\partial_i E_d)_{\rho, S} = -\partial_i (p + E_d) = 0$ , on the assumption that the elastic moduli are constant, independent of  $\rho$  and  $S$ . From the thermodynamical definition of pressure we have  $\partial_i p = \mu \partial_i \rho + \rho \partial_i \mu - \partial_i E + S \partial_i T + T \partial_i S$  and from the familiar

relation  $dE = TdS + \mu d\rho + (dE_d)_{\rho,S}$ ,  $\partial_i E = T\partial_i S + \mu\partial_i \rho + (\partial_i E_d)_{\rho,S}$  we find  $F_i = -\partial_i p - (\partial_i E_d)_{\rho,S} = -\rho\partial_i \mu - S\partial_i T$ . Hence, if  $T = \text{constant}$ , the presence of equilibrium requires  $\mu = \text{constant}$ .

If one considers a closed system whose state is described by the variables  $x_a$ ,  $a = 1, 2, \dots, N$ . Their equilibrium values are determined by the condition that the entropy of the system is a maximum in statistical equilibrium. The relevant conditions are  $X_a = -\partial S/\partial x_a = 0$ . If the system is in a state near to equilibrium,  $x_a$  differ only slightly from their equilibrium values and  $X_a$  are small. Processes occur that tend to restore equilibrium, hence  $x_a$  will be functions of time, with their rate of change being  $\dot{x}_a = -\sum_b \gamma_{ab} X_b$ . Onsager's principle states that the coefficients  $\gamma_{ab}$  (called kinetic coefficients) are symmetric under the exchange of the suffixes  $a$  and  $b$ . The rate of change of entropy is  $\dot{S} = \sum_a (\partial S/\partial x_a) \dot{x}_a = -\sum_a X_a \dot{x}_a = \sum_{a,b} \gamma_{ab} X_a X_b$ . Considering now deformations in nematic liquid crystals, in a weak departure from equilibrium, under the usual hydrodynamic approximation,  $\sigma'_{ik}$  is a linear function of  $v_{ik}$  ([5], [1]). The general form of such a linear dependence is

$$\sigma'_{ik} = \eta_{iklm} v_{lm}.$$

From the symmetry properties of the tensors  $\sigma'_{ik}$  and  $v_{ik}$ , as well as from the symmetry of the kinetic coefficients (here  $2R/T$  is the rate of change of entropy,  $\dot{x}_a$  are taken to be the components of  $\sigma'_{ik}$ , hence the corresponding conjugate variables  $X_a$  are identified with the components of the tensor  $-v_{lm}/T$ ) we obtain

$$\eta_{iklm} = \eta_{kilm} = \eta_{ikml} = \eta_{lmik}.$$

The rank-four tensor  $\eta_{iklm}$  (called the viscosity tensor) is constructed only from the unit tensor  $\delta_{ik}$  and the molecular director. The five independent linear combinations of that kind are

$$\begin{aligned} n_i n_k n_l n_m, \quad n_i n_k \delta_{lm} + n_l n_m \delta_{ik}, \quad n_i n_l \delta_{km} + n_k n_l \delta_{im} + n_i n_m \delta_{kl} + n_k n_m \delta_{il}, \\ \delta_{ik} \delta_{lm}, \quad \delta_{il} \delta_{km} + \delta_{kl} \delta_{im}. \end{aligned} \tag{1.34}$$

Hence, the viscosity tensor will comprise of five independent terms. In the following expression the above terms feature in reverse order so that the stress tensor can be written as

$$\begin{aligned} \sigma'_{ik} = \eta_1 2v_{ik} + (\eta_2 - \eta_1) \delta_{ik} v_{ll} + (\eta_4 + \eta_1 - \eta_2) (\delta_{ik} n_l n_m v_{lm} + n_i n_k v_{ll}) \\ + (\eta_3 - 2\eta_1) (n_i n_l v_{kl} + n_k n_l v_{il}) + (\eta_5 + \eta_1 + \eta_2 - 2\eta_3 - 2\eta_4) n_i n_k n_l n_m v_{lm}. \end{aligned} \tag{1.35}$$

The dissipative coefficients are presented here in a different form to the original given by Leslie (1966) and Parodi (1970). Selecting the  $z$ -axis to be parallel to the molecular director, we can write the dissipative function as

$$\begin{aligned} 2R = 2\eta_1 \left( v_{\alpha\beta} - \frac{1}{2} \delta_{\alpha\beta} v_{\gamma\gamma} \right)^2 + \eta_2 v_{\alpha\alpha}^2 \\ + 2\eta_3 v_{\alpha z}^2 + 2\eta_4 v_{zz} v_{\alpha\alpha} + \eta_5 v_{zz}^2 + \frac{1}{T} [\kappa_{\parallel} (\partial_z T)^2 + \kappa_{\perp} (\partial_{\alpha} T)^2] + \frac{h^2}{\gamma}, \end{aligned} \tag{1.36}$$

where  $\kappa_{ik} = \text{diag}(\kappa_{\perp}, \kappa_{\perp}, \kappa_{\parallel})$ ,  $\alpha, \beta, \gamma = 1, 2$  for the  $x$  and  $y$  components, respectively. Since the rate of change of entropy must be always positive  $\eta_{(1,2,3,5)} > 0$ ,  $\kappa_{(\perp, \parallel)} > 0$ ,  $\gamma > 0$  and the discriminant in the trinomial  $\eta_2 v_{\alpha\alpha}^2 + 2\eta_4 v_{zz} v_{\alpha\alpha} + \eta_5 v_{zz}^2$ , where  $v_{\alpha\alpha}$  is considered as a variable and  $v_{zz}$  as a parameter,

or the reverse. Hence the condition  $\eta_2\eta_5 > \eta_4^2$  must also be upheld. Similar conditions are derived in [6] The number of viscosity coefficients may be reduced if we regard the flow as incompressible, in which case  $\text{div}(\mathbf{v}) = v_{ll} = 0$ . Then the second term in the expression (1.35) for the stress tensor vanishes. In the third term of the same expression, the first summand does not contribute to dissipation since  $\delta_{ik}n_l n_m v_{lm} v_{ik} = n_l n_m v_{lm} v_{ii} = 0$ . The same applies for the term  $-p\delta_{ik}$  featuring in the complete stress tensor  $\sigma_{ik}$  and resulting in the redefinition of the pressure regarded as an unknown function of co-ordinates and time and not as a thermodynamic variable linked to others through a state equation [1]. The viscous stress tensor for an incompressible nematic fluid is the simplified as below

$$\sigma'_{ik} = 2\eta_1 v_{ik} + (\eta_3 - 2\eta_1)(n_i n_l v_{kl} + n_k n_l v_{il}) + (\bar{\eta}_3 + \eta_1 + \eta_2 - 2\eta_3)n_i n_k n_l n_m v_{lm}, \quad (1.37)$$

containing three independent viscosity coefficients (we have defined  $\bar{\eta}_3 = \eta_2 + \eta_5 - 2\eta_4$ ). The dissipative function is now written as

$$\begin{aligned} 2R &= 2\eta_1 \left( v_{\alpha\beta} - \frac{1}{2}\delta_{\alpha\beta} v_{\gamma\gamma} \right)^2 + (\eta_2 + \eta_5 - 2\eta_4) v_{\alpha\alpha}^2 \\ &\quad + 2\eta_3 v_{az}^2 + \frac{1}{T} [\kappa_{\parallel} (\partial_z T)^2 + \kappa_{\perp} (\partial_{\alpha} T)^2] + \frac{h^2}{\gamma} \\ &= 2\eta_1 \left( v_{\alpha\beta} - \frac{1}{2}\delta_{\alpha\beta} v_{\gamma\gamma} \right)^2 + \bar{\eta}_3 v_{\alpha\alpha}^2 \\ &\quad + 2\eta_3 v_{az}^2 + \frac{1}{T} [\kappa_{\parallel} (\partial_z T)^2 + \kappa_{\perp} (\partial_{\alpha} T)^2] + \frac{h^2}{\gamma}, \end{aligned} \quad (1.38)$$

since  $v_{\alpha\alpha} + v_{zz} = 0$ .

## 1.2 Chiral nematics

As we mentioned earlier, chiral nematic liquid crystals do not have a centre of inversion among their symmetry elements. The fact that no use of the presence of a centre of inversion was made in deriving the equations of motion and equilibrium for ordinary nematics, means that the general equations are also valid for chiral nematics. However, there are a number of differences since the free energy  $F_d$  contains a term linear in the derivatives (the pseudo-scalar  $\mathbf{n} \text{curl} \mathbf{n}$ ). The molecular field  $\mathbf{h}$  must be redefined and there is now a difference between the isothermal and adiabatic values of the modulus  $K_2$ . In what follows we consider the adiabatic elastic moduli as definite functions of  $\rho$  and  $S$ . Finally, there is a substantial change in the hydrodynamic equations for chiral nematics, when compared to those of nematics, in that further terms feature in the dissipative part of the equations as follows

$$\begin{aligned}
 \sigma'_{ik} &= (\sigma'_{ik})_{\text{nematic}} + \mu_1 (n_i \epsilon_{klm} + n_k \epsilon_{ilm}) n_m \partial_l T, \\
 N_i &= (N_i)_{\text{nematic}} + \nu_1 \epsilon_{ikl} n_k \partial_l T, \\
 q_l &= (q_l)_{\text{nematic}} + \nu_2 \epsilon_{lki} n_k h_i + \mu_2 (\epsilon_{lmi} n_k + \epsilon_{lmk} n_i) n_m v_{ik}.
 \end{aligned}
 \tag{1.39}$$

These terms were first introduced by Leslie [7] in an attempt to explain the Lehmann effect (rotation of the chiral nematic structure as a consequence of heat flow). The presence of the completely antisymmetric tensor creates a pseudo-tensor and pseudo-vectors, removing the symmetry under spatial inversion. Terms that are true tensors or vectors (like  $n_i \partial_k T + n_k \partial_i T$ ) are precluded by virtue of the invariance under a change in the sign of  $\mathbf{n}$ . Similarly, a term proportional to  $\partial_i T$  in  $N_i$  is impossible because it is invariant

under the change in the sign of  $\mathbf{n}$  whereas  $dn_i/dt$  and hence  $N_i$  would have to change sign. The coefficients in (1.39) are connected by relations derived by Osanger's principle. As before,  $\dot{S} = 2R/T$  and we identify  $\dot{x}_a$  with the quantities  $\sigma'_{ik}$ ,  $q_i$  and  $N_i$ . Then, the conjugate variables are the quantities  $-v_{ik}/T$ ,  $\partial_l T/T^2$  and  $-h_i/T$  respectively. As seen from their positions in (1.9), (1.10) and (1.25), the quantities  $\sigma'_{ik}$  are even and the quantities  $q_i$  and  $N_i$  are odd under time reversal. If two thermodynamic variables  $x_a$  and  $x_b$  have the same (opposite) parity under time reversal then the corresponding kinetic coefficients are symmetric (antisymmetric) under exchange of the indices  $a$  and  $b$ . Odd parity under time reversal signifies an odd correlation function. Expanding the expression  $\dot{x}_a = -\sum_b \gamma_{ab} X_b$  we have

$$\begin{pmatrix} \sigma'_{ik} \\ q_i \\ N_i \end{pmatrix} = - \begin{pmatrix} \gamma_{11} & \gamma_{12} & \gamma_{13} \\ \gamma_{21} & \gamma_{22} & \gamma_{23} \\ \gamma_{31} & \gamma_{32} & \gamma_{33} \end{pmatrix} \begin{pmatrix} -\frac{v_{ik}}{T} \\ \frac{\partial_l T}{T^2} \\ -\frac{h_i}{T} \end{pmatrix}, \quad (1.40)$$

where according to the symmetry under time reversal  $\gamma_{12} = -\gamma_{21}$  and  $\gamma_{23} = \gamma_{32}$ . Comparing with (1.39) we have  $[\mu_2(\epsilon_{lmi}n_k + \epsilon_{lmk}n_i)n_m]T = [\mu_1(n_i\epsilon_{klm} + n_k\epsilon_{ilm})n_m]T^2 \Rightarrow \mu_2 = \mu_1 T$ , since  $\epsilon_{lmk} = \epsilon_{klm}$  and  $-\nu_2\epsilon_{lki}n_k T = \nu_1\epsilon_{ikl}n_k T^2 \Rightarrow \nu_2 = \nu_1 T$  since  $\epsilon_{lki} = -\epsilon_{ikl}$ . The final form of (1.39) consequently reads

$$\begin{aligned} \sigma'_{ik} &= (\sigma'_{ik})_{\text{nematic}} - \mu_1[n_i(\mathbf{n} \times \nabla T)_k + n_k(\mathbf{n} \times \nabla T)_i], \\ \mathbf{N} &= \mathbf{N}_{\text{nematic}} + \nu_1 \mathbf{n} \times \nabla T, \\ \mathbf{q} &= \mathbf{q}_{\text{nematic}} + \nu_1 T \mathbf{n} \times \mathbf{h} + 2\mu_1 T \mathbf{n} \times (v\mathbf{n}), \end{aligned} \quad (1.41)$$

where  $(v\mathbf{n})_i = v_{ik}n_k$ .

From the equations above we note the dependence of the stress tensor and the molecular field on the temperature gradient. This gradient (contained in the term of the form  $\mathbf{n} \times \nabla T$ ) gives rise to twisting moments acting on the director and on the mass of the liquid crystal (responsible for the Lehmann rotation). Conversely, the molecular field which accompanies a rotation of the director relative to the liquid alongside the liquid velocity gradients generate a heat flux.

Having determined the mechanical properties of nematic and chiral nematic liquid crystals under deformations, we will now proceed to study the optical properties of the resonators comprised of these structures in their equilibrium configurations.



# Bibliography

- [1] L. D. LANDAU AND E. M. LIFSHITZ, *Theory of Elasticity, Vol. 7*, ch. 6, Butterworth-Heinemann, Oxford, 1999.
- [2] F. C. FRANK, *I. Liquid crystals. On the theory of liquid crystals*, Discuss. Faraday Soc., **25**, pp. 19-28 (1958).
- [3] F. M. LESLIE, *Some constitutive equations for liquid crystals*, Arch. Rotation. Mech. An., **28**, pp.265-283 (1968).
- [4] L. D. LANDAU AND E. M. LIFSHITZ, *Statistical Physics, Vol. 5*, ch. 2, Butterworth-Heinemann, Oxford, 1999.
- [5] L. D. LANDAU AND E. M. LIFSHITZ, *Fluid Mechanics, Vol. 6*, ch. 6, Pergamon Press, Oxford, 1966.
- [6] D. FORSTER, T. C. LUBENSKY, P. C. MARTIN, J. SWIFT, AND P. S. PERSHAN, *Hydrodynamics of Liquid Crystals*, Phys. Rev. Lett.**26**, pp. 1016-1019 (1971).
- [7] F. M. LESLIE, *Some Thermal Effects in Cholesteric Liquid Crystals*, Proc. R. Soc. Lond. A, **307**, pp. 359-372 (1968).

# Chapter 2

## Optical properties of LC cells

In this chapter we will review the basic optical properties of nematics and chiral nematics with a particular emphasis on formulating boundary value problems. We will consider the viewpoints of various workers analysing optical problems in anisotropic media, and we will aim to demonstrate a convergence of their methods regarding the nature of optical feedback in these periodic media.

### 2.1 The Belyakov formulation

#### 2.1.1 Kinematical approximation and exact solution

The eigenwaves corresponding to light propagation along the helix axis are solutions of the wave equation

$$\frac{\partial^2 \mathbf{E}}{\partial z^2} = \frac{\bar{\bar{\epsilon}}(z)}{c^2} \frac{\partial^2 \mathbf{E}}{\partial t^2}. \quad (2.1)$$

The solutions of the above are sought not in the form of a plane wave, as in

a homogeneous medium, but in the form of a Bloch wave <sup>†</sup>

$$\mathbf{E}(z, t) = \sum_s \mathbf{E}_s \exp[i(K + s\tau)z - i\omega t]$$

In the general case of a medium with one dimensional periodicity, an infinite number of amplitudes  $\mathbf{E}_s$  are non zero. In a chiral nematic medium the dielectric tensor assumes the form

$$\bar{\bar{\epsilon}}(z) = \begin{pmatrix} \bar{\epsilon}[1 + \delta \cos(\tau z)] & \pm \bar{\epsilon} \delta \sin(\tau z) & 0 \\ \pm \bar{\epsilon} \delta \sin(\tau z) & \bar{\epsilon}[1 + \delta \cos(\tau z)] & 0 \\ 0 & 0 & \epsilon_{\perp} \end{pmatrix}. \quad (2.2)$$

(the two signs in the components of the above tensor correspond to left and right handed chirality of the helical structure), which can be also expressed in terms of Fourier series as

$$\bar{\bar{\epsilon}}(\mathbf{r}) = \sum_{s=0, \pm 1} \bar{\bar{\epsilon}}_s \exp(is\tau \cdot \mathbf{r}).$$

The Fourier coefficients are written as

$$\bar{\bar{\epsilon}}_0 = \begin{pmatrix} \bar{\epsilon} & 0 & 0 \\ 0 & \bar{\epsilon} & 0 \\ 0 & 0 & \epsilon_{\perp} \end{pmatrix}, \quad \bar{\bar{\epsilon}}_1 = \bar{\bar{\epsilon}}_{-1}^* = \frac{\bar{\epsilon} \delta}{2} \begin{pmatrix} 1 & \mp i & 0 \\ \mp i & -1 & 0 \\ 0 & 0 & 0 \end{pmatrix},$$

where  $\bar{\epsilon} = \frac{\epsilon_{\parallel} + \epsilon_{\perp}}{2}$  is the mean dielectric constant,  $\delta = \frac{\epsilon_{\parallel} - \epsilon_{\perp}}{\epsilon_{\parallel} + \epsilon_{\perp}}$  is the dielectric anisotropy, and  $\mathbf{k}_0, \mathbf{e}_0, \mathbf{k}_1, \mathbf{e}_1$  are the wave and polarization vectors for the incident and scattered waves respectively.

---

<sup>†</sup>In relation with the previous chapter, we point out that  $\tau = 2q_0$ .

It is instructive to invoke the kinematical approximation for scattering of light in chiral nematic media, according to which the scattering cross-section for a sample is [1]

$$\frac{d\sigma(\mathbf{k}_0, \mathbf{e}_0; \mathbf{k}_1, \mathbf{e}_1)}{d\Omega_{\mathbf{k}_1}} = \left( \frac{\omega^2}{4\pi c^2} \right)^2 \left| \int [\mathbf{e}_1^\dagger (\bar{\bar{\epsilon}} - \bar{\epsilon}\mathbb{I}) \mathbf{e}_0] \exp[i(\mathbf{k}_0 - \mathbf{k}_1) \cdot \mathbf{r}] d\mathbf{r} \right|^2, \quad (2.3)$$

where

$$\tau = \frac{2\pi}{(p/2)} = \frac{4\pi}{p}$$

is the reciprocal lattice vector of the chiral nematic. By virtue of the specific form of the dielectric tensor given above, rearranging (2.3) yields

$$\frac{d\sigma(\mathbf{k}_0, \mathbf{e}_0; \mathbf{k}_1, \mathbf{e}_1)}{d\Omega_{\mathbf{k}_1}} = \left( \frac{\omega^2}{4\pi c^2} \right)^2 \left| \sum_s \mathbf{e}_1^\dagger \bar{\bar{\epsilon}}_s \mathbf{e}_0 \int \exp[i(\mathbf{k}_0 - \mathbf{k}_1) \cdot \mathbf{r} + s\boldsymbol{\tau} \cdot \mathbf{r}] d\mathbf{r} \right|^2. \quad (2.4)$$

In the limit of an infinite sample, the integral in the above relation is proportional to a delta function  $\delta(\mathbf{k}_0 - \mathbf{k}_1 + s\boldsymbol{\tau})$  and the scattering directions are given by the kinematical Bragg condition

$$\sin \theta = \frac{s\lambda}{p}$$

It is evident from (2.4) that only first order Bragg-reflection occurs. In an analogous fashion to X-ray diffraction, the structure amplitude role is played by the quantity

$$F(\mathbf{k}_0, \mathbf{e}_0; \mathbf{k}_1, \mathbf{e}_1) = \mathbf{e}_1^\dagger \bar{\bar{\epsilon}}_s \mathbf{e}_0$$

which is polarisation dependent and describes the scattering amplitude from a chiral nematic layer with thickness equal to a half helical pitch [1].

The two waves are written as a superposition of two circularly polarized plane waves of the form

$$\mathbf{E}(z, t) = \exp(-i\omega t)[E^+ \mathbf{n}_+ \exp(iK^+ z) + E^- \mathbf{n}_- \exp(iK^- z)], \quad (2.5)$$

with  $\mathbf{n}_\pm = \frac{1}{\sqrt{2}}(\mathbf{x} + i\mathbf{y})$  being the two unit circular polarization vectors. The wave-vectors satisfy the Bragg condition  $K^+ - K^- = \tau$  alongside the secular equation produced by substituting (2.5) into (2.1). The substitution yields the system of equations

$$\begin{cases} [1 - (\eta^+)^2] E^+ + \delta E^- = 0, \\ [1 - (\eta^-)^2] E^- + \delta E^+ = 0, \end{cases} \quad (2.6)$$

where

$$\eta^\pm = \frac{K^\pm}{\kappa}, \quad \kappa = (\omega/c)\bar{\epsilon}.$$

The compatibility condition generates the secular equation

$$[1 - (\eta^+)^2] [1 - (\eta^-)^2] - \delta^2 = 0.$$

The eigenvalues and ratios of values of eigenvectors, respectively, read

$$K_j^\pm = \frac{\tau}{2} \pm k^\pm, \quad (2.7)$$

with

$$k^\pm = \kappa \sqrt{1 + \left(\frac{\tau}{2\kappa}\right)^2 \pm \sqrt{\left(\frac{\tau}{\kappa}\right)^2 + \delta^2}}$$

and

$$\xi_j = \left( \frac{E^-}{E^+} \right)_j = \delta [(\eta_j^-)^2]^{-1}. \quad (2.8)$$

The eigensolutions are numbered in the following way:  $j = 1, 4$  for signs “+” and “-” before  $k^+$  in (2.7) and  $j = 2, 3$  for signs “+” and “-” before  $k^-$  in (2.7). Depending on the sign of  $K^+$  and  $K^-$  in equation (2.5), there are either two waves with circular polarizations of opposite handedness propagating in the same direction (corresponding to same signs of  $K^+$  and  $K^-$ ) or two waves with circular polarization of the same handedness propagating in opposite directions (corresponding to opposite signs of  $K^+$  and  $K^-$ ). Changes in the sign of the wave-vector in the phase vector of a circular wave is equivalent to the simultaneous change of the propagation direction and handedness of the circular polarization of the wave. The existence of eigensolutions where the constituent plane wave solutions propagate in opposite directions is indicative of reflection from the spatial structure of the chiral nematic. From the defining equations for the wave-vectors we deduce that the pair of solutions (1,4) containing  $k^+$  corresponds to two non-diffracting modes propagating in opposite directions, while the pair (2,3) containing  $k^-$  relates to modes experiencing diffraction in the chiral nematic.

For small values of the dielectric anisotropy  $\delta$  (assume  $\delta \ll 1$ ) we will now focus on the frequency dependence of the eigenvalues. For the solution 1,  $K^+$  and  $K^-$  have the same signs for all frequencies whereas for the ratio of amplitudes we have  $\xi_1 \sim \delta$  except for the high frequency region  $\omega/c \gg \tau/\delta$  where  $\xi_1 \rightarrow 1$ . Similar conclusions hold for solution 4 describing a wave propagating in the opposite direction. The wave-vector in this limit is  $\kappa\sqrt{1+\delta} \simeq \kappa(1+\delta/2)$  The dispersion relation for solutions 1 and 4 is

linear, resembling that of a wave propagating in a homogeneous medium. Solution 1, therefore, corresponds to a circularly polarized wave rotating with the opposite handedness from that of the chiral nematic helix, within the accuracy of the small dielectric anisotropy  $\delta$ , for all frequencies outside the region  $\omega/c > \tau/\delta$ . For  $\omega/c \gg \tau/\delta$  the solution corresponds to a linearly polarized standing wave with rotating plane of polarization matching the handedness of the chiral nematic helix. Depending on the frequency, the wave vectors  $K^+$  and  $K^-$  maybe either real with the same signs, real with opposite signs or complex quantities in the region  $\omega_B/\sqrt{1+\delta} < \omega < \omega_B/\sqrt{1-\delta}$ , where  $\omega_B = \tau c/(2\sqrt{\epsilon})$  denotes the center of the Bragg band (called also hereinafter forbidden band, stop band, photonic band-gap, or simply band-gap). Hence, no wave can propagate in this frequency range if their circular polarization matches the handedness of the chiral nematic helix. The above property is defined as selective reflection. In the forbidden band,  $|\xi_{2,3}| = 1$  independently of  $\delta$ . Outside the band-gap,  $|\xi_{2,3}| \sim \delta$  except in the high frequency limit. Consequently, solution 2 corresponds to a wave circularly polarised in the sense of the helix. In the limit of very short wavelengths that we have considered above,  $K^- \simeq \kappa(1 - \delta/2)$ . Solution 3 exhibits the same behaviour, with the difference that the corresponding wave propagate in the opposite direction outside the forbidden region. We should remark here that only first order reflection is possible, since  $|s| = 1$  in the Fourier components of the dielectric tensor.

### 2.1.2 Formation of the Boundary Value Problem

Having obtained the eigensolutions, we now proceed to address the problem of reflection and transmission for a chiral nematic sample of finite thickness. We will consider initially the case of normal incidence onto a plane parallel sample of thickness  $L$  with the helical axis (called also optical axis) normal to the plate surface. The boundary conditions requiring continuous tangential electric and magnetic field components at the boundary reduce to continuous electric and magnetic fields on the sample surfaces, since the waves are transverse. Hence, the boundary conditions attain the form

$$\left\{ \begin{array}{l} \mathbf{E}^i(0) + \mathbf{E}^r(0) = \mathbf{E}(0) \\ \mathbf{E}^t(L) = \mathbf{E}(L) \\ \{\mathbf{curl}[\mathbf{E}^i(z) + \mathbf{E}^r(z)]\}_{z=0} = [\mathbf{curl}\mathbf{E}(z)]_{z=0} \\ [\mathbf{curl}\mathbf{E}^t(z)]_{z=L} = [\mathbf{curl}\mathbf{E}(z)]_{z=L}. \end{array} \right. \quad (2.9)$$

The electric fields of the incident ( $\mathbf{E}^i$ ), reflected ( $\mathbf{E}^r$ ), transmitted ( $\mathbf{E}^t$ ) waves as well as the wave propagating inside the sample are given by the following relations.

$$\begin{aligned} \mathbf{E}^i(z, t) &= \exp[i(q_i z - \omega t)](E_i^+ \mathbf{n}_+ + E_i^- \mathbf{n}_-), \\ \mathbf{E}^r(z, t) &= \exp[-i(q_i z + \omega t)](E_r^+ \mathbf{n}_+ + E_r^- \mathbf{n}_-), \\ \mathbf{E}^t(z, t) &= \exp[i(q_i z - \omega t)](E_t^+ \mathbf{n}_+ + E_t^- \mathbf{n}_-), \\ \mathbf{E} &= \exp(-i\omega t) \sum_{j=1}^4 E_j^+ [\exp(iK_j^+ z) \mathbf{n}_+ + \xi_j \exp(iK_j^- z) \mathbf{n}_-], \end{aligned} \quad (2.10)$$

where  $q_i = \omega\sqrt{\varepsilon}/c$  is the wave-vector outside the chiral nematic. When waves

propagate in the positive (negative) direction of the z-axis, the unit vectors  $\mathbf{n}_+$  and  $\mathbf{n}_-$  describe left (right) and right (left)-handed circular polarizations, respectively. Substituting (2.10) into the boundary conditions we obtain the following system for the amplitudes of the eigenwaves

$$\begin{aligned}
\sum_j (1 + \eta_j^+) E_j^+ &= 2E_i^+, \\
\sum_j \exp(iK_j^+ L) (1 - \eta_j^+) E_j^+ &= 0, \\
\sum_j \xi_j (1 + \eta_j^-) E_j^+ &= 2E_i^-, \\
\sum_j \xi_j \exp(iK_j^- L) (1 - \eta_j^-) E_j^+ &= 0.
\end{aligned} \tag{2.11}$$

On determining these we can then find the reflected and transmitted wave amplitudes as follows

$$\begin{aligned}
E_r^+ &= \frac{1}{2} \sum_j \xi_j (1 - \eta_j^-) E_j^+, \\
E_t^+ &= \frac{1}{2} \sum_j \exp[i(K_j^+ - q_i)L] (1 + \eta_j^+) E_j^+, \\
E_r^- &= \frac{1}{2} \sum_j (1 - \eta_j^+) E_j^+, \\
E_t^- &= \frac{1}{2} \sum_j \xi_j \exp[i(K_j^- - q_i)L] (1 + \eta_j^-) E_j^+.
\end{aligned} \tag{2.12}$$

If light is incident from the outside half-space onto the half-space filled with a chiral nematic medium, then only two eigensolutions can be excited in the sample corresponding to propagation into the depth of the chiral nematic layer, i.e. solutions 1 and 2 (assuming a small imaginary part in  $\bar{\epsilon}$  the fields of solutions 3 and 4 would increase infinitely towards the direction of increasing

depth).

Extending our treatment to samples that are not thick ( $\delta L/p \sim 1$ ) we note that if we neglect light reflection at the CLC boundaries assuming that the dielectric constant of the ambient space is equal to  $\bar{\epsilon}$  up to the small dielectric anisotropy, then three eigensolutions are excited: two correspond to the diffracting wave and one one to the non-diffracting wave propagating along the direction of incidence. Hence the problem reduces into solving a system of three linear equations. Furthermore, the assumption of no boundary reflection allows the separation of the eigensolutions such that the incident wave with diffracting circular polarization excites only solutions 2 and 3, while the wave with the non-diffracting polarization excites solution 1 only. Neglecting boundary reflection introduces an error of the order of  $\delta$ , consistent with retaining only terms of the lowest order in  $\delta$  in the equations for the amplitudes of the diffracting eigensolutions 2 and 3.

Hereinafter, we will consider only the diffracting eigenwaves and replace the subscript index 2 (3) by  $+$  ( $-$ ). Then, after assuming that  $\eta_+^+ = \eta_-^+ = 1$  and  $\eta_+^- = \eta_-^- = -1$ , the last two equations of the system (2.11) take the form

$$\begin{aligned} E_+^+ + E_-^+ &= E_i^+, \\ \xi_+ \exp(iK_+^+ L) E_+^+ + \xi_- \exp(iK_-^+ L) E_+^- &= 0. \end{aligned} \tag{2.13}$$

From the first two equations of (2.12) we obtain the expressions for the reflected and the transmitted wave of the diffracting polarization

$$\begin{aligned} E_r^+ &= \xi_+ E_+^+ + \xi_- E_-^+, \\ E_t^+ &= \exp[i(K_+^+ - q_i)L] E_+^+ + \exp[i(K_-^+ - q_i)L] E_+^-. \end{aligned} \tag{2.14}$$

Solving system (2.13) for the amplitudes of the diffracting eigensolutions, and replacing in the expression for  $E_r^+$  and  $E_t^+$  above, we obtain the following expressions for the complex amplitude reflection and transmission coefficient

$$\begin{aligned} r &= \frac{E_r^+}{E_e} = \frac{i\delta \sin(k^- L)}{\left(\frac{k^- \tau}{q^2}\right) + i \left[ \left(\frac{\tau}{2q}\right)^2 + \left(\frac{k^-}{q}\right)^2 - 1 \right]}, \\ t &= \frac{E_t^+}{E_e} = \frac{\exp(iqL) \left(\frac{k^- \tau}{q^2}\right)}{\left(\frac{k^- \tau}{q^2}\right) + i \left[ \left(\frac{\tau}{2q}\right)^2 + \left(\frac{k^-}{q}\right)^2 - 1 \right]}. \end{aligned} \quad (2.15)$$

The squared modulus of the above quantities yields what is usually called the (intensity) reflection and transmission coefficients for the diffracting eigenwave, denoted by  $R^+$  and  $T^+$  respectively.

$$\begin{aligned} R^+ &= \frac{\delta^2 \sin(k^- L)^2}{\left(\frac{k^- \tau}{q^2}\right)^2 + \left[ \left(\frac{\tau}{2q}\right)^2 + \left(\frac{k^-}{q}\right)^2 - 1 \right]^2}, \\ T^+ &= \frac{\left| \exp(iqL) \left(\frac{k^- \tau}{q^2}\right) \right|^2}{\left(\frac{k^- \tau}{q^2}\right)^2 + \left[ \left(\frac{\tau}{2q}\right)^2 + \left(\frac{k^-}{q}\right)^2 - 1 \right]^2}. \end{aligned} \quad (2.16)$$

The secular equation reads

$$\tan(k^- L) = \frac{ik^- \frac{\tau}{q^2}}{\left(\frac{\tau}{2q}\right)^2 + \left(\frac{k^-}{q}\right)^2 - 1} \quad (2.17)$$

The solutions of the above transcendental equation can be written in the form  $\omega_{EM} = \omega_{EM}^0(1 + i\Delta)$ . For a sufficiently small  $\Delta$  and under the condi-

tion  $\Im(Lk^-) \ll 1$  the values  $\omega_{EM}^0$  coincide with the zeros of the reflection coefficient  $R$  of a non-absorbing chiral nematic sample. The real and imaginary part of the eigenfrequencies are determined by the conditions

$$k^-L = n\pi, \quad \Delta = -\frac{2^5\delta(n\pi)^2}{(L\delta\tau)^3}. \quad (2.18)$$

Also

$$\begin{aligned} \mathbf{E}(\omega_n, z, t) = i \exp(-i\omega_n t) & \left\{ \mathbf{n}_+ \exp\left(\frac{i\tau z}{2}\right) \sin\left(\frac{n\pi z}{L}\right) + \right. \\ \frac{1}{\delta} \mathbf{n}_- \exp\left(\frac{-i\tau z}{2}\right) & \left[ \left[ \left(\frac{\tau}{2q}\right)^2 + \left(\frac{n\pi}{Lq}\right)^2 - 1 \right] \sin\left(\frac{n\pi z}{L}\right) - i\frac{\tau n\pi}{Lq^2} \cos\left(\frac{n\pi z}{L}\right) \right] \right\}. \end{aligned} \quad (2.19)$$

For a non-absorbing CLC, the only source of the edge-mode amplitude decay is energy leakage through the sample surfaces. Applying relation (2.19) for  $z = 0, L$  we obtain

$$E_{out} = \frac{\tau n\pi}{q^2 L \delta}$$

for the leaking wave amplitude at the sample surfaces. The decrease in the edge-mode electromagnetic energy per unit time is equal to the energy flow of the outgoing waves given by the Poynting vector and is proportional to  $\mathbf{E} \cdot \mathbf{E}^* \hat{z}$ . The edge-mode lifetime can therefore be obtained as

$$\tau_m = \frac{\int_0^L |\mathbf{E}(\omega_{EM}, z, t)|^2 dz}{\frac{d}{dt} \int_0^L |\mathbf{E}(\omega_{EM}, z, t)|^2 dz} \propto L \left(\frac{L\delta}{pn}\right)^2$$

The amplitudes of the eigenwaves excited in the structure read [2]

$$E_+^+ = -E_i \exp(-ik^-L) \frac{\left(\frac{\tau}{2q}\right)^2 + \left(\frac{k^-}{q}\right)^2 - \frac{k^- \tau}{q^2} - 1}{2 \left\{ \frac{k^- \tau}{q^2} \cos(k^-L) + i \left[ \left(\frac{\tau}{2q}\right)^2 + \left(\frac{k^-}{q}\right)^2 - 1 \right] \sin(k^-L) \right\}}, \quad (2.20)$$

$$E_+^+ = E_i \exp(ik^-L) \frac{\left(\frac{\tau}{2q}\right)^2 + \left(\frac{k^-}{q}\right)^2 + \frac{k^- \tau}{q^2} - 1}{2 \left\{ \frac{k^- \tau}{q^2} \cos(k^-L) + i \left[ \left(\frac{\tau}{2q}\right)^2 + \left(\frac{k^-}{q}\right)^2 - 1 \right] \sin(k^-L) \right\}}. \quad (2.21)$$

Solving the inhomogeneous system for an excitation with a frequency close to that of an edge-mode, we obtain

$$E_{\pm}^{EM(+)} = \pm E_+^+ [1 + \tan(k^-L)],$$

where  $E_{\pm}^{EM}$  satisfy the homogeneous system. We can immediately see that

$$\frac{E_+^{EM(+)}}{E_-^{EM(+)}} = -1.$$

For a thick chiral nematic layer, it can be shown that the amplitudes  $E_{\pm}^+$  are very good approximations to  $E_{\pm}^{EM}$ .

In the presence of absorption the mean dielectric constant is written as  $\epsilon = \epsilon_0(1 + i\gamma)$ , where  $\gamma \ll 1$  in most situations. Under the condition  $\Im(Lk^-) \ll 1$  mentioned above, the reflection and transmission coefficients at the reflection minima read [2]

$$\begin{aligned}
R &= \frac{(a^3\gamma)^2}{[(n\pi)^2 + (a^3\gamma)^2]^2}, \\
T &= \frac{(n\pi)^4}{[(n\pi)^2 + (a^3\gamma)^2]^2}.
\end{aligned}
\tag{2.22}$$

Then, the absorption of light from the chiral nematic structure can be written as

$$\Gamma = 1 - R - T = \frac{2(n\pi)^2 a^3 \gamma}{[(n\pi)^2 + a^3 \gamma]^2},$$

with  $a = \frac{\tau L \delta}{4}$ . The absorption attains the maximum value of  $\Gamma = 1/2$  for  $(n\pi)^2 = a^3 \gamma$ . Under the presence of amplification, with  $\gamma < 0$ ,  $|\gamma| \ll 1$ , relations (2.22) hold, but now the coefficients become divergent for  $\gamma = -\frac{(n\pi)^2}{a^3}$ . These values correspond to the lasing threshold amplification values for the edge-modes numbered by  $n$ . As it can be deduced from the above relation, the threshold values of  $|\gamma|$  are inversely proportional to the third power of the chiral nematic layer thickness. The minimum threshold value corresponds to the dominant edge-mode with  $n = 1$ . Thus, as a zero approximation to the numerical solution of the solvability condition, the frequency of the first maximum for enhanced absorption  $\Gamma$  as well as for the first point where  $\Gamma$  diverges, coincide with that of the first zero of the reflection coefficient. This is impractical for a collinear pumping configuration, unless the pumping frequency coincides with the high-frequency edge of the reflection band and the lasing frequency with the low frequency edge.

## 2.2 The de Vries formulation

We will now summarize the main results of the de Vries theory for the optical properties of chiral nematic layers, as presented in his seminal monograph published in 1951. De Vries[3] transformed Maxwell's equations from the Cartesian into a rotating co-ordinate system, whose unit vectors are defined by

$$\begin{aligned}\hat{\xi} &= \cos\left(\frac{\tau z}{2}\right)\hat{\mathbf{x}} + \sin\left(\frac{\tau z}{2}\right)\hat{\mathbf{y}} \\ \hat{\eta} &= -\sin\left(\frac{\tau z}{2}\right)\hat{\mathbf{x}} + \cos\left(\frac{\tau z}{2}\right)\hat{\mathbf{y}} \\ \hat{\zeta} &= \hat{\mathbf{z}},\end{aligned}\tag{2.23}$$

where the vector  $\hat{\eta}$  is identical to the molecular director. Applying Faraday-Maxwell and Ampère-Maxwell law for an non-magnetic anisotropic medium (in our case uniaxial) we obtain

$$\mathbf{curl}(\mathbf{curl}\mathbf{E}) = -\mu_0\frac{\partial}{\partial t}(\mathbf{curl}\mathbf{H}) = -\mu_0\varepsilon_0\frac{\partial^2}{\partial t^2}\mathbf{D}$$

where it is understood that the dielectric tensor contains only relative (dimensionless) dielectric constants. If we assume a transverse field  $\mathbf{E} = \mathbf{E}(z)$  then for the dielectric tensor (2.2) we have  $\mathbf{div}(\mathbf{E}) = 0$  and we can thus write in Cartesian co-ordinates

$$\begin{aligned}\frac{1}{c^2}\frac{\partial^2 D_x}{\partial t^2} &= \frac{\partial^2 E_x}{\partial z^2}, \\ \frac{1}{c^2}\frac{\partial^2 D_y}{\partial t^2} &= \frac{\partial^2 E_y}{\partial z^2}, \\ E_z &= 0, \quad D_z = 0.\end{aligned}\tag{2.24}$$

In the rotating co-ordinate system we can write  $D_\xi = \varepsilon_\perp E_\xi$  and  $D_\eta = \varepsilon_\parallel E_\eta$ . The fields are transformed between the two frames according to the relation

$$\begin{pmatrix} E_x \\ E_y \end{pmatrix} = R^{-1} \left( \frac{\tau z}{2} \right) \begin{pmatrix} E_\xi \\ E_\eta \end{pmatrix}$$

where  $R \left( \frac{\tau z}{2} \right)$  is the rotation matrix corresponding to a rotation of the axes by  $\tau z/2$ . Equations (2.24), then, acquire the form

$$\begin{aligned} \frac{\varepsilon_\perp}{c^2} \frac{\partial^2 E_\xi}{\partial t^2} &= \frac{\partial^2 E_\xi}{\partial z^2} - \tau \frac{\partial E_\eta}{\partial z} - \frac{\tau^2}{4} E_\xi \\ \frac{\varepsilon_\parallel}{c^2} \frac{\partial^2 E_\eta}{\partial t^2} &= \frac{\partial^2 E_\eta}{\partial z^2} - \tau \frac{\partial E_\xi}{\partial z} - \frac{\tau^2}{4} E_\eta \end{aligned} \quad (2.25)$$

A trial solution representing an elliptically polarized wave of the form

$$\begin{pmatrix} E_\xi \\ E_\eta \end{pmatrix} = \exp \left[ 2\pi i \left( \frac{t}{T} - \frac{mz}{\lambda} \right) \right] \begin{pmatrix} \mathcal{A} \\ i\mathcal{B} \end{pmatrix}$$

produces the system of equations

$$\begin{cases} \frac{\varepsilon_\perp}{c^2} \mathcal{A} = \frac{m^2}{\lambda^2} \mathcal{A} + 2\mathcal{B} \frac{m}{\lambda p} + \frac{\mathcal{A}}{p^2} \\ \frac{\varepsilon_\parallel}{c^2} \mathcal{B} = \frac{m^2}{\lambda^2} \mathcal{B} + 2\mathcal{A} \frac{m}{\lambda p} + \frac{\mathcal{B}}{p^2} \end{cases} \quad (2.26)$$

The compatibility condition of the above system of equations yields an algebraic equation for the ‘effective refractive index’,  $m$ , which encompasses the characteristics of propagation in the chiral nematic medium. The equation reads

$$m^4 - m^2 \left( \varepsilon_\perp + \varepsilon_\parallel + 2 \frac{\lambda^2}{p^2} \right) + \left( \varepsilon_\perp - \frac{\lambda^2}{p^2} \right) \left( \varepsilon_\parallel - \frac{\lambda^2}{p^2} \right) = 0 \quad (2.27)$$

As expected, this equation is symmetric in the interchange of  $\varepsilon_{\perp}$  and  $\varepsilon_{\parallel}$ . De Vries introduced the reduced quantities  $\lambda' = \lambda/(p\sqrt{\varepsilon})$  and  $m' = m/\sqrt{\varepsilon}$ . Then, the eigenvalue equation (2.27) can be written as

$$m'^4 - m'^2(1 + \lambda'^2) + (1 - \delta - \lambda'^2)(1 + \delta - \lambda'^2) = 0 \quad (2.28)$$

From the eigenvectors, one obtains the "degree of ellipticity",  $f$ , as below

$$f = \frac{\mathcal{B}}{\mathcal{A}} = \frac{1 - \delta - m'^2 - \lambda'^2}{2m'\lambda'} \quad (2.29)$$

As the quartic eigenvalue equation has two roots, the ellipticity will also be given by two expressions with very different behaviour, corresponding to the diffracting and the non-diffracting eigenwave. The roots of the characteristic algebraic equation can be readily expressed as

$$m_{\pm}^2 = 1 + \lambda'^2 \pm \sqrt{4\lambda'^2 + \delta^2} \quad (2.30)$$

As we can immediately deduce, the solution  $m_{-}$  becomes imaginary for  $|\lambda'^2 - 1| < \delta$ . This inequality defines the Bragg-band, the same range for which  $k^{-}$  is imaginary, when the eigenvalue equation is produced in the Cartesian frame of co-ordinates. In that range of wavelengths, having  $m'_{-} = -i\mu$ , the eigenwave can be written as

$$\begin{pmatrix} E_{\xi} \\ E_{\eta} \end{pmatrix} = \exp\left(-2\pi\frac{\mu z}{\lambda}\right) \cos\left(\frac{2\pi t}{T}\right) \begin{pmatrix} \mathcal{A}_{-} \\ i\mathcal{B}_{-} \end{pmatrix}$$

The above expression corresponds to a linearly polarized wave in the  $\xi - \eta$  frame. At the edges of the Bragg-band, when  $\lambda' \rightarrow \sqrt{1 \pm \delta}$ , the ellipticity

diverges to  $0 (+\infty)$ , corresponding to a linearly polarized wave being perpendicular to (or, respectively, following) the molecular director. The magnetic field will be found with the help of Ampère-Maxwell law, according to which, in the Cartesian frame, we have

$$\frac{\partial B_x}{\partial t} = \frac{\partial E_y}{\partial z}, \quad \frac{\partial B_y}{\partial t} = -\frac{\partial E_x}{\partial z} \quad (2.31)$$

The above can be written as

$$\frac{\partial}{\partial t} \left[ R\left(-\frac{\tau z}{2}\right) \begin{pmatrix} B_\xi \\ B_\eta \end{pmatrix} \right] = \hat{\mathbf{z}} \times \frac{\partial}{\partial z} \left[ R\left(-\frac{\tau z}{2}\right) \begin{pmatrix} E_\xi \\ E_\eta \end{pmatrix} \right] \quad (2.32)$$

so that

$$\begin{pmatrix} B_\xi \\ B_\eta \end{pmatrix} = R\left(\frac{\tau z}{2}\right) \int \frac{\partial}{\partial z} \left[ R\left(-\frac{\tau z}{2}\right) \begin{pmatrix} E_\eta \\ -E_\xi \end{pmatrix} \right] dt = -i \frac{T}{2\pi} \begin{pmatrix} E_\xi \frac{\tau}{2} + \frac{\partial E_\eta}{\partial z} \\ E_\eta \frac{\tau}{2} - \frac{\partial E_\xi}{\partial z} \end{pmatrix} \quad (2.33)$$

given that  $\hat{\xi} \times \hat{\eta} = \hat{\mathbf{z}}$ . Finally

$$\begin{pmatrix} B_\xi \\ B_\eta \end{pmatrix} = \frac{A}{c} \begin{pmatrix} (-i) \left( \frac{\lambda}{p} + mf \right) \\ m + \frac{\lambda}{p} f \end{pmatrix} \exp \left[ 2\pi i \left( \frac{t}{T} - \frac{mz}{\lambda} \right) \right], \quad (2.34)$$

where  $c$  is the speed of light in the vacuum. As explained in [3] the quantity  $\mathfrak{r} = m' + \lambda' f$  plays the role of the normal refractive index, as it is nearly unity apart from the region where  $\lambda' \simeq 1$ . Furthermore, from the system (2.26) defining the eigenvectors, we also obtain

$$\frac{1}{f} = \frac{1 + \delta - m'^2 - \lambda'^2}{2m'\lambda'} = \frac{2m'\lambda'}{1 - \delta - m'^2 - \lambda'^2}$$

and hence we can write

$$(\lambda' + m'f)(\lambda'f + m') = f \left( \lambda'^2 + \frac{m'\lambda'}{f} + m'\lambda'f + m'^2 \right) = f, \quad (2.35)$$

after substituting the two equivalent expressions for the ellipticity. After the above considerations, the magnetic field component can be written as

$$B_\xi = -\frac{\sqrt{\bar{\epsilon}}}{\tau c} E_\eta, \quad B_\eta = \frac{\tau}{c} \sqrt{\bar{\epsilon}} E_\xi$$

We can see once more that the parameter  $\tau$  (through  $m$  and  $f$ ) encompasses the optical transmission properties of the chiral nematic in our consideration. In an isotropic medium  $\tau = 1$ ; this value is approached by the non-diffracting eigenwave, and by the diffracting one in the wavelength region considerably far from the stop-band. De Vries argues that the negative sign should be chosen for  $m_-$  in the region  $\lambda' > \sqrt{1 + \delta}$ , as follows. The time averaged Poynting vector in the rotating co-ordinate system is given by the relation

$$\begin{aligned} \langle \mathbf{S} \rangle &= \frac{\mu_0}{2c} \Re \{ \mathbf{E} \times \mathbf{B}^* \} = \frac{\mu_0}{2c} \Re \{ E_\xi B_\eta^* - E_\eta B_\xi^* \} \hat{\mathbf{z}} \\ &= \frac{\mu_0}{2c} \Re \left\{ \sqrt{\bar{\epsilon}} \left( \tau^* \mathcal{A}^2 + \frac{1}{\tau^*} \mathcal{B}^2 \right) \right\} \hat{\mathbf{z}}. \end{aligned} \quad (2.36)$$

Outside the Bragg band  $\tau \in \mathbb{R}$ , hence the sign of the Poynting vector (and hence the direction of power flow) will be determined by  $\tau$ . In the region  $\lambda' > \sqrt{1 + \delta}$  when  $m < 0$  then  $f > 0$ , since the numerator is always negative. In addition,  $|\lambda'f| > |m|$  since  $\frac{\lambda'^2 + m'^2 + \delta - 1}{2|m'|} > |m'| \Rightarrow m'^2 < \lambda'^2 + \delta - 1$ .

On the other hand, by the definition of  $m_-$  we have  $m^2 < 1 + \lambda'^2 - 2\lambda' + \delta$ , since for  $a, b \in \mathbb{R}^+$ ,  $a > b$ ,  $\sqrt{a^2 + b^2} > \sqrt{(a-b)^2}$ . It follows then that  $m^2 < (\lambda' - 1)^2 + \delta < (\lambda' - 1)(\lambda' + 1) + \delta = \lambda'^2 - 1 + \delta$ , as required. From the above argumentation, we infer that  $m$  must be negative in that region, otherwise  $\mathbf{r}$  would be negative, resulting in a power flow in the opposite ( $-z$ ) direction. We should also notice that since  $m = m_-$  is imaginary in the stop-band,  $f$  and  $\mathbf{r}$  are also imaginary and as a consequence  $\left(\mathbf{r}^* \mathcal{A}^2 + \frac{1}{\mathbf{r}^*} \mathcal{B}^2\right) \in \mathbb{I}$ . This result comes as well to verify that there is no propagation of electromagnetic power inside the band-gap, as anticipated.

We will now formulate a boundary value problem in exactly the same fashion as in [1],[2], but for the solution of Maxwell's equations in a rotating co-ordinate system inside the chiral nematic, in order to obtain an expression for the reflection and the transmission coefficient of the structure. The components of the incident and reflected waves propagating in the medium outside the liquid crystal cell (assumed to have a refractive index of  $n_0 = \sqrt{\bar{\epsilon}}$ ) read

$$\begin{pmatrix} E_x^{i(r)} \\ E_y^{i(r)} \end{pmatrix} = \begin{pmatrix} e_x^{i(r)} \\ i e_y^{i(r)} \end{pmatrix} \exp \left[ 2\pi i \left( \frac{t}{T} - \frac{mz}{\lambda} \right) \right], \quad (2.37)$$

$$B_{x[y]}^{i(r)} = \mp(\pm) \frac{\sqrt{\bar{\epsilon}}}{c} E_{y[x]}^{i(r)},$$

where it is understood that the sign choice follows the field component and the parenthesis follow the type of wave (incident or reflected). In the above relations we have assumed that the refractive index of the medium surrounding the crystal is the same as the the root of its mean dielectric constant, in order to avoid boundary reflection and hence conversion of the eigenwave

from one type to another (the reader should have been already familiar with that assumption). Imposing the boundary conditions for continuity of the tangential components of the electric and the magnetic fields at the interface  $z = 0$ , where  $\hat{\xi} = \hat{x}$  and  $\hat{\zeta} = \hat{y}$  we have

$$\begin{aligned} e_x^i + e_x^r &= \mathcal{A}, & e_y^i + e_y^r &= \mathcal{B} = f\mathcal{A}, \\ e_x^i - e_x^r &= \mathfrak{r}\mathcal{A}, & e_y^i - e_y^r &= \frac{f}{\mathfrak{r}}\mathcal{A}. \end{aligned} \quad (2.38)$$

The first two equations derive from equating the  $x$  and  $y$  components of the electric fields, respectively, whereas the relations in the last line derive from equating the  $y$  and  $x$  components of the magnetic field. From the four relations above, the following amplitudes and ratios can be deduced.

$$\begin{aligned} 2e_x^i &= \mathcal{A}(1 + \mathfrak{r}), & 2e_y^i &= \frac{\mathcal{A}f(1 + \mathfrak{r})}{\mathfrak{r}}, \\ 2e_x^r &= \mathcal{A}(1 - \mathfrak{r}), & 2e_y^r &= -\frac{\mathcal{A}f(1 - \mathfrak{r})}{\mathfrak{r}}, \end{aligned} \quad (2.39)$$

and

$$\begin{aligned} \frac{e_x^i}{e_y^i} &= -\frac{e_x^r}{e_y^r} = \lambda' + \frac{m'}{f}, \\ r &= \frac{e_x^r}{e_x^i} = -\frac{e_y^r}{e_y^i} = \frac{1 + \mathfrak{r}}{1 - \mathfrak{r}}. \end{aligned} \quad (2.40)$$

In our analysis it is assumed that only the eigenwave with the diffracting polarization results as a result of the incidence of the elliptically polarized wave  $\mathbf{E}^i$ . It is exactly the same assumption that we met in (2.13) and (2.14) when the summation index assumed values  $j = 2, 3$ , again corresponding to the diffracting polarization. The difference lies on the fact that the ratio of the component amplitudes of the incident wave, generating the diffracting eigenwave, is fixed in Belyakov's approach (and equal to 1 in modulus), in de

Varies it is a function of the wavelength and equal to  $f/\mathfrak{r}$ . This ratio, however is close to unity for the wavelength region of interest (approximately equal to  $1 + \delta/(2\lambda)$ ). On reflection from the boundary crystal-surrounding medium, the sign of  $m$ ,  $\mathfrak{r}$ , and consequently of  $f$  changes (consistent with having the power flux in the  $-z$  direction). At  $z = L = Np$  we have also  $\hat{\xi} = \hat{\mathbf{x}}$  and  $\hat{\zeta} = \hat{\mathbf{y}}$ . Applying the continuity boundary conditions we obtain

$$\begin{aligned} \mathcal{A} \exp\left(-\frac{2\pi imL}{\lambda}\right) + \mathcal{A}' \exp\left(+\frac{2\pi imL}{\lambda}\right) &= e_x^t \exp\left(-\frac{2\pi i\sqrt{\bar{\epsilon}}L}{\lambda}\right), \\ f \left[ \mathcal{A} \exp\left(-\frac{2\pi imL}{\lambda}\right) + \mathcal{A}' \exp\left(+\frac{2\pi imL}{\lambda}\right) \right] &= e_y^t \exp\left(-\frac{2\pi i\sqrt{\bar{\epsilon}}L}{\lambda}\right), \\ \mathfrak{r} \left[ \mathcal{A} \exp\left(-\frac{2\pi imL}{\lambda}\right) - \mathcal{A}' \exp\left(+\frac{2\pi imL}{\lambda}\right) \right] &= e_x^t \exp\left(-\frac{2\pi i\sqrt{\bar{\epsilon}}L}{\lambda}\right), \\ \frac{f}{\mathfrak{r}} \left[ \mathcal{A} \exp\left(-\frac{2\pi imL}{\lambda}\right) - \mathcal{A}' \exp\left(+\frac{2\pi imL}{\lambda}\right) \right] &= e_y^t \exp\left(-\frac{2\pi i\sqrt{\bar{\epsilon}}L}{\lambda}\right). \end{aligned} \quad (2.41)$$

Incorporating the phase factors in redefined complex amplitudes, as

$$\begin{aligned} \mathcal{C} &= \mathcal{A} \exp\left(-\frac{2\pi imL}{\lambda}\right), \quad \mathcal{C}' = \mathcal{A}' \exp\left(+\frac{2\pi imL}{\lambda}\right), \\ \mathcal{T}_{x(y)} &= e_{x(y)}^t \exp\left(-\frac{2\pi i\sqrt{\bar{\epsilon}}L}{\lambda}\right) \end{aligned} \quad (2.42)$$

we obtain

$$\frac{\mathcal{C}'}{\mathcal{C}} = \frac{\mathfrak{r} - 1}{\mathfrak{r} + 1}, \quad \frac{\mathcal{T}_x}{\mathcal{C}} = \frac{2\mathfrak{r}}{\mathfrak{r} + 1}, \quad \frac{\mathcal{T}_y}{\mathcal{C}} = \frac{2f}{\mathfrak{r} + 1}. \quad (2.43)$$

Let us assume a wave of the diffracting circular polarization with complex amplitude of a given modulus. We will first consider the  $x$  component. The amplitude of the first reflected wave from the interface reads  $e_x^i(1 - \mathfrak{r})/(1 + \mathfrak{r})$ .

The amplitude of the eigenwave then will be  $A = 2/(\tau + 1)$ . At the boundary  $z = L$ , the complex amplitude will have accumulated a phase factor  $s = \exp(2\pi i m' \sqrt{\varepsilon} L / \lambda)$ . This phase factor is a measure of the absorption when  $m_-$  is imaginary. On reflection, the amplitude will now be  $sA(\tau - 1)/(\tau + 1)$  and at the first interface,  $s^2A(\tau - 1)/(\tau + 1)$ . After  $N$  boundary reflections, the amplitude reflection coefficient reads

$$\begin{aligned} \mathcal{R} &= \frac{e_{\text{total}}^r}{e_x^i} = \frac{1 - \tau}{(1 + \tau)} - \frac{1 - \tau}{(1 + \tau)} \frac{2\tau}{(1 + \tau)} \frac{2}{(1 + \tau)} s^2 \\ &\quad - \frac{1 - \tau}{(1 + \tau)} \frac{2\tau}{(1 + \tau)} \frac{2}{(1 + \tau)} \left( \frac{1 - \tau}{1 + \tau} \right)^2 s^4 - \dots \\ &= \frac{1 - \tau}{1 + \tau} \left( 1 - \frac{4\tau}{(1 + \tau)^2} s^2 \sum_{k=0}^N v^k \right), \end{aligned} \quad (2.44)$$

where  $v = \left( \frac{s^2(1 - \tau)}{1 + \tau} \right)^2$ .

In the limit  $N \rightarrow \infty$ , the above sum converges since  $|v| < 1$ . The final result is

$$\begin{aligned} \mathcal{R} &= \frac{1 - \tau}{1 + \tau} \left( 1 - \frac{4\tau}{(1 + \tau)^2} s^2 \frac{1}{1 - v} \right) = \frac{1 - \tau}{1 + \tau} \left( 1 - \frac{4\tau s^2}{(1 + \tau)^2 - s^2(1 - \tau)^2} \right) \\ &= \frac{1 - \tau}{(1 + \tau)} \frac{(1 + \tau)^2(1 - s^2)}{(1 + \tau)^2 - s^2(1 - \tau)^2} = \frac{(1 - \tau^2)(1 - s^2)}{(1 + \tau)^2 - s^2(1 - \tau)^2} \end{aligned} \quad (2.45)$$

We note that this formula is immediately comparable with the standard result derived for the amplitude reflection coefficient of a Fabry-Pérot resonator.

$$\mathcal{R}_{FP} = r + tt'r' \frac{\exp(2i\delta)}{1 - r'^2 \exp(2i\delta)} = \frac{r[1 - \exp(2i\delta)]}{1 - r^2 \exp(2i\delta)}, \quad (2.46)$$

where we identify the parameters  $s = \exp(i\delta)$ ,  $r = (1 - \mathfrak{r})/(1 + \mathfrak{r})$ ,  $r' = -r$ ,  $t = 2/(1 + \mathfrak{r})$  and  $t' = 2\mathfrak{r}/(1 + \mathfrak{r})$ . We also note that the familiar condition  $r^2 + tt' = 1$  is satisfied. Had we considered the component  $e_y$ , then the expressions for  $t$  and  $t'$  would have been interchanged, as well as the ones for  $r$  and  $r'$  (since  $f$  changes sign for the reflected wave), leaving the expression for  $\mathcal{R}$  unaltered apart from a change of sign. This is to be expected, as upon consideration of a circularly polarized wave with the diffracting polarization, the reflected wave is also of the same polarization and propagates in the opposite direction, hence the components of the Stokes vector acquire a phase difference of  $\pi$ . Using the same correspondence, the amplitude transmission coefficient, then, is readily available as

$$\mathcal{T} = \frac{tt' \exp(i\delta)}{1 - r^2 \exp(2i\delta)} = \frac{4\mathfrak{r}s}{(1 + \mathfrak{r})^2 - s^2(1 - \mathfrak{r})^2}. \quad (2.47)$$

Outside the region of total reflection  $s^2 = \cos(2\delta) + i \sin(2\delta)$  and the intensity reflection coefficient reads

$$R = |\mathcal{R}|^2 = \frac{(1 - \mathfrak{r}^2)^2 \sin^2 \delta}{(1 - \mathfrak{r}^2)^2 \sin^2 \delta + 4\mathfrak{r}^2}. \quad (2.48)$$

Inside the stop-band  $s$  is real and  $\mathfrak{r}^2$  becomes imaginary. The reflection coefficient, then, reads

$$R_b = |\mathcal{R}_b|^2 = \frac{(1 - \mathfrak{r}^2)^2 (1 - s^2)^2}{(1 - \mathfrak{r}^2)^2 (1 - s^2)^2 - 16s^2 \mathfrak{r}^2}. \quad (2.49)$$

## 2.3 Oblique incidence

We will now outline the main results of dynamic theory of light scattering in chiral nematic liquid crystal samples pertaining to oblique propagation of the eigenwaves, as detailed in [1]. Oblique incidence and propagation presents a number of differences from the case of normal incidence: there are higher order reflections with corresponding frequency bands centered at multiples of the Bragg frequency, there exist frequency regions in which every polarization is reflected and the polarization properties are in general more complicated, affected both by diffractive scattering and birefringence. In the two-wave approximation of the dynamic diffraction theory, one assumes two eigenwaves with wave-vectors  $\mathbf{k}_0$  and  $\mathbf{k}_1 = \mathbf{k}_0 + \boldsymbol{\tau}$ . The total field inside the chiral nematic reads  $\mathbf{E}(\mathbf{r}, t) = [\mathbf{E}_0 \exp(i\mathbf{k}_0 \cdot \mathbf{r}) + \mathbf{E}_1 \exp(i\mathbf{k}_1 \cdot \mathbf{r})] \exp(-i\omega t)$ . Then, Maxwell's equations  $c^2 \mathbf{curl}(\mathbf{curl}\mathbf{E}) = -\hat{\varepsilon}(\mathbf{r})\partial^2\mathbf{E}/\partial t^2$  reduce in the system

$$\begin{cases} \left(1 - \frac{\mathbf{k}_0^2}{\kappa^2}\right) \mathbf{E}_0 + \frac{\hat{\varepsilon}_{\boldsymbol{\tau}}}{\sqrt{\hat{\varepsilon}}} \mathbf{E}_1 = 0 \\ \frac{\hat{\varepsilon}_{-\boldsymbol{\tau}}}{\sqrt{\hat{\varepsilon}}} \mathbf{E}_0 + \left(1 - \frac{\mathbf{k}_1^2}{\kappa^2}\right) \mathbf{E}_1 = 0, \end{cases} \quad (2.50)$$

where  $\hat{\varepsilon}_{\boldsymbol{\tau}, -\boldsymbol{\tau}}$  are the Fourier components of the dielectric tensor as defined previously and

$$\kappa = \frac{\omega}{c} \sqrt{\hat{\varepsilon} \left(1 - \frac{\delta}{2} \cos^2 \theta\right)} \quad (2.51)$$

is the mean value of the wave-vector propagating at an angle  $\pi/2 - \theta$  to the optical axis (coinciding here with the  $z$ -axis). Analyzing the fields in components along the  $\sigma$  axis (perpendicular to the plane of incidence) and

two axes  $\pi, \pi_1$  perpendicular to the direction of propagation of the two waves in the plane of incidence results in the following four equations

$$\begin{aligned}
\left(1 - \frac{k_0^2}{\kappa^2} + \frac{\delta}{2} \cos^2 \theta\right) E_0^\sigma - \frac{\delta}{2} E_1^\sigma + \frac{i\delta}{2} \sin \theta E_1^\pi &= 0, \\
\left(1 - \frac{k_0^2}{\kappa^2} - \frac{\delta}{2} \cos^2 \theta\right) E_0^\sigma - \frac{\delta}{2} \sin^2 \theta E_1^\pi - \frac{i\delta}{2} \sin \theta E_1^\sigma &= 0, \\
-\frac{\delta}{2} E_0^\sigma + \frac{i\delta}{2} \sin \theta + \left(1 - \frac{k_0^2}{\kappa^2} + \frac{\delta}{2} \cos^2 \theta\right) E_1^\sigma &= 0, \\
\frac{i\delta}{2} \sin \theta E_0^\sigma - \frac{\delta}{2} \sin^2 \theta E_0^\pi + \left(1 - \frac{k_0^2}{\kappa^2} - \frac{\delta}{2} \cos^2 \theta\right) E_1^\pi &= 0.
\end{aligned} \tag{2.52}$$

Equating the determinant of the system matrix to zero yields the following equation

$$u^4 - (2\Delta^2 + 2n^2 - 1)u^2 - (2n^2 + 1)\Delta^2 + 2n^2\Delta = 0, \tag{2.53}$$

in which

$$u = \frac{k_1^2 - k_0^2}{\kappa^2 \delta (1 + \sin^2 \theta)}, \quad n = \frac{\cos^2 \theta}{1 + \sin^2 \theta}, \quad \Delta = \frac{2q^2 - k_0^2 - k_1^2}{\kappa^2 \delta (1 + \sin^2 \theta)}. \tag{2.54}$$

As shown in [1], the parameter  $\Delta$  measures the deviation of the angle of incidence (and propagation) from the angle dictated by the Bragg condition.

This constant can be recast in the more instructive form

$$\Delta = \frac{2 \sin \theta (2\kappa \sin \theta - \tau)}{\kappa \delta (1 + \sin^2 \theta)}. \tag{2.55}$$

The non-trivial case where  $\Delta = 0$  coincides within an accuracy of the order of  $\delta$  to the Bragg condition  $\sin \theta = \lambda/p$ . Equation (2.53) has four solutions

$$u_j = \pm \sqrt{\Delta^2 + n^2 - \frac{1}{2} \pm \sqrt{\left(\Delta^2 + n^2 - \frac{1}{2}\right) + (2n^2 + 1)\Delta^2 - 2n^2\Delta - \Delta^4}}, \quad (2.56)$$

which are enumerated as in the case of normal propagation:  $j = 1, 4$  for the sign “+” in front of the square brackets, and signs “+,” “−” in front of the braces, respectively;  $j = 2, 3$  for the sign “−” in front of the square brackets, and signs “+,” “−” in front of the braces, respectively. The eigensolutions of (2.52) are then written in the form

$$\mathbf{E}(\mathbf{r}, t) = [\mathbf{E}_{0j} \exp(i\mathbf{k}_{0j} \cdot \mathbf{r}) + \mathbf{E}_{1j} \exp(i\mathbf{k}_{1j} \cdot \mathbf{r})] \exp(-i\omega t), \quad (2.57)$$

with

$$\begin{aligned} \mathbf{E}_{0j} &= E_{0j}^\sigma \hat{\boldsymbol{\sigma}} + E_{0j}^\pi \hat{\boldsymbol{\pi}}_0, \\ \mathbf{E}_{1j} &= E_{1j}^\sigma \hat{\boldsymbol{\sigma}} + E_{1j}^{\pi_1} \hat{\boldsymbol{\pi}}_1 \end{aligned} \quad (2.58)$$

and

$$\begin{aligned} E_{0j}^\sigma &= a_{1j} = (\Delta - n + u_j)[(\Delta - u_j)^2 - n^2], \\ E_{0j}^\pi &= a_{2j} = -i \sin \theta (\Delta + n + u_j)[(\Delta - u_j)^2 - n^2], \\ E_{1j}^\sigma &= a_{3j} = (\Delta - n - u_j)(\Delta + u_j - n^2), \\ E_{1j}^{\pi_1} &= a_{4j} = -i \sin \theta (\Delta + n - u_j)(\Delta + u_j - n^2), \\ \mathbf{k}_{0j} &= \mathbf{q} + q\delta \frac{\Delta + n + u_j}{2(1+m) \sin \theta} \hat{\mathbf{z}}, \quad \mathbf{k}_{1j} = \mathbf{k}_{0j} + \boldsymbol{\tau}, \end{aligned} \quad (2.59)$$

where  $\mathbf{q}$  makes an angle  $\pi/2 - \theta$  with the  $z$ -axis. As we can see, the eigensolutions are superpositions of two waves with elliptical polarization in contrast

to normal incidence, where the eigenpolarizations are circular.

We will now formulate once more a boundary value problem whereby an elliptically polarized wave

$$\mathbf{E}^i(\mathbf{r}, t) = E^e \exp [i(\mathbf{q} \cdot \mathbf{r} - \omega t)] \hat{\mathbf{e}}_{\alpha, \beta}, \quad (2.60)$$

with

$$\hat{\mathbf{e}}_{\alpha, \beta} = \cos \alpha \hat{\boldsymbol{\sigma}} + \sin \alpha \exp(i\beta) \hat{\boldsymbol{\pi}}_0, \quad (2.61)$$

is incident obliquely upon the sample surface at a given  $z = z_1$ . The upper surface of the cell is located at  $z = z_1 + L$ . The amplitudes of the reflected and transmitted waves are sought in the forms  $\mathbf{E}^r = E_\sigma^r \hat{\boldsymbol{\sigma}} + E_\pi^r \hat{\boldsymbol{\pi}}_1$  and  $\mathbf{E}^t = E_\sigma^t \hat{\boldsymbol{\sigma}} + E_\pi^t \hat{\boldsymbol{\pi}}_0$ , respectively. It is assumed that the reflected (transmitted) wave has the polarization of the eigenwave with wave-vector  $\mathbf{k}_{1(0)}$ . Imposing the familiar boundary conditions of continuity for the tangential components of  $\mathbf{E}$  and  $\mathbf{B}$  yields the system of equations for the determination of the eigenwave amplitudes

$$\begin{aligned} \sum_j a_{1j} C'_j &= E_\sigma^i, & \sum_j a_{2j} C'_j &= E_\pi^i \\ \sum_j a_{3j} C'_j \exp(i\mathfrak{d}k_j L) &= 0, & \sum_j a_{4j} C'_j \exp(i\mathfrak{d}k_j L) &= 0, \end{aligned} \quad (2.62)$$

while for the reflected/transmitted waves we have

$$\begin{aligned}
\sum_j a_{3j} C'_j \exp(i\tau z_1) &= E_\sigma^r, & \sum_j a_{4j} C'_j \exp(i\tau z_1) &= E_\pi^r, \\
\exp[i(\mathbf{q} \cdot \hat{\mathbf{z}})L] \sum_j a_{1j} C'_j \exp(i\mathfrak{d}k_j L) &= E_\sigma^t, & & (2.63) \\
\exp[i(\mathbf{q} \cdot \hat{\mathbf{z}})L] \sum_j a_{2j} C'_j \exp(i\mathfrak{d}k_j L) &= E_\pi^t, & &
\end{aligned}$$

where  $C'_j = C_j \exp[i(\mathbf{k}_{0j} \cdot \hat{\mathbf{z}})z_1]$  and  $\mathfrak{d}k_j = q\delta(\Delta + n + u_j)/[2(1+m)\sin\theta]$  is the aforementioned diffractive correction of the order of  $\delta$ . The system matrix determinant of (2.62) is

$$D = \begin{vmatrix} a_{11} & a_{12} & a_{13} & a_{14} \\ a_{21} & a_{22} & a_{23} & a_{24} \\ \gamma_1 a_{31} & \gamma_2 a_{32} & \gamma_3 a_{33} & \gamma_4 a_{34} \\ \gamma_1 a_{41} & \gamma_2 a_{42} & \gamma_3 a_{43} & \gamma_4 a_{44} \end{vmatrix}, \quad (2.64)$$

with  $\gamma_j = \exp[i(\Delta + u_j + n)l]$  and  $l = (\delta q L)/[2(1+n)\sin\theta]$ . The  $\sigma$  polarized component of the reflected wave is obtained by the familiar relation

$$E_\sigma^r = \frac{E^i}{D} \begin{vmatrix} a_{11} & a_{12} & a_{13} & a_{14} & \cos\alpha \\ a_{21} & a_{22} & a_{23} & a_{24} & \sin\alpha \exp(i\beta) \\ \gamma_1 a_{31} & \gamma_2 a_{32} & \gamma_3 a_{33} & \gamma_4 a_{34} & 0 \\ \gamma_1 a_{41} & \gamma_2 a_{42} & \gamma_3 a_{43} & \gamma_4 a_{44} & 0 \\ a_{31} & a_{32} & a_{33} & a_{34} & 0 \end{vmatrix}. \quad (2.65)$$

Applying the numerical Newton-Raphson method to determine the solutions of the secular equation  $|D| = 0$  we have found that the imaginary parts of  $\omega_{EM}$  are identical to the expressions in (2.18) for propagation angles lying

from  $0^\circ - 30^\circ$  to normal. This result is consistent with the constant lasing threshold curve obtained also numerically in [4].

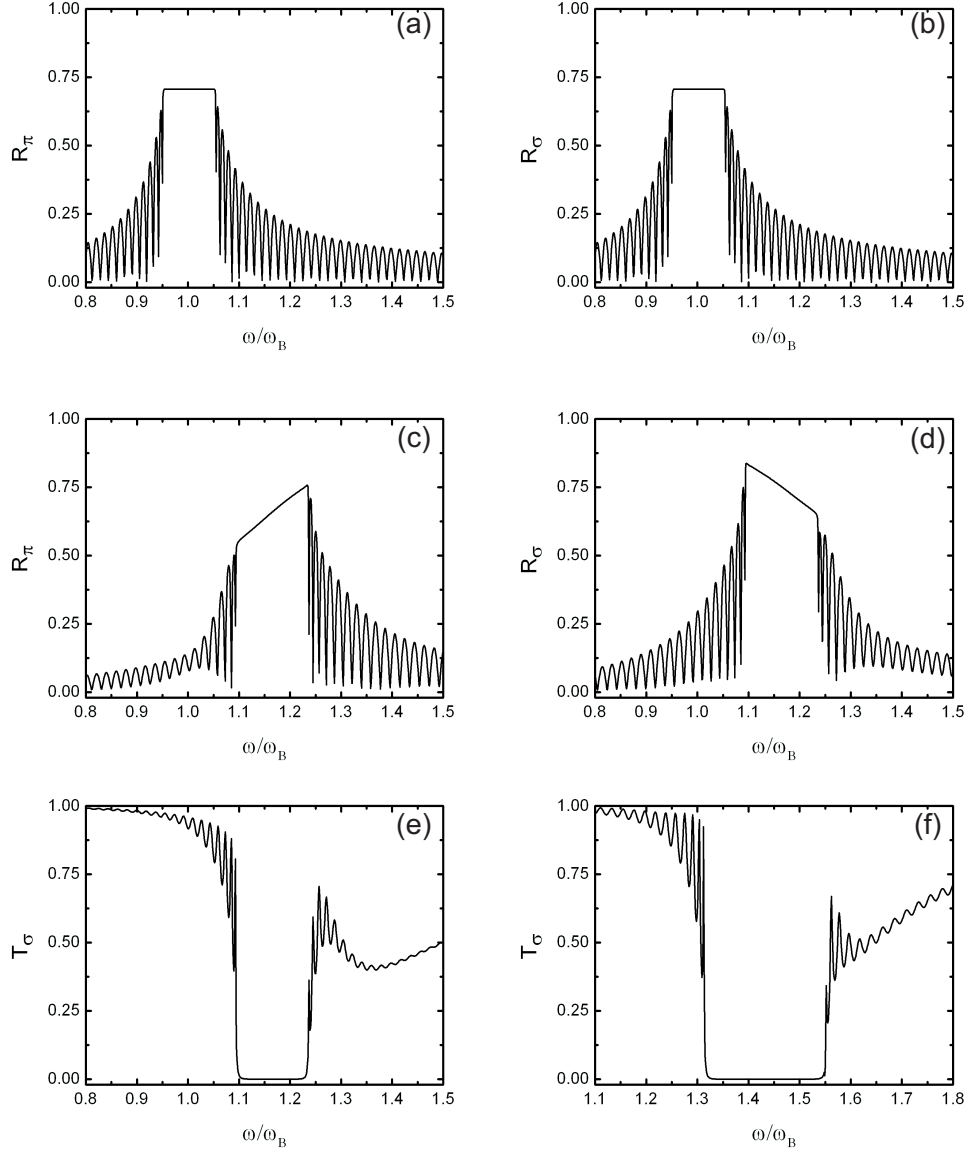


Figure 2.1: Transmission (T) and Reflection (R) coefficients for  $\sigma$  and  $\pi$  polarizations in oblique incidence. In (a, b)  $\theta \rightarrow \pi/2$ , in (c, d, e)  $\theta = \pi/3$  and in (f)  $\theta = \pi/4$ . In all cases  $\delta = 0.1$  and  $L = 30p$ .

The other components of the reflected and transmitted waves are obtained by similar relations, by modifying the elements of the last row in the previous matrix, as follows: for  $E_\pi^r$  by  $a_{4j}$ , for  $E_\sigma^t$  by  $\gamma_j a_{1j}$  and for  $E_\pi^t$  by  $\gamma_j a_{2j}$ . For crystals in which  $l \gg 1$  the kinematic approximation presented in the beginning of the section cannot account for the formation of reflection bands. In our consideration, the only eigensolutions with non-zero coefficients are those corresponding to wave attenuation inside the crystal length [1]. Evidently, the damping of eigenwaves is due to diffraction scattering (for real  $\hat{\epsilon}(\mathbf{r})$ ) and is due to the fact that the wave-numbers  $k_0$  and  $k_1$  are complex in a certain range of  $\Delta$ , where propagation is forbidden. From the solution of the eigenvalue equation (2.53) we can distinguish three different cases regarding light reflection based on the values of  $\Delta$ . If  $\Delta$  is such that all the solutions  $u_j$  are real and the waves pass un-attenuated from the crystal which presents a small reflectivity. The other case is such that the two solutions  $u_{2,3}$  are imaginary (and conjugates) while the others ( $u_{1,4}$ ) are real. Then, one of the waves (2,3) is attenuated and the other is amplified exponentially within the crystal. The incident wave with elliptical polarization corresponding to (2,3) experiences total reflection in the Bragg band and the orthogonally polarized (incident) wave excites the eigenwaves (1,4) that contribute only slightly to reflection. As unpolarized light can always be analyzed into two given orthogonal axes with zero correlation, the reflectivity of the sample for unpolarized light in that frequency (or angle) region will be approximately 1/2. Finally, there exists a region of  $\Delta$  where all solutions are complex in conjugate pairs. In that range, incident light of any polarization is almost completely reflected and the reflectivity of the sample approaches unity. For

a thick crystal, two parameters  $\gamma_j$  are exponentially large and the other two exponentially small (corresponding to negative and positive imaginary parts, respectively, from the complex conjugate pairs). As we can deduce from (2.65), then,  $E_\sigma^t = E_\pi^t = 0$ , because the rows in the corresponding determinants are linearly dependent, and  $D \neq 0$ .

Plots of the transmission and reflection coefficients as a function of frequency (for oblique incidence) are given in Figure 2.1 for the  $\sigma$  and  $\pi$  eigenpolarizations. We can deduce that the stop-band broadens with increasing deviation from normal incidence, and is also centered at higher frequencies. This result holds also for other distributed feedback structures, as we will see in the next chapter.

## 2.4 The Berreman method

The problem of oblique propagation in chiral nematics can be also addressed by the matrix method proposed by Berreman[5] in 1972 that we will briefly outline. After writing Faraday-Maxwell and Ampère-Maxwell law in the absence of sources in a 6x6 matrix form, and linking the electric field with the electric displacement and the magnetic field with the magnetic induction through a matrix relation as well (of the form  $(\mathbf{D}, \mathbf{B}) = \mathbf{M}(\varepsilon_0 \mathbf{E}, \mu_0 \mathbf{H})$ ) we end up in the following equation for transverse waves with a time dependence  $\exp(-i\omega t)$  with  $k_y = 0$

$$\partial_z \psi_i = \frac{i\omega}{c} \Delta_{ij} \psi_j, \quad (2.66)$$

where  $\psi = (E_x, \mu_0 c H_y, E_y, -\mu_0 c H_z)$  and  $\Delta_{ij} = f(k_x c / \omega, \varepsilon_{ij}, \mu_{ij}, \rho_{ij})$ . The

penultimate arguments are components of the magnetic permeability tensor and the last ones components of the optical-rotation tensors. If the matrix elements  $\Delta_{ij}$  are independent of (or vary very slowly with)  $z$  over some short interval  $\delta z$  equation (2.66) will have four periodic solutions of the form  $\psi_j(\delta z) = \exp(iq_j\delta z)\psi_j(0)$ . Substituting this form in (2.66) we obtain the eigenvalue equation

$$\left| \Delta - \frac{qc}{\omega} \mathbb{I} \right| = 0 \quad (2.67)$$

and subsequently determine the eigenvectors  $\psi_j$ . If the matrix  $\Delta$  is independent of  $z$  over some finite range  $h$ , as it happens with dielectric stacks then (2.66) can be integrated to give  $\psi_i(z+h) = P_{ij}(h)\psi_j(z)$ . This is familiar expression from one of the postulations of the Bloch-Floquet theorem for waves in periodic media [6] with  $h$  being the spatial period of the structure. The matrix in the above relation can be written as

$$\mathbf{P}(h) = \exp\left(\frac{i\omega h \Delta}{c}\right) = \sum_{n=0}^{\infty} \left(\frac{i\omega h \Delta}{c}\right)^n. \quad (2.68)$$

In many numerical problems, when  $(\omega h/c) \ll 1$  only the first few terms from the above expansion are retained. A secular equation for the eigenvalues  $q$  similar to (2.66) can be formed as

$$|P(h) - \exp(iqh)\mathbb{I}| = 0. \quad (2.69)$$

The matrix  $\mathbf{P}$  has the obvious symmetry property  $\mathbf{P}(kh) = [\mathbf{P}(h)]^k$ .

Focussing on chiral nematic liquid crystals, the dielectric tensor has the form (2.2) and the corresponding differential propagation matrix is

$$\mathbf{\Delta}(z) = \begin{pmatrix} 0 & 1 - \frac{\Xi^2}{\epsilon_{\parallel}} & 0 & 0 \\ \bar{\epsilon}[1 + \delta \cos(\tau z)] & 0 & \bar{\epsilon}\delta \sin(\tau z) & 0 \\ 0 & 0 & 0 & 1 \\ \bar{\epsilon}\delta \sin(\tau z) & 0 & \bar{\epsilon}[1 - \delta \cos(\tau z)] - \Xi^2 & 0 \end{pmatrix}, \quad (2.70)$$

where  $\Xi = (c/\omega)k_x = (c/\omega)k \sin \theta$  and  $\theta$  is the angle between the  $z$  axis and the direction of propagation. Having constructed the matrix  $\mathbf{\Delta}$  we can obtain numerical solutions for the field amplitudes in oblique propagation (when  $\Xi \neq 0$ ). For  $\Xi = 0$ , as noted in [5] the eigenvectors  $\psi(z)$  should have a form such that  $E_x$  and  $c\mu_0 H_y$  at  $z = 0$  are the same as  $E_y$  and  $-c\mu_0 H_x$  at  $z = p/4$  apart from a phase factor ( $p$  is the helix pitch). This spiral symmetry is reflected in the eigenvectors

$$\begin{aligned} \psi &= \exp(iqz) \begin{pmatrix} A \exp(i\frac{\tau}{2}z) + B \exp(-i\frac{\tau}{2}z) \\ c\mu_0[A' \exp(i\frac{\tau}{2}z) + B' \exp(-i\frac{\tau}{2}z)] \\ A \exp[i\frac{\tau}{2}(z - \pi/\tau)] + B \exp[-i\frac{\tau}{2}(z - \pi/\tau)] \\ c\mu_0\{A \exp[i\frac{\tau}{2}(z - \pi/\tau)] + B \exp[-i\frac{\tau}{2}(z - \pi/\tau)]\} \end{pmatrix} \\ &= \exp\left[i\left(q + \frac{\tau}{2}\right)z\right] \begin{pmatrix} A \\ c\mu_0 A' \\ -iA \\ -ic\mu_0 A' \end{pmatrix} + \exp\left[i\left(q - \frac{\tau}{2}\right)z\right] \begin{pmatrix} B \\ c\mu_0 B' \\ -iB \\ -ic\mu_0 B' \end{pmatrix}. \quad (2.71) \end{aligned}$$

It is evident from the above that the eigenvalue  $q$  is the Bloch wave-number which is to be determined. Substituting in (2.66) we obtain

$$\begin{aligned}
& \exp \left[ i \left( q + \frac{\tau}{2} \right) z \right] \begin{pmatrix} A' \\ \mu_0 c (\bar{\varepsilon} A + \bar{\varepsilon} \delta B) \\ -i A' \\ -i \mu_0 c (\bar{\varepsilon} A + \bar{\varepsilon} \delta B) \end{pmatrix} \\
& + \exp \left[ i \left( q - \frac{\tau}{2} \right) z \right] \begin{pmatrix} B' \\ \mu_0 c (\bar{\varepsilon} B + \bar{\varepsilon} \delta A) \\ i B' \\ i \mu_0 c (\bar{\varepsilon} B + \bar{\varepsilon} \delta A) \end{pmatrix} \\
& = \frac{c}{\omega} \left( q + \frac{\tau}{2} \right) \exp \left[ i \left( q + \frac{\tau}{2} \right) z \right] \begin{pmatrix} A \\ c \mu_0 A' \\ -i A \\ -i c \mu_0 A' \end{pmatrix} \\
& + \frac{c}{\omega} \left( q - \frac{\tau}{2} \right) \exp \left[ i \left( q - \frac{\tau}{2} \right) z \right] \begin{pmatrix} B \\ c \mu_0 B' \\ -i B \\ -i c \mu_0 B' \end{pmatrix}.
\end{aligned} \tag{2.72}$$

Equating the corresponding vector components from both handsides we obtain the following system of equations

$$\begin{cases} A' = \left( q + \frac{\tau}{2} \right) \frac{c}{\omega} A \\ B' = \left( q - \frac{\tau}{2} \right) \frac{c}{\omega} B \\ \bar{\varepsilon} A + \bar{\varepsilon} \delta B = \left( q + \frac{\tau}{2} \right) \frac{c}{\omega} A' = \left[ \left( q + \frac{\tau}{2} \right) \frac{c}{\omega} \right]^2 A \\ \bar{\varepsilon} B + \bar{\varepsilon} \delta A = \left( q - \frac{\tau}{2} \right) \frac{c}{\omega} B' = \left[ \left( q - \frac{\tau}{2} \right) \frac{c}{\omega} \right]^2 B. \end{cases} \tag{2.73}$$

The compatibility condition of the above system yields the eigenvalue quartic equation with solutions

$$q = \pm \sqrt{\frac{\tau^2}{4} + k^2 \bar{\epsilon} \pm k\tau \bar{\epsilon} \left(1 + \frac{\delta^2 k^2}{\tau^2}\right)} = km_{\pm}, \quad (2.74)$$

with  $k = \omega/c$  and  $m$  being the ‘effective refractive index’ in the de Vries formulation (see (2.27)).

## 2.5 Optical feedback in nematic LC slabs

We will conclude this chapter by treating laser radiation produced by liquid crystal samples as a feedback mechanism, based on the treatment in [4]. We consider a homogeneous liquid crystal cell  $B$  of thickness  $d$  which is unbounded in the  $x$  and  $y$  directions, as shown in Figure 2.2.

The slab  $B$  is surrounded by the regions  $A$  and  $C$ ; we assume that the electromagnetic fields in  $A$  and  $B$  are superpositions of forward and backward-travelling waves, whereas in region  $C$  only forward-travelling waves can exist. The monochromatic wave incident upon the slab from the medium  $A$  is represented by a column vector

$$\mathbf{E} = \begin{pmatrix} E_{s0} \exp(-i\mathbf{k}_0 \cdot \mathbf{r}) \\ E_{p0} \exp[-i(\mathbf{k}_0 \cdot \mathbf{r} + \delta_0)] \end{pmatrix}, \quad (2.75)$$

where  $\mathbf{k}_0$  is the wavevector in medium  $A$  and the indices  $s(p)$  refer to waves polarized in (perpendicular to) the plane of incidence. The phase shift  $\delta_0$  denotes the arbitrary ellipticity of the incident wave. The incident wave is partially transmitted in medium  $B$  with a complex amplitude following the

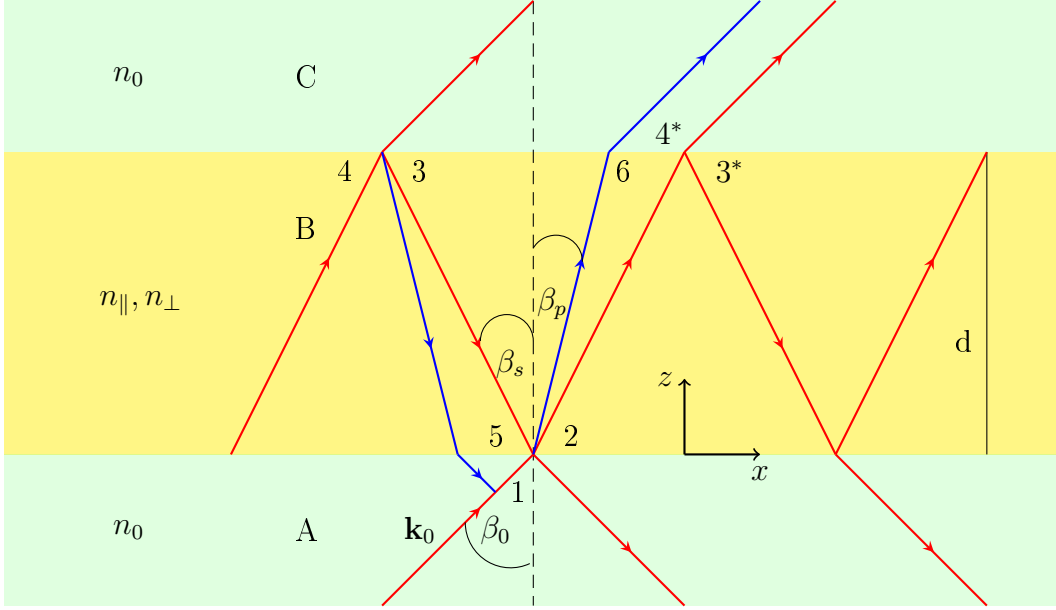


Figure 2.2: Schematic diagram of ray propagation in a nematic liquid crystal slab.

vector relation

$$\mathbf{E}_{21} = \mathbf{T}_{21}\mathbf{E}, \quad (2.76)$$

where  $\mathbf{T}_{21}$  is the transmission matrix of the interface 1 – 2. Hereinafter the order of suffixes in our expressions is indicative of the propagation direction of the wave that is travelling from the point denoted by the outer to the point denoted by the inner suffix. The resultant forward-propagating wave field at point 2 is written as

$$\mathbf{E}_2 = \mathbf{E}_{21} + \mathbf{R}_{21}\mathbf{P}_{23}\mathbf{R}_{34}\mathbf{E}_3, \quad (2.77)$$

where  $\mathbf{R}_{34}$  is the reflection matrix of the interface 3–4,  $\mathbf{P}_{23}$  is the propagation matrix from point 3 to point 2,  $\mathbf{R}_{21}$  is the reflection matrix of the interface

$2 - 1$  and  $\mathbf{E}_3$  is the forward propagating wave field at point 3. By virtue of the homogeneity of the sample in the  $x$  and  $y$  directions the difference between the waves at points 3 and  $3^*$  can only amount to a phase shift  $\delta_{33^*} = k_{0x}(x_3 - x_{3^*})$ , therefore

$$\mathbf{E}_3 = \mathbf{E}_{3^*} \exp(-i\delta_{33^*}) = \mathbf{P}_{3^*2} \mathbf{E}_2 \exp(-i\delta_{33^*}). \quad (2.78)$$

Substituting (2.76) and (2.77) into (2.78) we obtain

$$\begin{aligned} \mathbf{E}_3 &= \mathbf{P}_{3^*2} \mathbf{E}_2 \exp(-i\delta_{33^*}) (\mathbf{T}_{21} \mathbf{E} + \mathbf{R}_{21} \mathbf{P}_{23} \mathbf{R}_{34} \mathbf{E}_3) \Rightarrow \\ \mathbf{E}_3 &= [\mathbb{I} - \mathbf{P}_{3^*2} \mathbf{R}_{21} \mathbf{P}_{23} \mathbf{R}_{34} \exp(-i\delta_{33^*})]^{-1} \mathbf{P}_{3^*2} \mathbf{T}_{21} \exp(-i\delta_{33^*}) \mathbf{E}. \end{aligned} \quad (2.79)$$

On the other hand, combining (2.79) and (2.80) the outgoing wave at point 4 can be written as

$$\mathbf{E}_4 = \mathbf{T}_{43} \mathbf{E}_3 = \mathbf{T}_{43} [\mathbb{I} - \mathbf{P}_{3^*2} \mathbf{R}_{21} \mathbf{P}_{23} \mathbf{R}_{34} \exp(-i\delta_{33^*})]^{-1} \mathbf{P}_{3^*2} \mathbf{T}_{21} \exp(-i\delta_{33^*}) \mathbf{E}. \quad (2.80)$$

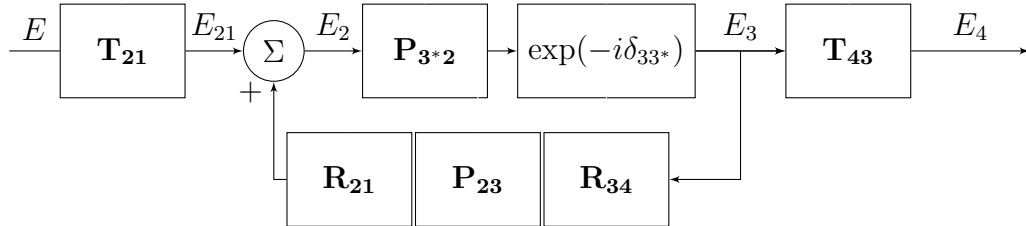


Figure 2.3: Feedback loop illustrating propagation of light in a liquid crystal cell.

The above relation can be construed in terms of the output function of the feedback loop outlined in Figure 2.3. Feedback is determined by the matrix

product  $\mathbf{P}_{3^*2}\mathbf{R}_{21}\mathbf{P}_{23}\mathbf{R}_{34}$  while the presence of an amplifying (or absorbing) medium in the liquid crystal is quantified through the propagation parameter  $\mathbf{P}_{3^*2}$  (and  $\mathbf{P}_{23}$ ). We draw attention on the fact that feedback is positive (denoted by the sign  $+$  on summation), hence the system may become unstable and the output unbounded with an arbitrarily small applied input (probe field). The singularity condition can be written in terms of the matrix  $\mathbf{F} = \mathbb{I} - \mathbf{P}_{3^*2}\mathbf{R}_{21}\mathbf{P}_{23}\mathbf{R}_{34} \exp(-i\delta_{33^*})$  as  $|\mathbf{F}| = 0$ . The role of the probe field can be played by any fluctuation. As noted in [4], the condition  $|\mathbf{F}| = 0$  must hold exactly. This means that when the gain exceeds its threshold value, lasing is quenched by saturation of the output wave. The inequality of gain exceeding losses is only meaningful under the condition that the density of photonic states in the resonating cavity must be sufficiently high for the quenched mode to dominate over adjacent modes reaching threshold. Although no assumption has been made for the properties of the slab  $B$  so far, we will now focus on the case of a homeotropically oriented nematic liquid crystal cell, where an analytical expression for the transfer matrices can be easily derived. We also assume that the liquid crystal cell is doped with a small amount of gain medium such that the values of the principal refractive indices are not altered when the medium is excited. If we suppose that the molecular director coincides with the unit direction along the  $z$ -axis ( $\mathbf{n} \equiv \hat{\mathbf{z}}$ ), then the refractive indices for the  $s$  and  $p$  polarized waves are given by the expressions

$$\begin{aligned} n_s &= n_\perp, \\ n_p^2(\beta_p) &= \frac{\varepsilon_\parallel \varepsilon_\perp}{\varepsilon_\parallel^2 \cos^2(\beta_p) + \varepsilon_\perp^2 \sin^2(\beta_p)}, \end{aligned} \tag{2.81}$$

where  $\beta_p$  is the angle between the  $z$ -axis and the wavevector of the  $p$  polarized wave. The reflection matrices are obtained by virtue of the continuity of the tangential components of the electromagnetic field and are given by the well-known Fresnel formulì

$$\mathbf{R}_{34} = \mathbf{R}_{21} = \begin{pmatrix} -\frac{\sin(\beta_0 - \beta_s)}{\sin(\beta_0 + \beta_s)} & 0 \\ 0 & \frac{\tan(\beta_0 - \beta_p)}{\tan(\beta_0 + \beta_p)} \end{pmatrix}, \quad (2.82)$$

where  $\beta_0$  is the angle between the  $z$ -axis and the direction of propagation of the wave in the homogeneous surrounding media  $A$  and  $C$  with refractive index  $n_0$ . The angles  $\beta_{0,p,s}$  are related by Snell's law as follows

$$n_0 \sin \beta_0 = n_s \sin \beta_s = n_p(\beta_p) \sin \beta_p.$$

By virtue of the symmetry of the problem and the uniformity of cell in the  $xy$  plane, the wave propagation matrices are diagonal. The matrix elements of  $\mathbf{P}_{23}$  will have the form of  $\exp(-i\mathbf{k}_{s,p}\mathbf{r}_{23})$  for the  $s, p$ -polarized waves. If we select the points 2 and 3 to be such that  $\mathbf{r}_{2,3} \parallel \mathbf{k}_s$ , then the matrix element for the  $p$ -wave will contain the phase shift  $\delta_{25} = k_0(x_2 - x_5) \sin \beta_0$  (as we have written  $\mathbf{r}_{23} = \mathbf{r}_{25} + \mathbf{r}_{53} = \mathbf{r}_{53} + (x_2 - x_5)\hat{\mathbf{x}}$ ) since the  $x$ -component of the wavevector is continuous across all regions (by virtue of the conservation of momentum in the  $x$ -direction). Also,  $|\mathbf{r}_{23}| = (d/\cos \beta_s)$  and  $|\mathbf{r}_{53}| = (d/\cos \beta_p)$  so that the propagation matrices  $\mathbf{P}_{3*2} = \mathbf{P}_{23}$  have the form

$$\begin{pmatrix} \exp \left[ -\frac{d}{\cos \beta_s} \left( \chi_s + i \frac{n_s}{n_0} k_0 \right) \right] & 0 \\ 0 & \exp \left[ -\frac{d}{\cos \beta_p} \left( \chi_p + i \frac{n_p(\beta_p)}{n_0} k_0 \right) - i \delta_{25} \right] \end{pmatrix}. \quad (2.83)$$

The above expression takes into account the the wavenumber has an imaginary part  $\chi_{s,p}$ , where  $\chi_{s,p} > 0 (< 0)$  corresponds to absorption (amplification). The experimentally measured coefficient is the one pertaining to the intensity of the wave,  $\alpha_{s,p} = 2\chi_{s,p}$ . If the gain medium is anisotropic, then  $\alpha_p$  depends on the angle  $\beta_p$ . In the case of weak absorption (or gain), where the condition  $|n_0\alpha_{s,p}/(2k_0)| \ll 1$  holds, the coefficients  $\alpha_{p,s}$  can be determined by considering the magnitude of the Poynting vector for each of the eigenwaves of the structure, which is proportional to  $\mathbf{e}_{p,s}(X\mathbf{e}_{p,s})$ , where  $X = \text{diag}(\chi_{\perp}, \chi_{\perp}, \chi_{\parallel})$ . The above inequality condition is necessary in order to write the components of the complex dielectric permittivity tensor as a sum where  $\chi_{s,p}$  appear only in the imaginary part, up to the first order. As derived in [6], the  $p$ - eigenwave belongs to the  $xz$  plane and the  $s$ -eigenwave is along the  $y$ -axis. More specifically,  $\mathbf{e}_p = (n_{\parallel}^2 \cos \beta_p, 0, -n_{\perp}^2 \sin \beta_p)$ ,  $\mathbf{e}_s = \hat{\mathbf{y}}$ , therefore

$$\begin{aligned} \alpha_s &= \alpha_{\perp} \\ \alpha_p(\beta_p) &= \frac{\alpha_{\parallel} \sin^2 \beta_p}{\sin^2 \beta_p + \left( \frac{n_{\parallel}}{n_{\perp}} \right)^4 \cos^2 \beta_p} + \frac{\alpha_{\perp} \cos^2 \beta_p}{\sin^2 \beta_p + \left( \frac{n_{\parallel}}{n_{\perp}} \right)^4 \sin^2 \beta_p}, \end{aligned} \quad (2.84)$$

where  $\alpha_{\perp, \parallel} = 2\chi_{\perp, \parallel}$ . Also we have

$$\begin{aligned}
\delta_{33^*} &= k_{0x}(x_3 - x_{3^*}) = -(2d \tan \beta_s)k_0 \sin \beta_0 = -(2d \tan \beta_s)k_0 \frac{n_s \sin \beta_s}{n_0} \\
&= -[2d(\tan \beta_s + \tan \beta_p - \tan \beta_p)]k_0 \frac{n_p \sin \beta_p}{n_0} \\
&= -(2d \tan \beta_p)k_0 \frac{n_p \sin \beta_p}{n_0} - 2k_0(x_3^* - x_6) \sin \beta_0 \\
&= -(2d \tan \beta_p)k_0 \frac{n_p \sin \beta_p}{n_0} - 2k_0(x_2 - x_5) \sin \beta_0 \\
&= -2 \left( k_0 d \tan \beta_p \frac{n_p \sin \beta_p}{n_0} + \delta_{25} \right)
\end{aligned} \tag{2.85}$$

Hence, the lasing condition  $|F| = 0$  is equivalent to two scalar equations obtained by equating each diagonal element of the resulting 2x2 matrix to zero. The conditions for the two waves  $s, p$  can be recast as follows

$$\begin{aligned}
&\mathbf{P}_{3^*2}\mathbf{R}_{21}\mathbf{P}_{23}\mathbf{R}_{34} \exp(-i\delta_{33^*}) = \mathbb{I} \\
\Rightarrow &\begin{cases} \frac{\sin^2(\beta_0 - \beta_s)}{\sin^2(\beta_0 + \beta_s)} \exp\left(-\frac{2\chi_s d}{\cos \beta_s}\right) \exp\left[-2ik_0 d \left(\frac{n_s}{n_0} \frac{1}{\cos \beta_s} - \frac{\sin^2 \beta_s}{\cos \beta_s}\right)\right] = 1 \\ \frac{\tan^2(\beta_0 - \beta_s)}{\tan^2(\beta_0 + \beta_s)} \exp\left(-\frac{2\chi_p d}{\cos \beta_p}\right) \exp\left(-2ik_0 d \frac{n_p(\beta_p)}{n_0}\right) = 1 \end{cases} \\
\Rightarrow &\begin{cases} \frac{\sin^2(\beta_0 - \beta_s)}{\sin^2(\beta_0 + \beta_s)} \exp\left(-\frac{2\chi_s d}{\cos \beta_s}\right) \exp\left(-2ik_0 d \frac{n_s}{n_0} \cos \beta_s\right) = 1 \\ \frac{\tan^2(\beta_0 - \beta_s)}{\tan^2(\beta_0 + \beta_s)} \exp\left(-\frac{2\chi_p d}{\cos \beta_p}\right) \exp\left(-2ik_0 d \frac{n_p(\beta_p)}{n_0}\right) = 1. \end{cases}
\end{aligned} \tag{2.86}$$

Exactly as in the case of a Fabry-Pérot etalon, since the left handside of the above equations is unity, we must impose the (phase) conditions

$$\begin{aligned}
k_0 d \frac{n_s}{n_0} \cos \beta_s &= m\pi, \\
k_0 d \frac{n_p(\beta_p)}{n_0} \cos \beta_p &= n\pi,
\end{aligned} \tag{2.87}$$

where  $n, m \in \mathbb{N}$ .

For these real frequencies (eigenfrequencies) there exist negative values of  $\chi_{s,p}$  which correspond to lasing. In the case of normal incidence,  $\beta_{s,p} = 0$  and  $\alpha_s = \alpha_p = \alpha_\perp$ . Since  $\beta_0 \rightarrow 0$  and  $\beta_s \rightarrow 0$  simultaneously, from the continuity of  $k_x$  we have  $\frac{d\beta_s}{d\beta_0} = \frac{n_0 \cos \beta_0}{n_s \cos \beta_s} \rightarrow \frac{n_0}{n_\perp}$ . We also apply l'Hôpital's rule for the matrix element  $\mathbf{R}_{2111}$  of the diagonal, to obtain

$$\lim_{\beta_0 \rightarrow 0} \frac{\sin(\beta_0 - \beta_s)}{\sin(\beta_0 + \beta_s)} = \lim_{\beta_0 \rightarrow 0} \frac{1 - \frac{d\beta_s}{d\beta_0} \cos(\beta_0 - \beta_s)}{1 + \frac{d\beta_s}{d\beta_0} \cos(\beta_0 + \beta_s)} = \frac{n_\perp - n_0}{n_\perp + n_0}, \quad (2.88)$$

so that we have the expression for the threshold gain

$$\alpha_{s,p} = \alpha_\perp = \frac{1}{d} \ln \left[ \left( \frac{n_\perp - n_0}{n_\perp + n_0} \right)^2 \right] < 0. \quad (2.89)$$

In the general case of oblique incidence where  $\beta_0 \in (0, \frac{\pi}{2})$ , the threshold gain is obtained by the following relations for the two polarizations

$$\begin{aligned} \alpha_s(\beta_0) = \alpha_\perp(\beta_0) &= -\frac{\cos \left[ \arcsin \left( \frac{n_0 \sin \beta_0}{n_\perp} \right) \right]}{d} \times \\ &\times \ln \left[ \frac{\sin^2 \left( \arcsin \left( \frac{n_0 \sin \beta_0}{n_\perp} \right) + \beta_0 \right)}{\sin^2 \left( \arcsin \left( \frac{n_0 \sin \beta_0}{n_\perp} \right) - \beta_0 \right)} \right], \quad (2.90) \\ \alpha_p(\beta_0) &= -\frac{\cos \beta_p}{d} \ln \left[ \frac{\tan^2(\beta_0 + \beta_p)}{\tan^2(\beta_0 - \beta_p)} \right] \left( \frac{K_D}{A} \sin^2 \beta_p + \frac{1}{B} \cos^2 \beta_p \right), \end{aligned}$$

where  $A = \sin^2 \beta_p + (n_\parallel/n_\perp)^4 \cos^2 \beta_p$ ,  $B = \cos^2 \beta_p + (n_\perp/n_\parallel)^4 \sin^2 \beta_p$ ,  $K_D = (\alpha_\parallel/\alpha_\perp)$  and  $\beta_p = \beta_p(\beta_0) = \arcsin \left[ n_0 n_\parallel \sin \beta_0 \sqrt{n_0^2 n_\parallel^2 + n_0^2 (n_\parallel^2 - n_\perp^2) \sin^2 \beta_0} \right]$ .

Consequently, lasing is in principle possible in any direction  $\beta_0$  associated with a unique discrete set of discrete wavelengths and threshold gain coefficients. When the thickness of the LC slab is small compared to the pumped surface, laser radiation can be produced within a broad spectral regime provided that the gain coefficients can vary within a sufficiently wide range (in practice, gain is provided only in a limited range of wavelengths, considered to be the FWHM of the luminescence spectrum of the gain medium). If the gain is very low, the lasing condition can still be satisfied for the case of the so-called sliding (or ‘leaky’) modes (where  $\beta_0 \rightarrow \pi/2$ ). Then, the phase condition (2.87) yields a number of (discrete) wavelengths for propagation in the free space (taking into account that  $n_s = n_\perp$  and  $n_p \rightarrow n_\parallel$ ), according to the relations

$$\begin{aligned} \frac{2\pi}{\lambda_s} dn_\perp \sqrt{1 - \left(\frac{n_0}{n_\perp}\right)^2} = m\pi &\Rightarrow \lambda_s(m) = \frac{2d}{m} n_\perp \sqrt{1 - \left(\frac{n_0}{n_\perp}\right)^2}, \\ \frac{2\pi}{\lambda_p} dn_\parallel \sqrt{1 - \left(\frac{n_0}{n_\parallel}\right)^2} = n\pi &\Rightarrow \lambda_p(n) = \frac{2d}{n} n_\parallel \sqrt{1 - \left(\frac{n_0}{n_\parallel}\right)^2}. \end{aligned} \quad (2.91)$$

It is obvious that the leaky modes can escape only through the edges of the substrate (in the form evanescent waves) if the condition for total internal reflection is satisfied on the substrate-air interface. Finally, as noted in [4], the presence of sliding modes is a significant channel of energy loss responsible for quenching band-edge lasing in chiral nematic LCs.

In this chapter we have detailed the principal analytical treatments employed in bibliography to analyse light propagation in nematic and chiral nematic

liquid crystal cells. Conclusions and formulae derived herein will serve as a basic means to develop our quantitative methods in the subsequent sections.



# Bibliography

- [1] V. A. BELYAKOV, *Diffraction Optics of Complex-Structured Periodic Media*, ch. 2, Springer-Verlag, New York, 1992.
- [2] V. A. BELYAKOV AND S. V. SEMENOV, *Optical Edge Modes in Photonic Liquid Crystals*, JETP, **109**, pp. 687-699 (2009).
- [3] HL. DE VRIES, *Rotatory Power and Other Optical Properties of Certain Liquid Crystals*, Acta Cryst., **4**, pp. 219-226 (1951).
- [4] S. P. PALTO, *Lasing in Liquid Crystal Thin Films*, JETP, **103**, pp.472-479 (2006).
- [5] DWIGHT. W. BERREMAN, *Optics in Stratified and Anisotropic Media:4x4 Matrix Formulation*, J. Opt. Soc. Am. , **62**, pp. 502-510 (1972).
- [6] A. YARIV AND P. YEH, *Photonics: Optical Electronics in Modern Communications*, ch. 12, 6th ed., Oxford University Press, US, 2006.

# Chapter 3

## The density of photon states

### 3.1 The rôle and the calculation of the DOS

In this chapter we will outline the main results of the analytic calculation of the DOS from the general treatment of 1D periodic media presented in [1]-[2], and we will subsequently focus on chiral nematics, where the aforementioned method has been applied to interpret experimental results [3].

Combining Maxwell's equations in the absence of charge density  $\rho$  (which implies also that the electrostatic potential  $\phi$  is zero) and current density  $\mathbf{J}$ , the vector potential  $\mathbf{A}$  is the solution of the equation

$$\mathbf{curl}(\mathbf{curl}\mathbf{A}) + \frac{\varepsilon(\mathbf{r})}{c^2} \frac{\partial^2}{\partial t^2} \mathbf{A} = \mathbf{0}. \quad (3.1)$$

The solution is sought in the form  $\mathbf{A}_{\mathbf{k}}(\mathbf{r}, t) = \mathbf{a}_{\mathbf{k}}(\mathbf{r}, t) \exp(-i\omega_{\mathbf{k}}t)$ . Substitution in the above yields the Helmholtz eigenvalue equation

$$\mathbf{curl}[\mathbf{curl}\mathbf{a}_{\mathbf{k}}(\mathbf{r})] - \frac{\omega_{\mathbf{k}}^2 \varepsilon(\mathbf{r})}{c^2} \mathbf{a}_{\mathbf{k}}(\mathbf{r}) = \mathbf{0}. \quad (3.2)$$

The amplitudes  $\mathbf{a}_{\mathbf{k}}(\mathbf{r})$  obey the transverse gauge condition  $\text{div}[\varepsilon(\mathbf{r})\mathbf{a}_{\mathbf{k}}(\mathbf{r})] = 0$  (called also a  $\varepsilon_{\perp}$  vector) and satisfy the orthogonality relation

$$\int \mathbf{a}_{\mathbf{k}}^*(\mathbf{r}')\mathbf{a}_{\mathbf{k}}(\mathbf{r})d^3\mathbf{k} = \overset{\leftrightarrow}{\delta}_{\varepsilon_{\perp}}(\mathbf{r}' - \mathbf{r}). \quad (3.3)$$

The inhomogeneous Helmholtz equation for the vector potential in the presence of  $\mathbf{J}$  reads

$$\text{curl}[\text{curl}\mathbf{A}(\mathbf{r}, t)] + \frac{\varepsilon(\mathbf{r})}{c^2} \frac{\partial}{\partial t^2} \mathbf{A}(\mathbf{r}, t) = \mu_0 \mathbf{J}, \quad (3.4)$$

assuming  $\mu = 1$ . The problem is solved with the help of the so-called dyadic Green's function  $\overset{\leftrightarrow}{\mathbf{G}}$  which satisfies the inhomogeneous wave equation

$$\text{curl}[\text{curl} \overset{\leftrightarrow}{\mathbf{G}}(\mathbf{r}, t; \mathbf{r}', t')] + \frac{\varepsilon(\mathbf{r})}{c^2} \frac{\partial^2}{\partial t^2} \overset{\leftrightarrow}{\mathbf{G}}(\mathbf{r}, t; \mathbf{r}', t') = \delta(t-t') \overset{\leftrightarrow}{\delta}_{\varepsilon_{\perp}}(\mathbf{r} - \mathbf{r}'), \quad (3.5)$$

with the time conditions

$$\begin{aligned} \overset{\leftrightarrow}{\mathbf{G}}(\mathbf{r}, t; \mathbf{r}', t')|_{t=t'} &= \mathbf{0}, \\ \frac{\partial}{\partial t} \overset{\leftrightarrow}{\mathbf{G}}(\mathbf{r}, t; \mathbf{r}', t')|_{t=t'} &= c^2 \overset{\leftrightarrow}{\delta}_{\varepsilon_{\perp}}(\mathbf{r} - \mathbf{r}') \end{aligned} \quad (3.6)$$

Green's function is often written in terms of the propagator  $\overset{\leftrightarrow}{\mathbf{D}}(\mathbf{r}, t; \mathbf{r}', t')$  as  $\overset{\leftrightarrow}{\mathbf{G}}(\mathbf{r}, t; \mathbf{r}', t') = u(t-t') \overset{\leftrightarrow}{\mathbf{D}}(\mathbf{r}, t; \mathbf{r}', t')$ , where  $u(t-t')$  is the Heaviside function. The function  $\overset{\leftrightarrow}{\mathbf{D}}(\mathbf{r}, t; \mathbf{r}', t')$  satisfies the same time conditions as  $\overset{\leftrightarrow}{\mathbf{G}}(\mathbf{r}, t; \mathbf{r}', t')$ .

The propagator can be written as an expansion in terms of the normal mode amplitudes. Considering the time translation invariance and the parity of the propagator, we can write

$$\overset{\leftrightarrow}{\mathbf{D}}(\mathbf{r}, t; \mathbf{r}', t') = \int \mathbf{b}_{\mathbf{k}}(\mathbf{r}') \mathbf{a}_{\mathbf{k}}(\mathbf{r}) \sin[\omega_{\mathbf{k}}(t - t')] d^3 \mathbf{k} = \int \mathbf{a}_{\mathbf{k}}^*(\mathbf{r}') \mathbf{a}_{\mathbf{k}}(\mathbf{r}) d^3 \mathbf{k}. \quad (3.7)$$

The coefficients  $\mathbf{b}_{\mathbf{k}}(\mathbf{r}')$  can be determined by the time derivative and the orthogonality conditions as follows

$$\begin{aligned} \frac{\partial}{\partial t} \overset{\leftrightarrow}{\mathbf{D}}(\mathbf{r}, t; \mathbf{r}', t') \Big|_{t=t'} &= c^2 \overset{\leftrightarrow}{\delta}_{\varepsilon_{\perp}}(\mathbf{r} - \mathbf{r}') \\ &= \int \mathbf{b}_{\mathbf{k}}(\mathbf{r}') \mathbf{a}_{\mathbf{k}}(\mathbf{r}) \omega_{\mathbf{k}} d^3 \mathbf{k} = c^2 \int \mathbf{a}_{\mathbf{k}}^*(\mathbf{r}') \mathbf{a}_{\mathbf{k}}(\mathbf{r}) d^3 \mathbf{k}. \end{aligned} \quad (3.8)$$

By virtue of the orthogonality relation

$$\int \mathbf{a}_{\mathbf{k}'}^*(\mathbf{r}) \mathbf{a}_{\mathbf{k}}(\mathbf{r}) dV = \delta(\mathbf{k} - \mathbf{k}'), \quad (3.9)$$

we obtain the relation  $\mathbf{b}_{\mathbf{k}}(\mathbf{r}') = \frac{c^2}{\omega_{\mathbf{k}}} \mathbf{a}_{\mathbf{k}}^*(\mathbf{r}')$ .

Then, the dyadic Green's function becomes

$$\overset{\leftrightarrow}{\mathbf{G}}(\mathbf{r}, t; \mathbf{r}', t') = c^2 u(t - t') \int \mathbf{a}_{\mathbf{k}}^*(\mathbf{r}') \mathbf{a}_{\mathbf{k}}(\mathbf{r}) \frac{\sin[\omega_{\mathbf{k}}(t - t')]}{\omega_{\mathbf{k}}} d^3 \mathbf{k}. \quad (3.10)$$

A current density (hence a radiating time varying electric dipole moment) will be immersed in its own electric field emitted at earlier times which has been Bragg-reflected in a periodic medium. The dyadic Green's function will be used to address the problem, since it contains all information about the boundary conditions and the dielectric permittivity profile. The rate of change of kinetic energy of a system of charged particles is equal (and opposite) to the rate of change of work done by the moving charges against a surrounding electric field. Denoting the latter by  $P(t)$  we have [4]

$$P(t) = - \sum_a q_a \mathbf{E} \mathbf{v}_a = - \int \mathbf{J}(\mathbf{r}, t) \cdot \mathbf{E}(\mathbf{r}, t) dV. \quad (3.11)$$

Since  $\mathbf{E} = -\frac{\partial \mathbf{A}}{\partial t}$  we have

$$P(t) = \int \mathbf{J}(\mathbf{r}, t) \cdot \mathbf{E}(\mathbf{r}, t) dV = \int \mathbf{J}(\mathbf{r}, t) \cdot \frac{\partial \mathbf{A}}{\partial t}(\mathbf{r}, t) dV, \quad (3.12)$$

where

$$\begin{aligned} \mathbf{A}(\mathbf{r}, t) &= \mu_0 \int_{-\infty}^{+\infty} \int_V \overset{\leftrightarrow}{\mathbf{G}}(\mathbf{r}, t; \mathbf{r}', t') \mathbf{J}(\mathbf{r}', t) dt' dV' \\ &= \mu_0 \int_{-\infty}^t \int_V \overset{\leftrightarrow}{\mathbf{D}}(\mathbf{r}, t; \mathbf{r}', t') \mathbf{J}(\mathbf{r}', t) dt' dV'. \end{aligned} \quad (3.13)$$

By virtue of Leibniz's rule we have

$$\begin{aligned} &\frac{\partial}{\partial t} \int_{-\infty}^t \int_V \overset{\leftrightarrow}{\mathbf{D}}(\mathbf{r}, t; \mathbf{r}', t') \mathbf{J}(\mathbf{r}', t) dV' dt' \\ &= \int_{-\infty}^t \int_V \frac{\partial \overset{\leftrightarrow}{\mathbf{D}}}{\partial t}(\mathbf{r}, t; \mathbf{r}', t') \mathbf{J}(\mathbf{r}', t) dV' dt' + \int_V \overset{\leftrightarrow}{\mathbf{D}}(\mathbf{r}, t; \mathbf{r}', t) \mathbf{J}(\mathbf{r}', t) dV' \\ &= \int_{-\infty}^t \int_V \frac{\partial \overset{\leftrightarrow}{\mathbf{D}}}{\partial t}(\mathbf{r}, t; \mathbf{r}', t') \mathbf{J}(\mathbf{r}', t) dV' dt', \end{aligned} \quad (3.14)$$

since the propagator has a time dependence of the form  $\sin[\omega_{\mathbf{k}}(t-t')]$ . Hence, the power can be written as

$$\begin{aligned} P(t) &= \mu_0 c^2 \int_k \int_{-\infty}^t \int_V \int_V [\mathbf{J}(\mathbf{r}, t) \cdot \mathbf{a}_{\mathbf{k}}(\mathbf{r})][\mathbf{J}(\mathbf{r}', t') \cdot \mathbf{a}_{\mathbf{k}}^*(\mathbf{r}')] \times \\ &\quad \times \cos[\omega_{\mathbf{k}}(t-t')] dt' dV dV' d^3 \mathbf{k}. \end{aligned} \quad (3.15)$$

The total energy emitted by the localized source up to time  $T$  is

$$\begin{aligned}
U(T) &= \mu_0 c^2 \int_{-\infty}^T P(t) dt \\
&= \mu_0 \frac{c^2}{2} \int_k \left| \int_{-\infty}^T \int_V \mathbf{J}(\mathbf{r}, t) \cdot \mathbf{a}_k(\mathbf{r}) \exp(-i\omega_k t) dV dt \right|^2 d^3 \mathbf{k},
\end{aligned} \tag{3.16}$$

where we have written  $\cos[\omega_k(t - t')] = \Re(\exp[i\omega_k(t - t')])$ , taken the  $\Re$  sign out of the integral since  $\mathbf{J}$  is real, and changed the limits  $\int_{-\infty}^T dt \int_{-\infty}^t dt' = \frac{1}{2} \int_{-\infty}^T \int_{-\infty}^T dt dt'$ , since the area of the triangle is half that of the parallelogram with edges

$$(-\infty, -\infty), \quad (-\infty, T), \quad (T, T), \quad (T, -\infty)$$

We will now draw parallels between the above procedure and the total excitation probability in the context of time-dependent perturbation theory [5] in the so-called ‘first quantization’ (where the fields are non-quantized). According to the standard first-order result, the transition probability (which is the modulus squared of the first order coefficient  $c_{fi}(t)$ ) between the bound atom states  $|i\rangle$  (initial) and  $|f\rangle$  (final) reads

$$|c_{fi}(t)|^2 = \frac{1}{\hbar^2} \left| \int_{-\infty}^t V_{fi}(t') \exp(i\omega_{fi} t') dt' \right|^2, \tag{3.17}$$

where  $V_{fi}(t) = \langle f | \hat{V}(t) | i \rangle$  are the matrix elements of the time-dependent perturbation (of the first order of smallness), and the term  $\exp(i\omega_{fi} t')$  is due to the inherent time dependence of the stationary states. If we assume a time-dependent perturbation operator of the form

$$\hat{V}(t) = [\hat{F} \exp(-i\omega_0 t) + \hat{G} \exp(i\omega_0 t)] u(t), \tag{3.18}$$

with  $\partial\hat{F}/\partial t = \partial\hat{G}/\partial t = 0$ . The Hermiticity condition of the operator  $\hat{V}(t)$  imposes that  $\hat{G} = \hat{F}^\dagger$  whence  $G_{fi} = F_{if}^*$ . Inserting the expression  $\hat{V}_{fi}(t) = \{F_{fi} \exp[i(\omega_{fi} - \omega_0)t] + F_{if}^* \exp[i(\omega_{fi} + \omega_0)t]\}u(t)$  in (3.17) we obtain

$$|c_{fi}(t)|^2 \cong \frac{1}{\hbar^2} |F_{fi}|^2 \frac{\sin^2\left(\frac{\omega_{fi} - \omega_0}{2}t\right)}{\left(\frac{\omega_{fi} - \omega_0}{2}\right)^2}, \quad (3.19)$$

where we have assumed  $\omega_{fi} \rightarrow \omega_0$  (resonance) so that the term containing the factor  $\sin[(\omega_{if} + \omega_0)t/(\omega_{if} + \omega_0)]$  is negligible in comparison to  $\sin[(\omega_{if} - \omega_0)t/(\omega_{if} - \omega_0)]$ .

We note that

$$\lim_{t \rightarrow \infty} \frac{\sin^2 at}{\pi t a^2} = \delta(a), \quad (3.20)$$

so that for  $t \rightarrow \infty$  (in the steady state) the transition probability reads

$$\mathcal{P}(t) = |c_{fi}(t)|^2 = \frac{2}{\hbar^2} |F_{fi}|^2 \pi t \delta(\omega_{fi} - \omega_0). \quad (3.21)$$

The transition rate then is

$$\Gamma = \frac{d\mathcal{P}}{dt} = \frac{2}{\hbar^2} |F_{fi}|^2 \pi \delta(\omega_{fi} - \omega_0). \quad (3.22)$$

In our case, the radiating dipole located at the position  $\mathbf{r} = \mathbf{r}_0$  corresponds to a current density

$$\mathbf{J}(\mathbf{r}, t) = \omega_0 \mathbf{d} \cos(\omega_0 t) \delta(\mathbf{r} - \mathbf{r}_0) u(t). \quad (3.23)$$

Taking the dot product with the normalized eigenwave amplitudes  $\mathbf{a}_{\mathbf{k}}(\mathbf{r})$  we produce the scalar quantity

$$\tilde{V} = \tilde{F}[\exp(-i\omega_0 t) + \exp(i\omega_0 t)]u(t), \quad (3.24)$$

where  $\tilde{F} \propto \mathbf{d} \cdot \mathbf{a}_{\mathbf{k}}(\mathbf{r})$  plays the rôle of the operator  $\hat{F}$ , and in our case  $\tilde{F} = \tilde{G}$ . We also write  $\omega_{\mathbf{k}}$  instead of  $\omega_{fi}$ , as we are dealing with unbound photon states with momentum  $\hbar\mathbf{k}$ . Neglecting the term containing  $\exp[i(\omega_{\mathbf{k}} + \omega_0)t]$ , the emission energy, according to (3.16) reads

$$U(t) = \int_k \tilde{F}^2 \frac{\sin^2\left(\frac{\omega_{fi} - \omega_0}{2}t\right)}{\left(\frac{\omega_{fi} - \omega_0}{2}\right)^2} d^3\mathbf{k}. \quad (3.25)$$

Similarly, according to (3.16), the emitted energy for the localized dipole reads

$$U(t) = \mu_0 \frac{c^2 \omega_0^2 d^2}{2} \int_k \left| \hat{\mathbf{d}} \cdot \mathbf{a}_{\mathbf{k}}(\mathbf{r}) \right|^2 \delta(\mathbf{r} - \mathbf{r}_0) \frac{\sin^2\left[\left(\frac{\omega_{\mathbf{k}} - \omega_0}{2}\right)t\right]}{\left(\frac{\omega_{\mathbf{k}} - \omega_0}{2}\right)^2} d^3\mathbf{k}. \quad (3.26)$$

Hence, for  $t \rightarrow \infty$ , the emission rate can be written according to (3.20) as

$$\begin{aligned} P(t \rightarrow \infty) &= \mu_0 \frac{\pi c^2}{4} \omega_0^2 d^2 \int_k \int_V \left| \hat{\mathbf{d}} \cdot \mathbf{a}_{\mathbf{k}}(\mathbf{r}) \right|^2 \delta(\mathbf{r} - \mathbf{r}_0) \delta(\omega_{\mathbf{k}} - \omega_0) dV d^3\mathbf{k} \\ &= \mu_0 \frac{\pi c^2}{4} \omega_0^2 d^2 \int_k \left| \hat{\mathbf{d}} \cdot \mathbf{a}_{\mathbf{k}}(\mathbf{r}_0) \right|^2 \delta(\omega_{\mathbf{k}} - \omega_0) d^3\mathbf{k}. \end{aligned} \quad (3.27)$$

In the free space (where  $\varepsilon(\mathbf{r}) = 1$ ), the modes are plane waves

$$\mathbf{a}_{\mathbf{k}}(\mathbf{r}) = (2\pi)^{-3/2} \exp(-i\mathbf{k} \cdot \mathbf{r}) \hat{\mathbf{e}}_{\mathbf{k}}, \quad (3.28)$$

where  $\hat{\mathbf{e}}_{\mathbf{k}}$  is the unit polarization vector. The waves, being transverse, satisfy  $\mathbf{k} \cdot \mathbf{e}_{\mathbf{k}} = 0$ . These solutions immediately also satisfy the orthogonality/normalization conditions (3.3), (3.9). The dispersion relation is  $k = \omega/c$ , so that we can write the ‘volume element’ in the  $k$ -space as  $d^3\mathbf{k} = d\Omega_{\mathbf{k}}k^2dk$ . The power-emitted by a dipole in free space is

$$\begin{aligned} P_{\text{free}}^{3D} &= \mu_0 \frac{c^2\pi}{4 \cdot 8\pi^3c} \omega_0^2 d^2 \int_k k^2 \delta(k - k_0) dk \int |\hat{\mathbf{d}} \cdot \hat{\mathbf{e}}_{\mathbf{k}}|^2 d\Omega_{\mathbf{k}} \\ &= \mu_0 \frac{k_0^2 \omega_0^2 d^2}{32\pi^2 c} \int \sin^2(\theta_{\mathbf{k}}) d\Omega_{\mathbf{k}}, \end{aligned} \quad (3.29)$$

where we have assumed that the electric dipole is oriented along the  $z$ -axis (in the  $k$ -space), so that  $\mathbf{e}_{\mathbf{k}} \equiv \hat{\theta}_{\mathbf{k}}$  (and  $\hat{\mathbf{z}} \cdot \hat{\theta}_{\mathbf{k}} = \sin\theta_{\mathbf{k}}$ ). The final result can be recast in the familiar form

$$P_{\text{free}}^{3D} = \frac{1}{12} \frac{\mu_0 \omega_0^4 d^2}{\pi c}, \quad (3.30)$$

in which the multiplicative factor of 2 accounts for the two independent polarizations (degrees of freedom) of the plane wave.

Let us now return to the expression (3.22), and consider explicitly spontaneous emission of an atom in a medium with a non-uniform dielectric profile. We will distinguish two states: the state  $|1, \{0\}\rangle$ , corresponding to the excited state of the atom with the photon occupation number equal to 0, and the state  $|0, \{1\}_{\mathbf{k}}\rangle$ , corresponding to the ground state with one photon in the transverse mode with wave-vector  $\mathbf{k}$ . Assuming a continuous distribution of modes in the  $k$ -space, the spontaneous emission probability in the steady state can be written as <sup>†</sup>

---

<sup>†</sup>Hereinafter in this chapter, the vectors will denote (formally) vector operators.

$$\begin{aligned}
\mathcal{P}_{\text{total}} &= \frac{1}{\hbar^2} \int_k |\langle 0, \{1\}_{\mathbf{k}} | \mathbf{d} \cdot \mathbf{E}_{\mathbf{k}}(\mathbf{r}_0) | 1, \{0\} \rangle|^2 \frac{\sin^2\left(\frac{\omega_{\mathbf{k}} - \omega_0}{2} t\right)}{\left(\frac{\omega_{\mathbf{k}} - \omega_0}{2}\right)^2} dV_{\mathbf{k}} \\
&= \frac{\pi}{\hbar^2} \int |\langle 0, \{1\}_{\mathbf{k}} | \mathbf{d} \cdot \mathbf{E}_{\mathbf{k}}(\mathbf{r}_0) | 1, \{0\} \rangle|^2 \frac{\sin^2\left(\frac{\omega_{\mathbf{k}} - \omega_0}{2} t\right)}{\left(\frac{\omega_{\mathbf{k}} - \omega_0}{2}\right)^2} \frac{dV_{\mathbf{k}}}{d\omega_{\mathbf{k}}} d\omega_{\mathbf{k}}.
\end{aligned} \tag{3.31}$$

We define  $\rho(\omega_{\mathbf{k}}) = \frac{dV_{\mathbf{k}}}{d\omega_{\mathbf{k}}}$  as the Density of Photon States (DOS), and also change variables in the above integral to  $\alpha = (\omega_{\mathbf{k}} - \omega_0)/2$ , so that:

$$\begin{aligned}
\mathcal{P}_{\text{total}} &= \frac{2\pi}{\hbar^2} \int |\langle 0, \{1\}_{\mathbf{k}} | \mathbf{d} \cdot \mathbf{E}_{\mathbf{k}}(\mathbf{r}_0) | 1, \{0\} \rangle|^2 t \frac{\sin^2(\alpha t)}{\pi t \alpha^2} \rho(2\alpha + \omega_0) d\alpha \\
&\stackrel{t \rightarrow \infty}{=} \frac{2\pi}{\hbar^2} \int |\langle 0, \{1\}_{\mathbf{k}} | \mathbf{d} \cdot \mathbf{E}_{\mathbf{k}}(\mathbf{r}_0) | 1, \{0\} \rangle|^2 t \delta(\alpha) \rho(2\alpha + \omega_0) d\alpha \tag{3.32} \\
&= \frac{2\pi}{\hbar^2} |\langle 0, \{1\}_{\mathbf{k}} | \mathbf{d} \cdot \mathbf{E}_{\mathbf{k}}(\mathbf{r}_0) | 1, \{0\} \rangle|^2 t \rho(\omega_0),
\end{aligned}$$

yielding the spontaneous transition rate

$$\Gamma = \frac{2\pi}{\hbar^2} |\langle 0, \{1\}_{\mathbf{k}} | \mathbf{d} \cdot \mathbf{E}_{\mathbf{k}}(\mathbf{r}_0) | 1, \{0\} \rangle|^2 \rho(\omega_0). \tag{3.33}$$

The above expression is known as ‘‘Fermi’s Golden Rule’’ [1]. As we have mentioned, this is a result derived by applying first order perturbation theory for the small perturbation  $\mathbf{d} \cdot \mathbf{E}_{\mathbf{k}}(\mathbf{r}_0)$  in the Hamiltonian. Hence, the result is said to be valid for weak coupling between the atom and the field. An analogous result can be derived classically from (3.16), according to which the emission rate normalized to the free space rate is

$$\gamma_{\text{classical}} = \omega_0 |\mathbf{d} \cdot \mathbf{a}_{\mathbf{k}}(\mathbf{r}_0)|^2 \left. \frac{dk}{d\omega} \right|_{\omega_0} \quad (3.34)$$

and the quantity  $\left. \frac{dk}{d\omega} \right|_{\omega_0}$  is the DOS, defined as the number of wave-numbers  $k$  per unit frequency  $\omega$ , and consequently is the reciprocal of the group velocity,  $v_g(\omega) = \frac{1}{\rho(\omega)} = \frac{d\omega}{dk}$ . This is the velocity of the pulse envelope moving through the one-dimensional (1D) ‘potential’  $n(x)$ .

Let us assume a lossless and dispersion-less refractive index profile  $n(x)$ , non-zero over an interval  $[0, L]$ . The Helmholtz equation (3.2) reduces to

$$\frac{d^2 a}{dx^2} + \frac{\omega_k^2}{c^2} \varepsilon(x) a(x) = 0. \quad (3.35)$$

The DOS can be obtained by extracting the dispersion relation  $k = k(\omega)$  from the above equation, solved by numerical methods. It can be also obtained by a more elegant technique (known as the Wigner method) based on the complex transmission coefficient of a structure, as detailed below. The complex transmission coefficient of any structure can be written as  $t(\omega) = x(\omega) + iy(\omega) = \sqrt{T} \exp(i\phi)$ , where  $\phi = \arctan[y(\omega)/x(\omega)]$ . Here,  $\phi$  is the total phase accumulated as the light propagates through the potential. It can be also written as  $\phi = kL$ , where  $L$  is the physical path traversed by the light waves (for normal propagation it coincides with the thickness of the structure). Therefore, the dispersion relation can be written as  $\tan(kL) = y(\omega)/x(\omega)$ . Differentiating with respect to  $\omega$  we obtain

$$\frac{d}{d\omega} [\tan(kL)] = \frac{L}{d\omega} \left( \frac{x(\omega)}{y(\omega)} \right) \Rightarrow \frac{1}{\cos^2(kL)} \frac{dk}{d\omega} = \frac{1}{L} \frac{y'x - x'y}{x^2}, \quad (3.36)$$

where the prime denotes differentiation with respect to  $\omega$ . Since  $1/\cos^2\theta = 1 + \tan^2\theta$ , solving the above for  $dk/d\omega$  we obtain

$$\rho(\omega) = \frac{dk}{d\omega} = \frac{1}{L} \frac{y'x - x'y}{x^2 + y^2}. \quad (3.37)$$

We note that the above derivation is independent of the specific form of  $n(x)$  and that the transmission coefficient can be easily obtained in periodic media with the help of transfer matrix methods. More precisely, if we write the general solution of (3.35) as a superposition of right and left-propagating waves, written as  $u^\pm(x) = f^\pm(x) \exp(\pm ikx)$ , where  $f^\pm(x)$  are real envelope functions, then the column vectors  $\mathbf{u} = \begin{pmatrix} u^+ \\ u^- \end{pmatrix}$  at  $x = 0, L$  are related by

$$\mathbf{u}(0) = \begin{pmatrix} 1 \\ r \end{pmatrix} = \mathbf{M}\mathbf{u}(L) = \begin{pmatrix} A & B \\ C & D \end{pmatrix} \mathbf{u}(L) = \begin{pmatrix} A & B \\ C & D \end{pmatrix} \begin{pmatrix} t \\ 0 \end{pmatrix}, \quad (3.38)$$

where  $\mathbf{M}$  is the transfer matrix. Under time reversal, due to the symmetry of the scattering system we have

$$\begin{pmatrix} u(0)^{+*} \\ u(0)^{-*} \end{pmatrix} = \mathbf{M} \begin{pmatrix} u(L)^{+*} \\ u(L)^{-*} \end{pmatrix}. \quad (3.39)$$

Also, we have

$$\begin{pmatrix} u(0)^{-*} \\ u(0)^{+*} \end{pmatrix} = \mathbf{M}^* \begin{pmatrix} u(L)^{-*} \\ u(L)^{+*} \end{pmatrix}, \quad (3.40)$$

and combining the two we obtain the condition

$$\mathbf{M}^* = \begin{pmatrix} 0 & 1 \\ 1 & 0 \end{pmatrix} \mathbf{M} \begin{pmatrix} 0 & 1 \\ 1 & 0 \end{pmatrix}. \quad (3.41)$$

Hence, the final form of the transfer matrix reads

$$\mathbf{M} = \begin{pmatrix} \frac{1}{t} & \frac{r^*}{t^*} \\ r & \frac{1}{t^*} \end{pmatrix}. \quad (3.42)$$

By virtue of the energy conservation, we also obtain the condition  $|r|^2 + |t|^2 = R + T = 1 \Rightarrow |\mathbf{M}| = 1$  (i.e. the transfer matrix is unimodular).

From (3.42), we deduce that the eigenvalues of  $\mathbf{M}$  satisfy the equation

$$\mu^2 + \left(\frac{1}{t} + \frac{1}{t^*}\right)\mu + \frac{1 - |r|^2}{|t|^2} = 0 \Rightarrow \mu^2 + 2\Re\left(\frac{1}{t}\right)\mu + 1 = 0. \quad (3.43)$$

Since the matrix is unimodular, the two eigenvalues  $\mu^\pm$  satisfy the relation  $\mu^+\mu^- = 1$ . Furthermore, the refractive index is periodic  $n(x) = n(x + d)$ , so that Bloch's theorem is applicable, according to which only the phase of the wavefunction ( $u^\pm$  in our case) changes on moving from one cell to the other. Denoting by  $\beta$  the phase (called also the Bloch's phase), we can then write

$$\mathbf{M}\mathbf{u}_B = \exp(\pm i\beta)\mathbf{u}_B, \quad (3.44)$$

where  $\mathbf{u}_B$  are called the Bloch eigenfunctions. Evidently,

$$\mu_B^+\mu_B^- = \exp(i\beta)\exp(-i\beta) = 1. \quad (3.45)$$

Substituting the eigenvalues  $\mu_B^\pm$  into (3.43) we find that  $\cos\beta = \Re(1/t)$ . We know from the Cayley-Hamilton theorem that a square matrix is a root of its characteristic polynomial. Hence, the transfer matrix satisfies the equation

$$\mathbf{M}^2 - 2\mathbf{M}\cos\beta + \mathbb{I} = 0. \quad (3.46)$$

Will now prove by induction that

$$\mathbf{M}^N = \frac{1}{\sin \beta} \{ \sin(N\beta)\mathbf{M} - \sin[(N-1)\beta]\mathbb{I} \}. \quad (3.47)$$

For  $N = 1$  we have the trivial relation  $\mathbf{M} = \mathbf{M}$ . For  $N = 2$  the above relation yields

$$\mathbf{M}^2 = \frac{1}{\sin \beta} [\sin(2\beta)\mathbf{M} - \sin \beta \mathbb{I}] = 2 \cos \beta \mathbf{M} - \mathbb{I}, \quad (3.48)$$

which is the eigenvalue equation. Let us assume that the equality holds for  $N$ . We will prove it is true for  $N + 1$ . Multiplying the equation for  $N$  by  $\mathbf{M}$  from the right, we have

$$\begin{aligned} \mathbf{M}^{(N+1)} &= \frac{1}{\sin \beta} \{ \sin(N\beta)\mathbf{M}^2 - \sin[(N-1)\beta]\mathbf{M} \} \\ &= \frac{1}{\sin \beta} \{ \sin(N\beta)[2 \cos \beta \mathbf{M} - \mathbb{I}] - \sin[(N-1)\beta]\mathbf{M} \} \\ &= \frac{1}{\sin \beta} \{ (2 \sin[(N-1)\beta] \cos^2 \beta + 2 \cos[(N-1)\beta] \cos \beta \sin \beta - \sin[(N-1)\beta])\mathbf{M} - \sin(N\beta)\mathbb{I} \} \\ &= \frac{1}{\sin \beta} \{ (\sin[(N-1)\beta](2 \cos^2 \beta - 1)) + \sin(2\beta) \cos[(N-1)\beta]\mathbf{M} - \sin(N\beta)\mathbb{I} \} \\ &= \frac{1}{\sin \beta} \{ (\sin[(N-1)\beta] \cos(2\beta) + \sin(2\beta) \cos[(N-1)\beta])\mathbf{M} - \sin(N\beta)\mathbb{I} \} \\ &= \frac{1}{\sin \beta} \{ \sin[(N+1)\beta]\mathbf{M} - \sin(N\beta)\mathbb{I} \}, \end{aligned} \quad (3.49)$$

which we need to show. We note that the same result can be obtained via Chebyshev's identity applied to calculate  $\mathbf{M}^N$ . Identifying the components of  $\mathbf{M}^N$  with those of the matrix

$$\begin{pmatrix} \frac{1}{t_N} & \frac{r_N^*}{t_N^*} \\ \frac{r_N}{t_N} & \frac{1}{t_N^*} \end{pmatrix}, \quad (3.50)$$

we obtain

$$\begin{aligned} \frac{1}{t_N} &= \frac{1}{t} \frac{\sin(N\beta)}{N\beta} - \frac{\sin[(N-1)\beta]}{N\beta} \\ \frac{r_N}{t_N} &= \frac{r}{t} \frac{\sin(N\beta)}{N\beta}. \end{aligned} \quad (3.51)$$

For a  $N$ -period structure we can express the real and imaginary parts of  $t_N = x_N + iy_N = \sqrt{T_N} \exp(i\phi_N)$  in terms of the constituents of  $t = x + iy$  as follows

$$\begin{aligned} x_N &= \frac{x \sin(N\beta) \sin \beta - (x^2 + y^2) \sin \beta \sin[(N-1)\beta]}{\sin^2(N\beta) - 2x \sin(N\beta) \sin[(N-1)\beta] + (x^2 + y^2) \sin^2[(N-1)\beta]} \\ y_N &= \frac{y \sin(N\beta) \sin \beta}{\sin^2(N\beta) - 2x \sin(N\beta) \sin[(N-1)\beta] + (x^2 + y^2) \sin^2[(N-1)\beta]} \end{aligned} \quad (3.52)$$

The Bloch-phase determines the pass-bands and stop-bands of the infinite-length structure, which are very close to the bands of the  $N$ -period potential mirror, exactly as it happens with chiral nematics. The Bloch phase is real when  $|\Re\{1/t\}| \leq 1$  and complex when  $|\Re\{1/t\}| > 1$  with  $\beta = i\theta$  for  $\Re\{1/t\} > 1$  and  $\beta = \pi + i\theta$  for  $\Re\{1/t\} < -1$ . In the pass-bands, the intensity transmission coefficient  $T_N$  varies sinusoidally with the Bloch phase. Taking the squared modulus of the second equation from (3.51) we obtain

$$\frac{1 - |t_N|^2}{|t_N|^2} = \frac{1 - |t|^2}{|t|^2} \frac{\sin(N\beta)}{N\beta} \Rightarrow T_N = |t_N|^2 = 1 + \frac{\sin^2(N\beta)}{\sin^2 \beta} \left( \frac{1}{|t|^2} - 1 \right), \quad (3.53)$$

which shows that  $T_N$  is periodic in  $\beta$  with period  $\pi/N$ . In the pass-band,  $\beta$  traverses a distance of  $\pi$ . In the first pass-band  $\beta \in [0, \pi]$  in the second  $\beta \in [\pi, 3\pi]$  and so forth. If we make the substitution  $z_N = y_N/x_N$ , then the DOS for the  $N$ -period structure can be calculated as follows

$$\rho_N = \frac{dk_N}{d\omega} = \frac{1}{L} \frac{d}{d\omega} \arctan(z_N) = \frac{1}{L} \frac{z'_N}{1+z_N^2}, \quad (3.54)$$

with  $L = Nd$  being the total length of the structure. Since the expressions for  $x_N$  and  $y_N$  have the same denominator, we can write

$$z_N = \frac{y \sin(N\beta)}{x \sin(N\beta) - (x^2 + y^2) \sin[(N-1)\beta]}. \quad (3.55)$$

Since we have defined  $\cos \beta = \Re(1/t)$  we can use the scalar quantities  $\eta_1 \equiv \cos \beta = x/|t|^2$  and  $\eta_2 = y/|t|^2$  to recast  $z_N$  into the simpler form

$$z_N = \frac{z \cos \beta \sin(N\beta)}{\cos \beta \sin(N\beta) - \sin[(N-1)\beta]} = \frac{z \cos \beta \sin(N\beta)}{\cos(N\beta) \sin(\beta)} = z \cot \beta \tan(N\beta), \quad (3.56)$$

where  $z = y/x$ . Substitution into the expression (3.54) yields

$$\rho_N = \frac{1}{L} \frac{\frac{1}{2} \left[ \frac{\sin(2N\beta)}{\sin \beta} \right] \left[ \eta'_2 + \frac{\eta_1 \eta_2 \eta'_1}{1 - \eta_1^2} \right] - N \frac{\eta_2 \eta'_1}{1 - \eta_1^2}}{\cos^2(N\beta) + \eta_2^2 \left[ \frac{\sin(N\beta)}{\sin \beta} \right]^2}. \quad (3.57)$$

In many cases, the unit cell of the periodic structure has the form of a series of steps, namely  $n(x) = n_i$ , where  $x \in [x_{i-1}, x_i)$ , with  $i = 1, 2, \dots, m$  and  $x_0 = 0$ ,  $x_m = d$ . We assume that  $n_i$  do not depend on the frequency. The transfer matrix for such a potential will be a product of matrices of two types, exactly as in the case of light propagation in a LC slab we examined in the previous

chapter. The first is the so-called ‘discontinuity’ matrix  $\Delta_{ij}$  providing information regarding reflection and transmission between the interfaces  $i$  and  $j$ . The second type is a propagation matrix  $\mathbf{P}(\mathbf{p}_i)$ , where  $\mathbf{p}_i = n_i b_i (\omega/c)$  is the phase accumulated as the light wave propagates from left to right traversing a distance  $b_i = |x_i - x_{i-1}|$  where the refractive index  $n_i$  is constant. The aforementioned matrices have the form

$$\Delta_{ij} = \begin{pmatrix} \delta_{ij}^+ & \delta_{ij}^- \\ \delta_{ij}^- & \delta_{ij}^+ \end{pmatrix}, \quad (3.58)$$

where  $\delta_{ij}^\pm = \frac{1}{2}(1 \pm n_i/n_j)$  and

$$\mathbf{P}(\mathbf{p}_i) = \begin{pmatrix} \exp(i\mathbf{p}_i) & 0 \\ 0 & \exp(-i\mathbf{p}_i) \end{pmatrix}. \quad (3.59)$$

Comparison between the form of (3.42) and  $\Delta_{ij}$  allows the identification  $\delta_{ij}^+ = 1/t_{ij}$  and  $\delta_{ij}^- = r_{ij}/t_{ij}$ . For normal incidence the elements are given by the familiar expressions

$$\begin{aligned} t_{ij} &= \frac{2n_j}{n_i + n_j}, \\ r_{ij} = -r_{ji} &= \frac{n_i - n_j}{n_i + n_j} \end{aligned} \quad (3.60)$$

We define the double-transmission and double-reflection coefficients on going across interfaces 1 and 2 as follows

$$\begin{aligned} R_{12} = -r_{12}r_{21} &= \left( \frac{n_1 - n_2}{n_1 + n_2} \right)^2, \\ T_{21} = t_{21}t_{12} &= \frac{4n_1n_2}{(n_1 + n_2)^2}. \end{aligned} \quad (3.61)$$

In order to construct the transfer matrix  $\mathbf{M}$  for a two layer unit-cell with a step-like refractive index profile

$$n(x) = \begin{cases} n_1, & x \in [0, a) \\ n_2, & x \in [a, a + b) \end{cases}. \quad (3.62)$$

The matrix propagating from left to right is

$$\begin{aligned} \mathbf{M}^{-1} &= \mathbf{P}(\mathbf{p})\mathbf{\Delta}_{12}\mathbf{P}(\mathbf{q})\mathbf{\Delta}_{21} \Rightarrow \\ \mathbf{M} &= \mathbf{\Delta}_{12}\mathbf{P}(-\mathbf{q})\mathbf{\Delta}_{21}\mathbf{P}(-\mathbf{p}), \end{aligned} \quad (3.63)$$

since  $\mathbf{P}^{-1}(\mathbf{p}) = \mathbf{P}(-\mathbf{p})$  and  $\Delta_{ij} = \Delta_{ji}^{-1}$ . Here we define  $\mathbf{p} = n_1 a \omega / c$  and  $\mathbf{q} = n_2 b \omega / c$ , with  $d = a + b$  being the period of the stack. Performing the calculations we obtain

$$\begin{aligned} \frac{1}{t} &= M_{11} = \delta_{12}^+ \delta_{21}^+ \exp[-i(\mathbf{p} + \mathbf{q})] + \delta_{12}^- \delta_{21}^- \exp[-i(\mathbf{p} - \mathbf{q})] \\ \frac{r}{t} &= M_{21} = \delta_{12}^+ \delta_{21}^- \exp[-i(\mathbf{p} + \mathbf{q})] + \delta_{12}^- \delta_{21}^+ \exp[-i(\mathbf{p} - \mathbf{q})], \end{aligned} \quad (3.64)$$

with  $M_{22} = M_{11}^*$  and  $M_{12} = M_{21}^*$ .

For a two-layer unit cell, we thus have

$$\begin{aligned} \frac{1}{t} &= \frac{1}{4n_1 n_2} [(n_1 + n_2)^2 \exp[-i(\mathbf{p} + \mathbf{q})] - (n_1 - n_2)^2 \exp[-i(\mathbf{p} - \mathbf{q})]] \\ &= \frac{(n_1 + n_2)^2}{4n_1 n_2} \exp[-i(\mathbf{p} + \mathbf{q})] \left[ 1 - \left( \frac{n_1 - n_2}{n_1 + n_2} \right)^2 \exp(2i\mathbf{q}) \right] \\ &\Rightarrow t = \frac{T_{21} \exp[-i(\mathbf{p} + \mathbf{q})]}{1 - R_{12} \exp(2i\mathbf{q})}. \end{aligned} \quad (3.65)$$

The real and imaginary parts of  $t$  for an arbitrary two-layer unit cell read

$$\begin{aligned}
x &= \frac{1}{2}(t + t^*) \\
&= \frac{1}{2}T_{12} \frac{\exp[-i(\mathbf{p} + \mathbf{q})][1 - R_{12} \exp(2i\mathbf{q})] + \exp[i(\mathbf{p} + \mathbf{q})][1 - R_{12} \exp(-2i\mathbf{q})]}{[1 - R_{12} \exp(-2i\mathbf{q})][1 - R_{12} \exp(2i\mathbf{q})]} \\
&= T_{12} \frac{\cos(\mathbf{p} + \mathbf{q}) - R_{12} \cos(\mathbf{p} - \mathbf{q})}{1 - 2R_{12} \cos(2\mathbf{q}) + R_{12}^2}.
\end{aligned} \tag{3.66}$$

Likewise,

$$\begin{aligned}
y &= \frac{1}{2i}(t - t^*) \\
&= \frac{1}{2i}T_{12} \frac{\exp[i(\mathbf{p} + \mathbf{q})][1 - R_{12} \exp(-2i\mathbf{q})] - \exp[-i(\mathbf{p} + \mathbf{q})][1 - R_{12} \exp(2i\mathbf{q})]}{[1 - R_{12} \exp(-2i\mathbf{q})][1 - R_{12} \exp(2i\mathbf{q})]} \\
&= T_{12} \frac{\sin(\mathbf{p} + \mathbf{q}) - R_{12} \sin(\mathbf{p} - \mathbf{q})}{1 - 2R_{12} \cos(2\mathbf{q}) + R_{12}^2}.
\end{aligned} \tag{3.67}$$

### 3.1.1 The quarter-wave stack

We will now focus on the special case of a quarter-wave stack (QWS), for which  $n_1 a = n_2 b = \lambda_0/4 = \pi c/(2\omega_0)$ . This case results in a significant simplification, as we can deduce from the expressions for  $x$  and  $y$ , since then  $\mathbf{p} = \mathbf{q} = \pi\omega/(2\omega_0)$ . Therefore, we can write

$$\begin{aligned}
\eta_1 &= \frac{\cos\left(\pi\frac{\omega}{\omega_0}\right) - R_{12}}{T_{12}}, & \eta_2 &= \frac{\sin\left(\pi\frac{\omega}{\omega_0}\right)}{T_{12}}, \\
\eta'_1 &= -\frac{\pi}{\omega_0} \frac{\sin\left(\pi\frac{\omega}{\omega_0}\right)}{T_{12}}, & \eta'_2 &= \frac{\pi}{\omega_0} \frac{\cos\left(\pi\frac{\omega}{\omega_0}\right)}{T_{12}},
\end{aligned} \tag{3.68}$$

required for determining  $\rho_N$ . The latter is normalized to the bulk group

velocity, defined as the period divided by the time required by the light to traverse it neglecting reflections. For a QWS this quantity is

$$v_{\text{bulk}} = \frac{1}{\rho_{\text{bulk}}} = \frac{a+b}{\frac{an_1}{c} + \frac{bn_2}{c}} = c \left( \frac{1}{n_1} + \frac{b}{a} \frac{1}{n_1} \right) = c \left( \frac{1}{n_1} + \frac{1}{n_2} \right). \quad (3.69)$$

The peaks of  $\rho_N$  and  $T_N$  nearly coincide, with the approximation improving with increasing  $N$ . In the left pass-band, the latter occur at  $\beta N = m\pi$ , with  $m \in 0, 1, \dots, N-1$  and at these values of the Bloch phase the denominator of  $\rho_N$  attains nearly its smallest value. The approximation improves for large  $N$  since then  $\eta_2 \rightarrow 0$ . Since at these values of  $\beta$ ,  $\sin(2N\beta) = 0$ , the numerator is proportional to  $N$ . At these approximate maxima, the expression for the DOS is

$$\rho_N^{\text{max}} \cong -\frac{1}{Nd} N \frac{\eta_2 \eta_1'}{1 - \eta_1^2} \Big|_{\beta = \frac{m\pi}{N}}. \quad (3.70)$$

For a QWS, the period of the structure can be written as

$$d = a + b = \frac{\pi c}{2\omega_0} \left( \frac{1}{n_1} + \frac{1}{n_2} \right) = \frac{\pi}{\rho_{\text{bulk}} \omega_0}. \quad (3.71)$$

We can also write

$$\begin{aligned} \sin^2 \left( \pi \frac{\omega}{\omega_0} \right) &= 1 - (T_{12} \cos \beta + 1 - T_{12})^2 \\ &= T_{12}^2 (1 - \cos \beta)^2 - 2T_{12} (1 - \cos \beta) \\ &= 4T_{12}^2 \sin^4 \left( \frac{\beta}{2} \right) - 4T_{12} \sin^2 \left( \frac{\beta}{2} \right) \end{aligned} \quad (3.72)$$

and

$$1 - \eta_1^2 = \sin^2 \beta = 4 \sin^2 \left( \frac{\beta}{2} \right) \cos^2 \left( \frac{\beta}{2} \right). \quad (3.73)$$

The DOS maxima for a QWS are then

$$\rho_{\max}^{\lambda/4} \Big|_{\beta = \frac{m\pi}{N}} = \rho_{\text{bulk}} \frac{1 - T_{12} \sin^2 \left( \frac{m\pi}{2N} \right)}{T_{12} \cos^2 \left( \frac{m\pi}{2N} \right)}. \quad (3.74)$$

For the closest edge to the band-gap (called the ‘long-wavelength edge’ below)  $m = N - 1$  (corresponding to the last maximum in the pass-band), and when  $N \rightarrow \infty$  we can keep in our expression terms up to the second order as below

$$\begin{aligned} \rho_{\max}^{\lambda/4} \Big|_{\beta = \frac{(N-1)\pi}{N}} &= \rho_{\text{bulk}} \frac{1 - T_{12} \cos^2 \left( \frac{\pi}{2N} \right)}{T_{12} \sin^2 \left( \frac{\pi}{2N} \right)} \simeq \rho_{\text{bulk}} \frac{1 - T_{12} \left( 1 - \frac{1}{2} \left( \frac{\pi}{2N} \right)^2 \right)^2}{T_{12} \left( \frac{\pi}{2N} \right)^2} \\ &\simeq \rho_{\text{bulk}} \frac{1 - T_{12} + T_{12} \left( \frac{\pi}{2N} \right)^2}{T_{12} \left( \frac{\pi}{2N} \right)^2} = \rho_{\text{bulk}} \frac{R_{12} + T_{12} \left( \frac{\pi}{2N} \right)^2}{T_{12} \left( \frac{\pi}{2N} \right)^2} \\ &\propto \frac{R_{12}}{T_{12}} N^2 \propto \frac{(n_1 - n_2)^2}{n_1 n_2} N^2. \end{aligned} \quad (3.75)$$

Regarding the latter symmetric expression with respect to  $n_1, n_2$  as a function of  $n_2$  (without loss of generality) with fixed  $n_1 < n_2$  then the above function increases with increasing difference  $n_2 - n_1$ . Keeping fixed the product  $n_1 n_2$  we find that for  $N$  sufficiently large, the maximum value of the DOS at the LWE is determined by the product  $(n_1 - n_2)N = (\Delta n)N$ . Increasing any of these terms of the product leads to enhanced feedback in the distributed Bragg-structure. The above conclusions are verified by Figure 3.1 that follows.

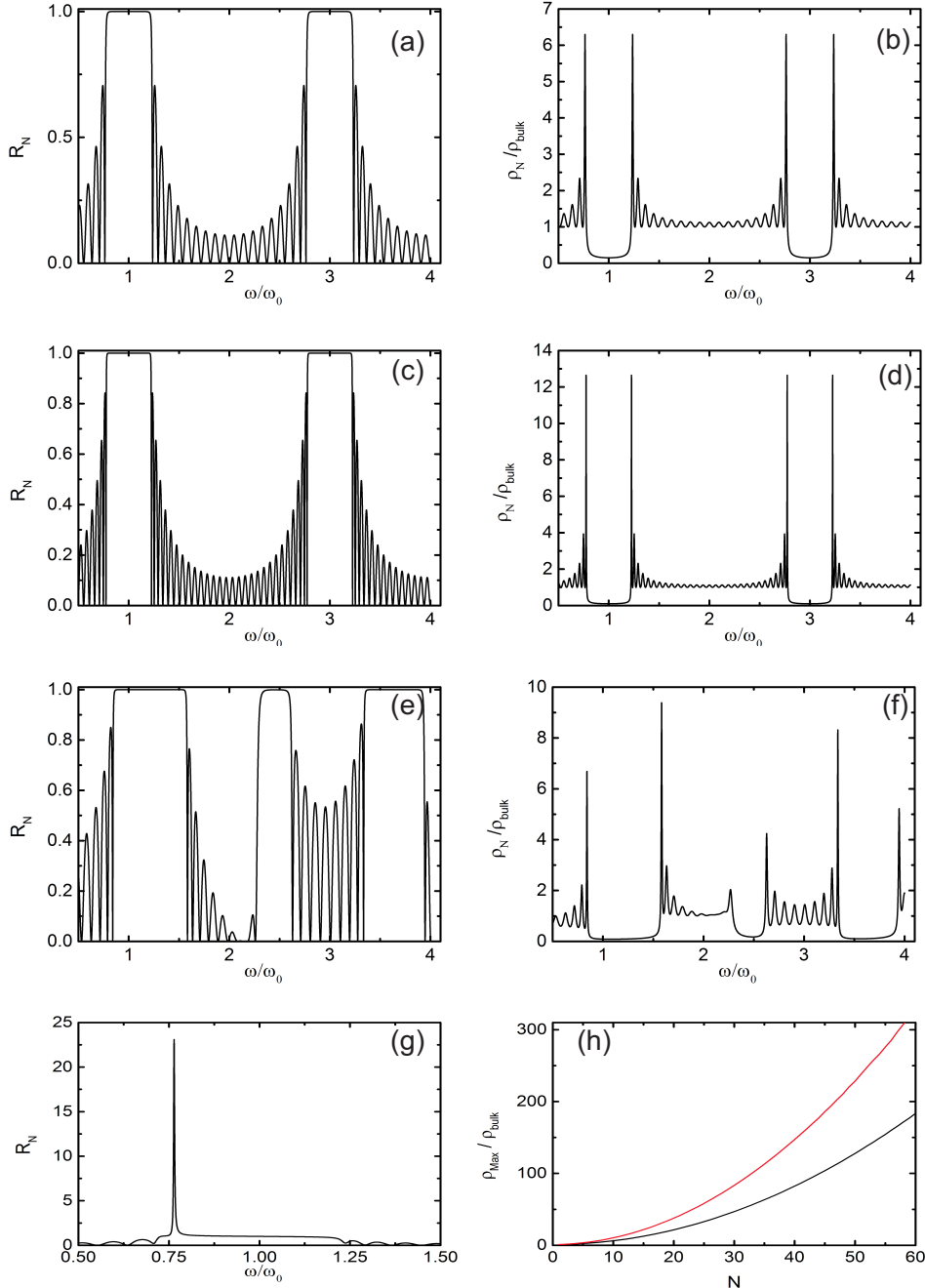


Figure 3.1: Quarter Wave Stack. In (a), (b) Intensity Reflection Coefficient and DOS respectively for  $n_1 = 1, n_2 = 2$  and  $N = 10$ . In (c), (d) Intensity Reflection Coefficient and DOS respectively for  $n_1 = 1, n_2 = 2$  and  $N = 15$ . In (e), (f) Intensity Reflection Coefficient and DOS respectively for  $n_1 = 1, n_2 = 2$  and  $N = 10$  for oblique propagation in the structure such that  $k_{\perp} = (\sqrt{2}/2)k_0$ . In (g) Intensity Reflection for  $n_1 = 1 - 0.05i, n_2 = 2 - 0.05i$  and  $N = 10$  and in (h) Maximum value of DOS as a function of the number of layers  $N$  for a stack with  $n_1 = 1, n_2 = 2$  (black curve) and for a stack with  $n_1 = 1, n_2 = 2.5$  (red curve).

At the mid-gap (mg) frequency, the Bragg-phase is  $\beta_{mg} = \pi + i\theta_{mg}$ , such that  $\cos \beta$  has there an extremum. This implies that at  $\omega = \omega_0$ ,  $\eta'_1 = 0$ . For the Bragg-phase we write

$$\begin{aligned} \cos \beta_{mg} &= \cos(\pi + i\theta_{mg}) = -\cosh \theta_{mg} = \frac{\cos \pi - R_{12}}{T_{12}} \Rightarrow \\ \cosh \theta_{mg} &= \frac{1 + R_{12}}{T_{12}} = \frac{n_1^2 + n_2^2}{2n_1n_2} = \frac{1}{2} \left( \frac{n_2}{n_1} + \frac{n_1}{n_2} \right). \end{aligned} \quad (3.76)$$

Without loss of generality we consider again  $n_2 > n_1$  and set  $r = \exp(a) = n_2/n_1 > 1$ , so that

$$\cosh \theta_{mg} = \frac{\exp(a) + \exp(-a)}{2} = \cosh(a) \Rightarrow \theta_{mg} = a = \ln \left( \frac{n_2}{n_1} \right) = \ln r. \quad (3.77)$$

The DOS at the midgap frequency (where  $\eta'_1 = 0$ ) is

$$\rho_N \Big|_{\eta'_1=0} = -\frac{1}{L} \frac{\frac{\eta'_2 \sinh(2N\theta_{mg})}{2 \sinh \theta_{mg}}}{\cosh^2 N\theta_{mg} + \eta_2^2 \left( \frac{\sinh N\theta_{mg}}{\sinh \theta_{mg}} \right)^2}. \quad (3.78)$$

For  $N \rightarrow \infty$  we can approximate  $\sinh(N\theta_{mg}) = \frac{1}{2} \exp(N\theta_{mg})$  and then write the DOS as

$$\rho_N = -\frac{1}{Nd} \frac{\frac{1}{4} \frac{\exp(2N\theta_{mg})}{\sinh \theta_{mg}} \eta'_2}{\left( \exp(2N\theta_{mg}) + \eta_2^2 \frac{\exp(2N\theta_{mg})}{\sinh^2(N\theta_{mg})} \right)} = -\frac{1}{Nd} \frac{\eta'_2 \sinh \theta_{mg}}{\eta_2^2 + \sinh^2 \theta_{mg}}. \quad (3.79)$$

For a QWS, in the mid-gap where  $\eta_2 = 0$ , expression (3.78) can be recast in the simpler form

$$\begin{aligned}\rho_N^{\lambda/4} &= -\frac{1}{2Nd} \frac{\pi}{\omega_0 T_{12}} \frac{2 \sinh(N\theta_{mg}) \cosh(N\theta_{mg})}{\cosh^2(N\theta_{mg})} = \frac{\rho_{\text{bulk}}}{NT_{12}} \frac{\sinh(N\theta_{mg})}{\cosh(N\theta_{mg}) \sinh \theta_{mg}} \\ &\propto \frac{1}{NT_{12}} \frac{r^N - r^{-N}}{r^N + r^{-N}}.\end{aligned}\tag{3.80}$$

As  $N \rightarrow \infty$  then  $(r^N - r^{-N})/(r^N + r^{-N}) \rightarrow 1$  and we obtain the asymptotic behaviour  $1/N$ .

### 3.2 The DOS in radiative chiral nematics

For chiral nematic liquid crystals Dirac's rule can be stated to account for the modification of the fluorescence of dye molecules embedded in the so-called 'mirror-less' cavity with a given photonic density of states (DOS). The relative fluorescence intensity, then reads [3]

$$I_j = \frac{\rho_j \int_0^L \langle |\mathbf{e}_j^* \hat{\mathbf{d}}|^2 \rangle_{\text{cn}} dz}{\rho_{\text{iso}} \int_0^L \langle |\mathbf{e}_i^* \hat{\mathbf{d}}|^2 \rangle_{\text{iso}} dz},\tag{3.81}$$

where  $j = 1(2)$  denotes the diffracting (non-diffracting) eigenwave, the brackets denote the spatial average over the orientational distribution of the transition dipole moment. If we assume that the fluorescent molecules are homogeneously distributed in the LC slab, the spatial dependence of the eigenwaves is not important and the integrals can be omitted. After having calculated the DOS for each of the eigenwaves, we need to determine the orientational average of the squared projections of the transition dipole moment  $\mathbf{d}$  on the unit vectors  $\hat{\mathbf{e}}_i$ . If  $\theta$  is the angle between the aforementioned vectors, we

characterize the degree of order of the transition dipole moment by the order parameter  $S_d$  defined as follows

$$S_d = \frac{3}{2} \langle \cos^2 \theta \rangle - \frac{1}{2}, \quad (3.82)$$

in a similar fashion to the orientational order parameter in uniaxial nematic liquid crystals (average of the second Legendre polynomial). It is found in [3] that

$$\langle |\mathbf{e}_i \cdot \mathbf{d}|^2 \rangle = \frac{2f_i^2 - 1}{3f_i^2 + 1} S_d + \frac{1}{3}, \quad (3.83)$$

where  $f_i$  is the degree of ellipticity for each eigenwave, as defined in the previous chapter. In order to calculate the transmission properties of the helical structure we use the relative dielectric anisotropy  $\delta$  at optical frequencies and the reduced wavelength  $\lambda'$  that we have defined in the previous chapter. Without loss of generality we may assume that  $p > 0$  which corresponds to a right-handed helical structure [3]. The dielectric anisotropy at optical frequencies is an alternative measure of the birefringence of the LC host and an implicit indication of feedback strength in an analogous way to the mirror reflectivities in a FP resonator.

### 3.2.1 Inclusion of absorption

When considering absorption in a dye-doped LC laser configuration we must keep in mind that the same host is an absorbing medium for the pump beam and simultaneously for the spontaneous emission of the fluorescent dyes. For the dye emission (as well as for the pumping beam propagation inside the

active medium), one has to take into account various loss mechanisms including linear absorption, light scattering from imperfections, cavity losses due to light escaping from the cavity and Förster resonance energy transfer when two chromophores are involved [6]. While spontaneous emission in free space is considered as randomly polarized, we assume that fluorescence is coupled to a particular normal mode with specific polarization properties in the presence of a chiral nematic LC medium. Both losses and gain can be incorporated into our analysis through introducing a small imaginary part to the dielectric constants parallel and perpendicular to the director, as  $\gamma_{\parallel}$  and  $\gamma_{\perp}$ , respectively, altogether amassed to the dimensionless constant  $\gamma = \gamma_{\parallel} + \gamma_{\perp}$  for which we assume no frequency dispersion and  $|\gamma| \ll 1$ , following a similar treatment to [7]. For a complex dielectric constant, the diffraction coefficient for the diffracting eigenwave (for convenience we drop the suffix  $j = 1$ ) is modified to

$$T \propto A(m, \lambda) \frac{\exp(ikNp)}{1 - r^2 \exp(2ikNp)} = A(m, \lambda) T'(\lambda, m, N), \quad (3.84)$$

where  $k = k_a(\lambda) + ik_b(\lambda) = \frac{2\pi m}{\lambda}$  and  $r = r_a(\lambda) + ir_b(\lambda) = -\frac{n - \frac{\lambda}{p}f - m}{n + \frac{\lambda}{p}f + m}$ ,

with

$$f = \frac{\lambda p \left[ \frac{\varepsilon_{\perp} + i\gamma_{\perp}}{\lambda^2} - \frac{1}{p^2} - \left( \frac{m}{\lambda^2} \right) \right]}{2m} = \frac{2m}{\lambda p \left[ \frac{\varepsilon_{\parallel} + i\gamma_{\parallel}}{\lambda^2} - \frac{1}{p^2} - \left( \frac{m}{\lambda^2} \right) \right]}. \quad (3.85)$$

Based on the de Vries formulation the modified ‘effective’ refractive index is the solution of the algebraic equation

$$m^4 - m^2 \left[ \varepsilon_{\parallel} + \varepsilon_{\perp} + i\gamma + 2 \left( \frac{\lambda}{p} \right)^2 \right] + \left[ \varepsilon_{\perp} + i\gamma_{\perp} - \left( \frac{\lambda}{p} \right)^2 \right] \left[ \varepsilon_{\parallel} + i\gamma_{\parallel} - \left( \frac{\lambda}{p} \right)^2 \right] = 0. \quad (3.86)$$

The real and imaginary parts of  $T'(\lambda, m, N)$  can be written as

$$\begin{aligned} X' &= -\cos(k_a N p) r_a^2 + 2r_a r_b \sin(k_a N p) + \cos(k_a N p) r_b^2 + \exp(2k_b N p) \cos(k_a N p), \\ Y' &= \sin(k_a N p) r_a^2 + 2r_a r_b \cos(k_a N p) - \sin(k_a N p) r_b^2 + \exp(2k_b N p) \sin(k_a N p), \end{aligned} \quad (3.87)$$

respectively, where we have omitted common real prefactors and wavelength independent terms. The expression for  $A(m, \lambda)$  can be obtained from the boundary conditions in the glass-chiral nematic and chiral nematic-glass interface [8] and in our case reads

$$A(m, \lambda) = \frac{\frac{\lambda}{p} f + m}{\frac{\lambda}{p} f + m + n}, \quad (3.88)$$

where  $n = \sqrt{\varepsilon}$ . It is then possible to calculate the DOS of the chiral nematic structure using (4.19). If we consider only the diffracting wave, the eigenfield to which emission is coupled is  $\mathbf{E}_1 = \exp(ikz)\hat{\mathbf{e}}_1$  (where  $\hat{\mathbf{e}}$  is the unit polarization vector, which is wavelength dependent as we have shown). Regarding the sign of the small additive imaginary term to the dielectric constant,  $\gamma > 0$  and  $\gamma < 0$  correspond to losses and gain, respectively. As we have no prior knowledge to assume otherwise, we assume that the losses,

etc., are the same for both the dielectric constants parallel and perpendicular to the director, i.e.,  $\gamma_{\perp} = \gamma_{\parallel}$ . This is the case when spontaneous emission is isotropic in terms of polarization and it is perhaps reasonable to assume that the stimulated absorption and emission are also isotropic. A similar approach is also followed in [9], where equal small imaginary parts are added to the ordinary and extraordinary refractive indices of the chiral nematic LC slab in order to account for gain in an active cell and therefore calculate the corresponding transmission coefficient of a defect mode structure.

If we assume an isotropic absorption of the dye we can see directly from equation (3.81) that the relative fluorescent intensities are then only directly proportional to the DOS when the spatial dependence of the normal modes is deemed unimportant in the calculation of the orientational average of the electric dipole moment of the gain medium [3]. On the other hand, one can consider that absorption is characterized by dichroism as in [10] because the dye molecules (usually rod-like with a length exceeding that of the liquid crystal molecules) tend to adopt to some extent the local nematic order. However, in our analysis we will not take into account dichroism in the absorption/fluorescence of the gain medium as we will assume the dye order parameter  $S_d \rightarrow 0$ , pertaining to the case of an isotropic dye. In that case, the relative intensity contributions for each eigenmode are directly proportional to the DOS. When taking into account losses and gain we employ relation (3.84) to calculate the transmission coefficient and then equation (4.19) for the corresponding DOS of the diffracting eigenwave.

Examples of the normalized DOS for the diffracting eigenwave as a function of the reduced wavelength are depicted in Figure 3.2 for different values of  $\delta$

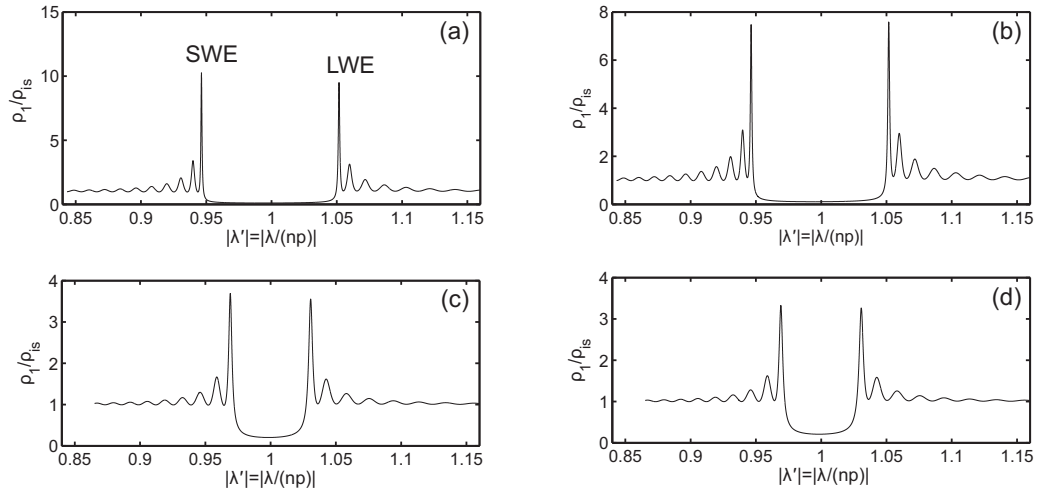


Figure 3.2: Theoretical results of the normalized DOS of the eigenwave  $\mathbf{E}_1(\rho_1/\rho_{iso})$  for a chiral nematic cell as a function of reduced wavelength for different values of the loss coefficient and the optical anisotropy. For all plots, the cell thickness was fixed at  $L = 30p$ . (a)  $n = 1.581$ , relative dielectric anisotropy at optical frequencies  $\delta = 0.1$ , loss coefficient  $\gamma = 2\gamma_{\parallel} = 0.0002$ , (b)  $n = 1.581$ , relative dielectric anisotropy at optical frequencies  $\delta = 0.1$ , loss coefficient  $\gamma = 2\gamma_{\parallel} = 0.002$  (c)  $n = 1.541$ , relative dielectric anisotropy at optical frequencies  $\delta = 0.0526$ , loss coefficient  $\gamma = 2\gamma_{\parallel} = 0.0002$  (d)  $n = 1.541$ , relative dielectric anisotropy at optical frequencies  $\delta = 0.0526$ , loss coefficient  $\gamma = 2\gamma_{\parallel} = 0.002$ .

and the loss coefficient  $\gamma$ . Figures 3.2(a) and 3.2(b) are for the same optical anisotropy but with different magnitudes of the losses. On the other hand, Figures 3.2(c) and 3.2(d) show the profile of the DOS for the same values of the loss coefficient but a smaller optical anisotropy. As it can be seen from the plots, the DOS decreases dramatically with increasing losses, regardless of the magnitude of the optical anisotropy, which is a result that can be shown for a FP resonator in the presence of losses [6]. Additionally, the DOS is larger at the band-edges for a greater optical anisotropy with the same number of pitches and loss coefficient. In this example, as an order of magnitude increase in the loss coefficient (from  $\gamma = 0.0002$  to  $\gamma = 0.002$ ) results in a reduction of the DOS by a factor of 2. The decrease in the DOS has also been noted when an imaginary term is included only in the dielectric constant parallel to the director [6]. In such a case, the short wavelength edge (SWE) is unaffected by the loss factor as opposed to the long wavelength edge (LWE) whose value is diminished.

What is interesting to note is the reversal of the maximum value of the normalized DOS between the SWE and LWE. Unlike the DOS in a quarter-wave stack [2], the DOS profile of a non-absorbing chiral nematic LC is non-symmetric with respect to the centre of the stop-band.

Figure 3.3 shows the ratio of the difference of DOS at the SWE and the LWE to the isotropic DOS as a function of  $\gamma$ . For small values of  $\gamma$ , the maximum value of  $\rho$  occurs at the SWE. As  $\gamma$  increases, the difference in  $\rho$  at the two edge modes (EM) approaches zero before the LWE dominates for large losses. Therefore, when choosing the optimum EM for laser emission it is important to consider the losses in addition to the projection of the optical field onto the

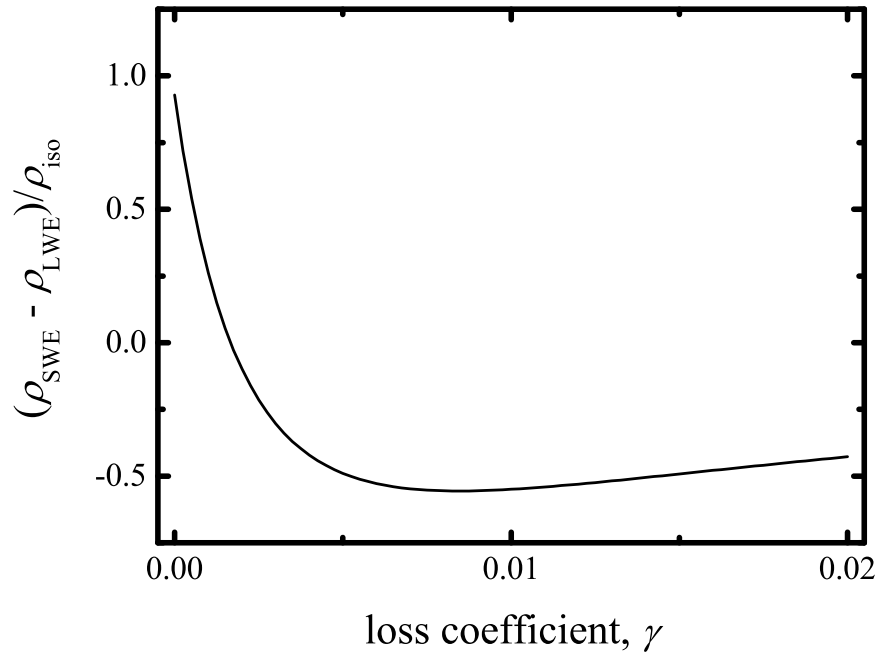


Figure 3.3: The asymmetry in the DOS at the first edge modes either side of the photonic band gap of a chiral nematic LC. A plot of the difference of the maximum DOS between the short and long wavelength edges ( $\rho_{\text{SWE}} - \rho_{\text{LWE}}$ ) of the eigenwave  $\mathbf{E}_1$  that is normalized to isotropic DOS as a function of the loss coefficient. In this case  $n = 1.581$ , the optical anisotropy is  $\delta = 0.1$  and the cell thickness is  $L = 30p$ .

transition dipole moment of the laser dye. It should be noted that the profile is symmetric with respect to the centre of the stop band occurring at  $\lambda' = 1$  for an infinitely thick non-absorbing cell and that the SWE and LWE are located at  $\lambda' = \sqrt{1 - \delta}$  and  $\lambda' = \sqrt{1 + \delta}$ , respectively [3]. For a finite cell, however, the position of the SWE is displaced towards shorter wavelengths (and the position of the LWE is displaced towards longer wavelengths) [3]. As losses become more dominant, we find that the DOS peaks broaden and are further shifted, in direct analogy with the behaviour of the resonance peak in damped steady state oscillating systems.

The variation of the value of the maximum DOS at either wavelength edge for different loss coefficients in cells with varying thickness is considered in Figure 3.4. The position of that maximum is found to shift to smaller values of the pitch with greater optical anisotropy, which is an indication of enhanced feedback. In particular, in this case we can observe that, when losses are present, the position of the maximum value DOS of the LWE is  $L = 40p$  for a cell with optical anisotropy  $\delta = 0.1$  [Figure 3.4(b)], which is reduced to the value of  $L = 35p$  for a 25% increase in  $\delta$  [Figure 3.4(d)]. These results also highlight the interchange between the SWE and LWE as the value of  $\gamma$  is increased. For example, in Figure 3.4(a) the SWE exhibits the largest value of  $\rho$  for all values shown of the pitch. However, when sufficiently large losses are incorporated, the LWE exhibits the largest DOS for sufficiently large  $N$ . The same occurs for a larger optical anisotropy (birefringence) although the maximum DOS is found to be slightly higher. Regarding the variation of the maximum value of the DOS with cell thickness the relation

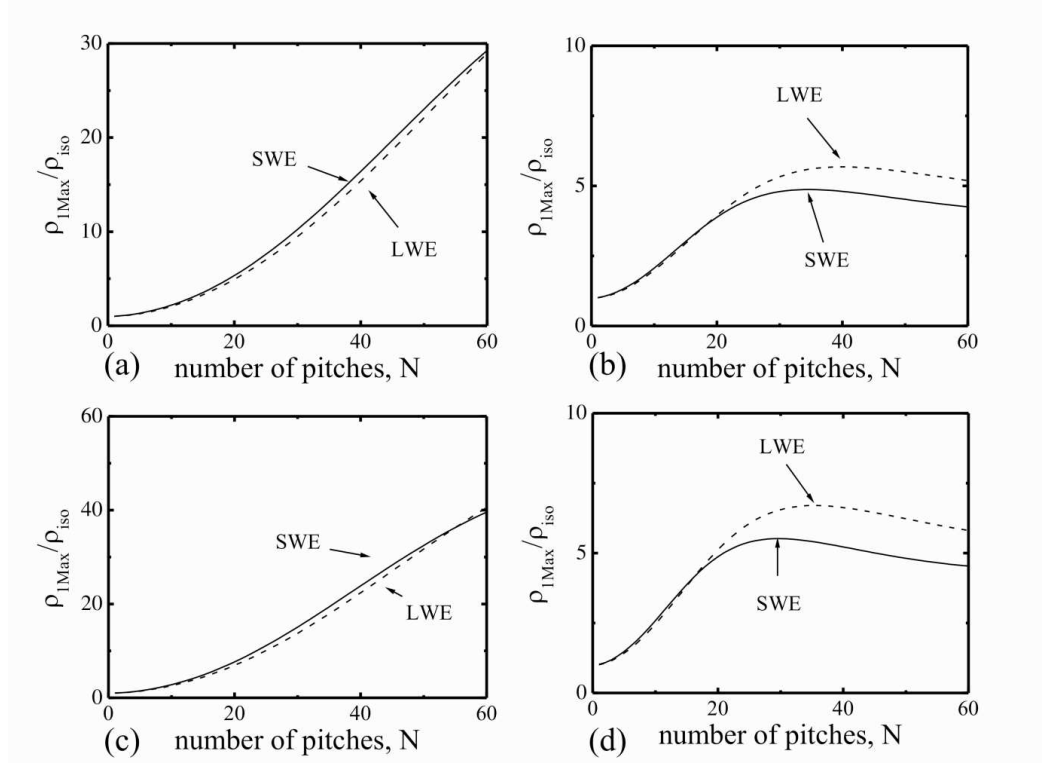


Figure 3.4: Theoretical plots of the maximum normalized DOS ( $\rho_{\text{Max}}/\rho_{\text{iso}}$ ) of the eigenwave  $\mathbf{E}_1$  at the two wavelength edges either side of the stop-band as a function of the chiral nematic LC. The cell thickness is  $L = Np$ . (a) for  $n = 1.581$   $\delta = 0.1$ , and  $\gamma = 2\gamma_{\parallel} = 0.0002$ , (b) for  $n = 1.581$   $\delta = 0.1$ , and  $\gamma = 2\gamma_{\parallel} = 0.006$  (c) for  $n = 1.603$   $\delta = 0.125$ , and  $\gamma = 2\gamma_{\parallel} = 0.0002$ , (d) for  $n = 1.603$   $\delta = 0.125$ , and  $\gamma = 2\gamma_{\parallel} = 0.006$ . The arrows mark the number of pitches where the peak DOS is attained for each wavelength edge. The short-wavelength and long-wavelength edges are shown as solid and dashed lines, respectively.

$$\rho_{\max} \propto L^2 \exp(-\beta L) \quad (3.89)$$

has previously been proposed to pertain to the experimental data of the energy-excitation threshold of cells as a function of  $L = Np$  with  $N$  being the length of the cell and  $\beta$  the collective absorption coefficient [6]. The general trend suggested by equation (3.89) is indeed vindicated by our theoretical findings: the deviation from the parabolic profile is more ostensible with increasing losses and a maximum is observed whose position and value depend on both the loss coefficient and the optical anisotropy. The parabolic dependence of the DOS at the wavelength of the photonic band edges is a known result for large  $N$  in quarter-wave stacks [2] as well as for non-absorbing chiral nematic LCs [6].

Experimentally, the dependence of the DOS upon the number of pitches for different optical anisotropies is verified, albeit indirectly, by determining the excitation threshold as a function of cell thickness, as depicted in Figure 3.5(a). As shown in [6] the excitation threshold is inversely proportional to  $\rho$  for a Fabry-Pérot resonator. The figure shows the excitation threshold as a function of the cell thickness for two different LC laser samples. These measurements were obtained using two different laser samples: one consisting of the nematic LC E7 ( $\delta = 0.13$  and  $\Delta n = 0.2$  at  $25^\circ\text{C}$ ) and the other with the nematic LC mixture E49 ( $\delta = 0.15$  and  $\Delta n = 0.25$  at  $25^\circ\text{C}$ ). The optical anisotropies were determined from the refractive indices parallel and perpendicular to the director of the nematic sample at a fixed wavelength of  $\lambda_0 = 589.6$  nm using an Abbe refractometer. Both mixtures were doped with a high twisting power chiral dopant (BDH1281, Merck KGaA) and the laser

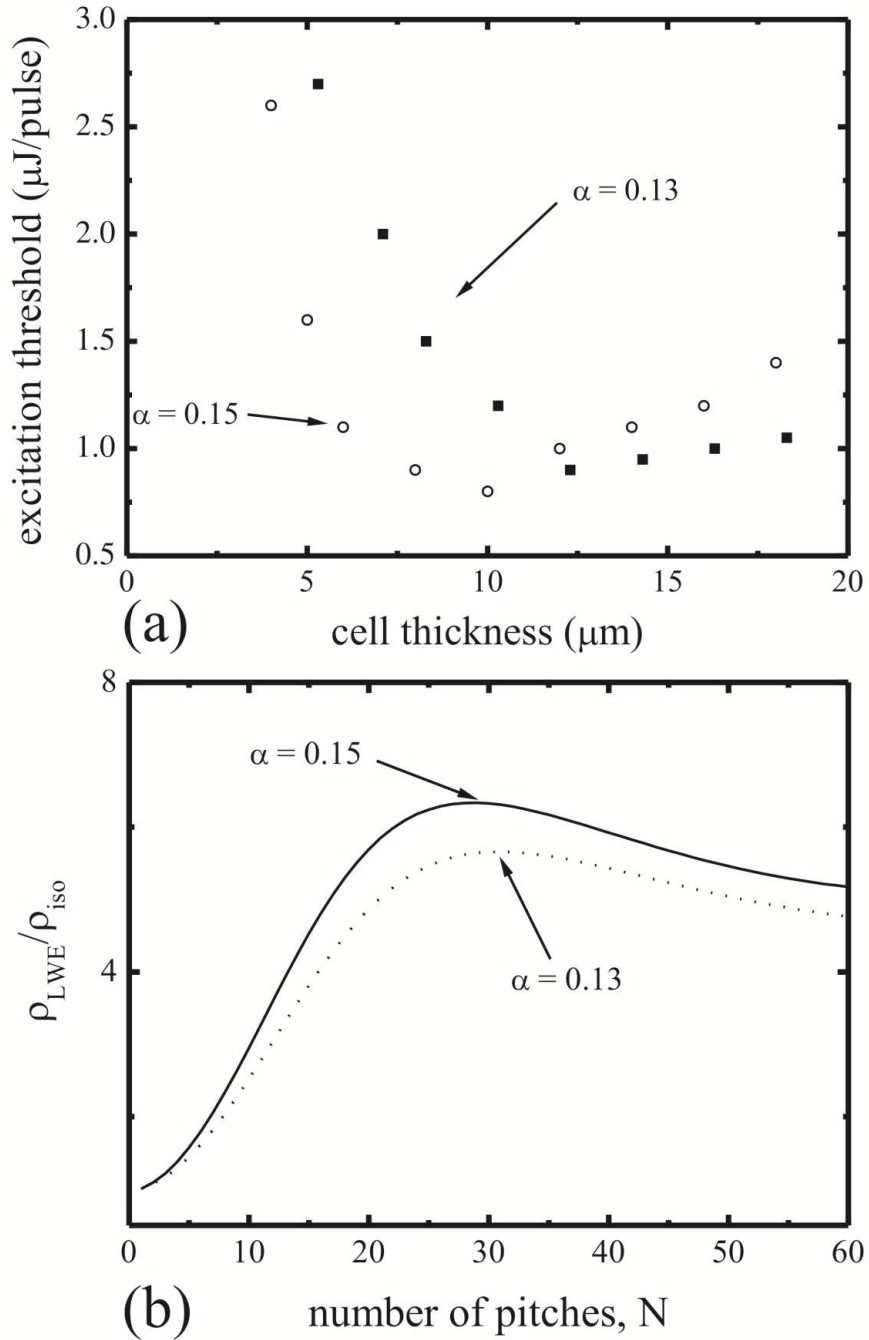


Figure 3.5: (a) Experimental results of the dependence of the laser excitation threshold on the cell thickness for a low optical anisotropy ( $\delta = 0.13$ ) (closed squares) and a high optical anisotropy ( $\delta = 0.15$ ) (open circles) LC host. (see A. D. Ford, PhD thesis, 2006) (b) Theoretical plots of the DOS for the long-wavelength band-edge for two different chiral nematic LCs for the same optical anisotropies as those used in the experiment. The loss coefficient in this case is  $\gamma = 0.0084$  for  $n = 1.608$  and  $n = 1.627$  respectively.

dye DCM (Exciton). The samples were capillary filled into wedge cells that were fabricated in-house and were coated with a rubbed polyimide alignment layer to ensure that a Grandjean texture was obtained after filling. Each cell was optically excited by the second harmonic of an Nd:YAG laser (Polaris II, New Wave Research) at positions within the wedge cell for which the dimensions of the cell gap were known. In both cases the emission wavelength and the pitch ( $p \simeq 350$  nm) were the same but the main difference was the optical anisotropy of the nematic host. The profile of the plot resembles the inverse of the dependence of the DOS on the number of pitches confined within the device (c.f., Figure 3.4) as suggested in [6]. The minimum in the excitation threshold is found to occur at smaller cell thicknesses (corresponding to a smaller  $N$  required for the maximum value of the DOS) for the higher optical anisotropy compound (E49) than that obtained for the laser sample with a lower optical anisotropy (E7). In this case, the minimum excitation threshold is found to occur at  $L = 12.5 \mu\text{m}$  for the sample consisting of E7 ( $\delta = 0.13$ ) and is shifted to  $L = 10 \mu\text{m}$  when the LC host is replaced with E49 ( $\delta = 0.15$ ). For the purposes of comparison, theoretical curves for the DOS for two different samples with the same optical anisotropy as E7 and E49 are shown in Figure 3.5(b) for a suggested value of  $\gamma = 0.0084$ . Theoretically, we find that the number of pitches required to obtain the maximum DOS for the higher optical anisotropy sample is reduced from  $N = 32$  to  $N = 28$ , which is in good agreement with the experimental results whereby the difference in the number of pitches for the two lasers is found to be  $\Delta N \simeq 5$ .

### 3.2.2 Inclusion of amplification

We will now take into consideration the gain of the active material in the process of laser emission. For an amplifying medium with  $\gamma < 0$  we find that the DOS of various EMs diverges at particular values of  $\gamma$ , which are the lasing excitation gain coefficients for these modes. The behaviour is consistent with the case of an active medium filling a FP resonator, where the DOS diverges at threshold [11].

In Figure 3.6 we depict the DOS of an amplifying chiral nematic LC for different values of  $\gamma$ . For  $|\gamma| \ll 1$  and for sufficiently thick cells, the threshold gain coefficient  $\gamma_{th}/n^2$  is found to be inversely proportional to  $\delta^2$  as well as to  $L^3$ , as we have shown in the previous chapter. As the threshold value for a chiral nematic LC with a given thickness is approached, the DOS rapidly diverges suggesting a theoretically infinite group time of photons residing in the resonating cavity. In actuality, the DOS does not reach infinity due to the finite lifetime of the excited state or due to the collision with a phonon [10]-[12]. Its value depends on the microscopic properties of the sample and the duration of the pumping. If the gain factor exceeds slightly the threshold value the DOS is still very high and the phase derivative changes sign [11]. Such values of  $\gamma$  belong to the regime of “superamplification”. As the gain coefficient is further increased the EM that first attained threshold (in one of the wavelength edges) is now quenched and laser action is triggered for successive EMs [Figure 3.6(c)]. Hence, as the author notes in [10] and we have mentioned in the previous chapter, the region of superamplification does not only correspond to the case where losses are slightly higher than the active medium gain but also to the case in which they are marginally

overcompensated. That behaviour can be traced also in the transmission and reflection coefficients in the region of anomalous absorption for amplifying chiral nematic LCs and other DFB structures [7]-[12].

Our results are in good agreement with the behaviour of the threshold values obtained from the maximisation of transmittance and the solvability condition of the system produced by satisfying the continuity conditions of tangential electric field components in a boundary value problem formulation for light propagation in chiral nematic LCs [7]. As we also observe in Figure 3.6(d), a smaller gain constant is required for the DOS of the lasing mode to diverge in a chiral nematic LC with greater birefringence, which is an indication of enhanced feedback.

Using the semi-classical laser theory, once the threshold gain has been identified, it can be directly linked to the critical population inversion  $\Delta N_{\text{th}}^e$  via [12]

$$\gamma_{\text{th}} \propto g_{\text{th}} = \Delta^e N_{\text{th}} \frac{\lambda^2}{8\pi n_0^2 \tau_{\text{sp}}} g(\omega), \quad (3.90)$$

where  $g(\omega)$  is the linewidth function,  $n_0$  is the refractive index of the medium away from resonance, and  $\tau_{\text{sp}}$  is the spontaneous lifetime of the radiative transition. For dye-doped cells, the population inversion is equal to threshold gain divided by the molecular cross section for spontaneous emission, which is experimentally determined from the luminescence spectrum (under low pumping) of the fluorescent dyes normalized to the ratio  $\Phi/(8\tau_{\text{sp}})$ , where  $\Phi$  is the fluorescence quantum yield [13].

The vector potential operator in a cavity sustaining transverse modes is expressed as [15]

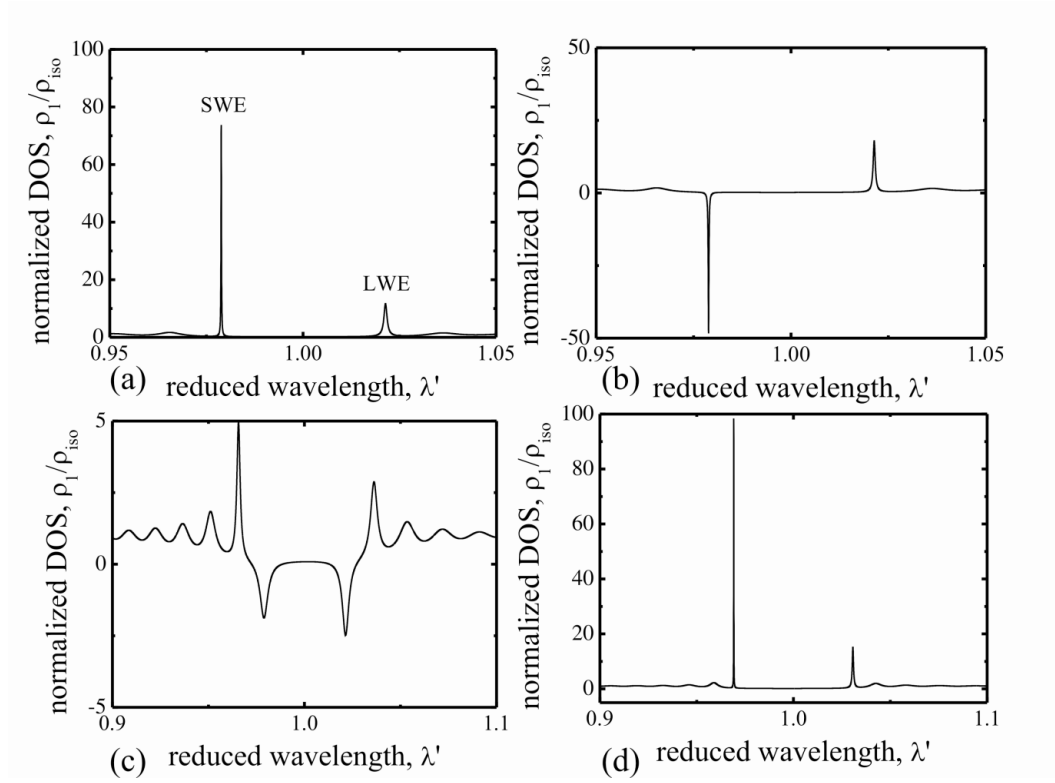


Figure 3.6: The behaviour of the DOS in the presence of gain. Normalized DOS of the eigenwave  $\mathbf{E}_1$  for a chiral nematic LC cell with thickness  $L = 30p$ ,  $n = 1.523$ ,  $\delta = 0.03$  and (a)  $\gamma = 2\gamma_{\parallel} = -0.0304$ , (b)  $\gamma = 2\gamma_{\parallel} = -0.0320$ , (c)  $\gamma = 2\gamma_{\parallel} = -0.0540$  (d)  $n = 1.541$ ,  $\delta = 0.05206$  and  $\gamma = 2\gamma_{\parallel} = -0.0134$ .

$$\hat{\mathbf{A}}(\mathbf{x}) = \sum_{\mathbf{k}, \lambda=1,2} \sqrt{\frac{\hbar}{2\epsilon_0\omega_{\mathbf{k}}V}} \left[ a_{\mathbf{k},\lambda} \exp(i\mathbf{k} \cdot \mathbf{x}) \hat{\mathbf{e}}_{\mathbf{k}\lambda} + a_{\mathbf{k},\lambda}^\dagger \exp(i\mathbf{k} \cdot \mathbf{x}) \hat{\mathbf{e}}_{\mathbf{k}\lambda}^* \right], \quad (3.91)$$

where a time dependence  $\exp(-i\omega_{\mathbf{k}}t)$  is assumed and  $\lambda = 1, 2$  denotes the polarization of the plane waves in the cavity (two degrees of freedom). This operator has non-zero matrix elements only for each mode where the photon (occupancy) number differs by one, consistent with first-order perturbation theory. In the dipole approximation, if  $N_{\mathbf{k},\lambda}$  photons are present in a cavity then the emission rate is

$$\Gamma_{i \rightarrow f} = \frac{\pi \omega_{\mathbf{k}}}{\epsilon_0 V} \langle |\hat{\mathbf{e}} \cdot \mathbf{d}|^2 \rangle (N_{\mathbf{k},\lambda} + 1) \delta(E_i - E_f - \hbar\omega), \quad (3.92)$$

in agreement with (3.34). The above is still a first-order perturbative result in the context of the second quantization, whereby the number of photons has been extracted by the ladder operator  $a_{\mathbf{k},\lambda}$  acting on the initial state with  $N_{\mathbf{k},\lambda}$  photons. In the framework of the first-quantization, the role of the photon number in stimulated emission is played by the DOS (as a distribution function) multiplied by the total number of photons in the cavity (of all frequencies), thus representing the selective amplification of the field in a resonator with Bragg-reflection (which is the case in chiral nematics). Hence, although the DOS diverges for particular values of amplification (threshold values) in the presence of a gain medium, formula (3.81) holds within first-order perturbation theory.

We consider a system with two weakly interacting parts. The parts have definite energies at a particular instant, denoted by  $E$  and  $\epsilon$  respectively. If the energy is measured again after some time interval  $\tau = \Delta t$ , the values  $E', \epsilon'$  are obtained and are different in general from  $E, \epsilon$ . We will use the results of first-order perturbation theory to determine the order of magnitude of the most probable value of the difference  $E' + \epsilon' - E - \epsilon$ . According to relation (3.19) the transition probability from a state with energy  $E$  to a state with energy  $E'$  under the action of a weak time-independent perturbation ( $\omega = 0$ ) is proportional to [5]

$$\frac{\sin^2 \left[ \frac{(E - E')t}{2\hbar} \right]}{(E' - E)^2}, \quad (3.93)$$

from which we infer that the most probable value of the energy difference  $E - E'$  is of the order of  $\hbar/t$ . Applying this result to our system with the two weakly interacting parts, we obtain the relation

$$|E + \epsilon - E' - \epsilon'| \Delta t \sim \hbar. \quad (3.94)$$

The quantities  $\epsilon, \epsilon'$  are related to the measuring “particle/apparatus” and are supposed to be known exactly, so that  $|\Delta E - \Delta E'| \sim \hbar/\tau$ . The same conclusion can be reached from another standpoint, by considering the transition of one system from one state to another, under the action of a perturbation. If  $E_0 + \epsilon_0$  is some energy level of the system (‘atom’ and field photon of the initial frequency) and  $E, \epsilon$  are the energies of the two parts into which the system decays (‘atom’ and photon of the final frequency), then we find again

$$|E_0 - E' - \epsilon'| \tau \sim \hbar, \quad (3.95)$$

where  $\tau$  is the reciprocal of the decay rate (called also the lifetime of the state). Since the sum  $E + \epsilon$  is the estimate of the energy of the system before it decays, the above result shows that the energy of a system is some “quasi-stationary” state can be determined only up to  $\hbar/\tau$ . This quantity is inversely proportional to the spectral width of emission. The experimentally determined emission spectral width (full width at half-maximum, FWHM) of both fluorescence and lasing can be directly related to the DOS via the uncertainty principle  $\Delta\tau\Delta\omega \propto \pi$ , bearing in mind that the DOS is linked to the characteristic time  $\Delta\tau$  as [11]-[14]  $\rho = \Delta\tau/L \propto \pi/(L\Delta\omega)$ . As the behaviour of the DOS can also reflect mode quenching in lasing structures in the regime beyond the threshold gain, we can immediately infer that the

FWHM of the lasing radiation profile, corresponding to the dominant mode, will decrease in the “super-amplification” regime.

In conclusion, in this chapter we have used the concept of the density of photon states to study amplified emission in chiral nematic LC samples doped with a gain medium, within the semi-classical first order perturbation treatment encompassed in Dirac’s rule (most commonly referred to as Fermi’s Golden Rule). Absorption and gain were introduced phenomenologically and were linked to the inhibition and enhancement of the optical feedback in these structures, respectively, through the density of states. In the next chapter we will examine the enhancement of spontaneous emission in these resonators, using one of the most common models employed in quantum optics.



# Bibliography

- [1] J. P. DOWLING AND C. M. BOWDEN, *Atomic transition rates in inhomogeneous media with applications to photonic band structures*, Phys. Rev. A **46**, pp. 612-622 (1992).
  
- [2] J. M. BENDICKSON, J. P. DOWLING, AND M. SCALORA, *Analytic expressions for the electromagnetic mode density in finite, one-dimensional, photonic band-gap structures* Phys. Rev. E **53**, pp. 4107-4121 (1996).
  
- [3] J. SCHMIDTKE AND W. STILLE, *Fluorescence of a dye-doped cholesteric liquid crystal film in the region of the stop-band: theory and experiment*, Eur. Phys. J. B **31**, pp. 179-194 (2003).
  
- [4] L. D. LANDAU AND E. M. LIFSHITZ, *The Classical Theory of Fields*, Vol. 2, ch. 4, Pergamon Press, 1971.
  
- [5] L. D. LANDAU AND E. M. LIFSHITZ, *Quantum Mechanics (Non-relativistic theory)*, Vol. 3, ch. 6, Elsevier, 2007.

- [6] M. F. MOREIRA, S. RELAIX, W. CAO, B. TAHERI, AND P. PALFFY-MUHORAY, *Liquid Crystal Microlasers*, Chap. 12, Transworld Research Network, Kerala, India, 2010.
- [7] V. A. BELYAKOV AND S. V. SEMENOV, *Optical Edge Modes in Photonic Liquid Crystals*, JETP, **109**, pp. 687-699 (2009).
- [8] HL. DE VRIES, *Rotatory Power and Other Optical Properties of Certain Liquid Crystals*, Acta Cryst., **4**, pp. 219-226 (1951).
- [9] Y. ZHOU, Y. HUANG, Z. GE, L.-P. CHEN, Q. HONG, T. X. WU, AND S.-T. WU, *Enhanced photonic band edge laser emission in a cholesteric liquid crystal resonator* Phys. Rev. E **74**, 061705 (2006).
- [10] S. P. PALTO, *Lasing in Liquid Crystal Thin Films*, JETP, **103**, pp.472-479 (2006).
- [11] S. P. PALTO, *Liquid Crystal Microlasers*, Chap. 8, Transworld Research Network, Kerala, India, 2010.
- [12] A. YARIV AND P. YEH, *Photonics: Optical Electronics in Modern Communications*, ch. 12, 6th ed., Oxford University Press, US, 2006.
- [13] L. M. BLINOV, *Lasers on cholesteric liquid crystals: Mode density and lasing threshold* JETP Lett. **90**, 166-171 (2009).
- [14] S. P. PALTO, L. M. BLINOV, M. I. BARNIK, V. V. LAZAREV, B. A. UMANSKII, AND N. M. SHTYKOV, *Photonics of liquid-crystal structures: A review* Crystallogr. Rep. **56**, pp. 667-697 (2011).

- [15] V. B. BERESTETSKII, E. M. LIFSHITZ, AND L. P. PITAEVSKII, *Quantum Electrodynamics, Vol. 4*, ch. 5, Elsevier (Singapore), 2008.

# Chapter 4

## The Jaynes-Cummings model

As we have seen in the previous chapter, the concept of the density of photon states (DOS) is regularly employed to study the photonic crystal properties that determine emission and absorption of electromagnetic radiation of a given frequency from guest atoms [1]. For the case of (dye-doped) chiral nematic liquid crystal (LC) films, which constitute a representative example of partial 1D photonic crystals, the link between the behaviour of the DOS and fluorescence under weak-coupling conditions and in the context of first-order perturbation theory is attempted in [2], where Dirac's rule (often referred to as 'Fermi's golden rule') is employed to calculate the photon emission rate.

With regard to the interaction of a gain medium and the electromagnetic field in the resonant cavity, a two-level system coupled to a quantum harmonic oscillator is frequently described with the Jaynes-Cummings (JC) Hamiltonian in which only 'resonant' terms feature [3], [4], [5]. Such a consideration is permissible in the case of near resonance and weak coupling [3]. Both conditions are satisfied for spontaneous emission in these periodic structures

for small detuning [4]. It should be mentioned here, that through a change of basis, a much greater range of coupling strength and detuning values can be allowed [4]. In [5] the JC model is employed to describe emission in the vicinity of the saddle point of 2D photonic crystals, where the DOS exhibits a logarithmic peak. In order to analyze the behavior of the DOS near its logarithmic peak and at the edge of the band gap, one can resort to a critical point analysis through an expansion in the region of the saddle point [1].

In this chapter, we put the analysis of spontaneous emission from 2D photonic crystals on a firmer basis providing analytical results, and explore in more detail the fluorescence properties in chiral nematic LCs, outlining common features that are attributed to resonance. Moreover, the discrepancy between the experimentally obtained emission spectra and the theoretically calculated DOS is addressed. Such a consideration aims to further the understanding of spontaneous and induced emission from these distributed feedback resonators. The case of chiral nematic LCs is selected because these structures have the additional advantage of allowing an exact analytic solution of Maxwell's equations [6].

## 4.1 Hamiltonian, states and equations of motion

We will now outline the basic formulation of an atom-field interaction in a resonant environment, within the framework of the JC model. In many cases, the frequency of the electric field in a resonant structure is near the transition frequency of a two-level system. Such a two-level system is called

an ‘atom’ for convenience [7]. The JC Hamiltonian for the atom-field system is written in the form [3], [5]

$$\hat{H} = \frac{1}{2}\hbar\omega_{10}\hat{\sigma}_z + \hbar \sum_{\kappa} \omega_{\kappa} \hat{a}_{\kappa}^{\dagger} \hat{a}_{\kappa} + i \sum_{\kappa} (\mu_{\kappa} \hat{a}_{\kappa}^{\dagger} \hat{\sigma}_- - \mu_{\kappa}^* \hat{a}_{\kappa} \hat{\sigma}_+), \quad (4.1)$$

where

$$\mu_{\kappa} = (\mathbf{d} \cdot \mathbf{e}_{kl}) \omega_{10} \sqrt{\frac{2\pi\hbar}{V\varepsilon\omega_{\kappa}}}, \quad (4.2)$$

is the atom-field coupling constant,  $\omega_{10}$  is the atomic transition frequency,  $\omega_{\kappa}$  is the electromagnetic mode frequency,  $\sigma_z$  is the inversion operator,  $\hat{\sigma}_{\pm} = (\hat{\sigma}_x \pm \hat{\sigma}_y)/2$  are the raising and lowering operators for Pauli matrices acting on qubit states,  $\hat{a}_{\kappa}^{\dagger}$  &  $\hat{a}_{\kappa}$  are the bosonic creation and annihilation operators for the  $\kappa^{th}$  mode,  $\mathbf{d} = e\mathbf{r}_{10}$  is the transition dipole moment,  $\mathbf{e}_{kl}$  is the unit field polarization vector and  $\varepsilon$  is the frequency independent dielectric constant of the medium with volume  $V$ . In writing the Hamiltonian in the form (4.1), we assume that the energies of the upper and lower states of the atom are equal and opposite, i.e.,  $E_1 = -E_0 = (1/2)\hbar\omega_{10}$ . The first term in the interaction part of the JC Hamiltonian in the so-called ‘rotating field’ approximation corresponds to the electronic transition from the lower to the upper level with the absorption of a photon from the field mode, while the second term represents the reverse process, i.e., the electronic transition from the upper to the lower atomic level and the emission of a photon that contributes into the mode field. The remaining terms in the interaction Hamiltonian (of the form  $\hat{H}_{int} = G(\hat{\sigma}_+ + \hat{\sigma}_-)(E^* \hat{a}^{\dagger} + E \hat{a})$ ) that do not feature in equation (4.1) correspond to non-resonant, virtual processes [7], namely to the electronic transition upwards accompanied by the emission of one photon

and the transition downward accompanied by the absorption of one photon. Due to their smallness, these terms are usually omitted [7]. We consider the atom-field system to be described by the wavefunction

$$|\psi\rangle = \exp(-i\omega_{10}t/2) [c_1(\mathbf{R}, t)|1, \{0\}\rangle + \sum_{\kappa} \exp(i\delta_{\kappa}t)c_0^{\kappa}(\mathbf{R}, t)|0, \{1\}_{\kappa}\rangle], \quad (4.3)$$

where  $\delta_{\kappa} = \omega_{10} - \omega_{\kappa}$ . This expression is a superposition of the state  $|1, \{0\}\rangle$ , corresponding to the excited state of the atom with the photon occupation number equal to 0, and the state  $|0, \{1\}_{\kappa}\rangle$ , corresponding to the ground state with one photon in the  $\kappa^{th}$  mode. Hence, the mechanism of spontaneous emission is quantified. In order to account for cavity losses and linewidth broadening, we introduce phenomenologically a small imaginary part to the field and transition frequencies, respectively, as in [5], such that

$$\omega_{\kappa} = \omega'_{\kappa} - i\gamma \quad \text{and} \quad \omega_{10} = \omega'_{10} - i\gamma_{10}. \quad (4.4)$$

Expressions for the imaginary part of the edge mode frequencies (eigenfrequencies) in the case of a chiral nematic LC layer can be found in [6]. The appearance of such an imaginary contribution is related to the energy leakage through the surfaces of the LC film. Substituting the wavefunction of relation (4.3) into the time-dependent Schrödinger equation yields a system of equations of motion for the time varying amplitudes  $c_1(t)$  and  $c_0^{\kappa}(t)$ . For the left-hand side of Schrödinger's equation applied for the state  $|\psi\rangle$  in (4.3), we have

$$\begin{aligned}
\hat{H}|\psi\rangle &= \exp(-i\omega_{10}t/2) \left[ \frac{1}{2}\hbar\omega_{10}c_1(\mathbf{R}, t)|1, \{0\}\rangle \right. \\
&- \frac{1}{2}\hbar\omega_{10} \sum_{\kappa} \exp(i\delta_{\kappa}t)c_0^{\kappa}(\mathbf{R}, t)|0, \{1\}_{\kappa}\rangle + \hbar \sum_{\kappa} \omega_{\kappa} \exp(i\delta_{\kappa}t)c_0^{\kappa}(\mathbf{R}, t)|0, \{1\}_{\kappa}\rangle \\
&\left. + i \sum_{\kappa} \mu_{\kappa}c_1(\mathbf{R}, t)|0, \{1\}_{\kappa}\rangle - i \sum_{\kappa} \mu_{\kappa}^* \exp(i\delta_{\kappa}t)c_0^{\kappa}(\mathbf{R}, t)|1, \{0\}\rangle \right].
\end{aligned} \tag{4.5}$$

The right-hand side of Schrödinger's equation reads

$$\begin{aligned}
i\hbar \frac{\partial \psi}{\partial t} &= i\hbar \cdot \exp(-i\omega_{10}t/2) \frac{dc_1}{dt}(\mathbf{R}, t)|1, \{0\}\rangle \\
&+ \frac{1}{2}\hbar\omega_{10} \cdot \exp(-i\omega_{10}t/2)c_1(\mathbf{R}, t)|1, \{0\}\rangle \\
&+ \exp(-i\omega_{10}t/2) \left[ \sum_{\kappa} i\hbar \cdot \exp(i\delta_{\kappa}t) \frac{dc_0^{\kappa}}{dt}(\mathbf{R}, t)|0, \{1\}_{\kappa}\rangle \right. \\
&- \hbar(\omega_{10} - \omega_{\kappa}) \exp(i\delta_{\kappa}t)c_0^{\kappa}(\mathbf{R}, t)|0, \{1\}_{\kappa}\rangle \left. \right] \\
&+ \frac{1}{2}\hbar\omega_{10} \exp(-i\omega_{10}t/2) \sum_{\kappa} \exp(i\delta_{\kappa}t)c_0^{\kappa}(\mathbf{R}, t)|0, \{1\}_{\kappa}\rangle \\
&= i\hbar \cdot \exp(-i\omega_{10}t/2) \frac{dc_1}{dt}(\mathbf{R}, t)|1, \{0\}\rangle + \frac{1}{2}\hbar\omega_{10} \exp(-i\omega_{10}t/2)c_1(\mathbf{R}, t)|1, \{0\}\rangle \\
&+ \exp(-i\omega_{10}t/2) \left[ \sum_{\kappa} i\hbar \cdot \exp(i\delta_{\kappa}t) \frac{dc_0^{\kappa}}{dt}(\mathbf{R}, t)|0, \{1\}_{\kappa}\rangle \right. \\
&+ \hbar\omega_{\kappa} \exp(i\delta_{\kappa}t)c_0^{\kappa}(\mathbf{R}, t)|0, \{1\}_{\kappa}\rangle \left. \right] \\
&- \frac{1}{2}\hbar\omega_{10} \cdot \exp(-i\omega_{10}t/2) \sum_{\kappa} \exp(i\delta_{\kappa}t)c_0^{\kappa}(\mathbf{R}, t)|0, \{1\}_{\kappa}\rangle.
\end{aligned} \tag{4.6}$$

Upon cancelling the common terms, one obtains

$$\begin{aligned}
& i \sum_{\kappa} \mu_{\kappa} c_1(\mathbf{R}, t) |0, \{1\}_{\kappa}\rangle - i \sum_{\kappa} \mu_{\kappa}^* \exp(i\delta_{\kappa} t) c_0^{\kappa}(\mathbf{R}, t) |1, \{0\}\rangle \\
& = i\hbar \frac{dc_1}{dt}(\mathbf{R}, t) |1, \{0\}\rangle + \sum_{\kappa} i\hbar \cdot \exp(i\delta_{\kappa} t) \frac{dc_0^{\kappa}}{dt}(\mathbf{R}, t) |0, \{1\}_{\kappa}\rangle.
\end{aligned}$$

After taking the inner product with the states  $(|0, \{1\}_{\kappa}\rangle)^{\dagger}$  and  $(|1, \{0\}\rangle)^{\dagger}$  we arrive at the equations of motion presented in [5]

$$\begin{cases} \frac{dc_1}{dt}(\mathbf{R}, t) = - \sum_{\kappa} \mu_{\kappa}^* \exp(i\delta_{\kappa} t) c_0^{\kappa}(\mathbf{R}, t) \\ \frac{dc_0^{\kappa}}{dt}(\mathbf{R}, t) = \exp(-i\delta_{\kappa} t) \mu_{\kappa} c_1(\mathbf{R}, t) \end{cases} . \quad (4.7)$$

The system is reduced to

$$\frac{dc_1}{dt}(\mathbf{R}, t) = - \int_0^t g(\mathbf{R}, t - \tau) c_1(\mathbf{R}, \tau) d\tau , \quad (4.8)$$

with the Green's function taking the form of

$$g(\mathbf{R}, t) = u(t) \sum_{\kappa} |\mu_{\kappa}|^2 \exp(i\delta_{\kappa} t) \equiv \beta u(t) \int_{\omega_1}^{\omega_2} \frac{\exp[i(\omega_{10} - \omega)t]}{\omega - i\gamma} \rho_l(\mathbf{R}, \omega) d\omega ,$$

in which  $\rho_l(\mathbf{R}, \omega)$  is the local density of photon states,  $u(t)$  is the unit step function and, assuming periodic boundary conditions,

$$\beta \propto \frac{\omega_{10}^2 |\mathbf{r}_{10}|^2 L}{\varepsilon L S} \frac{L}{2\pi} \propto \frac{\omega_{10}^2 |\mathbf{r}_{10}|^2}{\varepsilon S}.$$

Here, we will derive an expression for the Fourier transform of the Green's function for the determination of the emission spectrum. Applying the

Fourier transform to both sides of (4.8) and invoking the convolution theorem, as well as the conjugate symmetry of the coefficients under time reversal, we obtain

$$\begin{aligned} \mathcal{F}\left\{\frac{dc_1}{dt}\right\}(\mathbf{R}, t) &= -\mathcal{F}\{g(\mathbf{R}, t)\}\mathcal{F}\{c_1(\mathbf{R}, t)\} \\ &\Rightarrow -i(\Omega - \omega_{10})\tilde{c}_1(\Omega - \omega_{10}) = -\tilde{g}(\mathbf{R}, \Omega - \omega_{10})\tilde{c}_1(\Omega - \omega_{10}) \\ &\Rightarrow -i(\Omega - \omega'_{10} + i\gamma_{10})\tilde{c}_1(\Omega - \omega_{10}) = -\tilde{g}(\mathbf{R}, \Omega - \omega_{10})\tilde{c}_1(\Omega - \omega_{10}) \end{aligned}$$

Hence

$$\tilde{c}_1(\Omega - \omega_{10}) = \frac{1}{\gamma_{10} - i(\Omega - \omega'_{10}) + \tilde{g}(\mathbf{R}, \Omega - \omega_{10})}, \quad (4.9)$$

where

$$\tilde{f}(\omega) = \int_0^\infty f(t)e^{i\omega t} dt. \quad (4.10)$$

Also, we have

$$\mathcal{F}\{g(\mathbf{R}, t)\} = \beta \int_{\omega_{min}}^{\omega_{max}} \frac{\mathcal{F}\{u(t) \exp(At)\}}{\omega - i\gamma} \rho_l(\mathbf{R}, \omega) d\omega \quad (4.11)$$

hence

$$\tilde{g}(\mathbf{R}, \Omega - \omega_{10}) = -\beta \int_{\omega_{min}}^{\omega_{max}} \frac{\rho_l(\mathbf{R}, \omega)}{(\omega - i\gamma) [(\Re\{A\} - \Im\{\Omega - \omega_{10}\}) + i(\Im\{A\} + \Re\{\Omega - \omega_{10}\})]} d\omega, \quad (4.12)$$

where  $A = \gamma_{10} - \gamma + i(\omega'_{10} - \omega)$ .

The integral above can be recast in the form

$$\tilde{g}(\mathbf{R}, \Omega - \omega_{10}) = -i\beta \int_{\omega_{min}}^{\omega_{max}} \frac{\rho_l(\mathbf{R}, \omega)}{(\omega - i\gamma)(\omega - \Omega - i\gamma)} d\omega. \quad (4.13)$$

The emission spectrum is then determined by the relation

$$S(\Omega) = 2\Re\{\tilde{c}_1(\Omega - \omega_{10})\} = \frac{2[\gamma_{10} + \Sigma_2(\Omega)]}{[\Omega - \omega'_{10} + \Sigma_1(\Omega)]^2 + [\gamma_{10} + \Sigma_2(\Omega)]^2}, \quad (4.14)$$

with

$$\tilde{c}_1(\Omega - \omega_{10}) = \int_0^\infty c_1(t) e^{i(\Omega - \omega_{10})t} dt$$

and

$$\Sigma_1 = \beta |\hat{\mathbf{e}}_{kl}(\mathbf{R}) \hat{\mathbf{r}}_{10}|^2 \Re \left\{ \int_{\omega_{min}}^{\omega_{max}} \frac{\rho(\omega)}{(\omega - i\gamma)(\omega - \Omega - i\gamma)} d\omega \right\}, \quad (4.15)$$

$$\Sigma_2 = \beta |\hat{\mathbf{e}}_{kl}(\mathbf{R}) \hat{\mathbf{r}}_{10}|^2 \Im \left\{ \int_{\omega_{min}}^{\omega_{max}} \frac{\rho(\omega)}{(\omega - i\gamma)(\omega - \Omega - i\gamma)} d\omega \right\}, \quad (4.16)$$

where  $\rho(\omega)$  is the density of photon states (DOS). The term  $\Sigma_1$  is linked to the Lamb shift, while the term  $\Sigma_2$  is related to the broadening of the transition between the two states of the system.

## 4.2 Photonic Density of States revisited

We will next consider the characteristic case of chiral nematic LCs, which are partial 1D photonic crystals, where the DOS can be derived from the transmission properties of a layer with finite thickness [2], enabling the emission spectrum to be predicted using equations (4.15).

For the extraction of the transmission coefficient and subsequently the density of photon states in chiral nematic LCs, we proceed as follows. We consider a boundary value problem formulated such that two plane waves of the diffracting polarization are incident on a chiral nematic LC layer. The assumption of no boundary reflection allows the separation of eigenpolarizations, introducing an error of the order of the relative dielectric anisotropy [8]. By demanding a continuous tangential component of the electric and magnetic field at the layer-glass interface, we formulate a system, the solution of which yields the transmission coefficient for light of diffractive circular polarization. The transmission coefficient for a layer with  $N$  full precessions of the molecular director, and hence thickness  $L = Np$ , reads [6]

$$T = \frac{\exp\left(\frac{i\tau L}{2}\right) \left(\frac{q\tau}{k^2}\right)}{\frac{q\tau}{k^2} \cos(qL) + i \left[ \left(\frac{\tau}{2k}\right)^2 + \left(\frac{q}{k}\right)^2 - 1 \right] \sin(qL)}, \quad (4.17)$$

where

$$q = k \sqrt{1 + \left(\frac{\tau}{2k}\right)^2} - \sqrt{\left(\frac{\tau}{k}\right)^2 + \delta^2}.$$

In these expressions,  $\tau = (4\pi)/p$ ,  $k = (\omega/c)\epsilon_0$ , with  $\epsilon_0 = (\epsilon_{\parallel} + \epsilon_{\perp})/2$  being the average dielectric constant where  $\epsilon_{\parallel}$  and  $\epsilon_{\perp}$  are the relative dielectric constants parallel and perpendicular to the director, respectively, and  $\delta = (\epsilon_{\parallel} - \epsilon_{\perp})/(\epsilon_{\parallel} + \epsilon_{\perp})$  the relative dielectric anisotropy,  $p$  the helical pitch and  $c$  the speed of light in the vacuum. This relation is a different expression to the one given in [2], where Maxwell's equations are solved in a frame rotating with the molecular director. Omitting common real prefactors and frequency independent terms, the real and imaginary parts, respectively, of

the transmission coefficient (equation (4.17)) read

$$\begin{aligned} X &= \left(\frac{q\tau}{k^2}\right) \cos(qL), \\ Y &= - \left[ \left(\frac{\tau}{2k}\right)^2 + \left(\frac{q}{k}\right)^2 - 1 \right] \sin(qL). \end{aligned} \quad (4.18)$$

The normalized DOS can be written as we have shown in the previous chapter

$$\rho = \frac{c}{Np\sqrt{\epsilon_0}} \frac{X \frac{dY}{d\omega} - Y \frac{dX}{d\omega}}{X^2 + Y^2}. \quad (4.19)$$

Focusing in the region of the band gap, we can write:  $q = i\tilde{q}$ . The real and imaginary parts become, respectively,

$$\begin{aligned} \tilde{X} &= \left[ \left(\frac{\tau}{2k}\right)^2 - \left(\frac{\tilde{q}}{k}\right)^2 - 1 \right] \sinh(\tilde{q}L), \\ \tilde{Y} &= \left(\frac{\tilde{q}\tau}{k^2}\right) \cosh(\tilde{q}L). \end{aligned} \quad (4.20)$$

One can easily verify that in this region

$$\tilde{\rho} = \frac{c}{Np\sqrt{\epsilon_0}} \frac{\tilde{X} \frac{d\tilde{Y}}{d\omega} - \tilde{Y} \frac{d\tilde{X}}{d\omega}}{\tilde{X}^2 + \tilde{Y}^2} = \frac{c}{Np\sqrt{\epsilon_0}} \frac{X \frac{dY}{d\omega} - Y \frac{dX}{d\omega}}{X^2 + Y^2} = \rho.$$

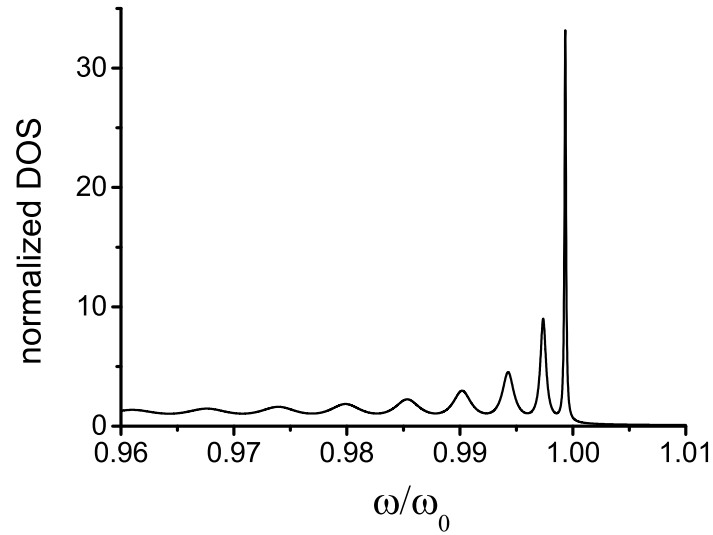
Hence, we find that the expressions in relation (4.18) can also be used inside the band gap. Letting now  $N \rightarrow \infty \Rightarrow L \rightarrow \infty$  and approximating  $\sinh(\tilde{q}L) = \cosh(\tilde{q}L) \simeq (1/2) \exp(\tilde{q}L)$ , we reproduce the asymptotic behaviour  $\rho \sim (1/N)$  in the middle of the band-gap, in a similar fashion to a QWS, as we have shown in the previous chapter. The low frequency band-edge for a chiral nematic LC is given by the formula  $\omega_0 = \omega_c / \sqrt{1 + \delta}$  where  $\omega_c = (2\pi c)/p$  is the center of the reflection band [6]. Similarly to a QWS,

also, we find that for a chiral nematic the value of the DOS at a wavelength edge is a quantity increasing with the product  $N\delta$ , which is an indication of feedback-strength in the cavity. In our treatment, we approximate the edge mode frequency in the long wavelength edge with  $\omega_0$ . For a layer with finite thickness, this approximation increases in validity as  $N\delta$  is appreciably higher than unity [6]. The expressions in (4.15) should be averaged over all possible orientations of the dipole moment and from this procedure we obtain the pertinent transition dipole order parameter, as shown in [2]. In what follows, we will assume that the dipole order parameter is zero; this corresponds to an isotropic distribution of the dyes i.e., absence of preferential alignment. We also consider a uniform distribution of the fluorescent molecules in the chiral nematic host, so that our results are not affected by the spatial distribution of the eigenmodes. In [2] it is shown that using these assumptions  $\langle |\hat{\mathbf{e}}_{kl}(\mathbf{R})\hat{\mathbf{r}}_{10}|^2 \rangle = 1/3$ .

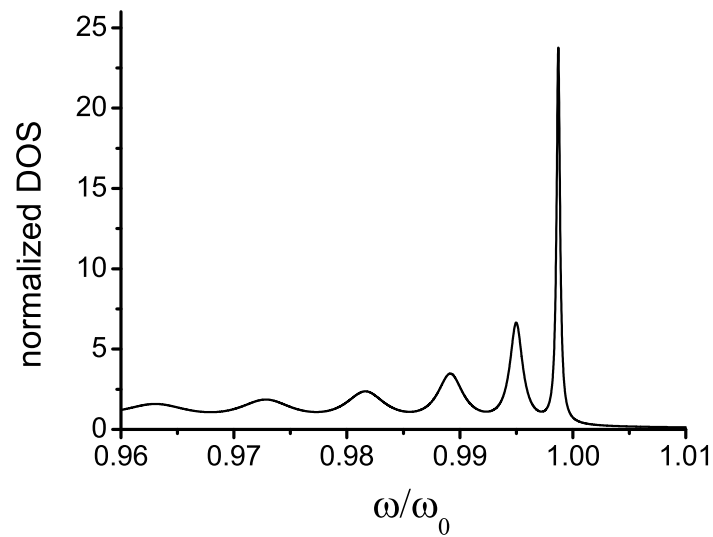
### 4.3 Main results for radiative chiral nematic LCs

Equations (4.15) allow the calculation of the emission spectrum, subject to the the determination of the DOS in the resonating structure.

First of all, Figure 4.1 depicts the DOS profile for a chiral nematic LC layer with different values of thickness and relative dielectric anisotropy, for the low frequency edge. It is shown that the value of the DOS increases with increasing product of thickness and relative dielectric anisotropy. Both these quantities determine distributed feedback within the structure. The DOS



(a)



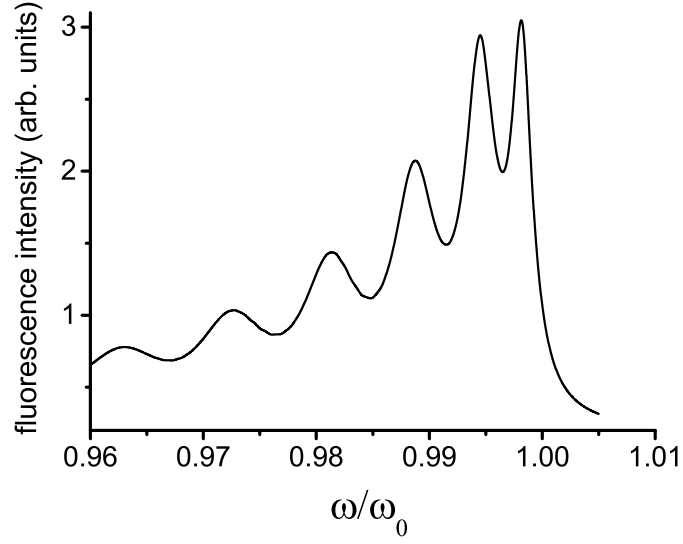
(b)

Figure 4.1: (a) Theoretically obtained normalized DOS using (4.19) for  $N = 65$  precessions of the director and  $\delta = 0.091$ . (b) Theoretically obtained normalized DOS using equation (4.19) for  $N = 40$  precessions and  $\delta = 0.13$ .

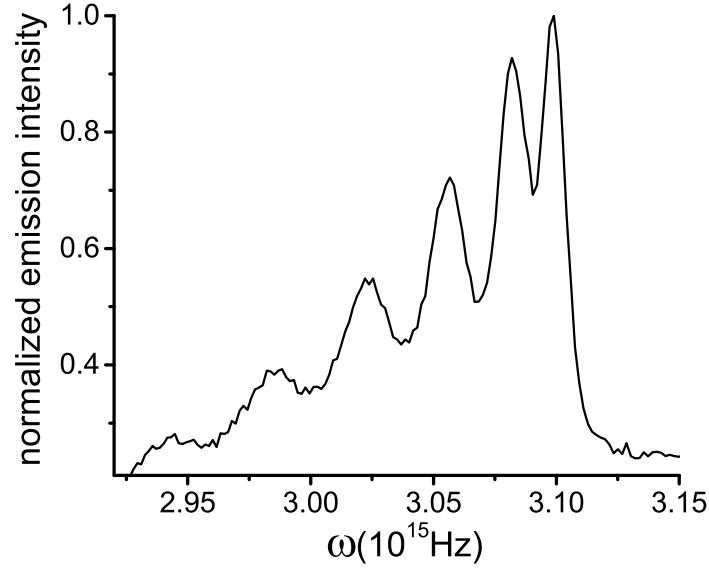
exhibits a distinct peak at the short frequency edge alongside some minor resonance peaks decreasing in magnitude with decreasing frequency. Similar results have been also reported elsewhere [2] and appear in the graphs of the previous chapter. The DOS value for the dominant edge mode diverges to infinity for a given relative dielectric anisotropy and  $N \rightarrow \infty$ .

The DOS calculated for a sample with  $N = 40$  precessions of the molecular director and relative dielectric anisotropy  $\delta = 0.13$  is now employed to calculate the emission profile from equation (4.14). Figure 4.2 shows a comparison between the theoretically obtained fluorescence spectrum and that measured experimentally for a cell with thickness  $L \simeq 12 \mu\text{m}$  ( $N \simeq 40$ ) consisting of the chiral nematic LC mixture E49 doped with the fluorescent dye DCM. The LC sample was illuminated by a frequency-doubled continuous-wave Nd:YAG laser producing an almost-monochromatic beam of  $\lambda = 532\text{nm}$  which was strongly attenuated by two cross-polarizers. The beam was subsequently converted to the circular polarization of the opposite handedness to that of the sample, in order to excite the fluorescent dye uniformly (see [2]), and then collimated and focussed onto the LC sample. Radiation collected from the sample was collimated by an achromatic lens and then coupled to an optical fibre. The fluorescence spectrum was obtained using a universal serial bus spectrometer with a resolution of 0.3 nm. There is a good agreement between theoretical and experimental results, from which we deduce that the spontaneous emission spectrum exhibits significant differences from the pattern dictated by the DOS presented in Figure 4.1.

However, by accounting for the emission spectrum using the approach discussed herein appears to provide a better match with experimental observa-



(a)



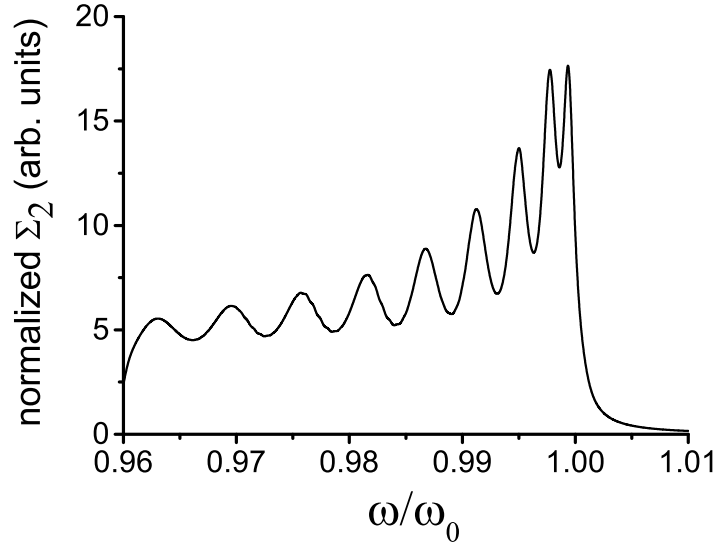
(b)

Figure 4.2: In all the figures that follow, we use the symbol  $\omega$  instead of  $\Omega$  that appears in the relations for the radiation terms, for convenience. (a) Theoretically obtained emission spectrum for a chiral nematic LC with a gain medium for  $N = 40$  precessions of the director,  $\delta = 0.13$ ,  $\gamma_{10} = 1.25 \cdot 10^{-4} \cdot \omega_0$  and  $\gamma = 9.36 \cdot 10^{-4} \cdot \omega_0$ . In this case  $\omega'_{10} = 1.06 \cdot \omega_0$ . (b) Experimentally determined fluorescence spectrum obtained from a chiral nematic LC sample doped with DCM (with a fluorescence peak in the LC host at  $\lambda_{max} \simeq 580nm$ ) and  $N \approx 40$  full precessions of the molecular director. For (a) the integration limits in Equations (4.14),(4.15) are  $\omega_{min} = 0.96 \cdot \omega_0$  and  $\omega_{max} = 1.01 \cdot \omega_0$ . Here,  $\beta = 1.05 \cdot 10^{29}[SI]$

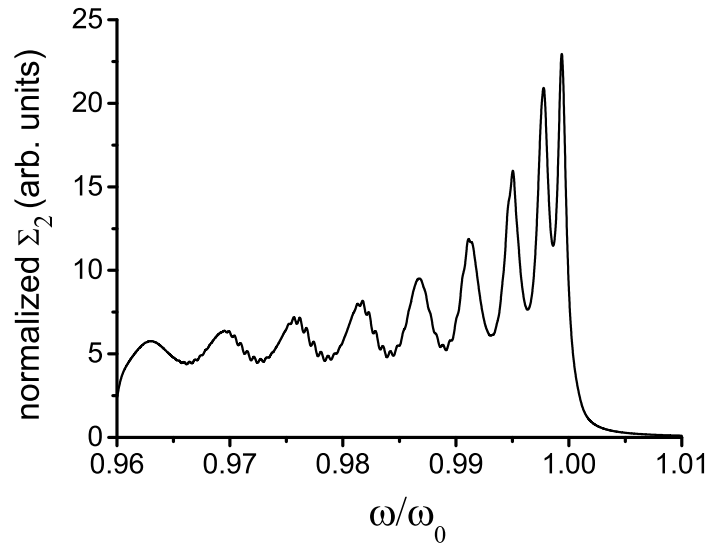
tions. Our results demonstrate that we ought to account additionally for the relative position of the transition frequency with respect to the edge mode location in order to describe more accurately the emission spectrum from these periodic structures. At large oscillator strengths of the atomic transition, there is a Fano-resonant mechanism between the discrete spectrum of the atomic transition and the continuum of photon states in the chiral nematic feedback structure, occurring when the atomic transition frequency lies in the region of the continuum. The same mechanism is associated with the splitting of the fluorescence into two components in the region of the logarithmic singularity due to the saddle point in the dispersion curve of a 2D photonic crystal [5].

Figure 4.3 depicts the transition broadening term  $\Sigma_2$  (equation (4.16)) normalized by the same arbitrary constant, for two different values of the cavity losses. We find that apart from the change in magnitude of the term with decreasing losses, there is also a change in the relative height of the first two edge-mode peaks. Moreover, we quantify the effect of resonance for a chiral nematic LC resonator in which the feedback properties are enhanced.

Figure 4.4 depicts the emission profile calculated from equation (4.14) for small and large detuning, i.e., varying the frequency offset between the electronic transition and the dominant edge mode. Our theoretical results show that the first two peaks which correspond to the two edge modes closest to the band gap are less pronounced than those in the DOS profile, when under the condition of exact resonance. This can be inferred from Figures 4.1(a), (b) and Figure 4.4(a). Their magnitude also decreases with increasing detuning (Figure 4(b)). The presence of residual attenuation due to a variety of

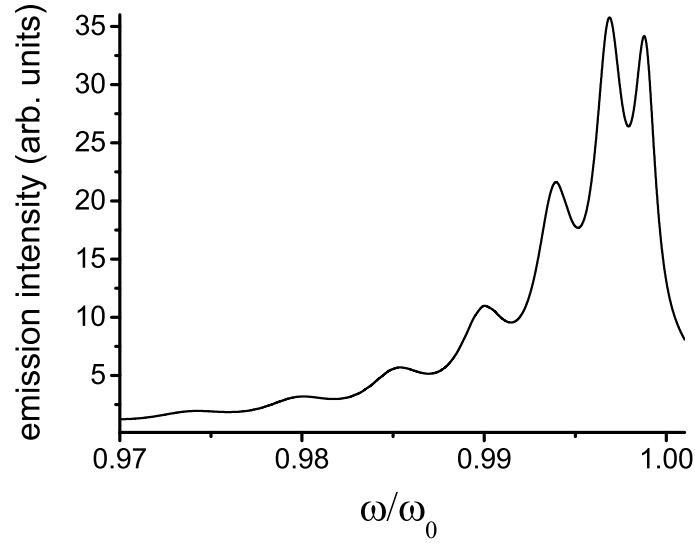


(a)

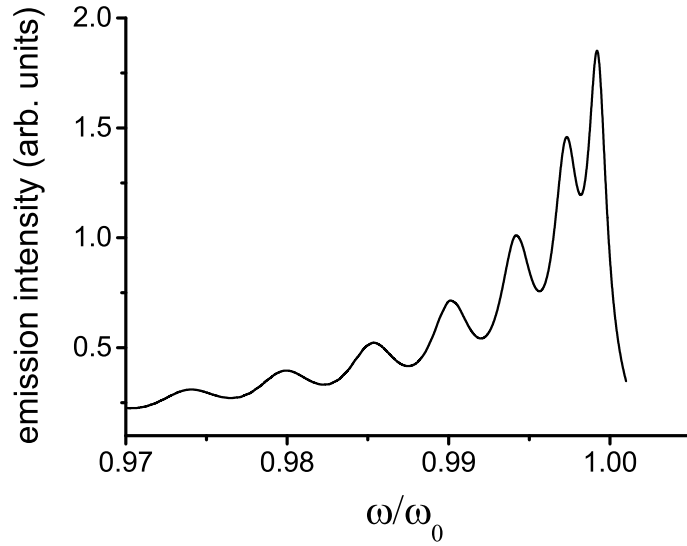


(b)

Figure 4.3: Transition broadening  $\Sigma_2$  term as a function of frequency for a chiral LC with a gain medium, for  $N = 60$  precessions of the director,  $\delta = 0.13$  and two different values of cavity losses. In (a)  $\gamma = 5.55 \cdot 10^{-4} \cdot \omega_0$  and in (b)  $\gamma = 3.70 \cdot 10^{-4} \cdot \omega_0$ .



(a)



(b)

Figure 4.4: Theoretically obtained emission spectrum for a chiral nematic LC with a gain medium for  $N = 65$  precessions of the director,  $\delta = 0.091$ ,  $\gamma_{10} = 1.25 \cdot 10^{-4} \cdot \omega_0$ ,  $\gamma = 7.02 \cdot 10^{-4} \cdot \omega_0$  for two different detuning values. In (a)  $\omega'_{10} = 1.005 \cdot \omega_0$  and in (b)  $\omega'_{10} = 1.05 \cdot \omega_0$ . In (a),  $\omega_{min} = 0.95 \cdot \omega_0$  and  $\omega_{max} = 1.001 \cdot \omega_0$  whereas in (b),  $\omega_{min} = 0.97 \cdot \omega_0$  and  $\omega_{max} = 1.001 \cdot \omega_0$ . Here,  $\beta = 3 \cdot 10^{28} [SI]$ .

mechanisms, such as scattering from long range thermal fluctuations of the molecular director and absorption from excited atomic levels, inhibits the feedback mechanism inside the resonator, which is manifested as a decrease in the DOS [10]. This result can also be demonstrated for a Fabry-Pérot resonator [10].

## 4.4 A 2D photonic crystal and the DOS

We will now address a particular case in which one can derive analytic expressions for the Lamb shift and the transition broadening featuring in equation (4.14). Unlike 1D photonic crystals, where the DOS displays Van Hove singularities at the band extrema, spontaneous emission in 2D crystals is not enhanced at these points despite the fact that the group velocity assumes zero values there. The exact dispersion relationship depends on the lattice of the periodic structure and the polarization of the modes considered. Here it is assumed that the atomic transition frequency is close to a saddle point ( $P_1$  type) in one of the branches of the photonic band spectrum, irrespective of the lattice and the emission direction from the periodic structure. Therefore, our findings will pertain to the general case. It is known that near the saddle point in the dispersion curve of a 2D photonic crystal, the DOS exhibits a logarithmic divergence [1], [5]. We start by calculating the integral (the expression for the DOS has a minus sign in front of the logarithm that we omit here and restore in the final expressions)

$$I = \int_{-\infty}^{+\infty} f(\omega) d\omega, \quad \text{with } f(\omega) = \frac{\log(|a(\omega_0)(\omega - \omega_0)|)}{(\omega - \omega_1)(\omega - \omega_2)}, \quad (4.21)$$

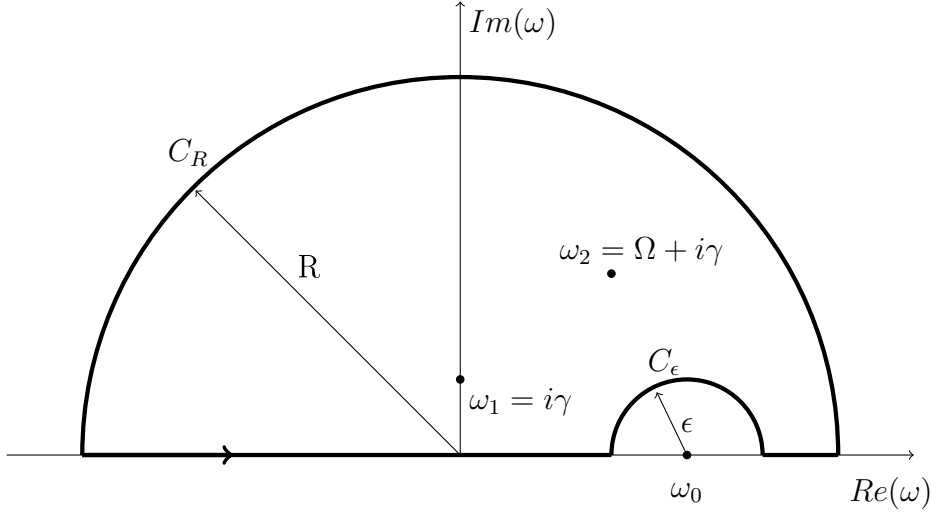


Figure 4.5: The integration contour for the application of the residue theorem in (4.22).

where  $a(\omega_0)$  has dimensions of  $\text{Hz}^{-1}$  and is related to the specific photonic crystal properties and the expansion near the saddle point [5]. We will find, however, that our final results are independent of this factor. Since the residue theorem is applied for single-valued functions, we consider the branch of the logarithm defined by  $\log(z) = \log|z| + i\theta$ ,  $-\frac{\pi}{2} \leq \theta < \frac{3\pi}{2}$ .

The integration contour is shown in Figure 4.5.

According to the residue theorem, we have

$$\begin{aligned} \int_{\omega_0+\epsilon}^R f(\omega)d\omega + \int_{C_R} f(\omega)d\omega + \int_{-R}^{\omega_0-\epsilon} f(\omega)d\omega + \int_{C_\epsilon} f(\omega)d\omega \\ = 2\pi i \left\{ \frac{\log[a(\omega_2 - \omega_0)]}{\omega_2 - \omega_1} + \frac{\log[a(\omega_1 - \omega_0)]}{\omega_1 - \omega_2} \right\}, \end{aligned} \quad (4.22)$$

where  $\omega_1 = i\gamma$  and  $\omega_2 = \Omega + i\gamma$ . We also have

$$\begin{aligned} \left| \int_{C_\epsilon} \frac{\log[a(\omega - \omega_0)]}{(\omega - \omega_1)(\omega - \omega_2)} d\omega \right| &= \left| \int_0^\pi \frac{\log(a\epsilon e^{i\theta})}{(\omega_0 + \epsilon e^{i\theta} - \omega_1)(\omega_0 + \epsilon e^{i\theta} - \omega_2)} i\epsilon e^{i\theta} d\theta \right| \\ &\leq \frac{|\log(a\epsilon)| + \pi}{(|\omega_0 - \omega_1| - \epsilon)(|\omega_0 - \omega_2| - \epsilon)} \pi\epsilon \rightarrow 0, \end{aligned}$$

as  $\epsilon \rightarrow 0$ , since  $\epsilon \log \epsilon \rightarrow 0$  when  $\epsilon \rightarrow 0$ . For  $R$  sufficiently large, we also have

$$\begin{aligned} \left| \int_{C_R} \frac{\log[a(\omega - \omega_0)]}{(\omega - \omega_1)(\omega - \omega_2)} d\omega \right| &= \left| \int_0^\pi \frac{\log[a(Re^{i\theta} - \omega_0)]}{(Re^{i\theta} - \omega_1)(Re^{i\theta} - \omega_2)} iRe^{i\theta} d\theta \right| \\ &\leq \frac{|\log[a(R + \omega_0)]| + \pi}{(R - |\omega_1|)(R - |\omega_2|)} \pi R \rightarrow 0, \end{aligned}$$

since  $\frac{\log R}{R} \rightarrow 0$  when  $R \rightarrow \infty$ . Hence, we deduce that

$$\begin{aligned} \int_{-\infty}^{+\infty} f(\omega) d\omega &= \int_{-\infty}^{+\infty} \frac{\log|a(\omega - \omega_0)|}{(\omega - \omega_1)(\omega - \omega_2)} d\omega + i\pi \int_{-\infty}^{\omega_0} \frac{d\omega}{(\omega - \omega_1)(\omega - \omega_2)} \\ &= \frac{2\pi i}{\omega_2 - \omega_1} \log\left(\frac{\omega_2 - \omega_0}{\omega_1 - \omega_0}\right), \end{aligned} \quad (4.23)$$

since

$$\int_{-\infty}^{\omega_0} \frac{d\omega}{(\omega - \omega_1)(\omega - \omega_2)} = \frac{1}{\omega_2 - \omega_1} \log\left(\frac{\omega_2 - \omega_0}{\omega_1 - \omega_0}\right). \quad (4.24)$$

We must note here that the behaviour of the DOS far from the saddle point may be different (usually we assume  $\rho \propto \omega$  far from the critical point). In that case, the upper integration limit is replaced by the Compton frequency [5], [7],  $\omega_c = \frac{mc^2}{\hbar} \cong 10^{21}$  Hz, which is many orders of magnitude higher than the frequencies in the visible part of the electromagnetic spectrum. Therefore, the integration to infinity can be justified. We conclude that

$$\int_{-\infty}^{+\infty} \frac{\log |a(\omega - \omega_0)|}{(\omega - \omega_1)(\omega - \omega_2)} d\omega = \frac{\pi i}{\omega_2 - \omega_1} \log \left( \frac{\omega_2 - \omega_0}{\omega_1 - \omega_0} \right) = \frac{\pi i}{\Omega} \log \left( \frac{\Omega + i\gamma - \omega_0}{i\gamma - \omega_0} \right). \quad (4.25)$$

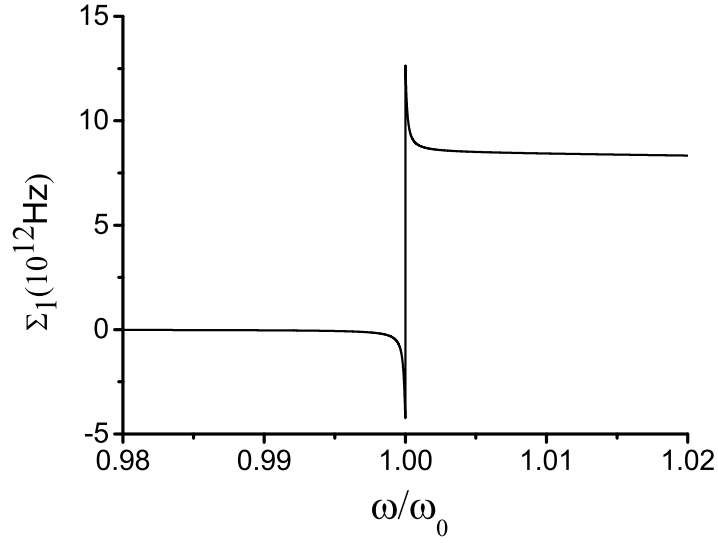
As we have selected the particular branch of the logarithmic function with  $-\frac{\pi}{2} \leq \theta < \frac{3\pi}{2}$ , the real part of the resulting integral will have a discontinuity since the phase of the logarithm varies between  $-\pi$  and  $0$  for an argument selection  $-\pi \leq \theta < \pi$ . This is also understood from the fact that in order for the identity  $\log(z_1 z_2) = \log(z_1) + \log(z_2)$  to be applied, then  $\arg(z_1) + \arg(z_2)$  must lie within the phase range of the chosen branch—otherwise there is an offset by  $2\pi$ . The same discontinuity, linked to the Lamb shift would have been exhibited if we had chosen any other branch cut outside our integration contour. The Lamb shift and the transition broadening term, in this case, read

$$\Sigma_1 = -\beta' |\hat{\mathbf{e}}_{kl} \hat{\mathbf{r}}_{10}|^2 \Re \left\{ \int_{-\infty}^{+\infty} \frac{\log |a(\omega - \omega_0)|}{(\omega - i\gamma)(\omega - \Omega - i\gamma)} d\omega \right\}, \quad (4.26)$$

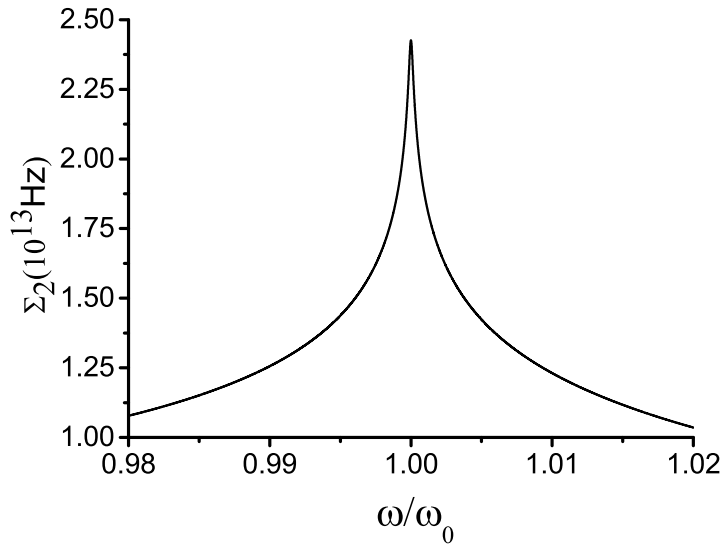
$$\Sigma_2 = -\beta' |\hat{\mathbf{e}}_{kl} \hat{\mathbf{r}}_{10}|^2 \Im \left\{ \int_{-\infty}^{+\infty} \frac{\log |a(\omega - \omega_0)|}{(\omega - i\gamma)(\omega - \Omega - i\gamma)} d\omega \right\}, \quad (4.27)$$

where we have assumed that the normalization term  $\beta$  in equations (4.15) is modified by some parameters particular to the expression of the DOS for a photonic crystal [5], to yield  $\beta'$ . We can deduce that for 2D photonic crystals in the saddle point of the dispersion function, resonance is associated with a Lamb dip in the fluorescence spectrum and a split in the real part of the Fourier transform of the Green's function.

The split (term  $\Sigma_1$ ) here is due to the behaviour of the complex logarithmic function; however, as we can observe in Figures 4.6(a), (b), the magnitude of



(a)



(b)

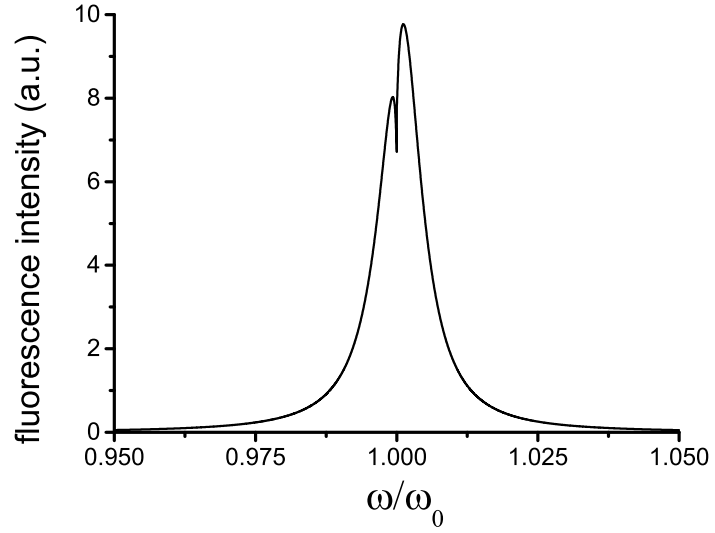
Figure 4.6: (a) The Lamb shift ( $\Sigma_1$ ) as a function of frequency for a 2D photonic crystal with a logarithmic singularity in the DOS at  $\omega_0$ . (b) Transition broadening ( $\Sigma_2$ ) as a function of frequency for a photonic crystal with a logarithmic singularity in the DOS at  $\omega_0$ . In all cases above,  $\omega'_{10} = 1.001 \cdot \omega_0$  and  $\gamma = 1.25 \cdot 10^{-4} \cdot \omega_0$

that term is significantly lower than the broadening term  $\Sigma_2$  of the transition  $|1, \{0\}\rangle \rightarrow |0, \{1\}_\kappa\rangle$ .

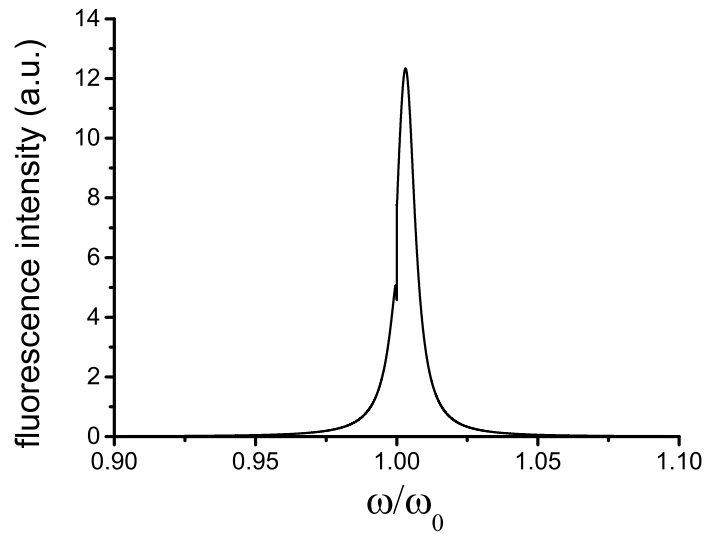
The Lamb dip essentially vanishes for larger detunings, as we can see in the emission spectra of Figures 4.7(a), (b). A Lamb shift has also been reported inside the (complete) photonic band gap for hydrogenic atoms embedded in 1D periodic structures [11].

## 4.5 Discussion of results

Concerning the validity of our results, we note that the rotating wave approximation we relied upon, requires a small detuning from the atomic transition frequency, in order for the ‘non-resonant’ terms to be much smaller than the ‘resonant’ ones when averaging over a time period of the order of  $1/\omega$  in the interaction picture [3],[7]. This constraint is met by selecting an appropriate upper and lower integration limit in equations (4.15) and by the presence of the function  $\log |a(\omega - \omega_0)|$  in equations (4.26) ensuring that the major contribution to the integral originates from the region  $|\omega - \omega_{10}| \ll (\omega + \omega_{10})$ . Likewise, the most significant contribution in the emission from chiral nematics will be from the first two edge mode peaks on the same side of the band gap, for  $N\delta \gg 1$ . Regarding the the Generalized Rotating Wave Approximation (GRWA) in [3], one can effect the change of basis from  $|\mp x, N\rangle$  to the adiabatic eigenstates  $|\Psi_\pm, N\rangle$  through a unitary transformation using the operator (for simplicity we denote by  $\omega_0$  the electromagnetic-field frequency and by  $\Omega$  the atomic transition frequency)



(a)



(b)

Figure 4.7: (a) Emission spectrum for a 2D photonic crystal with a logarithmic singularity in the DOS at  $\omega_0$ , as a function of frequency for  $\omega'_{10} = 1.002 \cdot \omega_0$ . (b) Emission spectrum for the photonic crystal as a function of frequency for  $\omega'_{10} = 1.005 \cdot \omega_0$ . In all cases above,  $\beta' = 3 \cdot 10^{27} [SI]$ ,  $\gamma = 1.25 \cdot 10^{-4} \cdot \omega_0$  and  $\gamma_{10} = 1.25 \cdot 10^{-5} \cdot \omega_0$ .

$$\hat{D} \left( \frac{\mu}{\omega_0} \hat{\sigma}_z \right) = \exp \left[ -\frac{\mu}{\omega_0} \hat{\sigma}_z (\hat{a}^\dagger - \hat{a}) \right]. \quad (4.28)$$

As we can readily verify,  $\hat{D}^\dagger \hat{D} = \mathbb{I}$ . We apply this transformation to the general Hamiltonian

$$\hat{H} = \omega_0 \hat{a}^\dagger \hat{a} + \frac{1}{2} \Omega \hat{\sigma}_x + \mu \hat{\sigma}_x (\hat{a}^\dagger + \hat{a}) = \omega_0 \hat{a}^\dagger \hat{a} + \frac{1}{2} \Omega \hat{\sigma}_x + \mu (\hat{\sigma}_- \hat{a}^\dagger + \hat{\sigma}_+ \hat{a} + \hat{\sigma}_+ \hat{a}^\dagger + \hat{\sigma}_- \hat{a}), \quad (4.29)$$

where  $\hat{\sigma}_\pm = (1/2)(\hat{\sigma}_z \mp i\hat{\sigma}_y)$  are the ladder operators in the basis of  $\hat{\sigma}_x$ , and  $\mu$  is the interaction constant. This Hamiltonian, then, is transformed to

$$\hat{H}' = \omega_0 \hat{a}^\dagger \hat{a} + \frac{1}{2} \Omega \hat{\sigma}_x \exp \left[ -\frac{2\mu}{\omega_0} \hat{\sigma}_z (\hat{a}^\dagger - \hat{a}) \right] = \omega_0 \hat{a}^\dagger \hat{a} + \frac{1}{2} \Omega \hat{\sigma}_x + \hat{H}_{1,x} + \hat{H}_{1,y}, \quad (4.30)$$

Using the properties of the Pauli matrices:  $\hat{\sigma}_x^2 = \mathbb{I}$  and  $\hat{\sigma}_x \hat{\sigma}_z = -i\hat{\sigma}_y$ , and setting  $\hat{u} = -\frac{\mu}{\omega_0} (\hat{a}^\dagger - \hat{a})$  we expand the second term in (4.29) and we obtain

$$\hat{\sigma}_x \exp(-\hat{\sigma}_z \hat{u}) = \hat{\sigma}_x \left( \mathbb{I} + \sum_{\kappa=1}^{+\infty} \frac{\hat{u}^{(2\kappa)}}{(2\kappa)!} \right) - \hat{\sigma}_x \hat{\sigma}_z \sum_{\kappa=1}^{+\infty} \frac{\hat{u}^{(2\kappa-1)}}{(2\kappa-1)!}, \quad (4.31)$$

so that the last two terms in the transformed Hamiltonian have the form

$$\begin{aligned} \hat{H}_{1,x} &= \frac{\Omega \hat{\sigma}_x}{2} \sum_{\kappa=1}^{+\infty} \frac{\left( \frac{2\mu}{\omega_0} (\hat{a}^\dagger - \hat{a}) \right)^{2\kappa}}{(2\kappa)!}, \\ \hat{H}_{1,y} &= \frac{i\Omega \hat{\sigma}_y}{2} \sum_{\kappa=1}^{+\infty} \frac{\left( \frac{2\mu}{\omega_0} (\hat{a}^\dagger - \hat{a}) \right)^{2\kappa-1}}{(2\kappa-1)!}. \end{aligned} \quad (4.32)$$

Carrying out the GRWA by keeping the “energy-conserving” terms, the contribution of  $\hat{H}_{1,x}$  is neglected since the only terms that do not have a rapid time-dependence contain only powers of the number operator resulting in zero net-excitation of the oscillator. Also,  $\hat{H}_{1,y}$  reduces to the coupling term

$$\Omega \left( \frac{\mu}{\omega_0} \right) [\hat{\sigma}_- \hat{a}^\dagger f(\hat{a}^\dagger \hat{a}) + \hat{\sigma}_+ f^*(\hat{a}^\dagger \hat{a}) \hat{a}], \quad (4.33)$$

which is a generalization of the term  $\mu(\hat{\sigma}_- \hat{a}^\dagger + \hat{\sigma}_+ \hat{a})$  in the standard RWA. At this point, we ought to mention that the two-level system approach is certainly a considerable simplification for fluorescent dyes. These complex molecules have states with many vibrational and rotational levels determining their spectra. In this analysis, mechanisms such as triple state generation and resonant energy transfer have also been ignored. Under the assumption of very small detuning, the effect of these phenomena can be quantified through the introduction of an imaginary part in the mode frequency. A model of coherent control of fluorescence would be that of a three-level system where the transition  $|2\rangle \rightarrow |1\rangle$  between the two upper levels is driven by a laser field and that the spontaneous emission transitions  $|2\rangle \rightarrow |1\rangle$  and  $|1\rangle \rightarrow |0\rangle$  are precluded by either symmetry or the presence of the band-gap [12]. In one of these configurations the levels  $|0\rangle$  and  $|1\rangle$  have the same symmetry (hence there is no allowed dipole-transition between them). We also assume that the dipole allowed transition occurs between the levels  $|2\rangle$  and  $|1\rangle$  and that the transition frequency  $\omega_{21}$  is far inside the band-gap, such that the transition  $|2\rangle \rightarrow |1\rangle$  will create a photon-atom bound state whose radiative lifetime is the same as the two photon  $|1\rangle \rightarrow |0\rangle$  transition. In this configuration  $|1\rangle \rightarrow |0\rangle$  is a dipole allowed transition and it is assumed that  $\omega_{21}$  is near the band edge. The Hamiltonian of the system is  $\hat{H} = \hat{H}_A + \hat{H}_F + \hat{H}_I + \hat{H}_L$ ,

where

$$\begin{aligned}
\hat{H}_A &= \hbar \sum_{j=0}^2 \omega_j \hat{\sigma}_{jj}, \\
\hat{H}_R &= \hbar \sum_{\lambda=1}^2 \sum_{\mathbf{k}} \omega_{\mathbf{k}} \hat{a}_{\mathbf{k}\lambda}^\dagger \hat{a}_{\mathbf{k}\lambda}, \\
\hat{H}_I &= i\hbar \sum_{\lambda=1}^2 \sum_{\mathbf{k}} g_{\mathbf{k}\lambda} (\hat{a}_{\mathbf{k}\lambda}^\dagger \hat{\sigma}_{02} - \hat{\sigma}_{20} \hat{a}_{\mathbf{k}\lambda}), \\
\hat{H}_L &= id_{21} E_0 \{ \hat{\sigma}_{21} \exp [i(\omega_{21}t + \phi)] - \hat{\sigma}_{21} \exp [-i(\omega_{21}t + \phi)] \},
\end{aligned} \tag{4.34}$$

where  $\hat{\sigma}_{ij} = |i\rangle\langle j|$  are fermionic operators (the energy of the  $j^{\text{th}}$  level is  $\hbar\omega_j$ ) and

$$g_{\mathbf{k}\lambda} = \frac{\omega_{20}d_{20}}{\hbar} \left( \frac{\hbar}{2\varepsilon_0\omega_{\mathbf{k}}V} \right)^{1/2} \hat{\mathbf{e}}_{\mathbf{k},\lambda} \cdot \hat{\mathbf{d}}_{20}, \tag{4.35}$$

is the atom-field coupling constant for the  $|2\rangle \rightarrow |0\rangle$  transition (in this expression, the hat denotes a unit vector). The last term in the Hamiltonian represents the interaction of the atom with the laser field. We assume that the latter is sufficiently strong such that it is treated classically in the context of the first quantization, with the pre-factor in front of the square-brackets being  $\hbar\Omega_R$ , where  $\Omega_R$  is the Rabi frequency, much larger than the detuning. Recently, rare-earth-doped nanocrystals have been used as the gain medium hosted in chiral nematic LCs [13]. In this case, the assumption of a two-level atom interacting with the electromagnetic field maybe much more appropriate to describe spontaneous emission from the resonator. Employing the DOS in the JC model is then expected to lead to a better match between theory and experiment. Moreover, for a further insight to spontaneous emission

from such periodic structures, we could resort to the resolvent method [7], in which the matrix elements of the time evolution operator can be calculated. We will detail the fundamental concepts and techniques of this method in the last chapter.

## 4.6 More on the Fano-Anderson model

We relate now our analysis to the Fano-Anderson model, pertaining to the interaction of a discrete state  $|d\rangle$  with a continuum described by a set of states  $|k\rangle$ . As before, the ‘atom’-field Hamiltonian in a frame rotating with frequency  $\omega_d$  assumes the form

$$H = \int \hbar\delta\omega(k)|k\rangle\langle k|dk + \hbar \int [v(k)|d\rangle\langle k| + v^*(k)|k\rangle\langle d|] dk, \quad (4.36)$$

where the second (Hermitian) interaction term accounts for a ‘coloured-coupling’ (dependent on the wavenumber). Evidently, this Hamiltonian is Hermitian. Likewise, the wavefunction of the system is written as  $|\psi\rangle = c_d(t)|d\rangle + \int c(k,t)v(k)dk$  and the expansion coefficients satisfy the coupled equations of motion (obtained by Schrödinger’s equation)

$$\left\{ \begin{aligned} i \frac{dc_d(t)}{dt} &= \omega_d c_d(t) + \int c(k,t)v(k)dk \end{aligned} \right. \quad (4.37a)$$

$$\left\{ \begin{aligned} i \frac{dc(k,t)}{dt} &= \omega(k)c(k,t) + v^*(k)c_d(t) \end{aligned} \right. \quad (4.37b)$$

Denoting the Laplace Transform of  $c_d(t)$  by

$$\tilde{c}_d(s) = \int_0^\infty c_d(t) \exp(-st)dt, \quad (4.38)$$

and then applying the Laplace Transform in both handsides of relations of the system (4.37a) we obtain (assuming that  $c_d(t = 0) = 1$  and  $c(k, t = 0) = 0$ )

$$\tilde{c}_d(s) = \frac{i}{is - \omega_d - \Sigma(s)}, \quad (4.39)$$

where  $\Sigma(s)$  is called the ‘self-energy’ term reading

$$\Sigma(s) = \int \frac{|v(k)|^2}{is - \omega(k)} dk = \int_{\omega_1}^{\omega_2} \frac{\rho(\omega')|v(\omega')|^2}{is - \omega'} d\omega', \quad (4.40)$$

where  $\rho(\omega)$  is the density of photon states. Applying the inverse Laplace Transform, we finally obtain

$$c_d(t) = \frac{1}{2\pi} \int_{\sigma - i\infty}^{\sigma + i\infty} \frac{e^{st}}{is - \omega_d - \Sigma(s)} ds, \quad (4.41)$$

where  $\sigma = 0^+$ , since the poles of  $\tilde{c}_d(s)$  if they exist, belong to the imaginary axis. Using the Sokhotski-Plemelj theorem, for  $\omega \in (\omega_1, \omega_2)$  we have

$$\Sigma(s = -i\omega \pm 0^+) = \Delta(\omega) \mp i\pi\rho(\omega)|v(\omega)|^2, \quad (4.42)$$

where

$$\Delta(\omega) = \mathcal{P} \int_{\omega_1}^{\omega_2} \frac{\rho(\omega')|v(\omega')|^2}{\omega - \omega'} d\omega' \quad (4.43)$$

The poles  $s_p = -i\Omega$  of  $\tilde{c}_d(s)$  correspond to bound states of the Hamiltonian, since they lead to the exponential term  $\exp(-i\Omega t)$  with constant magnitude, after applying the residue theorem. These poles satisfy the conditions

$$\Omega - \omega_d = \Delta(\Omega), \quad \rho(\Omega)|v(\Omega)|^2 = 0 \quad (4.44)$$

For an infinitely-thick chiral nematic LC sample, the density of photon states reads

$$\rho_j = \frac{dk_j}{d\omega} = \frac{dk_j}{d\lambda'} \frac{d\lambda'}{d\omega} = -\frac{p\sqrt{\varepsilon}}{c} \lambda'^2 \left( \frac{1}{\lambda'} \frac{dm'_i}{d\lambda'} - \frac{m'_i}{\lambda'^2} \right), \quad (4.45)$$

where

$$\frac{dm_j}{d\lambda'} = \left( 1 \mp \frac{2}{\sqrt{4\lambda'^2 + \delta^2}} \right) \frac{\lambda'}{m'_j}. \quad (4.46)$$

The index  $j$  assumes values 1, 2 for the non-diffracting and diffracting eigenwave respectively. As we have seen in the different chapters,  $m_1$  takes the value of zero, for  $\lambda' = \sqrt{1 \pm \delta}$ , hence  $\rho_1$  is divergent at these wavelengths. For a broad density of states, as the one corresponding to the non-diffracting eigenwave, one can use the Wigner-Weisskopf approximation [15] according to which only the pole contribution  $s \rightarrow 0^+$  is retained and we can apply the Sokhotski-Plemelj theorem for the calculation of  $\Sigma(s)$ , as

$$\lim_{s \rightarrow 0^+} \frac{1}{s + i(\omega_k - \omega_d)} = -i\mathcal{P} \frac{1}{\omega_k - \omega_d} + \pi\delta(\omega_k - \omega_d). \quad (4.47)$$

In that case, in the absence of poles of  $\tilde{c}_d(s)$  we find that  $c_d(t)$  decays exponentially to zero.

In this chapter we have outlined the application of the Jaynes-Cummings model in quantifying spontaneous emission from chiral nematic LCs, as an alternative to the semi-classical Dirac's rule discussed previously. The linking element between the current and the previous chapter is the photonic density of states, showing a selective emission enhancement characteristic of the opti-

cal feedback in the liquid crystal resonator. In light of this approach, we have tried to interpret differences between the profile of the density of states and the experimentally measured fluorescence from these LC samples, refining our model phenomenologically in the context of the second quantisation.



# Bibliography

- [1] R. C. MCPHEDRAN, L. C. BOTTEN, J. MCORIST, A. A. ASATRYAN, C. M. DE STERKE, AND N. A. NICOROVICI, *Density of states functions for photonic crystals*, Phys. Rev. E **69**, 016609 1-16 (2004).
- [2] J. SCHMIDTKE AND W. STILLE, *Fluorescence of a dye-doped cholesteric liquid crystal film in the region of the stop-band: theory and experiment*, Eur. Phys. J. B **31**, pp. 179-194 (2003).
- [3] E. K. IRISH, *Generalized Rotating-Wave Approximation for Arbitrarily Large Coupling*, Phys. Rev. Lett. **99**, pp. 173601 1-4 (2007).
- [4] S. HAROCHE AND J.-M. RAIMOND, *Exploring the Quantum: Atoms, Cavities, and Photons*, Oxford University Press, Oxford, 2006.
- [5] E. YU. PERLIN, *Fluorescence of a Two-Level Atom in a Two-Dimensional Photonic Crystal in the Vicinity of the Saddle Point of the Photonic Band Spectrum*, Opt. Spectrosc., **98**, 320-325 (2005).
- [6] V. A. BELYAKOV AND S. V. SEMENOV, *Optical Edge Modes in Photonic Liquid Crystals*, JETP, **109**, pp. 687-699 (2009).

- [7] , V. P. BYKOV, *Radiation of Atoms in a Resonant Environment*, World Scientific Publishing, Singapore, 1993.
- [8] V. A. BELYAKOV, *Diffraction Optics of Complex-Structured Periodic Media*, ch. 2, Springer-Verlag, New York, 1992.
- [9] V. A. BELYAKOV AND S. V. SEMENOV, *Optical defect modes in chiral liquid crystals*, JETP **112**, 6947710 (2011).
- [10] M. F. MOREIRA, S. RELAIX, W. CAO, B. TAHERI, AND P. PALFFY-MUHORAY, *Liquid Crystal Microlasers*, Chap. 12, Transworld Research Network, Kerala, India, 2010.
- [11] J. SAJEEV AND W. JIAN, *Quantum Electrodynamics Near a Photonic Band Gap: Photons Bound States and Dressed Atoms*, Phys. Rev. Lett. **64**, pp. 2418-2421 (1990).
- [12] M. WOLDEYOHANNES AND S. JOHN, *Coherent control of spontaneous emission near a photonic band edge*, PhD tutorial, J. Opt. B: Quantum Semiclass. Opt. **5**, pp. R 43-82 (2003).
- [13] L. J. BISSELL, S. G. LUKISHOVA, A. W. SCHMID, C. R. STROUD, JR., AND R.W. BOYD, *Room-Temperature Single Photon Sources with Definite Circular and Linear Polarizations Based on Single-Emitter Fluorescence in Liquid Crystal Hosts*, Proc. SPIE, **7993**, 79931N (2010).
- [14] S. LONGHI, *Bound states in the continuum in a single-level Fano-Anderson model*, Eur. Phys. J. B **57**, pp. 45-51 (2007).

- [15] S. JOHN AND T. QUANG, *Spontaneous Emission near the Edge of a Photonic Bandgap*, Phys. Rev. A, **50**, pp. 1764-1769 (1994).

## Chapter 5

# Adaptive pumping of radiative LC cells

In the previous chapters we have included a discussion on lowering the laser excitation threshold of dye-doped chiral nematic cells. Here, we will focus on a pumping application where the input power is distributed to a group of spots, therefore a consideration of the excitation threshold of liquid crystal lasers is essential, as such a configuration is feasible only under the low-threshold lasing properties exhibited by these molecular structures. Organic solid-state dye lasers offer a number of advantages over their liquid-host counterparts, such as compactness and their easy-to-handle set-ups. However, the interaction time between the dye molecules and the pump beam must be minimized in order to circumvent bleaching issues, requiring a pulsed operation. To attain high repetition rates or continuous wave operation - which is necessary for many spectroscopic applications - excited dye molecules need to be removed from the pump volume [1],[2]. Hitherto, this has necessitated

the use of mechanical parts and/or fluid flow [3]. In this chapter, we demonstrate a new technique that involves dynamically controlling the position of incidence of a pump beam shone onto a thin film organic dye laser using holography, thus negating the need for moving parts and circulation of the dye. By moving the pump beam, the interaction time remains short enough that the triplet population is not increased and provides a means of accessing higher repetition rates. The method also provides additional functionality such as wavelength tuning and spatial shaping of the pump beam. Despite the advantages of organic solid-state dye lasers, liquid-dye lasers considerably outperform the solid-state organics when it comes to pulse duration. They can operate with pulses as short as 10 fs, and the pulse length can be made so long as to allow continuous-wave (CW) outputs. Solid-state dye lasers, which consist of an organic dye that is dispersed into a solid matrix, are not so versatile and are restricted to pulse durations are typically no longer than 10 ns. CW operation is generally prohibited because of bleaching issues caused by thermal degradation effects and also the accumulation of triplet excitons. In the case of triplet excitons, which possess an absorption band that overlaps the stimulated emission spectrum, suppression of the gain in the active region can occur, resulting in laser action being switched off. In order to ensure that the population of triplet states is dissipated between the pulses, repetition rates of the pump laser are usually restricted to less than 10 kHz. However, even if the repetition rate is low enough that triplet excitons do not build-up it is still not necessarily the case that thermal effects are absent.

In order to combat these thermal and excited-state absorption effects, a so-

lution is to remove the excited dye molecules out of the pump volume in sufficient timescales so as to maintain laser action. For liquid dye lasers, this involves a constant convective circulation of the organic species using a jet-stream with velocities on the order of 10s of  $\text{ms}^{-1}$  to replenish the dye molecules and thus avoid the bleaching effects that ultimately shut down laser action [1]. Alternatively, for solid-state organic dye lasers, methodologies that mimic the approach of ‘flushing out’ the excited dye molecules have been demonstrated such as mechanically rotating a disc-shaped active gain medium at high speeds to constantly refresh the dye molecules [4]. A common feature of the techniques that have been demonstrated to date require physically translating the active region in some way relative to the pump. This, therefore, requires the use of moving parts or fluid flow. In this chapter, we demonstrate a solution in which the pump beam is moved relative to the solid-state organic dye laser using adaptive optics, which bypasses the need for any moving parts as the position of the pump beam is adjusted through the diffraction of light. In our experimental work, a chiral nematic liquid crystal (LC) laser [5]-[8] is used as a representative thin-film organic dye laser. As we have shown, the chiral nematic LC provides the feedback mechanism as it possesses a 1-d photonic band gap for visible light, which suppresses fluorescence within the band gap [9] but enhances it at the band edges [10]-[13]. The gain medium consists of a laser dye that is based upon the pyrromethene class, which are known to exhibit reduced triplet-triplet absorption across the emission spectral region and high quantum efficiencies [14]-[20] as well as LC media [21]. The LC laser was chosen for this study because of the ease with which the laser wavelength can be selected across the

visible spectrum, which is particularly important for demonstrating the additional functionality available using the adaptive pumping technique. Studies have shown that illumination of a chiral nematic LC with high excitation energies, and even relatively low repetition rates (e.g. 20 Hz), can lead to a dramatic reduction in the output energy of the LC laser within a short time [22]. The motivation for this study is to demonstrate that the repetition rate of the LC laser can be significantly improved using an adaptive dynamic pumping approach. Although the results demonstrated in this chapter are for an LC laser, in principle, the technique is applicable to all organic solid-state and even liquid dye laser systems.

## 5.1 The method of adaptive pumping

Below we will detail the method of holographic adaptive pumping. An incident pump beam from the solid-state laser-the excitation source-is reflected from a spatial light modulator (SLM) displaying a computer generated hologram (CGH). The reflected light from the SLM is then focussed to form the replay field on a glass cell containing a dye-doped LC. This optically excites the dye and triggers lasing. By changing the hologram displayed on the SLM, it is possible to form different spot positions or different spot patterns incident on the sample in real-time. This enables both static pumping - in which the position of the pump beam remains fixed, and dynamic pumping- in which the pump beam can be translated across the cell in 2D, enabling the active gain region to be refreshed. For static pumping, a single hologram is continuously displayed; for dynamic pumping, a sequence of holograms is

displayed on the SLM. In this study, the CGHs were generated using the Gerchberg-Saxton (GS) phase retrieval algorithm [23]-[24]. The most common steps followed to calculate a CGH are given below [23]

- (1) Sampling of the continuous intensity distribution  $I(x, y)$  in the image plane.
- (2) Square-root of the intensity samples to obtain the (sampled) amplitude distribution  $|u(x, y)|$ .
- (3) Initial superposition of a random phase to create  $|u(x, y)| \exp[i\phi(x, y)]$ .
- (4) Calculation of the Fast Fourier Transform (FFT) of the samples of the complex amplitude  $u(x, y)$  and extraction of the corresponding phase distribution.
- (5) Sampling of the intensity distribution  $I(x, y)$  in the diffraction plane.
- (6) Square-root of the intensity samples to obtain the (sampled) amplitude distribution  $|u'(x, y)|$ .
- (7) Initial superposition of a random phase to create  $|u'(x, y)| \exp[i\phi'(x, y)]$ .
- (8) Iterations until constraints are satisfied.

The superposition of a random phase distribution (as a multiplicative exponential factor) is analogous to the introduction of a diffuser between the source and the object. A global rearrangement of the phase samples is then necessary to eliminate first-order zeros in the amplitude distribution [25]. This algorithm is frequently used in holographic applications and has recently been employed to realize optical tweezing [26].

An illustration of the operating principle of the technique used to optically

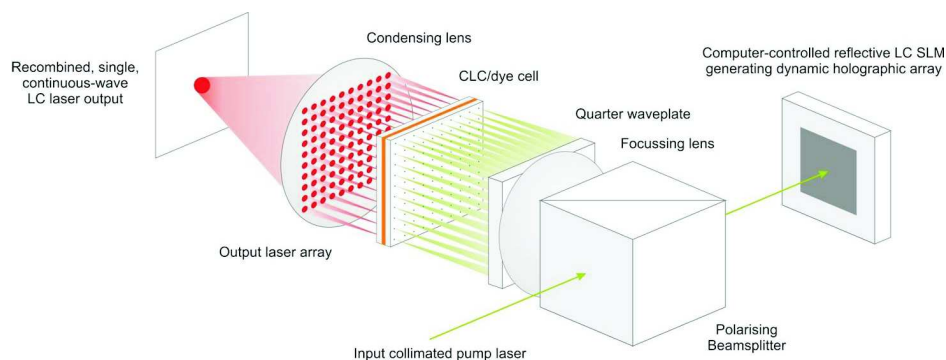


Figure 5.1: Illustration of the principle of dynamic optical pumping using computer generated holograms.

excite thin-film organic laser samples is shown in Figure 5.1.

### 5.1.1 Sample preparation

In our experiment, the single wavelength laser cell consisted of the nematic mixture E49 (Merck KGaA) doped with the chiral dopant BDH1281 (Merck KGaA) and the laser dye Pyrromethene 580 (PM-580; Exciton) so as to form a chiral nematic liquid crystal with a short-wavelength band-edge at 574 nm. The cell had a thickness of 13  $\mu\text{m}$  which has been shown to be suitable for low-threshold lasing. The pitch-gradient cell, of 10  $\mu\text{m}$  thickness, consisted of two different dye-doped liquid crystal mixtures which are drawn into the cell by capillary action to form two regions gradually diffusing together and creating a continuous pitch-gradient. Both of these mixtures comprised of the liquid crystal E49 (Merck) and the chiral dopant BDH1281 (Merck; 3.9 wt% for red and 4.3 wt% for green). DCM (Exciton; 1.5 wt%) was added to make the red mixture and PM580 (Exciton; 0.5 wt%) was added to make the green mixture.

### 5.1.2 Pumping process

The pump source is a frequency-doubled Nd:YAG laser (CryLaS, FDSS 532-Q) which produces 1 ns pulses at 532 nm and has a variable repetition rate (up to 3000 Hz, although in this work it was varied from 100 - 600 Hz). For direct control of the pump beam energy, a half-waveplate between crossed polarisers was implemented into the set-up before the spatial light modulation. Two lenses act as collimating optics to expand the beam so that the entire area of the SLM was illuminated. The beam is reflected from a nematic, multi-level phase spatial light modulator (Cambridge Correlators, SDE1280) with a maximum input frame addressing rate of 60 Hz displaying a CGH. A beam splitter redirects it through a 532 nm half waveplate followed by a 532 nm quarter waveplate in order to convert the light into the appropriate circular polarization so as to improve the penetration depth through the sample and avoid further losses due to the reflection band of the chiral nematic LC. A focussing lens ( $f = 12.5$  cm) forms the replay field on the dye-doped LC cell. Two high-pass filters (cut-off 530 nm) remove the pump beam and a 4x microscope objective with numerical aperture 0.1 is used to collect the light over a narrow forward angle. Emission energies of the pulses emitted from the LC laser were recorded using a calibrated pyroelectric head (PD10-SH-V2) connected to an energy meter (USB-2, Ophir) whereas spectra were obtained using a universal serial bus spectrometer with a resolution of 0.3 nm (HR2000, Ocean Optics). 2D and 3D beam profiles were captured using a Spiricon beam profiler, and photographic images of the polychromatic LC laser were taken using a high resolution digital camera (Canon, EOS 550D). The experimental set-up detailed above is illustrated in Figure 5.2.

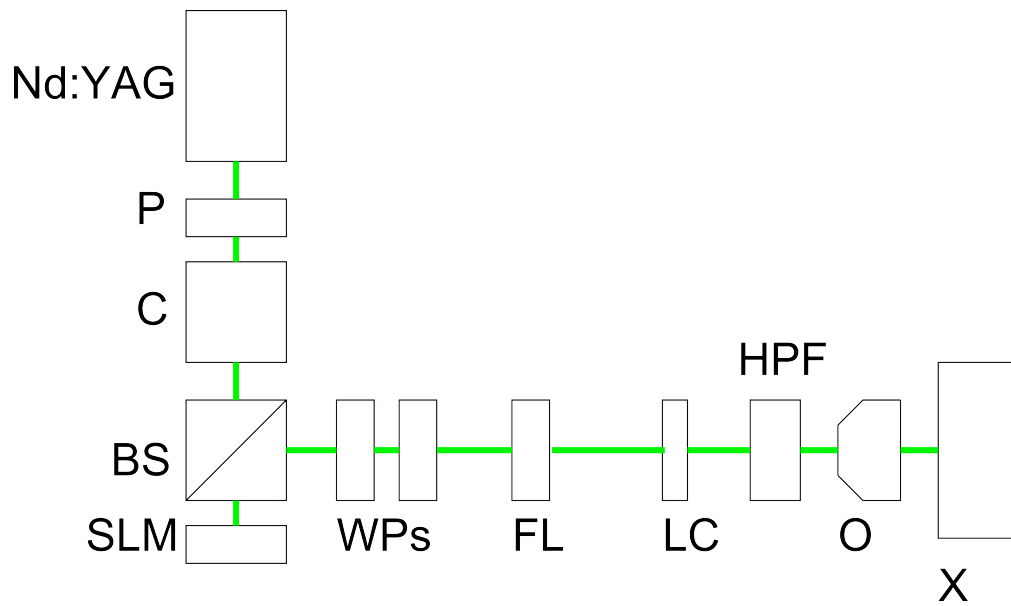


Figure 5.2: Experimental setup. P: polariser; C: collimating optics; BS: beam-splitter; SLM: spatial light modulator; WPs: wave-plates- $\lambda/2$  wave-plate followed by a  $\lambda/4$  waveplate; FL: focussing lens ( $f = 125\text{mm}$ ); LC: dye doped chiral nematic liquid crystal sample; HPF: high-pass filter; O: objective lens (4x); X: camera, spectrometer or beam-profiler depending on the purpose of the experiment.

## 5.2 Main results

In order to prove the principle of hologram-steered optical pumping, we created a hologram that would generate a single spot in the replay field. Examples of a CGH for a 2D array of 6 pump spots at the LC cell is shown in Figure 5.3(a). The corresponding replay field for a single and multiple spot array is presented in Figure 5.3(b). However, our SLM was not capable of true  $2\pi$  modulation meaning that a fraction of a conjugate image is formed in the replay field. This is because the Fourier transform of a real function is always  $180^\circ$ -symmetric about the origin, as  $|\psi(u, v)|^2 = |\psi(-u, -v)|^2$ , where  $\psi(u, v)$  is the complex amplitude of light in the diffraction plane. This reduces the efficiency of the hologram by 50%. Hence, if a hologram displayed on the SLM is used to generate a single first order spot, there will actually be two first order spots in the replay field. Thus, due to conjugate-image formation, two spatially separate pump beams were incident on the LC and therefore two LC laser beams-corresponding to two spatially separated active regions-were generated. The first order pump spot in the replay field at the sample position was found to be approximately circular with an area of  $0.003 \text{ mm}^2$ , an excitation energy threshold of  $130 \text{ nJ/pulse}$  and a corresponding excitation fluence of  $4.3 \text{ mJ/cm}^2$ .

A beam profiler (Spiricon, LW 230) was used to record the spatial profile of the intensity emitted by the LC laser beam at a distance of 7 cm from the cell and it was found to be near-Gaussian as shown by the two- and three-dimensional plots in Figures 5.4(a) and 5.4(b), respectively. In this case, two separate beams are emitted from the LC laser device corresponding to two spatially separated active regions. From these measurements, the waist of

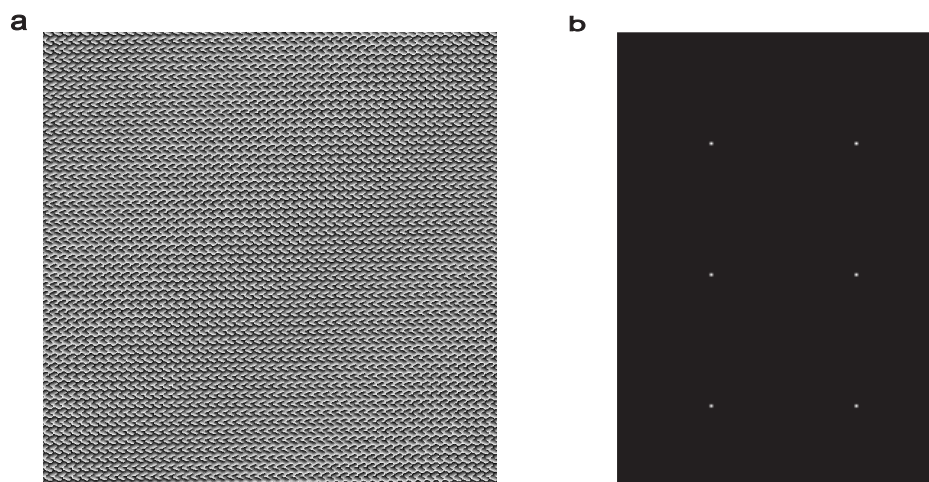


Figure 5.3: Hologram and replay field used for and multi-spot beam. In (a) Phase CGH (grey-scale) for the generation of six first order spots in the replay field (768 x 768 pixels), (b) Replay field of the ideal CGH.

the two quasi-Gaussian beams were calculated to be approximately  $70 \mu\text{m}$ . When the CGH was removed from the SLM the spots vanished, confirming that the output from the LC cell was caused by the hologram. The emission spectrum was recorded on a spectrometer, which was shown to occur at a wavelength of  $\lambda = 560.2 \text{ nm}$  for both beams, Figure 5.4(c). Additionally, CGHs used to generate single spots in different positions and also patterns of spots were created: Figure 5.4(d) shows a pattern of six spots (which becomes twelve due to the presence of the conjugate image). In this case, the CGH divides the pump beam into twelve spots of equal intensity. This is in contrast to a previous approach using a micro lens array [27] which results in a non-uniform distribution of energy across the array of spots due to the spatial variation in the pump-beam energy.

Subsequently, the benefits of pumping the organic laser dynamically were shown. A sequence of holograms displaying spots at different positions was

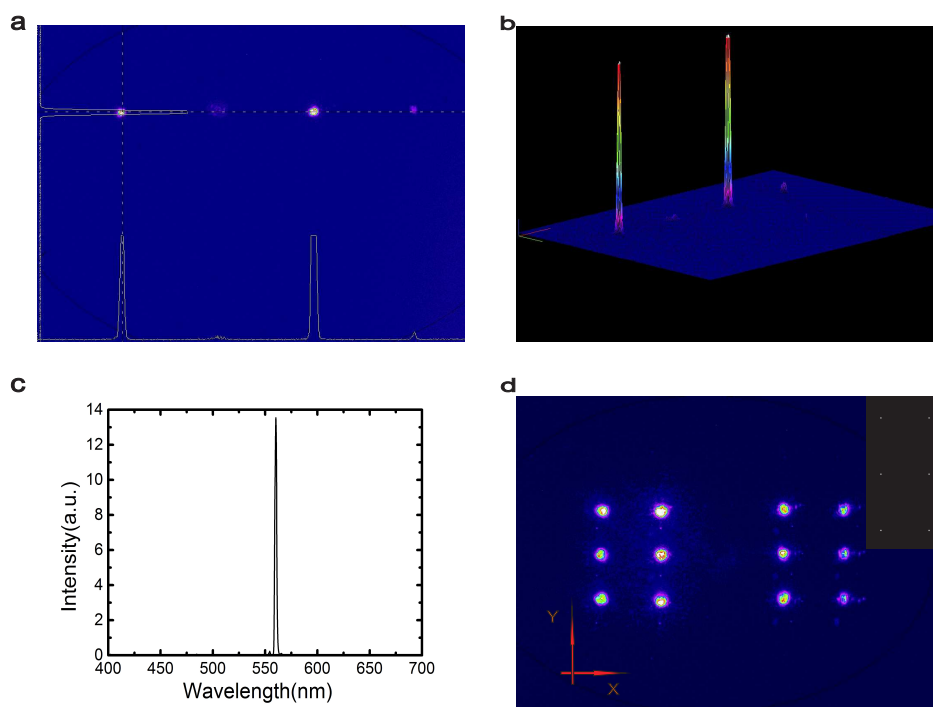


Figure 5.4: Optically pumping an organic laser using the replay field of a multi-level phase CGH.(a) 2D profile for one spot, (b) 3D profile for one spot, (c) emission spectrum from a cell pumped with a one replay field spot in four different locations, (d) 2D profile for six spots (inset: ideal replay-field pattern). In (a,b,d) the symmetric order is displayed and in (a,b) the zero order is present alongside a second order spot.

created with the holograms displayed at 0.5 s intervals. This dynamic pumping process was then exploited to increase the repetition rate accessible to the LC laser. To this end, the pump beam was scanned around the lasing medium so that it was only incident on a given active region for a short period of time, thus minimizing the interaction time between the dye and the pump beam to avoid triplet state generation and other degradation effects.

Results obtained for pumping the LC laser in the static case with a single spot at a fixed location over a total of 12,000 pulses is presented in Figure 5.5(a), which highlights the degradation in performance for high repetition rates. The data shows how the normalised pump energy decreases with the number of pulses and is found to be more extreme for the higher repetition rates. In particular, at a repetition rate of 600 Hz the output drops exponentially to 40% of the initial value in approximately 2000 pulses (around 4 seconds). Before comparing this behavior with that observed for dynamic pumping it was necessary to determine the best frame rate for the holograms displayed on the SLM; that is, how often should a new hologram be displayed to change the position of the pump spots and refresh the dye. Therefore, videos displaying different CGHs at various frame-rates were made. The LC laser outputs for these different replay fields at a pump repetition rate of 300 Hz were then recorded, as shown in Figure 5.5(b). It can be seen that a frame rate of 1 frame per second (fps) yields laser pulses with a significantly larger rate of degradation of LC laser output. Subsequent experiments were performed using a frame rate of 2 fps as this resulted in a relatively stable output on the order of some minutes. Increasing the rate to 10 fps did not lead to any significant improvement in the stability although it did reduce the output

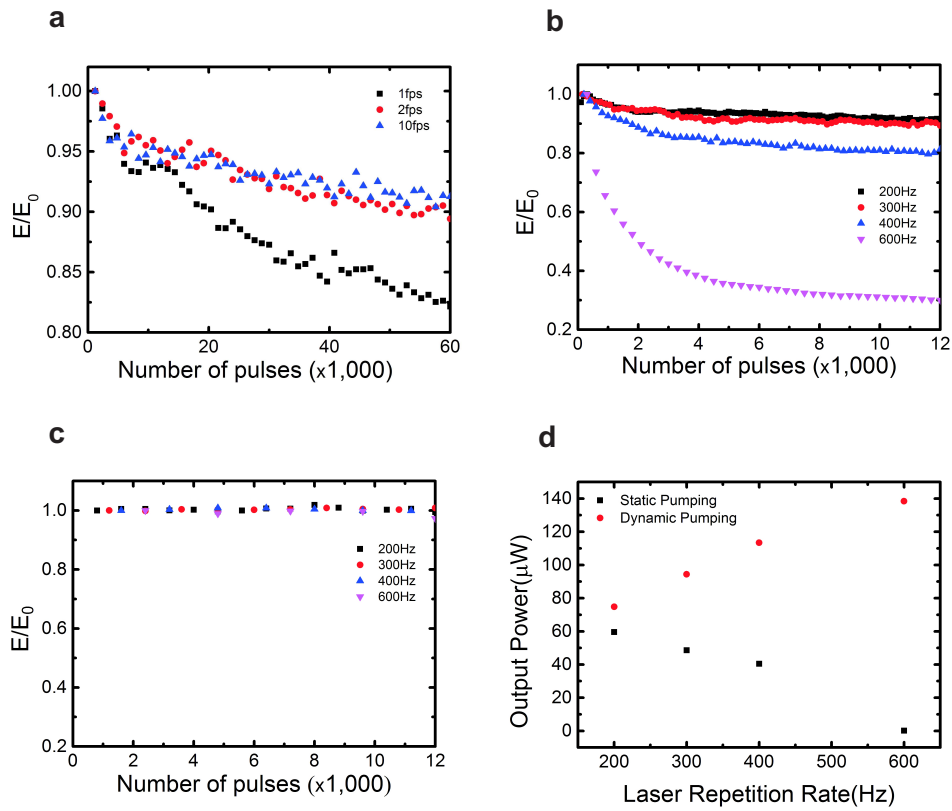


Figure 5.5: Accessing higher repetition rates using dynamic pumping. The energy was recorded for each pulse, but in (a-c) results are averaged over 2 s. The energies are normalized to the first pulse. (a) Dynamic pumping at 600 Hz with different frame rates - 1 fps (■), 2 fps (●) and 10 fps (blue ▲) (b) Static pumping of a LC laser. (c) Dynamic pumping with 2 fps at different repetition rates. In (b) and (c): 200 Hz (■), 300 Hz (●), 400 Hz (blue ▲), 600 Hz (pink ▼) (d) Total power output over 1 minute for different repetition rates for both the static (■) and dynamic (●) case.

power due to the rise time of the LC laser which became more pronounced at greater frame rates. Figure 5.5(c) demonstrates the improvement in the performance of the LC laser for dynamic illumination. The results show that output is almost independent of the number of pulses even for the highest repetition rate used in this study and the output is thus significantly more stable. When the LC laser was statically pumped with a single spot in a fixed location at different repetition rates (Figure 5.5b), the normalized output energy decreased with the number of pulses and the effect was more pronounced at higher repetition rates: at 600 Hz the output dropped to 60% of its value in roughly 2000 pulses (4 s). Increasing the repetition rate did not significantly alter the pump pulse energy. In contrast, when dynamic pumping is employed, the LC laser output is almost independent of the pulse number, even at the highest repetition rate that we used; the output is significantly more stable [Figure 5.5(c)]. For example, in the case of a 400 Hz repetition rate, it took 29 minutes to decay by 10%, compared with 5s using static pumping. The measured normalized photostabilities for the different repetition rates, corresponding to a 10% decrease in the output pulse energy and for the pumping volume in the LC cell based upon the cell thickness and pump spot area, are calculated to be 0.028GJ/mol (200 Hz), 0.182 GJ/mol (300 Hz), 1.19 GJ/mol(400 Hz) and 1.41 GJ/mol (600 Hz). We also compared mean output powers over a given length of time [Figure 5.5(d)] and this was greater at all repetition rates when dynamic pumping was employed. The mean output power for the first minute of emission increased with repetition rate when dynamically pumped, but decreased (due to bleaching) when statically pumped.

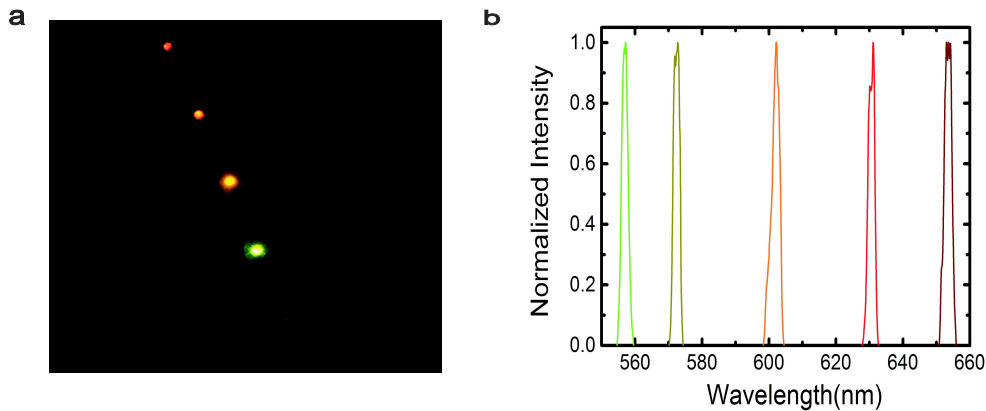


Figure 5.6: Multicolor laser arrays and dynamic wavelength tuning. (a) 4 spots (one zero order, two first order and one second order) corresponding to different colours from red to green. (b) Emission spectra from different regions of the cell, obtained by static addressing of different regions.

CGHs can also be designed such that they increase the functionality of the LC laser by configuring the pump beam to steer the beam onto different regions of the cell. By combining this function with a pitch-gradient LC cell - a cell consisting of two LCs that emit at different ends of the visible spectrum which have diffused together to form a continuum of wavelength regions - it is possible to ‘tune’ the wavelength of the laser or create a multi-colored array. Changing the position of the pump beam on the cell enables a different output wavelength to be obtained. LC lasers have previously been tuned by deforming the molecular structure using temperature variation, electric fields, magnetic fields, mechanical stresses [8] or UV radiation [28]-[29]. Figure 5.6(a) depicts a pattern of spots, each of which is a different colour due to the pitch variation across the cell. Figure 5.6(b) shows the laser emission spectra from five different regions of the cell. Each region was isolated by changing the hologram so that the pump beam was incident on a different region. The

method presented here can be directly applied to configurations relying on the energy transfer between two dyes [30], allowing tuneable output across the entire visible range. In this study, we demonstrate a simple approach to wavelength tuning and multi-chromatic outputs simultaneously, but it is equally possible to envisage that novel pump beam profiles that optimise propagation through the medium could also be demonstrated. This work has focused on the behavior of an organic solid-state dye laser, however, the same approach could be used in the field of organic semiconductor lasers [31].

In conclusion, in this chapter we describe a system for pumping an organic solid-state dye laser using computer generated holography. This technique provides a means with which to vary the location of the pump beam on the active medium in real-time enabling fresh active gain regions to be addressed in rapid succession, thus preventing build-up of triplet states and ensuring optimum thermal management. Both static and dynamic hologram-defined pumping have been shown to be possible, with dynamic pumping leading to improved stability, larger average output powers and access to higher repetition rates. With higher repetition rate pump lasers, it is feasible that this approach could enable these organic lasers to reach operating frequencies on the order of a MHz, without the need of mechanically moving parts. Additionally, due to the unique nature of the adaptive pumping method, it is possible to precisely control the spatial wavefront and configuration of the pumping wave allowing greater versatility and functionality to be realised.



# Bibliography

- [1] E. P. SCHAFER ED., *Dye Lasers*, 3rd Ed., Springer-Verlag, 1990.
- [2] F. J. DUARTE AND L. W. HILLMAN EDS., *Dye Laser Principles*, Academic, New York, 1990.
- [3] O. G. PETERSON, S. A. TUCCIO AND B. B. SNAVELY, *Cw operation of an organic dye solution laser*, Appl. Phys. Lett., **17**, pp. 245-247 (1970).
- [4] R. BORNEMANN, U. LEMMER AND E. THIEL, *Continuous wave solid state dye laser*, Opt. Lett. **31**, pp. 1669-1671 (2006).
- [5] I. P. IL'CHISHIN, E. A. TIKHONOV, V. G. TISHCHENKO AND M. T. SHPAK, *Generation of a tunable radiation by impurity cholesteric liquid crystals*, JETP Lett., **32**, pp. 24-27 (1980).
- [6] V. I. KOPP, B. FAN, H. K. M. VITHANA, AND A. Z. GENACK, *Low-threshold lasing at the edge of a photonic stop band in cholesteric liquid crystals*, Opt. Lett. **23**, pp. 1707-1709 (1998).
- [7] B. TAHERI, A. MUNOZ, P. PALFFY-MUHORAY AND R. TWIEG, *Low threshold lasing in cholesteric liquid crystals*, Mol. Cryst. Liq. Cryst. **358**, pp. 73-82 (2001).

- [8] H. J. COLES AND S. M. MORRIS, *Liquid Crystal Lasers (review article)*, Nature Photon. **4**, pp. 676-685 (2010).
- [9] E. YABLONOVITCH, *Inhibited spontaneous emission in solid state physics and electronics*, Phys. Rev. Lett. **58**, pp. 2059-2062 (1987).
- [10] S. JOHN, *Strong localization of photons in certain disordered dielectric superlattices*, Phys. Rev. Lett. **58**, pp. 2486-2489 (1987).
- [11] J. P. DOWLING, M. SCALORA, M. J. BLOEMER AND C. M. BOWDEN, *The photonic band-edge laser: A new approach to gain enhancement*, J. Appl. Phys. **75**, pp. 1896-1899 (1994).
- [12] J. SCHMIDTKE AND W. STILLE, *Fluorescence of a dye-doped cholesteric liquid crystal film in the region of the stop-band: theory and experiment*, Eur. Phys. J. B **31**, pp. 179-194 (2003).
- [13] J. M. BENDICKSON, J. P. DOWLING, AND M. SCALORA, *Analytic expressions for the electromagnetic mode density in finite, one-dimensional, photonic band-gap structures* Phys. Rev. E **53**, pp. 4107-4121 (1996).
- [14] T. G. PAVLOPOULOS, M. SHAH AND J. H. BOYER, *Efficient laser action from 1,3,5,7,8-pentamethylpyrromethene-BF<sub>2</sub> complex and its disodium 2,6-disulfonate derivative*, Opt. Commun. **70**, pp. 425-427 (1989).
- [15] T. G. PAVLOPOULOS, J. H. BOYER, M. SHAH, K. THANGARAJ AND M. L. SOONG, *Laser action from 2,6,8-position trisubstituted 1,3,5,7-tetramethylpyrromethene-BF<sub>2</sub> complexes: part 1*, Appl. Opt. **29**, pp. 3885-3886 (1990).

- [16] T. G. PAVLOPOULOS, J. H. BOYER, K. THANGARAJ, G. SATHYAMOORTHY, M. SHAH AND M. L. SOONG, *Laser dye spectroscopy of some pyrromethene-BF<sub>2</sub> complexes*, Appl. Opt. **31**, pp. 7089-7094 (1992).
- [17] M. FALOSS, M. CANVA, P. GEORGES, A. BRUN, F. CHAPUT AND J. P. BOILOT, *Toward millions of laser pulses with pyrromethene - and perylene - doped xerogels*, Appl. Opt. **36**, pp. 6760-6763 (1997).
- [18] M. D. RAHN, T. A. KING, A. GORMAN AND I. HAMBLETT, *Photostability enhancement of Pyrromethene 567 and Perylene Orange in oxygen-free liquid and solid dye lasers*, Appl. Opt. **36**, pp. 5862-5871 (1997).
- [19] M. AHMAD, M. D. RAHN AND T. A. KING, *Singlet Oxygen and Dye-Triplet-State Quenching in Solid-State Dye Lasers Consisting of Pyrromethene 567-Doped Poly(Methyl Methacrylate)*, Appl. Opt. **38**, pp. 6337-6342 (2000).
- [20] A. COSTELA, I. GARCA-MORENO, J. BARROSO AND R. SASTRE, *Laser performance of pyrromethene 567 dye in solid matrices of methyl methacrylate with different comonomers*, Appl. Phys. B: Lasers Opt. **70**, pp. 367-373 (2000).
- [21] C. MOWATT, S. M. MORRIS, M. H. SONG, T. D. WILKINSON, R. H. FRIEND AND H. J. COLES, *Comparison of the performance of photonic band-edge liquid crystal lasers using different dyes as the gain medium*, J. Appl. Phys. **107**, pp. 043101 (1-9) (2010).

- [22] S. M. MORRIS, A. D. FORD, M. N. PIVNENKO AND H. J. COLES, *The effects of Optical Reorientation on The Emission Properties of Liquid Crystal Photonic Band Edge Lasers*, J. Opt. A: Pure Appl. Opt., **7**, pp. 215-223 (2005).
- [23] R. W. GERCHBERG AND W. O. SAXTON, *A practical Algorithm for the Determination of Phase from Image and Diffraction Plane Pictures*, Optik **35**, pp. 237-246 (1972).
- [24] J. R. FIENUP, *Phase retrieval algorithms: A personal tour*, Appl. Optics, **52**, pp. 45-56 (2013).
- [25] F. WYROWSKI AND O. BRYNGDAHL, *Iterative Fourier-transform algorithm applied to computer holography*, J. Opt. Soc. Am. A, **5**, pp. 1058-1065 (1988).
- [26] H. CHEN, Y. GUO, Z. CHEN, J. HAO, J. XU, H.-T. WANG AND J. DING, *Holographic optical tweezers obtained by using the three-dimensional Gerchberg-Saxton algorithm*, J. Opt., **15**, pp. 035401 (1-8) (2013).
- [27] S. M. MORRIS, P. J. W. HANDS, S. FINDEISEN-TANDEL, R. H. COLE, T. D. WILKINSON AND H. J. COLES, *Polychromatic liquid crystal laser arrays towards display applications*, Opt. Express, **16**, pp. 18828-18837 (2008).
- [28] A. CHANISHVILI, G. CHILAYA, G. PETRIASHVILI, R. BARBERI, R. BARTOLINO, G. CIPPARRONE, A. MAZZULLA AND L. ORIOL, *Lasing*

- in dye-doped cholesteric liquid crystals: Two new tuning strategies*, Adv. Mater. **16**, pp. 791-795 (2004).
- [29] T.-H. LIN, Y.-J. CHEN, C.-H. WU, A.Y.-G. FUH, J.-H. LIU AND P.-C. YANG, *Cholesteric liquid crystal laser with wide tuning capability*, Appl. Phys. Lett., **86**, pp. 161120 (1-3) (2005).
- [30] K. SONOYAMA, Y. TAKANISHI, K. ISHIKAWA AND H. TAKEZOE, *Position-sensitive cholesteric liquid crystal dye laser covering a full visible range*, Jpn. J. Appl. Phys., **46**, L874-L876 (2007).
- [31] I. D. W. SAMUEL AND G. A. TURNBULL, *Organic semiconductor lasers*, Chem. Rev., **107**, pp. 1272-1295 (2007).

# Chapter 6

## Suggestions for further research

### 6.1 Decay dynamics in the Jaynes-Cummings model

This chapter we will outline the salient parts of the resolvent method and provide some insight leading to the full treatment of atomic radiation in the resonant environment of a photonic crystal. We will commence our discussion in the framework of the JC model, where the existence of the so-called ‘quasi dressed-states’ (the ones leading to the oscillatory behaviour of the spontaneous emission decay) was firstly demonstrated in [1], and we will see how similar conclusions can be reached with the resolvent method, which is consistent with perturbation theory. In connection to the 4th chapter, for a(n isotropic) 3D photonic crystal, the Laplace Transform of the bound state amplitude is <sup>†</sup> [1]

---

<sup>†</sup>To avoid misunderstanding, in this chapter we no longer designate unit vectors by a hat on top, but we reserve this symbol to designate operators only.

$$\begin{aligned}
\tilde{c}_d(s) &= \left[ s + \sum_{\kappa} |\mu_{\kappa}|^2 \frac{1}{s + i(\omega_{\kappa} - \omega_d)} \right]^{-1} \\
&= \left[ s + \frac{(\omega_{10}d_{10})^2}{2\hbar\varepsilon_0V} \int \int \frac{(\mathbf{e}_{\mathbf{k}\lambda} \cdot \hat{\mathbf{r}})^2}{s + i(\omega_{\mathbf{k}} - \omega_d)} \frac{d\Omega_{\mathbf{k}}d\mathbf{k}}{\left(\frac{2\pi}{L}\right)^3} \right]^{-1} \\
&= \left[ s + \frac{(\omega_{10}d_{10})^2}{16\hbar\varepsilon_0\pi^3} \int_0^{\Lambda} \int_0^{\pi} 2\pi \frac{\sin^3\theta}{s + i(\omega_{\mathbf{k}} - \omega_d)} k^2 d\theta d\mathbf{k} \right]^{-1} \\
&= \left[ s + \frac{(\omega_{10}d_{10})^2}{6\hbar\varepsilon_0\pi^2} \int_0^{\Lambda} \frac{k^2}{s + i(\omega_{\mathbf{k}} - \omega_d)} d\mathbf{k} \right]^{-1},
\end{aligned} \tag{6.1}$$

where  $\Lambda$  is the cutoff in the photon wave-vector corresponding to the Compton wavelength. Near the band-edge  $\omega_c$  of the crystal, the dispersion relation is written as

$$\omega_{\mathbf{k}} \simeq \omega_c + \frac{\omega_c}{k_1^2} (k - k_1)^2, \tag{6.2}$$

where  $k_1 = \pi/L$  is the first spatial frequency in the Fourier series expansion of the dielectric profile function ( $L$  is the lattice constant). Substituting this expression into (6.1) the following analytic expression is obtained

$$\tilde{c}_d(s) = \frac{(s - i\delta\omega)^{\frac{1}{2}}}{s(s - i\delta\omega)^{\frac{1}{2}} - (i\beta)^{\frac{3}{2}}}, \tag{6.3}$$

where  $\beta = \frac{\omega_{10}^{\frac{7}{2}}d_{10}^2}{6\pi\varepsilon_0\hbar c^3}$  is related to the coupling strength and  $\delta\omega = \omega_{10} - \omega_c$  measures the detuning. Furthermore, based on the residue theorem, the inverse Laplace transform can be also calculated in a closed form

$$\begin{aligned}
c_d(t) &= \frac{1}{2\pi i} \int_{\sigma-i\infty}^{\sigma+i\infty} \tilde{c}_d(s) e^{st} ds = f_1(\delta, \beta) \exp(\beta x_1^2 t + i\delta\omega t) \\
&+ f_2(\delta, \beta) \exp(\beta x_2^2 t + i\delta\omega t) + f_3(\delta, \beta) \frac{\exp(i\delta t)}{(\beta t)^{\frac{3}{2}}},
\end{aligned} \tag{6.4}$$

where we have used the asymptotic expansion of the complementary error function and approximated for large  $\beta t$  as follows

$$\begin{aligned} \operatorname{erfc}(\sqrt{\beta x_i^2 t}) &= \frac{\exp(-\beta x_i^2 t^2)}{\sqrt{\pi \beta x_i^2 t}} \sum_{n=1}^{\infty} (-1)^n \frac{(2n-1)!!}{(2\beta x_i^2 t^2)^n} \\ &\simeq \frac{\exp(-\beta x_i^2 t^2)}{\sqrt{\pi \beta x_i^2 t}} \frac{(-1)}{2\beta x_i^2 t^2} = \frac{\exp(-\beta x_i^2 t^2)}{2\sqrt{\pi}(\beta t)^3}, \end{aligned} \quad (6.5)$$

where  $i = 1, 2, 3$ . As can be shown in [1]  $x_1^2 = i|x_1|^2$ , so that the first term in (6.4) represent a bound atom-photon state with no exponential decay and frequency  $\omega_c - \beta|x_1|^2$ . The second term (representing also a bound state) in (6.4) depends on the relative position between the band-gap and the atomic radiation frequency. If the latter is far inside the band-gap, then this term vanishes (for the pertinent condition see [1]). The third term in (6.4) arises from the branching point of the square root and yields a state responsible for a non-exponential decay with an amplitude oscillating with the band-edge frequency  $\omega_c$ .

For a 1-D (partial) photonic crystal, as chiral nematics are, and for a given orientational distribution of the gain medium the expression (6.1) needs to be modified as follows

$$\begin{aligned} \tilde{c}_d(s) &= \left[ s + \sum_{\kappa} |\mu_{\kappa}|^2 \frac{1}{s + i(\omega_{\kappa} - \omega_d)} \right]^{-1} \\ &= \left[ s + \frac{(\omega_{10} d_{10})^2}{2\hbar \varepsilon_0 V} \int \frac{\langle (\mathbf{e}_{\mathbf{k}\lambda} \cdot \hat{\mathbf{r}})^2 \rangle}{s + i(\omega_k - \omega_d)} \frac{dk}{\left(\frac{2\pi}{L}\right)} \right]^{-1} \\ &= \left[ s + \frac{(\omega_{10} d_{10})^2}{2\hbar \varepsilon_0 S} \int_{\omega_{\min}}^{\omega_{\max}} \frac{f(S_g)}{s + i(\omega - \omega_d)} \rho(\omega) d\omega \right]^{-1}, \end{aligned} \quad (6.6)$$

where  $\rho(\omega)$  is the photonic DOS,  $f(S_g)$  is a function of the order parameter

pertaining to the orientational distribution of the gain molecule (see [2]). A numerical study of this integral can reveal the time-evolution characteristics of the atom-photon states. For  $N \rightarrow \infty$  (where  $N$  is the number of full helicoidal director precessions in the LC sample) and for oblique propagation in the structure, the spontaneous emission intensity is calculated in [4] for  $t \rightarrow \infty$  within the JC formulation for Floquet's theorem applied for Mathieu's equation (In the system of equations obtained, the contribution of field amplitudes with subscript  $n \pm 2$  is neglected in comparison to those having suffixes  $n, n - 1$ . This is consistent with deriving the first-order Brillouin dispersion relation).

## 6.2 The basic principles of the Resolvent Method

We will now approach the same problem within the context of the resolvent method, which is consistent with perturbation theory. The method involves the calculation of the matrix elements of the operator  $R(z) = 1/(z\mathcal{I} - H)$  (called the 'resolvent' operator) which features in the expression for the time-evolution operator (in this section we drop the hats denoting the operators, for convenience)

$$U(t) = \frac{1}{2\pi i} \oint_C \frac{e^{-izt/\hbar}}{z\mathcal{I} - H} dz, \quad (6.7)$$

where  $C$  is a closed contour around the axis of  $\Re(z)$  where are located all the eigenvalues of the unperturbed Hamiltonian (which are real, since the operator is Hermitian). For a Hamiltonian of the form  $H = H_0 + V$ , the matrix elements of the resolvent operator are written as [3]

$$R_{nm} = -\frac{1}{\Delta(z)} \frac{\partial \Delta(z)}{\partial V_{mn}} = -\frac{\partial \ln \Delta(z)}{\partial V_{mn}}, \quad (6.8)$$

and the determinant  $\Delta(z)$  of the matrix  $(z\mathcal{I} - H)$  is written in the form

$$\Delta(z) = \det(z\mathcal{I} - H) = \det(z\mathcal{I} - H_0) \det[\mathcal{I} - (z\mathcal{I} - H_0)^{-1}V]. \quad (6.9)$$

Setting  $A = \mathcal{I} - (z\mathcal{I} - H_0)^{-1}V$  we write

$$\det A = \exp[\text{Tr}(\ln A)] = \exp\left(\text{Tr} \sum_{n=1}^{\infty} \frac{1}{n} B^n\right), \quad (6.10)$$

where  $B = (z\mathcal{I} - H_0)^{-1}V$ . The above can be written as

$$\det A = \exp[\text{Tr}(\ln A)] = \exp\left[\sum_{n=1}^{\infty} \frac{1}{n} S_n\right], \quad (6.11)$$

where  $S_n = \text{Tr}(B^n)$ . Expanding (6.9) in terms up to the second order of  $V$ , as it is usually done in practice, we have

$$\Delta(z) = \det(z\mathcal{I} - H) = \det(z\mathcal{I} - H_0) \left[1 - S_1 + \frac{1}{2!}(S_1^2 - S_2)\right], \quad (6.12)$$

where

$$S_1 = \text{Tr}(B) = \sum_{n=0}^{\infty} \frac{V_{nn}}{z - E_n^0} \quad (6.13)$$

and

$$S_2 = \text{Tr}(B^2) = \sum_n \sum_m \frac{V_{mn}V_{nm}}{(z - E_m^0)(z - E_n^0)}, \quad (6.14)$$

where  $E_l^0$  are the eigenvalues of the unperturbed Hamiltonian. Using these expressions, the denominator in the expression for the matrix elements of the resolvent operator reads

$$\begin{aligned} \Delta(z) &= \prod_n (z - E_n^0) - \sum_m \Delta_m \prod_{n \neq m} \frac{(z - E_n^0)}{(z - E_m^0)} \\ &+ \frac{1}{2!} \sum_m \sum_p \Delta_{mp} \prod_{n \neq m, p} \frac{(z - E_n^0)}{(z - E_m^0)(z - E_p^0)} - \dots, \end{aligned} \quad (6.15)$$

in which  $\Delta_m = V_{mm}$ ,  $\Delta_{mp} = V_{mm}V_{pp} - V_{mp}V_{pm}, \dots$  are the principal minors of the perturbation matrix  $V$ . This determinant can be also written as

$$\Delta(z) = \prod_n (z - E_n^0)[1 - F(z)], \quad (6.16)$$

with

$$F(z) = \sum_m C_m (z - E_m^0)^{-1}, \quad (6.17)$$

and

$$C_m = \Delta_m - \frac{1}{2!} \sum_{p \neq m} \frac{\Delta_{pm}}{z - E_p^0} + \dots \quad (6.18)$$

Based on the definitions (6.16) and (6.8) we write

$$R_{nm} = \frac{\frac{\partial F(z)}{\partial V_{mn}}}{1 - F(z)} \quad (6.19)$$

The decay law for the excited state  $|b, 0\rangle$  (where photons are absent in all oscillators) is described by the matrix element  $U_{b_0, b_0}(t) = \langle b, 0 | U(t) | b, 0 \rangle$ , and the corresponding matrix elements of the resolvent operator are

$$R_{b_0, b_0} = -\frac{1}{\Delta(z)} \frac{\partial \Delta(z)}{\partial V_{b_0, b_0}} = -\frac{\partial \ln \Delta(z)}{\partial V_{b_0, b_0}}. \quad (6.20)$$

The denominator  $\Delta(z)$  is written as

$$\Delta(z) = \prod_n \Delta_n = \prod_{n \neq m} \left[ z - E_n^0 - \left( V_{nn} + \frac{1}{2!} \sum_p \frac{V_{np} V_{pn}}{z - E_m^0} \right) \right], \quad (6.21)$$

since the zeros of the denominator,  $z_i$  closest to  $E_n^0$  correspond to leading terms multiplied by the large quantity  $\partial F(z)/\partial V_{nn}|(z = z_i)$ . In (6.21) we have retained terms proportional to the first order of the interaction constant  $1/\mu \cong e^2/\hbar c$ . The numerator of  $R_{b_0, b_0}$  is

$$\begin{aligned} N_{b_0, b_0} &= -\frac{\partial \Delta(z)}{\partial V_{b_0, b_0}} = \left( 1 + \frac{|V_{b_0, b_0}|}{z - E_{b_0}^0} \right) \prod_{n \neq b_0} \left[ z - E_n^0 - \left( V_{nn} + \frac{1}{2!} \sum_p \frac{V_{np} V_{pn}}{z - E_m^0} \right) \right] \\ &\simeq \prod_{n \neq b_0} \left[ z - E_n^0 - \left( V_{nn} + \frac{1}{2!} \sum_p \frac{V_{np} V_{pn}}{z - E_m^0} \right) \right], \end{aligned} \quad (6.22)$$

where in the approximation effected we have omitted terms of the second order in the interaction constant. Hence, under this approximation only one term remains in the denominator and therefore the matrix elements of the time evolution operator can be written in the form

$$\begin{aligned} U_{b_0, b_0} &= \frac{1}{2\pi i} \oint_C e^{-izt/\hbar} R_{b_0, b_0}(z) dz \\ &= \frac{1}{2\pi i} \oint_C e^{-izt/\hbar} \left[ (z - E_{b_0}) - \left( V_{b_0, b_0} + \frac{1}{2!} \sum_k \frac{|V_{b_0, gk}|^2}{z - E_{gk}^0} \right) \right]^{-1}. \end{aligned} \quad (6.23)$$

### 6.3 Atomic radiation in free space

We now consider the sum featuring in the expression above for the case of spontaneous radiation in free space, as a limiting case of a system with a discrete spectrum that approaches the continuum as a parameter changes. The simplest example is that of a cubic cavity where the field is subject to periodic boundary conditions. Letting the volume of the cavity tend to infinity we obtain the transition from the discrete spectrum

$$\mathbf{k}_d = \frac{2\pi}{\sqrt[3]{V}}(l_d, m_d, n_d), \quad \omega_d = \frac{2\pi c}{\sqrt[3]{V}}\sqrt{l_d^2 + m_d^2 + n_d^2}. \quad (6.24)$$

In a resonant cavity (where the modes are denoted by the subscript  $j$ , and the states of the unperturbed atomic Hamiltonian are denoted by  $|g\rangle$ ) the sum featuring in the expression (6.23) takes the form

$$S = \frac{1}{2!} \sum_{g,j} \frac{V_{b0,gj} V_{gj,b0}}{z - E_{gj}^0} = \frac{\pi e^2 \hbar}{m^2 V} \sum_{g,j} \frac{|(\hat{\mathbf{p}} \cdot \mathbf{e}_j)_{bg}|^2}{\omega_j (z - E_g - \hbar \omega_j)}, \quad (6.25)$$

since the matrix elements of the interaction Hamiltonian are

$$V_{b0,gj} = -\frac{e}{m} \sqrt{\frac{2\pi \hbar}{\omega_j V}} [(\hat{\mathbf{p}} \cdot \mathbf{e}_j) e^{i\mathbf{k}_j \cdot \hat{\mathbf{r}}}]_{bg} \quad (6.26)$$

and

$$\sum_g |[(\hat{\mathbf{p}} \cdot \mathbf{e}_j) e^{i\mathbf{k}_j \cdot \hat{\mathbf{r}}}]_{bg}|^2 = \sum_g \langle b | (\hat{\mathbf{p}} \cdot \mathbf{e}_j) e^{i\mathbf{k}_j \cdot \hat{\mathbf{r}}} | g \rangle \langle g | e^{-i\mathbf{k}_j \cdot \hat{\mathbf{r}}} (\hat{\mathbf{p}} \cdot \mathbf{e}_j) | b \rangle = \sum_g |(\hat{\mathbf{p}} \cdot \mathbf{e}_j)_{bg}|^2. \quad (6.27)$$

In the expression for (6.25) the summation is over all the field oscillators including the energy degenerate modes that differ only in the direction of

propagation or polarization. Converting the sum to an integral over  $k$  with  $\sum_k \rightarrow \int \frac{d\Omega_k k^2 dk}{(2\pi)^3/V}$  and using the dispersion relation  $k = \omega/c$  we can write

$$S = \frac{e^2 \hbar}{3\pi c^3 m^2} \sum_g |\mathbf{p}_{bg}|^2 \int_0^{\omega_{\max}} \frac{\omega d\omega}{z - E_g - \hbar\omega}, \quad (6.28)$$

where we have integrated over all polarization directions. After having determined  $S$ , and effecting the mass renormalization<sup>‡</sup> by introducing an operator  $\hat{W}$  with

$$W_{b_0, b_0} = \frac{1}{2\mu} \langle b | \mathbf{p}^2 | b \rangle = \frac{1}{2\mu} \sum_g \langle b | \mathbf{p} | g \rangle \langle g | \mathbf{p} | b \rangle, \quad (6.29)$$

we can write the denominator of the resolvent as  $\Delta_{b_0} = z - E_{b_0} - (W_{b_0, b_0} + S)$  with

$$W_{b_0, b_0} + S = \frac{e^2 \hbar}{3\pi c^3 m^2} \sum_g |\mathbf{p}_{bg}|^2 (z - E_g) \int_0^{\omega_{\max}} \frac{d\omega}{z - E_g - \omega} \quad (6.30)$$

In the calculation of these matrix elements appear the Cauchy integrals of the form

$$I(\zeta) = \int_a^b \frac{F(\omega)}{\omega - \zeta} d\omega, \quad (6.31)$$

defining an analytical function of  $\zeta$ . This function has a cut along the segment  $(a, b)$ , is single-valued along the entire complex plane excluding this segment,

---

<sup>‡</sup>We assume that the perturbation Hamiltonian is written in the form  $\hat{H}' = \hat{V} + \hat{W}$  with  $\hat{W} = \hat{\mathbf{p}}^2/(2\mu)$  being a term that accounts for the large changes occurring due to the interaction of the atom with the field. This term has the structure of the kinetic energy operator and the 'effective mass'  $\mu$  is chosen following the form of  $S$ .

and decreases monotonically with  $|\zeta| \rightarrow \infty$ . Using the Sokhotski-Plemelj theorem, for  $\omega_0 \in (a, b)$  we have

$$\lim_{\zeta \rightarrow \omega_0 \pm i0} \int_a^b \frac{F(\omega)}{\omega - \zeta} d\omega = \pm i\pi F(\omega_0) + \mathcal{P} \int_a^b \frac{F(\omega)}{\omega - \omega_0} d\omega. \quad (6.32)$$

In the interval  $0 < z < \hbar\omega_m$  (where  $\hbar\omega_m$  is the upper limit of integration) we obtain the following expression

$$\Delta_{b0} = z - E_{b0} - \frac{\alpha}{3\pi} \sum_g \frac{|\mathbf{p}_{bg}|^2}{m^2 c^2} (z - E_g) \left[ i\pi u(z - E_g) + \ln \left| \frac{\hbar\omega_m}{z - E_g} - 1 \right| \right], \quad (6.33)$$

where  $\alpha = e^2/(\hbar c)$  is the fine structure constant. After the analytical continuation of the expression (6.33), the main contribution to the matrix element  $U_{b0,b0}(t)$  will originate from the residue at the pole  $z = z_b$

$$U'_{b0,b0}(t) = \frac{\exp\{-i[(E_{b0} + \Delta E_b)t] - \Gamma_b t/\hbar\}}{\left( \frac{\partial \Delta_{b0}}{\partial z} \right)_{z=z_b}}. \quad (6.34)$$

This contribution describes the exponential decay of the excitation. The derivative in the denominator evaluates to

$$\left( \frac{\partial \Delta_{b0}}{\partial z} \right)_{z=z_b} = 1 - \frac{\alpha}{3\pi} \sum_g \frac{|\mathbf{p}_{bg}|^2}{m^2 c^2} \left[ i\pi + \ln \left( \frac{\hbar\omega_m}{E_b - E_g} - 1 \right) + \frac{\hbar\omega_m}{\hbar\omega_m + E_g - E_b} \right]. \quad (6.35)$$

For the derivation of the above we have assumed that  $\Delta_{b0}$  can be written as a Taylor series of  $(z - z_b)$  up to the first order in the region of  $z_b$ . The contour  $C$  we defined above, along which the integral (6.23) is taken is deformed to encircle the pole  $z_b$  and to circumvent the branching points  $0, E_g$  and

$E_m$ , which is the upper limit of the integral  $I$ . The dominant contribution arises from the pole  $z_b$ , which is responsible for the exponential decay of the excitation, since the remaining terms are multiplied by the small fine structure constant and the small parameter  $|\mathbf{p}_{bg}|^2/(m^2c^2) \sim (\lambda/a)^2 \sim 10^{-7}$ , where  $a$  is the Bohr radius and  $\lambda$  the radiated wavelength from the transition  $b \rightarrow g$ . We will consider now a term, which, albeit small in comparison to  $U'_{b_0,b_0}(t)$ , yields a small deviation from the exponential excitation: the integral along a contour starting and ending at  $\pm\rho - i\infty$  (respectively), and circumventing the origin (which is a branching point) in the  $z$ -plane, can be recast in the form

$$\begin{aligned} U''_{b_0,b_0}(t) &= -\frac{\hbar}{2\pi} \left( \int_0^\infty \frac{e^{-\rho t}}{\Delta_{b_0}^-(\rho)} d\rho - \int_0^\infty \frac{e^{-\rho t}}{\Delta_{b_0}^+(\rho)} d\rho \right) \\ &= -\frac{\hbar}{2\pi} \int_0^\infty \frac{\Delta_{b_0}^+(\rho) - \Delta_{b_0}^-(\rho)}{\Delta_{b_0}^+(\rho)\Delta_{b_0}^-(\rho)} e^{-\rho t} d\rho, \end{aligned} \quad (6.36)$$

with the parametrization  $z = i\rho$  along the path. For large  $t$ , the only important contribution in the integral will arise for  $\rho \rightarrow 0$ . In that case, the difference  $\Delta_{b_0}^+(\rho) - \Delta_{b_0}^-(\rho)$  can be expressed, to first order in  $\rho$ , as

$$\Delta_{b_0}^+(\rho) - \Delta_{b_0}^-(\rho) = \frac{2\alpha |\mathbf{p}_{bg}|^2}{3\pi m^2 c^2} \rho, \quad (6.37)$$

while the denominator of (6.36) tends to the constant

$$D = E_{b_0} + \frac{\alpha}{3\pi} \sum_g \frac{|\mathbf{p}_{bg}|^2}{m^2 c^2} (z - E_g) \left[ i\pi u(E_b - E_g) + \ln \left| \frac{\hbar\omega_m}{z - E_g} - 1 \right| \right]. \quad (6.38)$$

Since  $\int_0^\infty \rho e^{-\rho t} d\rho = 1/t^2$ , the contribution of this term to the matrix element  $U_{b_0,b_0}(t)$  amounts to

$$U''_{b_0, b_0}(t) = \frac{\alpha |\mathbf{p}_{bg}|^2 \hbar^2}{3\pi m^2 c^2 D^2 t^2}, \quad (6.39)$$

representing a term responsible for the departure from exponential decay.

## 6.4 Atomic radiation in cavities and waveguides

The interaction of an atom with the cavity modes in the first order of perturbation theory shifts the energy levels of a subsystem, however the spectrum of the system as a whole, remains discrete. For an atom in a cavity without losses, the state

$$|\psi(t)\rangle = \exp(-iE_0 t/\hbar) \left[ C_0 |0\rangle + \sum_{n \neq 0} C_n \exp(iM_n \Delta \omega t) \right], \quad (6.40)$$

describes a periodical motion of the system (known as the ‘Poincaré cycle’) with period  $2\pi/\Delta\omega$ , where  $|n\rangle$  are stationary states of the unperturbed Hamiltonian and the coefficients of the stationary states  $D_n = D_n(t) = C_n \exp(iM_n \Delta \omega t)$  are of first order of smallness. These coefficients are periodic with period  $2\pi/\Delta\omega$ , since their expression contains the factor  $\exp(iM_n \Delta \Omega t)$  in the integrand, for a periodic perturbation (see Chapter 3). The phase factor  $\exp(-iE_0 t/\hbar)$ , common to all terms can be disregarded in deriving the equations of motion for the system. As we can infer, the system has ‘memory’ of the initial state, which is repeated for an infinite time and determines the motion of the system. In a cavity with a length much larger than the atomic radiation wavelength, the value of  $\Delta\omega$  is very small and consequently the initial state will be reproduced after a very long time interval. Hence, radiation

in a large cavity is practically aperiodic and can be compared to radiation in free space. Another important aspect which needs to be emphasized is that higher orders of perturbation give rise to new combination frequencies, approaching the continuum in the infinite limit. From this discussion, we can treat the optical cavity as a open system whose radiation spectrum is modified by the presence of Lorentz-type signatures, which are representative of the high-quality cavity resonances. For this reason, we write the denominator  $F(z)$  of the resolvent operator matrix element  $U_{b_0, b_0}(t)$  as

$$\Delta(z) = z - \hbar\Omega - \frac{1}{2!}(I_1 + I_2), \quad (6.41)$$

where

$$I_{1,2} = \int \frac{\rho(\omega) |V_{b_0, gk}|_{(1,2)}^2}{z - \hbar\omega} d\omega = \begin{cases} i \frac{\alpha |\mathbf{p}_{bg}|^2}{3m^2 c^2} \equiv -i\hbar\gamma & (1) \\ \sum_n \frac{h_n^2}{z - \hbar(\omega_n - i\Gamma_n)} & (2), \end{cases} \quad (6.42)$$

where the case (1) corresponds to the interaction of the atom with the free space modes (and is due to the  $i\pi F(\omega_0)$  term in (6.32), the other term being approximately equal to zero), and the integral (2) represents the interaction of the atom with the cavity modes (corresponding to Lorentzian profiles). For the case (2) we have applied the residue theorem for the integral

$$\begin{aligned} I' &= \int \sum_n \frac{h_n^2}{(z - \hbar\omega)[(\omega - \omega_n)^2 + \Gamma_n^2]} d\omega \\ &= \int \sum_n \frac{h_n^2}{(z - \hbar\omega)[\omega - (\omega_n + i\Gamma_n)][\omega - (\omega_n - i\Gamma_n)]} d\omega, \end{aligned} \quad (6.43)$$

where we have retained only the term

$$2\pi i \sum_n \frac{1}{z - \hbar(\omega_n - i\Gamma_n)} \frac{h_n^2}{(-2i\Gamma_n)} \equiv - \sum_n \frac{\tilde{h}_n^2}{z - \hbar(\omega_n - i\Gamma_n)}, \quad (6.44)$$

that would lead to the physically meaningful exponential decay of the excitation. Summing the two contributions, the denominator can be written as

$$\Delta(z) \cong z - \hbar\Omega + i\hbar\gamma - \sum_n \frac{\tilde{h}_m^2}{z - \hbar(\omega_m - i\Gamma_m)}, \quad (6.45)$$

where for illustrative purposes we will limit ourselves to only one cavity mode ( $n = m$ ). Equating the denominator of the resolvent to zero in order to find the (dominant) pole contribution, the following quadratic equation is produced

$$(z - E')(z - E'') = \tilde{h}_m^2, \quad (6.46)$$

where  $E' = \hbar(\Omega - i\gamma)$  and  $E'' = \hbar(\omega_n - i\Gamma_n)$ . The roots of this equation are

$$z_{1,2} = \frac{1}{2} \left[ (E' + E'') \pm \sqrt{(E' - E'')^2 - 4\tilde{h}_m^2} \right]. \quad (6.47)$$

On the assumption that  $|\tilde{h}_m| \ll |E'|, |E''|$ , which holds, then

$$\pm \sqrt{(E' - E'')^2 - 4\tilde{h}_m^2} = \pm(E' - E'') \sqrt{1 - \frac{4\tilde{h}_m^2}{(E' - E'')^2}} \quad (6.48)$$

the roots of the equation differ from  $E', E''$  only in terms of second order in the small parameter  $\tilde{h}_m$  (since  $-\pi < \arg[(E' - E'')^2] + \arg \left[ 1 - \frac{4\tilde{h}_m^2}{(E' - E'')^2} \right] \leq \pi$ ). Hence, the roots of the equation, written for convenience as  $z_{1,2} =$

$\hbar(\Omega_{1,2} - i\kappa_{1,2})$  have negative imaginary parts. Finally, the decay of the excitation is determined by the matrix element [3]

$$U_{b_0, b_0}(t) = \frac{[\Omega_1 - \omega_n - i(\kappa_1 - \Gamma_n)] \exp[-(\kappa_1 + i\Omega_1)t]}{\Omega_1 - \Omega_2 - i(\kappa_1 - \kappa_2)} - \frac{[\Omega_1 - \omega_n - i(\kappa_1 - \Gamma_n)] \exp[-(\kappa_1 + i\Omega_1)t]}{\Omega_1 - \Omega_2 - i(\kappa_1 - \kappa_2)}. \quad (6.49)$$

This is a simple illustrative case of a not purely exponential decay process, in which there is energy transfer between the atom and the resonator. If the coupling between the atom and the modes of free space is weak, then  $\gamma = 0$ , and only the cavity losses determine the decay law of the atomic excitation. In the case of an atom in a waveguide, the summation term in the expression for  $U_{b_0, b_0}(t)$  becomes

$$\sum_{\kappa} \frac{|V_{g\kappa, b_0}|^2}{z - \hbar\omega_{\kappa}} \rightarrow \frac{g^2 c}{2\pi} \int_0^{\infty} \frac{dk'}{\omega_{k'}(z - \hbar\omega_{k'})}, \quad (6.50)$$

where the dispersion relation reads

$$k' = c^{-1}(\omega^2 - \omega_c^2)^{\frac{1}{2}} \Rightarrow \frac{dk'}{d\omega} \omega [c(\omega^2 - \omega_c^2)^{\frac{1}{2}}]^{-1}, \quad (6.51)$$

where  $\omega_c$  is the cut-off frequency of the waveguide. For simplicity, hereinafter we assume that the atom is a two level system with transition frequency  $\Omega = (E_b - E_g)/\hbar$  and a momentum operator that takes the form  $\hat{\mathbf{p}} = m\Omega\mathbf{r}(|b\rangle\langle g| + |g\rangle\langle b|)$ . We introduce the dimension-less quantities

$$\nu = \omega/\Omega, \quad \nu_c = \omega_c/\Omega, \quad d\nu = d\omega/\Omega, \quad \zeta(\zeta') = z(z')/(\hbar\Omega) \quad (6.52)$$

and the integral above acquires the form

$$I(\zeta') = \frac{g^2}{2\pi\hbar\Omega} \int_{\nu_c}^{\infty} \frac{d\nu}{(\zeta' - \nu_c)(\nu^2 - \nu_c^2)^{\frac{1}{2}}}. \quad (6.53)$$

Applying the Sokhotski-Plemelj relation we have

$$\lim_{\zeta' \rightarrow \zeta \pm i0} I(\zeta') = \frac{g^2}{2\pi\hbar\Omega(\zeta^2 - \nu_c^2)^{\frac{1}{2}}} \left\{ \ln \left[ \frac{(\zeta + \nu_c)^{\frac{1}{2}} + (\zeta - \nu_c)^{\frac{1}{2}}}{(\zeta + \nu_c)^{\frac{1}{2}} - (\zeta - \nu_c)^{\frac{1}{2}}} \right] \mp i\pi \right\}. \quad (6.54)$$

Since this integral has a branch cut along the segment  $(\nu_c, \infty)$  we can separate the integral along the upper (+) and lower (-) parts of the contour  $C$ , as below

$$U_{b0,b0}(t) = \frac{1}{2\pi i} \oint_C \frac{e^{-i\zeta\Omega t}}{G(\zeta)^{-1}} d\zeta \equiv \frac{1}{2\pi i} \int_{\hbar\omega_c}^{\infty} \frac{e^{-izt/\hbar}}{\Delta_{b0}^{(-)}} dz - \frac{1}{2\pi i} \int_{\hbar\omega_c}^{\infty} \frac{e^{-izt/\hbar}}{\Delta_{b0}^{(+)}} dz, \quad (6.55)$$

and the denominators are

$$\Delta_{b0,b0}^{\pm}(z) = z - E_b - \Delta E_b(z) \pm i\Gamma(z), \quad (6.56)$$

where

$$\Delta E_b(z) = \frac{g^2}{2\pi} \ln \left[ \frac{(z + \hbar\omega_c)^{1/2} + (z - \hbar\omega_c)^{1/2}}{(z + \hbar\omega_c)^{1/2} - (z - \hbar\omega_c)^{1/2}} \right] (z^2 - \hbar^2\omega_c^2)^{-1/2} \quad (6.57)$$

and

$$\Gamma(z) = -\frac{g^2}{2} (z^2 - \hbar^2\omega_c^2)^{-1/2}. \quad (6.58)$$

From the form of the matrix element

$$U_{b0,b0}(t) = -\frac{1}{\pi} \int_{\hbar\omega_c}^{\infty} \frac{\Gamma(z)e^{-izt/\hbar}}{[z - E_b - \Delta E_b(z)]^2 + \Gamma_b^2(z)} dz, \quad (6.59)$$

we can deduce that the decay is not strictly exponential, as it would be in the case that  $\Delta E_b$  and  $\Gamma$  were independent of  $z$ . The integration contour may be deformed as follows: since the function  $G(\zeta)$  does not have any zeros in the lower half plane (lower part of the contour) and  $\exp(-i\zeta\Omega t) \rightarrow 0$  as  $\Im\zeta \rightarrow -\infty$  for  $t > 0$ , the integral along this part of the contour has a zero contribution. The upper part of the contour must be deformed such that it circumvents the branching point  $\zeta = \nu_c$ . One part of this contour encircles the pole  $\zeta = \zeta_b$ , that has a negative imaginary part. The pole is found by the analytic continuation of the function

$$G(\zeta) = \hbar\Omega(\zeta - 1) - \frac{g^2}{2\pi\hbar\Omega(\zeta^2 - \nu_c^2)^{\frac{1}{2}}} \left\{ \ln \left[ \frac{(\zeta + \nu_c)^{\frac{1}{2}} + (\zeta - \nu_c)^{\frac{1}{2}}}{(\zeta + \nu_c)^{\frac{1}{2}} - (\zeta - \nu_c)^{\frac{1}{2}}} \right] - i\pi \right\} \quad (6.60)$$

in the upper part of the contour onto another sheet of the Riemann surface (being consistent with our previous assumption that the deformed lower part of the contour does not ‘meet’ the pole). As it happens also with radiation in free space, the pole  $\zeta_b$  is responsible for the exponential decay of the excited atomic state, whereas the part of integral the contour enclosing the branching point  $\zeta = \nu_c$  accounts for small deviations from exponentiality. We will now focus on the transition from the discrete to the continuous spectrum. The denominator of the resolvent can be written (omitting prefactors) as

$$H(\zeta) = (\zeta - 1) - \frac{R\lambda}{L} \sum_m \frac{1}{\nu_m(\zeta - \nu_m)}, \quad (6.61)$$

where  $R = g^2/[2\pi(\hbar\Omega)^2]$  and the subscript  $m$  runs over the eigenfrequencies. As the residues of the integrand in  $U_{b0,b0}(t)$  are

$$\frac{e^{-i\zeta_n\Omega t}}{(\partial H/\partial\zeta)}\Big|_{\zeta_n}, \tag{6.62}$$

where  $H(\zeta_n) = 0$ , then as the roots  $\zeta_n$  become far from unity, the residue will diminish in magnitude, since the denominator tends to infinity (the root is very close to the asymptotes  $\nu_m$ ). We conclude that the most important contribution is made when  $\zeta \cong \nu_m \cong 1$ . The resonance frequencies are equidistant, so that we can write

$$\nu_m = 1 + \frac{\lambda}{L} \left(m + \frac{1}{2}\right), \quad m = 0, \pm 1, \pm 2... \tag{6.63}$$

The second term of  $H(z)$  in the region of interest can be written as

$$\begin{aligned} & \left\{ \left[ 1 + \frac{\lambda}{L} \left(m + \frac{1}{2}\right) \right] \left[ \zeta - 1 - \frac{\lambda}{L} \left(m + \frac{1}{2}\right) \right] \right\}^{-1} \\ &= \frac{\left(\frac{L}{\lambda}\right)^2 (\zeta - 1)}{\left(\frac{L}{\lambda}\right)^2 (\zeta - 1)^2 - \left(m + \frac{1}{2}\right)^2 (\zeta - 1) + \left(\frac{L}{\lambda}\right) \left(m + \frac{1}{2}\right) (\zeta - 1)(\zeta - 2)}. \end{aligned} \tag{6.64}$$

We have assumed however that

$$\zeta - 1 \cong \nu_m - 1 = \frac{\lambda}{L} \left(m + \frac{1}{2}\right), \tag{6.65}$$

so that the last two terms in the denominator can be recast in the form

$$\left(m + \frac{1}{2}\right)^2 [(\zeta - 2) - (\zeta - 1)] = - \left(m + \frac{1}{2}\right)^2 \tag{6.66}$$

Finally, we can write

$$H(\zeta) = (\zeta - 1) + \left(\pi \frac{R\lambda}{L}\right) \sum_m \left(\frac{L}{\lambda}\right) \frac{\left(\frac{L}{\lambda}\right) (\zeta - 1)\pi}{\left[\left(m + \frac{1}{2}\right) \pi\right]^2 - \left[\left(\frac{L}{\lambda}\right) (\zeta - 1)\pi\right]^2}. \quad (6.67)$$

By virtue of the series expansion of  $\tan x$  (see [5])

$$\tan(x) = \sum_{m=0}^{\infty} \frac{2x}{\left[\left(m + \frac{1}{2}\right) \pi\right]^2 - x^2}, \quad (6.68)$$

setting  $x = \pi(L/\lambda)(\zeta - 1)$  we obtain

$$H(\zeta) = (\zeta - 1) + \pi R \tan(x), \quad (6.69)$$

with derivative

$$\frac{\partial H}{\partial \zeta} = 1 + \pi R \sec^2(x) \frac{dx}{d\zeta} = 1 + \pi^2 \frac{RL}{\lambda} [1 + \tan^2(x)]. \quad (6.70)$$

In the limit  $L \rightarrow \infty$  we can disregard unity in the above and for the roots  $\zeta_n(x_n)$  we have

$$\tan^2(x_n) = \frac{(\zeta_n^2 - 1)^2}{\pi^2 R^2}, \quad (6.71)$$

so that

$$\left. \frac{\partial H}{\partial \zeta} \right|_{(\zeta=\zeta_n)} \cong \frac{L}{R\lambda} [(\zeta_n - 1)^2 + (\pi R)^2]. \quad (6.72)$$

Integration along the contour C produces the sum

$$\sum_n \frac{e^{-i\Omega\zeta_n t}}{(\zeta_n - 1)^2 + (\pi R)^2}, \quad (6.73)$$

which for large  $L$  is approximately equal to the integral

$$\int_{-\infty}^{+\infty} \frac{e^{-i\Omega\zeta t}}{(\zeta - 1)^2 + (\pi R)^2} \frac{dn}{d\zeta} d\zeta, \quad (6.74)$$

which is of Lorentzian form. Far from  $\zeta = 1$ , the roots  $\zeta_n$  are very close to the resonance frequencies  $\nu_m$ . In this region the roots are also equidistant (as are the  $\nu_m$ ). The distance between the roots gradually decreases and reaches its minimum when  $\zeta \cong 1$ . The limits are defined by the condition  $\zeta_n - 1 \simeq \pi R \Rightarrow |m| \simeq (\pi RL/\lambda)$ . In the region  $-(\pi RL/\lambda) < m < (\pi RL/\lambda)$  there is one additional root compared with the number of resonance frequencies in that region. This additional mode is distributed over a distance of  $(2\pi RL/\lambda)$ . Hence, the average distance between roots in that region differs from the distance between roots outside this region by

$$\left| \frac{d}{d(L/\lambda)} (\pi RL/\lambda)^{-1} \right| = \frac{\lambda^2}{2\pi RL^2}, \quad (6.75)$$

which is of the second order of smallness in terms of the (small) parameter  $\lambda/L$ . Hence, we can calculate  $U_{b_0, b_0}(t)$  assuming that the roots  $\zeta_n$  are equidistant and that small deviations from equidistance are regarded as a perturbation. Up to first order in  $\lambda/L$  we have  $\zeta_n^{(0)} = 1 + n(\lambda/L)$  and in that case, using that  $\Omega = 2\pi c/\lambda$  we write [3]

$$U_{b_0, b_0}(t) = \frac{\pi R L e^{-i\Omega t}}{2c\hbar} \sum_{n=-\infty}^{+\infty} \frac{\exp(-2\pi n i c t / L)}{(n\pi)^2 + \left(\frac{\pi^2 R L}{\lambda}\right)^2}. \quad (6.76)$$

Setting  $T = L/(2c)$  and  $\Gamma = \pi\Omega R$ , we can consider the above sum as the Fourier series expansion of a periodic function with

$$U_{b_0, b_0}(t) = \frac{e^{-i\Omega t} e^{-\Gamma t} + e^{\Gamma(t-2T)}}{\hbar\Omega (1 - e^{-2\Gamma T})}, \quad (6.77)$$

in the fundamental period  $t \in [0, 2T]$ . In the limit  $L \rightarrow \infty$  ( $T \rightarrow \infty$ ) we obtain the exponential decay

$$U_{b_0, b_0}(t) = \frac{1}{\hbar\Omega} e^{-\Gamma t - i\Omega t}. \quad (6.78)$$

We will consider now the effect of the deviation from equidistance on the matrix element  $U_{b_0, b_0}(t)$  by taking the difference

$$\Delta U_{b_0, b_0}(t) = \frac{R\lambda}{L\hbar\Omega} \sum_{n=-\infty}^{+\infty} \left[ \frac{e^{-i\Omega\zeta_n t}}{(\zeta_n - 1)^2 + (\pi R)^2} - \frac{e^{-i\Omega\zeta_n^{(0)} t}}{(\zeta_n^{(0)} - 1)^2 + (\pi R)^2} \right]. \quad (6.79)$$

The terms in the sum can be added to give

$$\frac{e^{-i\Omega\zeta_n^{(0)} t} \left\{ e^{-i\Omega\Delta\zeta_n t} \left[ (\zeta_n^{(0)} - 1)^2 + (\pi R)^2 \right] - (\zeta_n - 1)^2 - (\pi R)^2 \right\}}{\left[ (\zeta_n^{(0)} - 1)^2 + (\pi R)^2 \right] \left[ (\zeta_n - 1)^2 + (\pi R)^2 \right]}. \quad (6.80)$$

Keeping terms up to the first order in  $\Delta\zeta_n$ , the numerator (pre-multiplied by  $e^{-i\Omega\zeta_n^{(0)} t}$ ) becomes

$$(e^{-i\Omega\Delta\zeta_n t} - 1) \left[ (\zeta_n^{(0)} - 1)^2 + (\pi R)^2 \right] - 2(\zeta_n^{(0)} - 1) \Delta\zeta_n e^{-i\Omega\Delta\zeta_n t}, \quad (6.81)$$

while in the denominator  $\zeta_n^{(0)}$  replaces  $\zeta_n$ . After cancellation of common factors, the final result (to first order in  $\Delta\zeta_n$ ) reads

$$\Delta U_{b0,b0}(t) = \frac{R\lambda}{L\hbar\Omega} \sum_{n=-\infty}^{+\infty} e^{-i\Omega\zeta_n^{(0)}t} \left[ \frac{e^{-i\Omega\Delta\zeta_n t} - 1}{\left(\zeta_n^{(0)} - 1\right)^2 + (\pi R)^2} - \frac{2\left(\zeta_n^{(0)} - 1\right)\Delta\zeta_n e^{-i\Omega\Delta\zeta_n t}}{\left[\left(\zeta_n^{(0)} - 1\right)^2 + (\pi R)^2\right]^2} \right]. \quad (6.82)$$

The numerator of the first fraction in the sum can be recast in the form

$$- 2ie^{-i(\Omega\Delta\zeta_n t)/2} \sin\left(\frac{1}{2}\Omega\Delta\zeta_n t\right). \quad (6.83)$$

For finite time  $t$ ,

$$\sin\left(\frac{1}{2}\Omega\Delta\zeta_n t\right) \simeq \frac{1}{2}(\Omega t) \max|\Delta\zeta_n| \sim \left(\frac{\lambda}{L}\right)^2. \quad (6.84)$$

The second term in the numerator is also of the second order of smallness in  $(\lambda/L)^2$ . In the sum (6.79) the number of significant terms is approximately  $2\pi RL/\lambda$ , as we have claimed above. Hence the sum is of first order in  $(\lambda/L)$ , consequently the corrections to the exponential decay due to the non-equidistance of the spectrum decrease inversely proportional to  $L$  as  $L \rightarrow \infty$ . Finally, we note that (6.77) represents a periodic function in which the initial value appears with an arbitrary accuracy, as there is a periodic exchange of energy between the atom and the cavity modes. As  $L \rightarrow \infty$ , however, the period  $T$  tends also to infinity. As a result, the system becomes then aperiodic (the radius of the Poincaré cycle increases infinitely.)

## 6.5 Atomic radiation in a 1D periodic medium

In the dipole approximation, the Hamiltonian of the system comprised of the atom and the electromagnetic field has the form

$$\hat{H} = \frac{\hat{\mathbf{p}}^2}{2m} + V(\hat{\mathbf{q}}) + \sum_j \hbar\omega_j \hat{a}_j^\dagger \hat{a}_j - \frac{e}{m} \sum_j \left( \frac{\pi\hbar}{QSc\omega_j L_j} \right)^{\frac{1}{2}} \Lambda_j (\hat{\mathbf{p}} \cdot \mathbf{e}_j) (\hat{a}_j^\dagger + \hat{a}_j), \quad (6.85)$$

where the constant  $\Lambda_j$  quantifies the dependence of the Hamiltonian on the position of the atom and  $L_j$  reflects the frequency dependence of the  $j^{\text{th}}$  eigenwave. The denominator of  $U_{b_0, b_0}(t)$ , as usual, reads

$$G(z) = z - \hbar\Omega - \frac{1}{2} \sum_m \frac{|V_{b_0, gm}|^2}{z - \hbar\omega_m} \equiv z - \hbar\Omega - X(\omega). \quad (6.86)$$

Replacing the summation over the field oscillators with integration over the effective wavenumber  $k'$ , we find that

$$G(z) = z - \hbar\Omega - \int \frac{|V_{b_0, g\omega_{k'}}|^2 Q(\omega_{k'})}{\pi(z - \hbar\omega'_k)} dk', \quad (6.87)$$

where  $Q$  is a function characteristic of the periodic structure. The integration is carried over all branches of the dispersion curve, in particular over the allowed frequency bands. Hence,  $G(z)$  has cuts along the allowed bands on the real axis (according to the Sokhotski-Plemelj relations), while in the forbidden bands it takes real values. The boundaries between the allowed and forbidden bands define the branching points of this function. Similarly to our discussion for the properties of atomic radiation in a waveguide, only the upper part of the contour  $C$  will contribute to  $U_{b_0, b_0}(t)$ , and the function  $G(z)$  for  $z + i0$  assumes the value

$$G(z) = z - \hbar\Omega + i\frac{A}{z}|\mathbf{p}_{bg} \cdot \mathbf{e}|^2 f(k, a, b) - I, \quad (6.88)$$

where  $f$  is a function of the characteristic dimensions of the 1D structure and the dispersion relation, and the integral  $I$  is taken in the sense of a principal value at real  $z = \hbar\omega$ . This integral defines the Lamb shift, and in most cases it is neglected due to its smallness [3]. It can be seen that the function  $G(z)$  has a root situated at  $z_b = \hbar(\Omega - i\gamma)$ , which is at the analytical continuation of the upper edge of the physical sheet downwards. As usual, the residue at this pole is responsible for the exponential decay.

Deforming the integration contour accordingly, to encircle the pole in the non-physical sheet of the Riemann surface, to enclose the branch cuts and encircle the pole on the real axis in the forbidden band (giving rise to the so-called ‘dynamic state’), The matrix element  $U_{b_0, b_0}(t)$  breaks down into three components. The two of these components that decay with time correspond to the residue at the pole of the nonphysical sheet of the Riemann surface and the the integral over the cut. The amplitude of the third component, corresponding to the residue at the pole in the real axis, does not depend on time. As noted in [3], the decay of the initial state does not occur fully, but only up to a stationary level. When the transition frequency  $\Omega$  is in the band-gap, the exponential part of the radiation decay is very small, and the probability of the appearance of the dynamic state approaches unity. For the case of chiral nematic liquid crystals, the knowledge of the photonic DOS can lead to the numerical computation of the function  $G(z)$  and hence to the properties of spontaneous emission decay in the molecular resonator. An agreement with the results presented above is expected when  $L \rightarrow \infty$ .

In this chapter we have presented a treatment whereby the eigenwaves alongside the corresponding photonic density of states in chiral nematic liquid crystals can be incorporated into the matrix elements of the resolvent operator. This suggestion follows the transition from a discrete to a continuous spectrum when studying atomic radiation in resonant cavities and waveguides, and aims to investigate departures from the Markov approximation and the corresponding exponentially decaying temporal spontaneous emission profiles.



# Bibliography

- [1] S. JOHN AND T. QUANG, *Spontaneous Emission near the Edge of a Photonic Bandgap*, Phys. Rev. A, **50**, pp. 1764-1769 (1994).
- [2] J. SCHMIDTKE AND W. STILLE, *Fluorescence of a dye-doped cholesteric liquid crystal film in the region of the stop-band: theory and experiment*, Eur. Phys. J. B **31**, pp. 179-194 (2003).
- [3] V. P. BYKOV, *Radiation of Atoms in a Resonant Environment*, World Scientific Publishing, Singapore, 1993.
- [4] P. CARETTE, C. LI, J. BOYAVAL AND B. MEZIANE, *Spontaneous Emission of  $\text{Eu}^{3+}$  ions in a cholesteric liquid crystal*, Optical and Quantum Electronics **35**, pp. 909-929 (2003).
- [5] I. S. GRADSHTEYN AND I. M. RYZHIK, *Table of Integrals, Series and Products*, 7th Ed., Elsevier, 2007.

## Synoptic conclusions

In this work, we have derived analytic expressions for the calculation of the density of photon states (DOS) in dye-doped chiral nematic liquid crystal (LC) cells in the presence of an active lossy medium. Results are presented on the profile of the DOS as a function of the reduced wavelength for different macroscopic parameters such as the optical anisotropy and the magnitude of the losses. The results show that, for a fixed value of the pitch, the DOS at the photonic band-edges decreases with increasing losses. The band-edge that exhibits the largest DOS (e.g., short or long wavelength band-edge) is found to depend on the magnitude of the loss coefficient; above a critical value the long-wavelength edge exhibits the largest DOS. Using the analytical expressions, results have been presented on the DOS as a function of the number of pitches showing an optimal value of the pitch that corresponds to the maximum in the density of states. These findings are correlated with experimental results for the lasing threshold, which is found to be inversely proportional to the maximum DOS when only losses are considered (apart from spontaneous absorption). The behaviour of the DOS can also reflect mode quenching in these lasing structures in the regime beyond the threshold gain. It is understood that the consideration of the DOS proves to be an

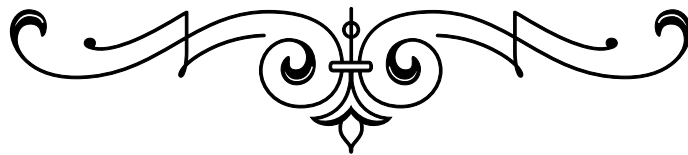
invaluable means for understanding lasing and such an approach should be implemented when determining the factors limiting the lasing threshold in chiral nematic films (e.g., leaky modes) as well as when studying the mode behaviour in more complicated configurations (e.g., defect modes).

We investigated resonance in a radiative chiral nematic LC (a characteristic example of a partial distributed feedback structure), for the diffractive polarization. We found that there is a disparity between the DOS and the calculated emission spectrum, which is also verified experimentally. We outlined the main effects occurring for different detuning values through deriving analytic results for the Lamb shift and the transition broadening following the logarithmic divergence of the DOS in a 2D photonic crystal. We conclude that incorporating cavity losses alongside broadening mechanisms, and including the effect of resonance leads to a more comprehensive treatment of spontaneous emission from these structures.

Subsequently, we have detailed a system for pumping an organic solid-state dye laser using computer generated holography. This technique provides a means with which to vary the location of the pump beam on the active medium in real-time enabling fresh active gain regions to be addressed in rapid succession, thus preventing build-up of triplet states and ensuring optimum thermal management. Both static and dynamic hologram-defined pumping have been shown to be possible, with dynamic pumping leading to improved stability, larger average output powers and access to higher repetition rates. With higher repetition rate pump lasers, it is feasible that this approach could enable these organic lasers to reach operating frequencies on the order of a MHz, without the need of mechanically moving parts. Ad-

ditionally, due to the unique nature of the adaptive pumping method, it is possible to precisely control the spatial wavefront and configuration of the pumping wave allowing greater versatility and functionality to be realised. In this study, we demonstrate a simple approach to wavelength tuning and multi-chromatic outputs simultaneously, but it is equally possible to envisage that novel pump beam profiles that optimise propagation through the medium could also be demonstrated.

The final chapter focusses on the relevance of the resolvent method in quantifying the decay of an excited atomic state in a chiral nematic. Following the determination of the pertinent diagonal matrix element of the time evolution operator in the case of a periodic waveguide, we can incorporate the density of states to examine the behaviour of integral functions albeit for a structure of finite length.



# Related publications

## Journal publications

(1) Th.K. Mavrogordatos, S.M. Morris, F. Castles, P.J.W. Hands, A.D. Ford, H.J. Coles, and T.D. Wilkinson, *Density of photon states in dye-doped chiral nematic liquid crystal cells in the presence of losses and gain*, Phys. Rev. E, **86**, pp. 011705(1-7) (2012).

(2) Th.K. Mavrogordatos, S.M. Morris, S. M. Wood, H.J. Coles, and T.D. Wilkinson, *Spontaneous emission from radiative chiral nematic liquid crystals at the photonic band-gap edge: An investigation into the role of the density of photon states near resonance*, Phys. Rev. E, **87**, pp. 062504(1-8) (2013).

(3) S. M. Wood, Th. K. Mavrogordatos, S. M. Morris, P. J. W. Hands, F. Castles, D. J. Gardiner, K. L. Atkinson, H. J. Coles, and T. D. Wilkinson, *Adaptive holographic pumping of thin-film organic lasers*, Opt. Lett., **38**, pp. 4483-4486 (2013).

**Conference proceedings**

(1) Th.K. Mavrogordatos, S. M. Morris, F. Castles, H. J. Coles, and T. D. Wilkinson, *The density of photon states in dye-doped chiral nematic liquid crystal cells in the presence of absorption and gain*, Laser Optics 2012, St. Petersburg, Russia, June 2012.

(2) Th.K. Mavrogordatos, S. M. Morris, F. Castles, H. J. Coles, and T. D. Wilkinson, *Fluorescence and lasing characteristics of dye-doped chiral nematic liquid crystal cells*, (International Liquid Crystal Conference) ILCC 2012. Mainz, Germany, August 2012.